FLOW INSTABILITY AND ACOUSTIC RADIATION MEASUREMENTS OF LOW REYNOLDS NUMBER SUPERSONIC JETS

By

GERALD LEE MORRISON

Bachelor of Science
Oklahoma State University
Stillwater, Oklahoma
1973

Master of Science
Oklahoma State University
Stillwater, Oklahoma
1974

Submitted to the Faculty of the Graduate College
of the Oklahoma State University
in partial fulfillment of the requirements
for the Degree of
DOCTOR OF PHILOSOPHY
December, 1977

FLOW INSTABILITY AND ACOUSTIC RADIATION MEASUREMENTS OF LOW REYNOLDS NUMBER SUPERSONIC JETS

Thesis Approved:

D K McLaughlin
Thesis Adviser

R F Lowery

W. A. Lieberman

R. Yarbrough

Norman N Durham
Dean of the Graduate College

ACKNOWLEDGMENTS

The author wishes to express his deepest appreciation to his wife, Nelda, for her support and help in the preparation of this dissertation and to his parents, Ed and Eleanor Morrison, whose help in the preparation of this dissertation was invaluable.

The author wishes to express his appreciation to his major adviser, Dr. Dennis K. McLaughlin, and to his other committee members, Dr. W. G. Tiederman, Dr. R. L. Lowery, and Dr. R. K. Yarlagadda, for their advice and guidance concerning this work. Appreciation is also expressed to Mr. T. R. Troutt and Mr. J. L. Stromberg, fellow graduate students working on this project, and to Charlene Fries whose expert typing and knowledge of the Graduate School's rules were invaluable.

The author would like to recognize the financial support of the National Science Foundation, whose grant number ENG 75-21405 made this study possible.

TABLE OF CONTENTS

LIST OF TABLES

LIST OF FIGURES

NOMENCLATURE

a_o	speed of sound in the ambient air
ALS	arbitrary linear scale
A_m	mass velocity fluctuation sensitivity coefficient
A_T	stagnation temperature fluctuation sensitivity coefficient
A_v	radial velocity fluctuation sensitivity coefficient
b	$(\gamma-1)\ M^2 s$
c	axial wave speed
d	nozzle diameter minus twice the displacement thickness
D	nozzle exit diameter
e'	fluctuating hot-wire voltage
E	mean hot-wire voltage
E_b	hot-wire bridge voltage
E_{KE}	axial kinetic energy flux
f	frequency (Hz)
k	complex wave number
k_i	imaginary part of the complex wave number
k_r	real part of the complex wave number
m	mass velocity
M	Mach number
n	azimuthal mode number
P	pressure
P_{atm}	standard atmospheric pressure
P_c	test chamber pressure

P_n	static nozzle exit pressure
r	radial distance from jet centerline
Re	Reynolds number
R_{mT_o}	correlation coefficient between mass velocity and stagnation temperature fluctuations
R_s	resistance in series with hot-wire in the hot-wire anemometer bridge
R_w	hot-wire resistance
s	$[1 + ((\gamma-1)/2)M^2]^{-1}$
St	Strouhal number, fd/U
T	static temperature
T_{aw}	adiabatic hot-wire temperature
T_o	stagnation temperature
$T_{o\infty}$	stilling chamber stagnation temperature
u	axial velocity
U	mean centerline jet velocity at the exit
v	radial velocity
x	downstream distance from the nozzle
x_c	length of the potential core
y	vertical distance from the centerline
z	horizontal distance from the centerline
α	yaw angle of crossed hot-wire probe relative to the local flow angle
γ	ratio of specific heats
ΔSt	width of a band pass in Strouhal number
η	recovery factor, T_{aw}/T_o
θ	azimuthal angle
θ^*	$\tilde{e}/A_T$
λ	axial wavelength

μ	Mach angle
ρ	density
ρ_o	density of ambient air
τ	period of the organized wave
ϕ	relative phase
ω	frequency (radians/sec)
$( )'$	instantaneous fluctuating component of quantity
$( )_{\Delta St}$	RMS value of the quantity in a frequency band St wide
$(\tilde{\ })$	RMS fluctuating quantity nondimensionalized by the local mean
$(\bar{\ })$	mean quantity
$( )_{rms}$	root mean square of a fluctuation quantity
$< >$	phase average

CHAPTER I

INTRODUCTION

During the last 25 years there have been many theories presented that mathematically describe the noise generation of a jet of air. The works of Lighthill (1) (2), Ffowcs Williams (3), Ribner (4), Phillips (5), Pao (6), Lilley (7), and Doak (8) are all capable of predicting the noise radiated from a jet of air with some degree of accuracy. However, in order to calculate the noise, all of these works must use empirical information about the flow fluctuations in the jet. Therefore, the only way to determine the source functions is to experimentally measure the flow fluctuations needed to calculate them. In jet flows this is an almost insurmountable task due to the complexity of the source terms. However, by using dimensional analysis with the theories it is possible to approximate the directivity of the acoustic field and the dependence of the sound intensity upon the velocity of the jet.

During the past several years a new class of jet noise theories has been developed by several authors (9) through (17). These theories are built on a substantial amount of experimental evidence which has demonstrated that there is an organized structure in turbulent free shear flows (18) through (24). It has also been hypothesized by several authors (9) (12) (25) (26) that the organized fluctuations, which are large scale in nature, are of fundamental importance in the noise generation process of a high speed jet.

One interpretation of the role of organized structures has been proposed by Laufer and his co-workers (27). They contend that the interaction (pairing) of large-scale eddies as they convect downstream is a dominant mechanism in (subsonic) jet noise. No conclusive evidence of such vortex pairing has been found in either high subsonic or supersonic jets.

The alternate interpretation, which is perhaps more appropriate for supersonic jets, is that the large-scale structure, in "fully turbulent" jets is a wave-like instability of the jet. The relatively new idea is that this coherent structure belongs in the same class as the large scale instability which has been analytically predicted and measured for the transition from laminar to turbulent flow in several shear flows (21), (28) through (41).

Tam (12), Chan (13), Liu (15), and Morris (17) calculate the flow fluctuations in the jet using quasi-linear stability methods. These theories divide the flow of a jet into three categories: a time independent mean flow, a coherent fluctuation and small scale turbulence. The small scale turbulence is accounted for by using eddy viscosity-type modeling. The growth of large scale wave-like eddies or instability waves are thus analyzed in high Reynolds number fully turbulent jets by using conventional stability theory methods. (This technique has been performed in a bounded turbulent channel flow by Reynolds and Hussain (42).) The calculated large-scale structure is then used to predict the noise radiated by the jet. In this manner some of the deficiencies of the previous theories are overcome,as a calculation of the primary noise is included.

In an effort to determine the noise-producing mechanisms in both subsonic and supersonic jets, many different types of experiments have been performed. Mollo-Christensen (25) first discovered the orderly structure in a subsonic jet by using space-time correlations of the near pressure field of the jet. The experiments of Crow and Champagne (20) confirmed the presence of the latent orderly structure in the subsonic jet and showed that the orderly structure can be approximately characterized as a flow instability of the jet. Chan (14), Lau, Fisher and Fuchs (22), and Moore (43) have all furthered the investigation of the orderly structure in subsonic jets. Chan has artificially excited a subsonic jet and measured the wave properties of three different modes having azimuth wave numbers of n =0, 1, and 2. The waves were modeled by a wave theory, and a linear stability solution of a divergent shear flow was found to describe the local properties of the waves. Thus, in subsonic jets an orderly structure has been observed and measured.

It has been suggested by Tam (9) through (12), Bishop et al. (26), and others that the noise-generating fluctuations in a supersonic jet may be even more organized than in the subsonic case. They came to this conclusion by viewing Schlieren, shadowgraph and holograph visualizations (44) through (50) which show distinct wave fronts propagating away from the jet in the acoustic field.

In our laboratory (51) (52) (53) we have shown that for low Reynolds number transitional supersonic jets there are instability waves present which can be characterized by a linear stability theory for the first several diameters of flow (as depicted in Figure 1). We have also shown that this instability produces a major portion of the noise radiated by the jet. The instability waves generate sound pressure level contours

which are very close in shape and amplitude to those generated by the high Reynolds number jet. We have thus shown that it is highly probable that the noise production mechanism in the low Reynolds number and high Reynolds number jets are the same. If so, the theoretical approach taken by Tam, Liu, Morris, and Chan is appropriate.

The present study extends the work that we have previously done. The wave properties of the instability of low Reynolds number jets are measured for Mach numbers of 1.4, 2.1 and 2.5. The sound radiated by the jet is also measured. From these measurements more detailed information about the noise-producing mechanism in the jet and the noise radiated by it is obtained.

Objectives

Recognizing the rising importance of large-scale coherent structures in high speed jets, this dissertation established an experimental program with the following objectives:

1. To characterize the dominant instability waves in low Reynolds number jets by measuring their wave properties and fluctuation levels and to determine how these properties vary as the disturbances progress downstream.

2. To measure the sound field radiated by the low Reynolds number jets.

3. To determine if the dominant instability waves in the low Reynolds number jets are producing a major portion of the noise.

In a high Reynolds number fully turbulent jet exhausting to atmospheric pressure it is very difficult to make instantaneous velocity measurements since the high dynamic pressures cause delicate hot-wire

probes to break. Also, in these high Reynolds number jets the level of turbulence is so high that one cannot determine if there is a coherent structure present in the jet without using some type of conditional sampling technique. To overcome these difficulties, we have constructed an anechoic vacuum test facility for supersonic jets. By lowering the Reynolds number (by lowering the density) we are now able to measure the flow fluctuations present in the jet using hot-wire anemometry. An added advantage of studying low Reynolds number jets is that the small scale turbulence which tends to mask the coherent flow structure is decreased, making the structure's detection and characterization much easier.

The theories of Tam, Liu, Morris, and Chan place the small scale turbulence of the jet into an eddy viscosity type model. They then use conventional instability methods to analyze the large-scale structure in the jet. Therefore, one should be able to study a low Reynolds number jet which is initially laminar and undergoes transition to turbulence and compare the measurements in the jet to the theories.* If the theories are not capable of predicting the flow fluctuations and noise field of a transitional low Reynolds number jet where they are most accurate, then their chance of characterizing high Reynolds number jets is very small.

The stability theories of Tam and Liu are based upon dividing the jet into several sections along the x-axis. At each one of these sections a local linear stability analysis is performed using the mean flow

---

*In comparing the present experimental results with the predictions of the noted theories it is interesting and important to note that the relatively low Reynolds numbers of our experiments are of the same order of magnitude as the Reynolds numbers based on the eddy viscosity of the conventional high Reynolds number turbulent jets.

properties at that section. A linear stability analysis assumes a solution for the flow disturbances Q (z, r, θ, t) in the form

$$Q(x, r, \theta, t) = \hat{Q}(r)\ \mathrm{Re}\ [\exp i\ (kx - \omega t - n\theta)] \qquad (1)$$

where $\hat{Q}(r)$ is the radial dependence of the wave's amplitude, ω is the frequency of the wave, k is a complex wave number such that $k = k_r + ik_i$ where k_r is the wave number in the downstream direction and $-k_i$ is the amplification factor for exponential growth in the downstream direction, and n determines the wave's dependence on the azimuth angle. Therefore, at each downstream location where the local linear stability analysis is performed, new values for $\hat{Q}$, k, ω, and n are calculated. Since the mean flow is changing, these values are not necessarily constant. In fact, Tam (12) hypothesizes that the changing mean flow will cause the flow fluctuations to be initially unstable, then neutrally stable, and then damped as the flow progresses downstream.

We (52) have observed in a Mach number 2.3 low Reynolds number jet that the instability waves propagate downstream at supersonic velocities. These waves are therefore capable of generating Mach wave type sound emissions. However, for a Mach number 1.3 jet the wave speed in the downstream direction is subsonic, thus eliminating the possibility of Mach wave emissions. In order to determine any dependence of the instability and the sound radiated by it on Mach number, this study examined the instability waves and acoustic field of three different Mach number jets: M = 1.4, 2.1, and 2.5.

In order to meet the objectives of this study the following measurements were made at one Reynolds number for each Mach number. The selection of the Reynolds number is discussed in detail later.

1. Axial and radial distributions of the Mach number and stagnation temperature were measured to establish the mean flow field.

2. Spectra of the flow fluctuations in the jet and pressure fluctuations in the acoustic field were measured. From these spectra the frequencies, ω, of the instability waves are readily identified and the amplitude of the instability waves relative to the random flow fluctuations can be observed. In the acoustic field the contribution of the organized structures to the sound emitted by the jet are determined from the spectra. Spectra of the flow fluctuations were made at several locations to determine changes in the spectral content as the flow progressed downstream. Spectra at different locations were also made in the acoustic field to determine the variation of relative amplitude of the different spectral components of the sound emitted by the instability waves.

3. The amplitude of the instability's fluctuations were measured for two reasons. First, the growth of the amplitude of the instability's fluctuations is part of the solution of the stability analyses. Second, the instability is a major noise producer, so information about its fluctuation levels indicates regions of potential noise generation. Therefore, radial and axial surveys of the axial flow fluctuations were made using a normal hot-wire probe. Radial surveys of the RMS values of the hot-wire voltage fluctuations were made at different downstream locations. The surveys were taken for the entire spectrum of the flow fluctuations and for the dominant spectral components of the instability.

Since we have shown that the dominant instability waves can be characterized by a linear stability theory for the first several diameters of flow, the growth rate, k_i, was evaluated from these

measurements over the region of exponential growth for the dominant spectral component of the instability.

4. Sound pressure level (SPL) contours were measured in the acoustic field of the jet. These contours were determined for the entire spectrum of the noise radiated and for the major noise-producing spectral component of the instability. In this way information about the acoustic directivity of the major noise-producing component and how it influences the overall SPL contours was obtained.

Tam (12) has stated that measurements of the mean flow and of the acoustic field of a supersonic jet are needed to compare with his theoretical results. The measurements noted above furnish the needed information.

5. The wave properties of the instability in the jet were measured by artificially exciting the jet. This was accomplished by measuring the relative phase between the excitation signal and the hot-wire. The relative phase distributions in the axial, radial and azimuth directions were determined for the dominant spectral components. From these measurements the mode number, n, and the wave number, k_r, were determined. The frequency of the disturbance is known, and hence, the wavespeed of the disturbance in the downstream direction was calculated. From these measurements the manner in which the disturbance propagates down the jet axis was determined. The measurements were made as far downstream as the structure remained correlated to the exciter. Microphone phase measurements were performed to determine the wave fronts in the acoustic field. From these measurements one can determine if the sound is radiated as Mach waves and the apparent location of the major noise-producing fluctuations in the jet.

6. Tam (12) hypothesizes that the radial velocity fluctuations generate the noise radiated by the jet. In our previous experiments (51) through (53) only the axial mass velocity fluctuations have been measured. In order to measure the radial velocity fluctuations a crossed hot-wire probe was used. This probe consists of two hot-wire mounted perpendicular to each other on the probe. The probe is aligned with the flow so that both wires are 45 degrees to the mean flow. To avoid transonic difficulties, radial velocity fluctuation measurements were made only in the Mach number 2.5 jet and relationships between the magnitude of the radial and axial fluctuations were observed.

CHAPTER II

EXPERIMENTAL APPARATUS AND PROCEDURE

General Facility

This study was conducted in the Oklahoma State University free jet test facility shown schematically in Figure 2. Four different axisymmetric supersonic nozzles were used in these measurements; they were designed for Mach 2.5 with exit diameters (D) of 6.86mm and 9mm, and for Mach 2.0 and 1.5 with exit diameters of 10mm. The inviscid nozzle contours were calculated by a NASA computer program (54) based upon the method of characteristics. Then a boundary layer correction computed using the method of Rott and Crabtree (55) was added to the inviscid contour. In this manner each nozzle was designed for uniform parallel flow at the exit. The Reynolds number used in the design of each nozzle ($10{,}000 \leq Re \leq 20{,}000$) was selected to be in the mid-range of all experiments being conducted at Oklahoma State University.

The two Mach 2.5 jets were used interchangeably since both have the same nondimensional contour and were operated at the same Reynolds number. There should be no difference in the nondimensional results. This was spot checked using spectra, mean hot-wire voltage profiles and axial wavelength measurements. The nondimensional flow and acoustic properties were identical for both jets. This evidence is important in establishing that the finite test chamber has a negligible influence on the results of the measurements.

The jet is exhausted into a 114 cm x 76 cm x 71 cm vacuum chamber which is lined with a five centimeter thick layer of Scott Pyrell acoustical foam. The foam effectively produces an anechoic environment for frequencies above one kiloHertz where the reverberant pressure field is always less than 2 db in the frequency ranges studied. The air in the vacuum chamber is evacuated through a variable throat diffuser which controls the pressure in the chamber. In this manner the chamber pressure can be adjusted in order to obtain perfectly expanded jets. The ratio of the static pressure (measured 1mm upstream of the exit of the nozzle) to the chamber pressure was used to determine the pressure balance of the jet. The diffuser is connected to a 0.1 m^3/sec Kinney vacuum pump by way of a 30 cubic meter storage tank. Vibrations due to the vacuum pump are effectively damped out by the vacuum storage tank and associated piping.

Compressed air (T_o = 294°K) is supplied to the nozzles by way of an air dryer, 1.8 cubic meter storage tank, pressure regulator, throttling valve, and a stilling chamber. The air compressor is shut off during measurements to eliminate vibrations. The stilling chamber is 15 cm in diameter and consists of a 5 cm thick layer of foam, several perforated plates, a 7.6 cm long honeycomb section, and six fine screens. A cubic contraction section is used to mate the stilling section to the nozzles. There is an area ratio of at least 200:1 between the stilling section and the nozzle exit. In this manner low levels of flow fluctuations ($\tilde{m}$ < 0.5%) are obtained at the exit of the nozzles.

The test chamber is equipped with a four degree-of-freedom probe drive on which a normal hot-wire probe, a crossed hot-wire probe, a pitot pressure probe, a static pressure probe, or a microphone can be mounted.

The probe drive has three orthogonal linear directions (x, y, z) and one stage of rotation. The rotation is used to calibrate the crossed hot-wire probe.

Instrumentation

Pressure probes were connected to either a silicone oil (specific gravity of 0.93) or a mercury manometer, both of which were referenced to a vacuum of 30 microns of mercury, absolute pressure. If the pressure measured was less than 3.5 cm of mercury, the silicone oil manometer was used for better resolution. The pitot probe was a square-ended tube epoxied onto a slender brass wedge. In supersonic flow the pitot probe measures the stagnation pressure behind a normal shock. Matthews (56) calibrated this type of probe and at the Reynolds number range of this study the viscous correction was negligible. The static pressure probe was a slender cone, cylinder probe with a diameter of 0.88 mm and is shown in Figure 3 along with the pitot probe. From Behrens' (57) calibration of a static pressure probe of this design, it was determined that the viscous correction is negligible for this application. Knowing the stagnation pressure behind a normal shock and the static pressure, one is able to calculate the Mach number at the location of the measurement. The Mach numbers presented in this paper were determined in this way.

If the stagnation temperature (T_o) is known at each location as well as the Mach number, then the velocity at that location can be calculated. Therefore, the stagnation temperature was measured using a normal hot-wire. It is known that the resistance of the hot-wire (made of platinum plated tungsten) varies 0.4%/°C. Therefore, by measuring the resistance of the hot-wire, the temperature of the wire is known. In supersonic

flow the hot-wire adiabatic wire temperature (T_{aw}) is related to the local stagnation temperature by $T_o = \frac{1}{\eta} T_{aw}$. The value of η was determined by measuring T_{aw} at the exit of the jet on the centerline for a range of hot-wire Reynolds numbers. The stagnation temperature in the stilling chamber ($T_{o\infty}$) was also measured. By assuming constant stagnation temperature along the centerline of the nozzle flow a value for η was calculated. This value of η was then used to calculate the local stagnation temperature in the jet. Changes in η with local Reynolds number of the flow over the hot-wire did not significantly affect the T_o estimates.

The normal hot-wires used in this study were Disa 55A53 subminiature hot-wire probes epoxied to brass wedges similar to the pitot probe wedge. For some probes the prongs were separated further apart, from 0.45 mm to about 1.5 mm, in order to reduce conduction end losses; however, this tends to reduce the frequency response of the wire. Normally a frequency response of 40 kHz or more was obtained when using a Disa 55M01 main frame with a Disa 55M10 constant temperature anemometer bridge. The output of the Disa 55M01 was measured using a Hickok model DP100 DC voltmeter and a Hewlett Packard 3400A RMS voltmeter.

The crossed hot-wire probes used in this study were made from round jewelers broaches, thermocouple ceramic insulators with four holes and 5 micron platinum-plated tungsten wire. These probes were operated with two Disa 55D05 constant temperature anemometers. There is a problem with limited frequency response encountered when using the 55D05 anemometers. This problem is discussed in Appendix B. Hot-wire voltage fluctuations were decomposed into axial mass velocity fluctuations, total temperature fluctuations, and radial velocity fluctuations, using

a technique similar to Rose's (58) (59) shown in Appendix B. By using this technique it is possible to simultaneously measure the instantaneous axial mass velocity fluctuations and the radial velocity fluctuations for the crossed wire probe. This data reduction technique for hot-wire anemometry in supersonic flow is valid where the Mach number of the flow normal to the wire is above 1.2. For a crossed hot-wire probe both wires are inclined to the mean flow at 45 degrees; thus, if measurements are being performed in the shear layer, the Mach number normal to the wire would definitely be below 1.2 for the Mach 1.5 and 2.0 jets. Therefore, the crossed hot-wire measurements were made only in the Mach number 2.5 jet.

Figure 4 shows the size of the crossed hot-wire probe relative to the 9 mm Mach number 2.5 jet. The distance between the probe supports perpendicular to the flow is 1.5 mm (the same as the remanufactured normal wire).

A Bruel and Kjaer 1/8 inch diameter type 4138 condenser microphone was used to measure the noise radiated by the jet. This microphone has omni-directional response within ± 3 db for frequencies up to 60 kHz. The microphone signal was high pass filtered at 3 kHz in order to eliminate the signal resulting from the test chamber resonance ($\approx$ 500 Hz). For consistency the hot-wire signal was also high pass filtered at 3 kHz. The signals were low pass filtered at either 60 or 40 kHz depending on the jet and the frequency response of the hot-wire. This also eliminated the signal due to the resonance of the microphone (100 kHz). These were determined to be acceptable band pass filter settings since all of the organized flow structure and the majority of the noise radiated by the jets had frequencies between 10 kHz and 30 kHz. A

Multimetrics model AF 120 active filter was used to band pass filter both the hot-wire and microphone signals.

Spectra of both the hot-wire and mcirophone were made using a Tektronix 7L5 Spectrum analyzer connected to a Hewlett Packard 135A X-Y plotter. A constant bandwidth of 1 kHz was used to generate all spectra. The frequencies in this study are presented in terms of the Strouhal number, fd/U, where U is the exit velocity of the jet and d is the effective diameter (exit diameter, D, minus twice the displacement thickness of the jet). The Tektronix Spectrum analyzer was also used as a narrow (1 kHz and 3 kHz) band pass filter in order to study individual spectral components.

The probe drive system is equipped with precision ten turn potentiometers which provide DC voltages proportional to the location of the probe. It was therefore possible to make mean hot-wire voltage profiles using the X-Y plotter. Similarly, profiles of the wide band (3-40 kHz) hot-wire voltage fluctuations are obtained by band pass filtering the hot-wire signal with the Multimetrics active filter, then using a Ballentine 710A Linear AC to DC converter to convert the fluctuating hot-wire voltage to a DC voltage. To obtain profiles of individual spectral components the Tektronix spectrum analyzer was used instead of the Ballentine AC to DC converter.

Artificial Excitation Mechanism

The jet was artificially excited in order to measure the orientation, wave speed, and wave length of the dominant spectral components of the flow fluctuations as well as the wave fronts in the acoustic field. The phase difference between the glow exciter input signal and the probe

(hot-wire or microphone) were measured in order to accomplish this. The method used to excite the jet in this study was similar to the technique used by Kendall (34). It consists of establishing an oscillating glow discharge at the exit of the jet. The oscillating glow is established by applying a 135 volt peak to peak alternating voltage biased to a negative potential of 415 volts DC to a 2% thoriated tungsten electrode at the exit of the jet. The frequency of the alternating voltage can be varied (using a signal generator). In this manner the jet is excited at one point. The electrode is 1/16 inch in diameter and is insulated from the nozzle (ground) by a ceramic tube. A current of 0.2 ma. DC was found to have established a glow of sufficient strength to cause the instability process to "lock" onto the exciter (the relative phase between the exciter and probe signal remains constant at one location of the probe) and yet not drastically alter the flow field or the acoustic field. The effects of artificial excitation are discussed more thoroughly in Appendix A.

The relative phase between the exciter and the probe was measured using a Saicor model SAI 43A correlation and probability analyzer by cross correlating the two signals. The Saicor correlator was also operated in the enhance mode in order to phase average* both hot-wire and microphone signals. In this manner the coherent structure can be extracted from the full signal and a measurement of the percent coherent structure present compared to the full wave was made. In addition, the

---

*The phase averaged signal is

$$q(t) = \lim_{N\to\infty} \frac{1}{N} \sum_{n=0}^{N} q(t + n\tau)$$

where τ is the period of the coherent structure in the jet.

waveform of the coherent structure was obtained and spectrum analyzed. This was done for both the microphone and hot-wire signals.

CHAPTER III

REYNOLDS NUMBER SELECTION

For several measurements made in this study the Reynolds number was varied over a moderate range. However, the majority of the measurements were made at one Reynolds number for each jet. The criteria used in the selection of the Reynolds number at which to operate the jets were as follows:

1. To maximize the amount of identifiable flow instability with respect to the turbulence, and to minimize the value of the eddy viscosity term used in the theories of Tam (12), Chan (13), Liu (15), and Morris (17). This makes the identification and characterization of the instability much easier.

2. To maximize the noise radiated by the organized structure with respect to the random sound generated.

In order to meet the criteria and establish the desired Reynolds number, microphone and hot-wire spectra were first made at different Reynolds numbers. Figures 5 through 7 show microphone and hot-wire spectra for the Mach 2.1 jet at three different Reynolds numbers. At a Reynolds number of 4,900 the flow fluctuation spectrum contains a peak at a Strouhal number of 0.22. However, the microphone spectrum does not contain a discrete peak at any frequency. When the Reynolds number is increased to 7,900 the flow again contains a peak at St = 0.22. However, there is now a discrete peak in the microphone spectrum at the same

Strouhal number, indicating that at this Reynolds number the instability in the jet is generating noise. With a further increase in Reynolds number to 11,750 the flow fluctuations show an increase in the amount of broadband fluctuations relative to the amplitude of the peak at St = 0.22. The microphone spectrum also no longer possesses a large discrete peak at St = 0.22. Therefore, this Reynolds number is higher than what the criteria specifies while the Reynolds number of 4,900 is too low. Consequently, the jet was operated at a Reynolds number of 7,900 where the Reynolds number criteria were best satisfied.

Following the same procedure, Reynolds numbers of 8,700 and 3,700 for the Mach 2.5 and 1.4 jets, respectively, were determined to satisfy the criteria. It was observed in all three jets that the frequencies of the discrete peaks did not significantly change as the Reynolds number was varied, only their amplitude relative to the other spectral components. Table I contains the test conditions and the constants used to nondimensionalize the results obtained in this study.

CHAPTER IV

FLOW MEASUREMENTS, MACH NUMBER 2.5 JET

The Mach number 2.5 jet was studied more extensively than the Mach number 1.4 and 2.1 jets and therefore the results of its measurements will be presented first. Measurements made in the Mach number 1.4 and 2.1 jets will then be presented and a comparison of the results will be made with the results from all three jets.

Mean Flow, Mach Number 2.5 Jet

Pitot pressure, static pressure and stagnation temperature measurements were made along the centerline of a Mach number 2.5 jet. Radial profiles of these quantities were also made at different downstream locations. The local Mach number was calculated from the ratio of the static pressure to the pitot pressure. Figure 8 shows the axial variation of the Mach number along the centerline of the jet. From this information it was determined that the average Mach number for the first ten diameters of the flow is 2.48 with a variation of $\pm$1.6%. This slight variation of Mach number along the centerline of the jet can be attributed to two factors. First, the jet is not operated at the design Reynolds number because the exact Reynolds number could not be determined until the nozzle had been constructed and tested. Therefore, an estimation of the proper Reynolds number was made in order to design and construct the nozzle. A design Reynolds number of 20,000 was used, but testing showed

that the jet should be operated at a Reynolds number of 8,700. This change in Reynolds number affects the boundary layer thickness. Thus, the boundary layer correction added to the inviscid contour is slightly off. Therefore, the flow at the exit of the nozzle will not be parallel, causing a system of weak expansion and compression waves (cell structure) to be present. This cell structure causes the variation in Mach number along the centerline of the jet. The second factor which can contribute to this Mach number variation along the centerline of the jet is that all of the jets used in this study were operated in a slightly underexpanded condition; that is, the ratio of the nozzle exit pressure to the pressure of the test chamber was held between 1.00 and 1.01. The slightly underexpanded pressure balance was used since more accurate control can be maintained over the operating condition of the jets. Underexpansion of a jet can generate a system of expansion and compression waves. However, measurements using a normal hot-wire have indicated that as long as the pressure balance is held between 0.98 and 1.02 there is no noticeable change in the strength of the cell structure.

Radial profiles of the Mach number are shown in Figure 9 for different downstream locations. At x/D = 1 the flow has a top hat profile with a very thin shear layer. At 15 diameters downstream the shear layers have grown together, indicating the end of the potential core. This is also the axial location where the centerline Mach number begins to decrease.

The axial variation of the local stagnation temperature, T_0, nondimensionalized by the stagnation temperature in the stilling chamber, $T_{0\infty}$, is shown in Figure 10. T_0 remains equal to $T_{0\infty}$ along the centerline

back to x/D = 15. This is the same axial location where the centerline Mach number begins to decrease in value and where the shear layer of the jet grows together on the centerline.

The value of T_0 along the centerline of the jet then approaches the value of T_0 outside the jet as the probe moves downstream. Radial profiles of $T_0/T_{0\infty}$ are shown in Figure 11. The local stagnation temperature is equal to $T_{0\infty}$ in the potential core of the jet, varies in the shear layer and finally approaches the value of the stagnation temperature in the test chamber. The same type of temperature profiles were measured in a supersonic wake by McLaughlin et al. (60). However, the jet shows less variation than the wake.

Spectra of Flow Fluctuations and Radiated Noise, Mach Number 2.5 Jet

Figure 12 is a far field microphone spectrum taken in a naturally excited jet at a Reynolds number of 8,700. There is a rather broad peak centered at a Strouhal number of 0.16. However, this spectrum does not have near the breadth that is found in higher Reynolds number jets (50). Figure 13 consists of normal hot-wire spectra taken at the radial location of maximum fluctuations at axial positions of 1, 5, 10, 15, and 19 diameters. This figure indicates that there is a band of unstable frequencies present in the Mach number 2.5 jet. However, the most prevalent spectral component is the Strouhal number 0.16 one. We have previously seen similar spectral characteristics in a Mach number 2.2 jet (52).

As the flow progresses downstream different frequencies become dominant in the spectra. However, the St = 0.16 spectral component is the only one producing a discrete peak from x/D = 1 to 19. At x/D = 15 the

spectrum shows that the amplitude of the St = 0.14 component is larger than the St = 0.16 component. However, closer to the centerline of the jet where the overall fluctuation level is slightly less, the St = 0.16 component's amplitude is larger. This indicates that the spectral components have different radial dependence (the radial dependence will be examined in detail later).

The longevity of the St = 0.16 spectral component in the flow field explains why it dominates the acoustic spectrum in Figure 12 and the growth and decay of the components around it account for the broad peak about the base.

Effect of Excitation on Spectra, Mach Number 2.5 Jet

In the following phases of this study extensive measurements were made to determine the wave properties of the St = 0.16 component and its acoustic radiation. The St = 0.16 component was selected because of its longevity in the flow field and larger contribution to the acoustic field than the other components. Measurements were made to show that the other components present in the jet possess wave properties similar to the St = 0.16 one and that studying the St = 0.16 component is representative of the band of unstable frequencies.

We chose to artificially excite the jet in order to measure the wave properties of the jet and its acoustic field. The alternate method available was the placing of an additional hot-wire probe into the flow. Then the wave properties could be determined by cross-correlating this hot-wire with either the microphone or another hot-wire. It was decided that the presence of the additional hot-wire would alter the flow and

acoustic fields more than the low amplitude artificial excitation used in our experiments. The level of excitation used in this study is low compared to that used by Crow and Champagne (20), Chan (14), and Hussain (61) in subsonic jets. C. J. Moore (43) has shown that large excitation levels can substantially change the flow field in a subsonic jet. Appendix A (which discusses the effect of excitation on the jets used in this study) shows that a supersonic jet can also be altered by large levels of excitation. However, the excitation levels used in this study are low and do not significantly alter the flow (as shown in Appendix A).

Hot-wire spectra made at x/D = 1, 5, 10, 15, and 19 are shown in Figure 14 for the Mach number 2.5 jet excited at St = 0.16. At x/D = 1 the spectrum shows three dominant peaks at St = 0.16, 0.32, and 0.48. The harmonics (0.32 and 0.48) are present because the glow exciter inputs a pulse into the flow occurring at the fundamental frequency. The Fourier decomposition of the exciter signal contains not only the fundamental frequency but its harmonics as well. The St = 0.09 mode is still present at x/D = 1 but at a reduced level. The excitation suppresses this mode, which has a comparatively low growth rate. As the flow progresses, the fundamental mode (St = 0.16) grows in amplitude faster than the harmonics indicating that it is more unstable. At x/D = 10 and x/D = 15 the excited spectrum shows the fundamental frequency still dominating the flow and the first and second harmonics are beginning to increase in amplitude. The excitation causes the jet to "lock" onto the St = 0.16 component (and its harmonics) and the St = 0.13 and St = 0.14 components, which were present in the unexcited jet, do not appear in the excited jet. At x/D = 19 (Figure 14(e)) the random fluctuations have increased significantly and are beginning to obscure the organized

structure. However, the St = 0.16 component remains more dominant in this jet in comparison to the natural jet. This occurs because the instability of the excited jet has consisted mainly of the St = 0.16 component. Thus the fluctuations are more coherent in the excited jet and the randomizing process of several other spectral components growing and decaying along with the St = 0.16 components not present.

The main effect of exciting the jet has been the suppression of other spectral components found in the natural jet and the increased presence of harmonics. When unstable components other than the one at St = 0.16 were excited, the jet amplified only the component being excited. Figures 15 and 16 show hot-wire spectra at x/D = 10 and 15 when the jet was excited at St = 0.14 and 0.18. In both cases the flow is dominated by the excited component and the St = 0.16 component is almost completely absent. This behavior indicates that the jet is unstable to several different frequencies. However, if any one spectral component possesses an initial level of fluctuation larger than the others, the jet will amplify that component in preference to the others.

When the jet is not excited, there are only small amplitude random fluctuations present at the exit of the nozzle. The behavior of the jet observed above indicates that the components present in the jet may vary with time as the fluctuations at the exit of the nozzle vary. This phenomenon has been observed in spectra made with a fast sweep rate (analyzing time). In these spectra, the amplitude of the St = 0.16 component may vary by a factor of 3 while other spectral components appear and disappear with consecutive sweeps of the analyzer. The spectra presented in this study were made using a much slower sweep rate (1 kHz/sec) and are thus indicative of the spectral content present over a long time

average. It is therefore apparent that in order to reliably measure the wave properties of the different spectral components, the excitation method should be used. In this manner the jet is stabilized onto one spectral component and its properties can be determined with reasonable accuracy.

We observed the same multi-frequency phenomenon discussed above in our earlier studies (51) (52) (53). At that time we referred to the instability as being multimodal based upon the multimodal instabilities experienced by Kendall (34), Mack (62), and McLaughlin (38) (41). However, measurements presented later in this chapter show that the wave properties of the spectral components in the St = 0.14 to 0.18 band are all similar. This indicates that the instability is comprised primarily of one mode which contains a band of spectral components. The higher harmonics such as the St = 0.32 and 0.48 components in the Mach number 2.5 jet should probably be classified as different modes based upon the measurements in an axisymmetric supersonic wake by McLaughlin (38) (41).

Phase Averaged Hot-Wire Signal, Mach Number 2.5 Jets

The hot-wire signal was phase averaged in the excited jet experiments using the Saicor Correlator. The time trace of the phase averaged signal was plotted and spectrum analyzed. Figure 17 shows the results at x/D = 15. As it must be the wave form is dominated by the St = 0.16 component and its harmonics, and is representative of the phase averaged signal measured at jet locations as far downstream as x/D = 19.

The RMS value of the phase averaged signal was obtained for the hot-wire voltage fluctuations at three axial positions. This quantity was

then divided by the RMS value of the hot-wire fluctuations contained in the frequency band from 3 kHz to 60 kHz.* In this way the fraction of the flow fluctuations due to the organized structure was obtained. For x/D = 10, 15 and 19 the fraction is equal to 0.90, 0.84, and 0.40, respectively. These fractions along with the previous spectra of the flow fluctuations show that the flow is very organized for x/D less than or equal to 15. Beyond the end of the potential core (x/D = 15) the centerline mean velocity begins to decay more rapidly and the flow fluctuations become less coherent.

Growth of Axial Flow Fluctuations, Mach Number 2.5 Jet

Normal hot-wires were used to measure the axial mass velocity fluctuations (normalized by the local mean mass velocity) $\tilde{m} = (\rho u)'_{rms}/\bar{\rho}\bar{u}$. Figure 18 shows the change in amplitude of $\tilde{m}$ as a function of axial position for the unexcited jet. This figure contains data from three different experiments and is shown to be fairly repeatable from day to day. The measurements were made at the radial location of maximum hot-wire voltage fluctuations. The hot-wire signal was band pass filtered from 3 kHz to 60 kHz (St = 0.03 to 0.64) and hence contains the full spectrum of flow fluctuations. The initial level of fluctuations is less than 0.5% and grows in amplitude approximately exponentially for the first 12 diameters of flow, as shown by the straight line on the semi log plot.

---

*The 3 kHz to 60 kHz frequency band corresponds to a range of nondimensional frequency from St = 0.03 to St = 0.64. From the spectra presented it is reasonable to assume that in the low Reynolds number jets the frequency range from 3 kHz to 60 kHz contains all the fluctuations of importance in the jet.

The growth of the fluctuations can be characterized by a linear stability type representation for the first 12 diameters of flow with a value of growth rate ($-k_i d$) calculated to be 0.29 ± 0.05 (95% confidence interval).

The level of fluctuations saturates at about 30% of the local mean and then begins to decay. The fluctuation amplitude saturates near the axial location of the end of the potential core. Tam's theory (12) predicts that for a Mach 2.2 jet the energy in the flow fluctuations will reach a maximum at the end of the potential core and then begin to decrease. The kinetic energy flux of the axial velocity fluctuations was estimated using mean flow profiles and hot-wire voltage fluctuation level profiles to evaluate the following integral.

$$E_{KE} = \frac{1}{\rho_o U^3} \int_o^\infty \frac{1}{2} \bar{\rho}\, \bar{u}\, (u')^2\, r dr \qquad (2)$$

This integral is the major portion of one of the primary outputs of Tam's stability theory (12). The axial distribution of E_{KE} is shown in Figure 19 for the natural jet. The distribution is very similar to the $\tilde{m}$ distribution shown earlier in Figure 18. The amplitude of E_{KE} maximizes near the end of the potential core and grows exponentially for the first 11 diameters of flow. The growth rate of E_{KE} is 0.72 ± 0.26 which is twice the growth rate of $\tilde{m}$ (within the uncertainty of the measurements). This result verifies one of the assumptions used by Tam in his analysis.

In order to better understand the frequency dependence of the instability the following measurements were made. The hot-wire was placed at x/D = 10, a point in the region of exponential growth where $\tilde{m}$ is large. The jet was then artificially excited at different frequencies while maintaining a constant input level of excitation. The response of the jet was measured by recording the level of fluctuations in a 1 kHz

($\Delta St = 0.01$) wide band centered on the frequency of excitation. The probe was moved radially at x/D = 10 to find and record the level of maximum fluctuations corresponding to each excitation frequency. The results of this experiment, contained in Figure 20, shows that there are several unstable frequencies contained in the frequency band from St = 0.10 to St = 0.20.

The effects of exciting the jet at three of the frequencies shown to be unstable in Figure 20 (St = 0.14, 0.16, and 0.18) are shown in Figure 21. Presented in this figure are the axial distribution of the full spectrum (St = 0.03 to 0.64) of the mass velocity fluctuations, $\tilde{m}$, in the natural jet and the jet excited at the three unstable frequencies. (The probe is located at the radial position of maximum hot-wire fluctuation voltage.) The data show that exciting the jet at different unstable frequencies does not alter the development of the overall flow fluctuations amplitude, just the spectral content.

Figure 20 shows that there were six spectral components present in the jet that attained large levels of fluctuation at x/D = 10. However, only a few of them appeared in the natural jet (as shown by spectra). The following experiment was made to determine the reason. The jet was excited at seven frequencies, one at a time: the six most unstable ones and one not as unstable. The axial distribution of the flow fluctuation amplitude contained in a 1 kHz wide band ($\Delta St = 0.01$) centered at the frequency of excitation was measured and is shown in Figure 22. The probe was located at the radial position of maximum fluctuations contained in the 1 kHz wide band.

The data of Figure 22 shows why only the St = 0.14 and 0.16 spectral components dominate the flow fluctuations in the unexcited jet.

The other components have higher rates of growth over a portion of the jet than do the St = 0.16 and 0.14 components. However, they do not maintain as high a level of fluctuation over the length of the jet. This indicates that the St = 0.14 and 0.16 components are unstable to a wider range of mean flow profiles than the others. Also, the St = 0.14 and 0.16 components possess levels of fluctuation at four diameters downstream from the exit of the jet that are twice as large as the levels of fluctuation possessed by the other frequencies. This shows that the top hat profile close to the exit of the nozzle is more unstable to the St = 0.14 and 0.16 components than to the other frequencies. Thus, the jet locks onto these two components and they dominate the flow in the unexcited jet. Therefore, an important factor in the frequency selection mechanism of the jet is the component's growth rate relative to a range of varying mean flow profiles. The components that are most unstable at the exit of the jet and that remain unstable for a wide range of mean flow profiles will be the ones that dominate the natural flow.

By observing the relative amplitude of the different spectral components shown in Figure 22 at various axial locations, it becomes apparent that at different axial locations the frequencies of the most unstable components may change from those shown in Figure 20. The changing mean flow may be responsible for this type of behavior. Thus, there does not seem to be just a few discrete frequencies that are unstable in the jet but a band of frequencies between St = 0.10 and 0.20.

From the above measurements it was shown that the jet responds about equally to excitation at St = 0.14 and 0.16. The St = 0.16 component is present in the unexcited jet from x/D = 1 to 19. However, the

St = 0.14 component is dominant at only one location (as shown by spectra). This indicates that the St = 0.16 component is preferred by the jet and therefore will be studied more extensively than the other spectral components in the remainder of the Mach 2.5 study.

Figure 23 contains axial growth measurements for the Mach 2.5 jet excited at St = 0.16. The full spectrum (St = 0.03 to 0.64), the St = 0.16 component (St = 0.155 to 0.165 band pass), the St = 0.32 component (St = 0.305 to 0.335 band pass), and the phase averaged components are shown. The full spectrum, the phase averaged component and the St = 0.16 component all grow exponentially at approximately the same rate for the first 12 diameters of flow and saturate in amplitude around x/D = 15. The growth of the St = 0.32 harmonic is delayed and begins to grow exponentially at x/D = 5 and continues to x/D = 14. Table II contains a summary of the values for the growth rates, $-k_i d$, along with the 95% confidence interval for each one. As would be expected, the growth rates of the full spectrum, the phase averaged component and the St = 0.16 component all have the same value within the confidence intervals since all three are comprised mainly of the St = 0.16 component over the region of exponential growth. The first harmonic (St = 0.32) component grows at a slower rate than the others.

The growth of the harmonic does not indicate a deviation from a linear stability representation since the fundamental and the harmonic both grow exponentially from x/D = 5 to 12. This occurs in both the excited and unexcited jets and hence it is not the excitation which causes the growth of the harmonic.

Growth of the Radial Velocity Fluctuations, Mach Number 2.5 Jet

Measurements of the radial velocity fluctuations were made in the Mach 2.5 jet excited at St = 0.18 using a crossed hot-wire probe. Recall from Figure 21 that the exact frequency of excitation in the St = 0.14 to 0.18 band in unimportant. The crossed hot-wire probe measures both axial and radial velocity fluctuations. The data reduction techniques are discussed in Appendix B. Due to the limited frequency response of the crossed wire probes, this data should be considered preliminary and is presented only to give the reader some insight into the general nature of the radial velocity fluctuations.

Figure 24 shows the growth of the axial and radial fluctuations as measured by two different crossed hot-wire probes and the axial mass velocity fluctuations as measured by a normal hot-wire. The axial mass velocity fluctuations as measured by the crossed hot-wire probe grow exponentially for the first 11 diameters of flow at a growth rate, $-k_i d$, of 0.29 $\pm$0.07. The corresponding normal wire measurements indicate a growth rate of 0.30 $\pm$0.05 when the jet is excited at St = 0.18. Thus, within the uncertainty of the measurements the rate of growth for the axial mass velocity fluctuations is the same as measured by both the normal hot-wire and the crossed hot-wire.

The radial velocity fluctuations (normalized with the local mean velocity) grow exponentially from x/D = 4 to 16. The rate of growth over this axial region is 0.17 $\pm$0.01 (substantially lower than the axial mass velocity fluctuation growth rate). At x/D = 15 the axial mass velocity flucutations attain a maximum amplitude of 0.30 while the radial velocity fluctuations attain a maximum amplitude of 0.16. By assuming negligible pressure fluctuations compared to the velocity, density and temperature fluctuations (a common assumption made by previous

investigators (63) through (68)), an estimation of the maximum axial velocity fluctuations is found to be $\tilde{u} = 0.21$. Comparisons of the peak velocity fluctuations (both radial and axial components) with other investigators are made later in Chapter VII.

Figure 25 contains spectra of the radial velocity fluctuations in the Mach 2.5 jet excited at St = 0.18. These spectra were made from the crossed hot-wire probe located at x/D = 5, 10 and 15. These spectra contain the same overall characteristics as do the axial flow fluctuations. As expected, the instability is a major portion of both the axial and radial flow fluctuations.

Radial Distributions of Hot-Wire Fluctuation Measurements, Mach Number 2.5 Jet

Profiles of the hot-wire voltage fluctuation amplitude were made in the Mach number 2.5 jet excited at St = 0.16 to determine the radial distribution of the full spectrum (St = 0.03 to 0.64), St = 0.16, component (ΔSt = 0.01) and phase averaged component. Profiles of the mean hot-wire voltage were also made. The profiles of the mean hot-wire voltage (Figure 26) can be used to obtain a qualitative measurement of how the mean flow of the jet is changing as it progresses downstream. As shown in Appendix B, for high overheat ratios the hot-wire responds primarily to mass velocity (ρu) and can be interpreted in this way. However, it should be noted that the hot-wire mean voltage profiles bear a strong resemblance to the Mach number profiles (see Figures 9 and 26). The mean hot-wire voltage profiles show that the potential core ends at about x/D = 15 and that the mean flow decays rapidly after that.

Profiles of the full spectrum in Figure 27 show the spreading of the high fluctuation region as the flow moves downstream with the maximum

fluctuations occurring at about the center of the shear layer (point of inflection in the man flow profile) which is common with free shear flows. The profiles also indicate that the end of the potential core is around x/D = 15. The radial profiles of the St = 0.16 component in Figure 28 show the same axial development as the full spectrum except at x/D = 15.7, where the profile peaks on the centerline instead of on the sides. The fluctuations of the +z side of the jet are larger in amplitude from x/D = 8.8 to 17.1. The reason for this asymmetric condition is puzzling since close to the exit of the jet (x/D < 7.1) the profiles show the same amplitude on either side of the jet. The asymmetry is not caused by the excitation of the jet since it is present in the unexcited jet also. The asymmetry is probably due to probe interference (the probe being slightly yawed in one direction), the machining of the nozzle, or a slight asymmetry in the exciter electrode near the exit of the nozzle.

The radial profiles of the phase averaged hot-wire voltage shown in Figure 29 develop the same as the St = .16 profiles. At x/D = 15.7 the profile has a distinct peak on the centerline of the jet. This shows that there is an increase in the level of organized fluctuations on the centerline of the jet when the shear layers grow together. The centerline fluctuations then subside at x/D = 17.1 into the profiles previously seen. At x/D = 20 almost all of the organized structure has disappeared. These measurements demonstrate that there is a violent organized interaction occurring on the centerline of the jet when the shear layers grow together which climaxes the growth of the fluctuations in the jet.

Experiments were also performed to investigate the radial amplitude distributions of the numerous spectral components which were discussed

in the axial growth rate section earlier. Figure 30 shows the radial distribution of the flow fluctuation amplitude in the natural Mach number 2.5 jet which are contained in a 1 kHz wide band ($\Delta St = 0.01$). At x/D = 10 the 1 kHz wide band is centered at St = 0.13 and 0.16. At x/D = 15 the 1 kHz wide band is centered at St 0.13, 0.14, 0.16, and 0.18. A 3 kHz wide band ($\Delta St = 0.03$) was also centered at St = 0.32 for both axial locations. An Ampex FR1300 tape recorder was used to record the flow fluctuations contained between 3 and 60 kHz measured by the hot-wire for one traverse through the shear layer of the jet. The recording was then replayed for each Strouhal number. In this manner the radial profiles of the amplitude of the different spectral components existing simultaneously in the unexcited jet were obtained. At x/D = 10 the St = 0.13 and 0.16 components attain levels of maximum fluctuations at different radial locations. The same trend is apparent at x/D = 15 for the five spectral components measured there. The radial distributions of the different spectral components display the dependence which has been found typical of other shear flow instabilities where more than one mode is present (37) (38) (41).

Relative Phase Measurements, Mach Number 2.5 Jet

The wavelength and wave orientation of the instability were determined by measuring the relative phase, ϕ, between the normal hot-wire and the excitation input signal. In this manner the axial wave number, k_r, and the azimuthal mode number, n, were determined for the St = 0.14, 0.16, and 0.18 components. The radial distribution of the relative phase was measured for the St = 0.16 component.

Figure 31 shows the axial distribution of the relative phase for the three spectral components mentioned above. Each measurement was made at the radial position of maximum fluctuations. Two different days' measurements are shown for the St = 0.16 component to demonstrate the repeatability of the technique. A first order linear regression curve fit was used to determine the wavelength and hence the wave number of the components. These results are presented in Table III. The phase distribution for each component fits a straight line for the entire region of the jet where the measurements were made. Beyond x/D = 20 the random flow fluctuations are so large in amplitude relative to the organized structure that it is impossible to reliably measure the relative phase with the correlation technique described. Thus the wavelengths of the disturbance remain constant for at least 12 diameters of the jet (x/D = 6 to 18). Since the wavelength and frequency of the disturbances are known, then the speed at which they travel downstream, c, can be calculated ($c = \lambda f$). The calculated value of c is also presented in Table III. All three spectral components are traveling downstream supersonically at about 68% of the exit velocity, and 112% of the ambient acoustic velocity, a_o.

Axial phase measurements of the radial velocity fluctuations and the axial mass velocity fluctuations were made for the St = 0.18 component using a crossed hot-wire probe positioned at $\theta = 270°$ (the previous measurements were made at $\theta = 180°$). From the relative phase distributions shown in Figure 32 it was determined that the axial and radial fluctuations are in phase. The wavelengths calculated from these measurements are 4.04 $\pm$.84 for the axial fluctuations and 3.77 $\pm$.61 for the radial fluctuations. Both of these fall within the 95% confidence

interval of each other and of the normal hot-wire measurements of the St = 0.18 axial component's mass velocity fluctuation wavelength. Morris (17) (69) analytically predicts that the axial and radial fluctuations will be in phase near the point of maximum fluctuations for an n = 1, St = 0.3 instability in a Mach number 1.4 isothermal jet. The same type of phase behavior was experimentally measured in a two-dimensional, incompressible shear layer by Browand and Weidman (23).

Figures 33 and 34 contain relative phase measurements made with the normal hot-wire in the radial and azimuthal directions at x/D = 8 for the St = 0.16 component. (The azimuthal measurements were made at the radial location of maximum fluctuations in the shear layer.) The radial phase measurements show that there is a rapid change in phase across each shear layer. (It is noteworthy that Winant and Browand (21) observed a 180° phase shift across a two-dimensional, incompressible free shear layer.) These measurements also indicate that the phase distribution is symmetrical about the vertical (y) axis of the jet but has a 180° phase shift across the horizontal (z) axis.

This symmetry and asymmetry together with the azimuthal phase distribution is consistent with an instability mode where the jet is flapping up and down. The flapping mode results from a superposition of two helical modes $e^{i(kx+\theta)}$ and $e^{i(kx-\theta)}$, which are often referred to as the n =)1 and n = -1 modes (see Equation (1)). The theoretical azimuthal phase distribution for the flapping mode is shown in Figure 34. The data show a smoother 180° phase shift at the θ = 90°, 270° points than the theoretical distribution.

One factor which influences the data and may cause the less rapid phase shift is that a normal hot-wire (wire oriented vertically) was

used to make the measurements. At the sides of the jet (90° and 270°) the hot-wire is aligned with the shear layer so as to measure the phase at that exact radial location making its phase very sensitive to the position of the probe due to the rapid variation of phase in the radial direction. However, at θ = 0° and 180° the hot-wire is perpendicular to the shear layer making the measurements less sensitive to the radial location. Yet another factor to consider is that the jet may not oscillate in the same plane continuously. The plane may vary slightly in the azimuth angle. These effects would cause the ideal phase distribution to be spread out and the sharp discontinuity to become more gradual.

At x/D = 12 the same radial dependence of the phase is present as indicated by Figure 35. The radial variation still changes approximately 180° across the shear layer but it occurs less rapidly since the shear layer has broadened. Again, the azimuthal phase distribution (Figure 36) is smoother than the ideal one but still representative of the flapping mode.

At x/D = 16 the radial phase variations have become less rapid, as would be expected, since the shear layers have grown together and become wider (see Figure 37). The azimuth distribution in Figure 38 has changed in a quite unexpected manner based upon the previous measurements. The disturbance has become a helix with an n = -1 mode number. It is evident that the jet undergoes a transition at approximately the end of the potential core where the flow fluctuations are at a maximum. In fact, this transition from a flapping mode into a helix is no doubt associated with the large level of fluctuations. It should be noted that the level of coherent structure decreases rapidly during and after the transition.

Measurements of the azimuth phase distributions for the St = 0.14 and 0.18 components were also made. Both of these components possess a flapping mode at x/D = 12. At x/D = 16 the St = 0.18 component has transformed into a helix (n = -1). However, the St = 0.14 component does not transform into a helix until x/D = 18. Again, the level of coherent structure decreases rapidly at this point. These measurements along with the axial phase measurements indicate that all of the spectral components are initially a flapping mode that transforms into a helix at a location near the end of the potential core. The waves all travel dwonstream at approximately 68% of the mean exit velocity of the jet. Tam (9) through (12), Liu (15), and Chan (13) all predict that the n = 1 mode is the most unstable for a supersonic jet and that it is this mode (or the superposition of n = 1 and n = -1) that is present in this Mach 2.5 jet.

The artificial exciter inputs a point excitation at $\theta = 0°$. The azimuth phase measurements show that the jet is flapping up and down in the plane that passes through $\theta = 0°$. This indicates that the exciter is exciting the n = +1 and -1 modes simultaneously. The theoretical developments for the jet's instability (9) (13) (15) show no preference for a left hand or right hand helix. Both are equally unstable. Therefore, the instability in the natural jet may be any combination of these modes. Measurements have shown that the frequency, growth rate and sound radiated by the jet (presented later) are the same for the natural and excited jet. In addition, in the excited jet the wavelength remained constant whether the instability was in the flapping mode or a helix. It is therefore apparent that the instability process is very similar for all the modes (whether the jet is flapping, n = +1 or n = -1). Thus, the

measurements of the instability present in the excited jet is representative of the one occurring in the natural jet.

CHAPTER V

ACOUSTIC MEASUREMENTS, MACH NUMBER 2.5 JET

Microphone SPL Contours, Mach Number 2.5 Jet

Figure 39(a) contains sound pressure level (SPL) contours of the full spectrum (St = 0.03-0.64) for an unexcited jet. Since these measurements have been made in a vacuum chamber, the reference pressure used to calculate the SPL was scaled to the ambient pressure in the test facility in the following manner:

$$SPL = 20 \log_{10} \frac{P'_{rms}}{(2\times10^{-5}\ Nt/m^2)\ (P_c/P_{ATm})} \qquad (1)$$

The sound pressure levels occurring in this jet have about the same magnitude as found in high Reynolds number atmosphere model jets at a similar position. This was shown in one of our earlier papers (53). The acoustic field is highly directional in its radiation pattern which is characteristic of supersonic jets and has been seen by other investigators (50) (69) (70).

Figure 39(b) shows the SPL contours for the jet excited at St = 0.16. The jet was excited at St = 0.16 since the spectra shown later in this section contained discrete peaks at St = 0.16 and its harmonics and not at the band of other frequencies found in the hot-wire data. The shape of the SPL contours is almost identical for the natural and excited jet; the main difference is the upstream shifting of the contours

in the excited jet case. This shift can be attributed to the flow fluctuations reaching a maximum sooner in the excited jet than in the natural jet. A somewhat surprising feature of the acoustic field of the excited jet is that at a radial distance of 10 diameters from the axis of the jet the SPL peaks at 2 db less than the value measured in the natural jet. This difference is even more pronounced in the lower Mach number jets (see Chapter VIII).

Figure 40 is the SPL contours for a 1 kHz wide band centered about St = 0.16 (St = 0.155 to 0.165). In this manner the sound pressure levels of the noise radiated at this frequency can be studied. Also shown are the SPL contours for the phase averaged pressure fluctuations. These SPL contours represent the level of the sound radiated by the instability. The maximum amplitudes shown for both SPL contours are only 6 db down from the full spectrum. This shows that a large portion of the noise is radiated at this frequency by the organized structure. The noise radiated by the organized structure is even more directional than the noise radiated by the full spectrum. This indicates that the directivity of the noise radiated by the jet is controlled by the St = 0.16 component.

Microphone Spectra, Mach Number 2.5 Jet

Noise spectra in an unexcited jet are shown in Figure 41 where the microphone was kept at a radial distance of 12 diameters from the centerline of the jet and moved in the downstream direction. At x/D = 6 the spectrum contains a peak at St = 0.16. However, at x/D = 14 the spectrum is very broad band. Both of these spectra were made in the acoustic field where the sound pressure level is below 140 db. This is

not in the region of large noise radiation. As the microphone approaches the contour of maximum noise radiation the spectra contain a more pronounced peak at St = 0.16. The spectrum at x/D = 40, which is outside the contour of maximum noise, shows the St = 0.16 component becoming less important as was the case before the contour of maximum noise level. This clearly indicates that the St = 0.16 component is a major noise generator in the areas of large sound pressure levels.

Figure 42 shows microphone spectra in the excited jet (St = 0.16) at the same locations as the previous spectra. The main effect of excitation is the slight enhancing of the St = 0.16 peak and the increased presence of harmonics.

A common way of representing spectral information in noise analysis is using the autocorrelation function. Presented in Figure 43 are the autocorrelation functions of microphone signals for both the natural and excited jets. The microphone is located at x/D = 30, and y/D = 12 and hence these figures correspond to the spectra presented in Figures 41(d) and 42(d). The features of the spectra discussed above are also evident on the autocorrelation function plots.

The fraction of sound radiated by the coherent portion of the jet at the locations of the above spectra is shown in Figure 44. The fraction of coherent sound drops considerably near x/D = 15. The coherent sound is comprised mainly of the St = 0.16 component as shown by the phase averaged wave form and spectrum at x/D = 30 and y/D = 12 in Figure 45. Therefore, the spectra presented earlier which showed low levels of the St = 0.16 component in the acoustic field near x/D = 15 confirm this drop in amplitude. These measurements reinforce the findings from the SPL contours that the directivity pattern of the jet is controlled mainly by the sound radiated from the coherent portion of the flow fluctuations.

Acoustic Wave Front Measurements, Mach Number 2.5 Jet

There has been speculation for the last ten years as to whether the flow disturbances in the jet that move downstream supersonically (which is the case in this Mach number 2.5 jet) produce noise in the form of Mach waves. To help establish the nature of the noise generation process, lines of constant phase were measured in the acoustic field of the jet. These lines of constant phase can be interpreted as acoustic wave fronts. Figure 46 is a plot of lines of constant phase (0° with respect to the excitation signal). Note the area of no correlation present around x/D = 15. The dashed line is the Mach angle corresponding to the instability wave speed ratioed to the ambient speed of sound. For the Mach number 2.5 jet $c/a_o = 1.11$. Therefore, the Mach angle corresponding to this wavespeed is $\mu = \sin^{-1}(1/1.11) = 64°$. Clearly, the Mach angle line does not correspond to any of the wave fronts. Between x/D = 15 and 25 there are some wave fronts that are straight lines. The angle they make with respect to the x-axis is approximately 53° which is not within the uncertainty range of the Mach angle above. Therefore, the sound radiation is not in the form of Mach waves, but is characteristic of waves emitted from a localized source around x/D = 15.

This type of radiation pattern is consistent with a noise source distribution which is moderately localized, having a length of 3 to 5 jet diameters for the dominant portion. (A point source would radiate perfectly circular wave fronts with no interference pattern of the type found here at x/D = 15.)

By using a simple ray tracing technique* in the region of the acoustic field where the sound pressure levels are large, one can approximate the position from where the major portion of the noise is radiated. The apparent source location is between x/D = 12 and 18. This seems to be reasonable since the flow fluctuation amplitude maximizes at approximately x/D = 15 (the end of the potential core) and the jet undergoes a transition from a flapping mode to a helical mode with large levels of fluctuations. Laufer et al. (72) have also observed (from directional microphone measurements) that the maximum noise seems to be radiated from the end of the potential core in supersonic jets. This situation is also predicted by Tam (12). However, the indication stated by Goldstein (73) that the maximum noise source location is just downstream of the sonic line is not borne out in the present measurements. (From Figure 8 one can see that the sonic line extends to x/D = 26.)

The dominant noise generation region in the Mach 2.5 jet is remarkably localized. No doubt it is the action of the rapid growth and decay of the instability that generates the noise. This takes place over a relatively short distance in the jet (approximately one wavelength of the instability). The coherence of the instability is drastically decreased after the flow fluctuation reaches this maximum. It is therefore hypothesized that rapid growth and decay of the instability generates noise in a manner similar to a whip cracking. Figure 47 is a schematic diagram of the jet configuration and noise radiation pattern envisioned from this study.

---

*This technique is a simplification of one proposed by Schubert (71) and consists of following lines drawn perpendicular to the orientation of the wave fronts presented in Figure 46.

A mechanism very similar to the one described has been hypothesized by Ffowcs Williams (74). He attributes the "crackle" (the intense spasmodic short duration compressive elements of the wave form) portion of the noise radiated by high Reynolds number supersonic jets to a "buckling" of the jet column. It appears that for the low Reynolds number jets used in this study a similar phenomenon is occurring. However, this study indicates that the instability is responsible for the major portion of the continuous noise radiated by the jet, and not simply an intermittent portion.

CHAPTER VI

SUMMARY, MACH NUMBER 2.5 JET

Flow field and acoustic measurements have been made in a low Reynolds number Mach 2.5 jet. There are several unstable frequencies present in the natural jet. The wave properties of the St = 0.14, 0.16 and 0.18 spectral components were measured. All three components are initially a flapping type mode (simultaneous n = +1 and n = -1 modes) that transform into a helix (n = -1) near the end of the potential core. This transformation occurs at the axial location of maximum flow fluctuations and is accompanied by a decrease in the level of coherence of the instability. Axial phase measurements show that all three spectral components travel downstream supersonically with respect to the ambient air ($1.12a_o$) at approximately 68% of the exit velocity of the jet. This wavespeed was found to be constant from x/D = 6 to 18. The growth rates of the full spectrum and St = 0.16 component are exponential over the first 12 diameters of flow. The St = 0.32 component also grows exponentially from x/D = 5 to 14. The growth of the harmonic does not cause the fundamental to deviate from its exponential growth indicating minimal nonlinear interaction. Thus, a linear stability theory can be applied to the jet using a wave representation for the flow fluctuations for at least the first 12 diameters of flow.

The spectra of the sound radiated from the jet contains a major peak at St = 0.16. This shows that the St = 0.16 spectral component of

the flow fluctuation is generating a major portion of the noise. The sound radiated by the flow instability governs the directivity of the acoustic field. Acoustic wave front measurements show that the sound is not radiated in the form of Mach waves. Instead, the sound is generated by a localized phenomenon, the rapid growth and decay of the instability which maximizes in fluctuation level and transforms from a flapping mode into a helix near the end of the potential core. At this location the fraction of coherent structure is greatly decreased.

CHAPTER VII

FLOW MEASUREMENTS, MACH NUMBER 1.4 AND 2.1 JETS

Mean Flow, Mach Number 1.4 and 2.1 Jets

Pitot and static pressure probe measurements were made in the Mach number 1.4 and 2.1 jets as was done in the Mach number 2.5 jet. The jet centerline Mach number distributions calculated from these measurements are shown in Figure 48 along with the Mach number 2.5 jet data. As in the Mach number 2.5 jet there is a cell structure present in the lower Mach number jets. The Mach number 2.1 jet possesses a centerline variation of $\pm 2\%$ in Mach number and the Mach number 1.4 jet has a $\pm 4\%$ variation. In the Mach number 1.4 jet there is a region of no cell structure from x/D = 0 to 3.5, even though it is found downstream of x/D = 3.5. The exact reason for this absence of cell structure from x/D = 0 to 3.5 is not known. It is interesting to note that both the static and pitot pressure measurements show the absence of the cell structure. The potential core ends at x/D = 8 and 7 for the Mach number 2.1 and 1.4 jets, respectively. Figure 49 shows how the axial location of the end of the potential core (x_c) changes with Mach number. Data for high Reynolds number cold jets measured by other investigators (75) (76) (77) and the isothermal jets studied by Lau et al. (78) are included. The location of x_c for the low Reynolds number jets used in this study follow the same trend as those measured by the other investigators. (The value of x_c increases with increasing jet Mach number.)

Radial profiles of Mach number are shown for the Mach number 1.4 and 2.1 jets in Figures 50 and 51, respectively. These can be compared with the profiles presented in Figure 9 for the Mach number 2.5 jet. All three jets have top hat profiles at x/D = 1 and develop in a similar fashion, except for the length of the potential core region as discussed above.

Axial variation of the local stagnation temperature for the jets is shown in Figure 52. As in the case of the Mach number 2.5 jet, T_o is constant along the centerline of the jet and equal to $T_{o\infty}$ until the end of the potential core. At the end of the potential core, T_o begins to increase and approaches the value of T_o for the ambient air. The radial profiles of T_o in Figures 53 and 54 show the local stagnation temperature varying across the shear layer of the jet from the value of $T_{o\infty}$ in the potential core to the value of the stagnation temperature of the ambient air. The same phenomenon was measured in the Mach number 2.5 jet (see Figure 11).

Spectra, Mach Number 1.4 and 2.1 Jets

Figure 55 contains a farfield microphone spectrum of the unexcited Mach number 2.1 jet. There is a peak present at St = 0.22. Figure 56 depicts hot-wire spectra made at x/D = 5, 10, and 15 in the unexcited jet. At x/D = 5 there is a peak at St = 0.22 and some less pronounced peaks at St = 0.19 and 0.38. At x/D = 10 only the St = 0.22 remains. As the flow progresses to x/D = 15 the spectrum is broad and contains no discrete peaks. The Mach number 2.1 jet was excited at St = 0.22 and the wave properties and acoustic field of this spectral component were studied. Only one component was selected since the measurements in the

Mach number 2.5 jet determined that the different spectral components behaved similarly. In addition, the St = 0.22 component possessed larger levels of fluctuation in the flow field and acoustic field than any other component present in the jet.

The effects of excitation upon the spectral content of the jet are shown in Figure 57. As in the Mach number 2.5 jet the excitation suppresses spectral components other than the one excited.

A far field microphone spectrum of the Mach number 1.4 jet (Figure 58) shows a very dominant peak at St = 0.33. The hot-wire spectra shown in Figure 59 explain this. At x/D = 4 and 8 the flow is clearly dominated by the St = 0.33 spectral component with no other component present. At x/D = 12 the spectrum is very broad with only a small peak at St = 0.33. When excited at St = 0.33 there is very little change in the hot-wire spectra as shown in Figure 60.

The Strouhal number of the spectral component most preferred by each jet is plotted as a function of Mach number in Figure 61. The Strouhal number decreases as the Mach number increases. Chan (13) predicts the same behavior for a helium jet. Tam (12), however, predicts increasing Strouhal number for increasing Mach number for a cold air jet. Tam's predicted values for the Strouhal number are shown in Figure 61 along with the measured values. This data indicates that the frequency selection mechanism in Tam's theory is invalid.

The fraction of organized structure present in the jets was measured by phase averaging the hot-wire signal. Figure 62 shows how the fraction changes as the flow progresses downstream for the Mach number 1.4, 2.1 and 2.5 jets. All of these jets are similar in that the

percentage of organized structure decreases as the flow progresses downstream with a dramatic drop after the end of the potential core.

Axial Growth of Flow Fluctuations, Mach Number 1.4 and 2.1 Jets

Figure 63 shows the axial variation of the mass velocity fluctuations for the unexcited Mach number 1.4, 2.1 and 2.5 jets. The flow fluctuations are band pass filtered from 3 to 40 kHz for the lower two Mach number jets. This includes a Strouhal number range from 0.05 to 0.72 for the Mach number 2.1 jet and from 0.07 to 0.92 for the Mach number 1.4 jet. This band width contains the full spectrum of the important jet fluctuations. The flow fluctuation amplitudes increase exponentially for about the first seven diameters of flow.

For all of the jets used in this study the flow fluctuation amplitude saturates near the end of the potential core. The growth of the fluctuations can be characterized by a linear stability type representation for the first several diameters of flow. Table IV contains the growth rates for all the spectral components measured in the three Mach number jets.

The growth rate of the full spectrum in the natural jet for different Mach numbers and Reynolds numbers are shown in Table V. The growth rates measured in jets with Reynolds numbers between 5,000 and 10,000 are grouped together. For this Reynolds number range the growth rate ($-k_i d$) decreases with increasing Mach number. Thus, increasing the Mach number tends to stabilize the flow. It is interesting to note that several of the jets were produced using simple conical contours instead of a contour designed by the exact method of characteristics. This

simple contour does not seem to significantly alter the development of the instability. Table V also contains a few growth rates measured at Reynolds numbers outside the 5,000 to 10,000 range. These measurements show that the growth rates increase with increasing Reynolds number.

The maximum level of $\tilde{m}$ remained between 0.3 and 0.4 for all Reynolds numbers for the measurements made between Mach numbers 2.3 and 2.5. This indicates that the maximum value of $\tilde{m}$ remains approximately constant for all Reynolds numbers greater than about three times the critical Reynolds number.

A deterministic trend is apparent in the maximum fluctuation levels attained in the jets. Figure 64 illustrates how the maximum level of mass velocity fluctuations increases with increasing jet Mach number. In the Mach number 1.4 jet the local flow Mach number at the point of maximum fluctuations is less than 1.2. Consequently, the Mach number independence assumed in the data reduction is invalid and the calculation of maximum $\tilde{m}$ is only an estimate.

The level of maximum axial velocity fluctuation can be estimated as was done earlier by assuming negligible pressure fluctuations. The levels of maximum axial velocity fluctuation normalized by the local mean velocity are also shown on Figure 64. Since the maximum level of velocity fluctuations is approximately the same for all three Mach number jets, the substantial increase in the maximum level of $\tilde{m}$ with Mach number can no doubt be attributed to an increased level of density fluctuations. (This also implies an increased level of temperature fluctuations at higher Mach numbers.)

Lau et al. (69) (78) have measured the radial and axial velocity fluctuations in a Mach number 1.4 isothermal jet (static temperature of

jet = static temperature of the ambient air) using a laser anemometer. Just past the end of the potential core they measured an axial velocity fluctuation level of approximately 0.14 and a radial velocity fluctuation level of 0.10 normalized by the exit velocity of the jet. Figure 64 also shows the maximum axial velocity fluctuation level measured in this study normalized by the exit velocity of the jet. The maximum radial velocity fluctuation level presented earlier when normalized by the exit velocity of the jet is 0.11. This shows that the maximum level of axial and radial velocity fluctuations measured in this study agree favorably with those measured by Lau et al. in a Mach number 1.4 isothermal jet, even though there is over a factor of 100 difference in the Reynolds numbers of the two experiments.

As in the case with the Mach number 2.5 jet, measurements were made in the Mach number 1.4 and 2.1 jets to determine which frequencies are most unstable. The techniques used in the Mach 2.5 jet were repeated. The hot-wire was placed at an axial location (x/D = 5 for M = 2.1 and x/D = 4 for M = 1.4) in the region of exponential growth. The signal was filtered by a 1 kHz band pass (ΔSt = 0.02 for M = 1.4 and 2.1) centered at the frequency of excitation. The response of the jets to the excitation was measured and the results are shown in Figure 65. The Mach number 2.1 jet contains several unstable frequencies as was the case for the Mach number 2.5 jet. However, the Mach number 1.4 jet has only one unstable frequency at St = 0.33.

The growth of the four spectral components in the Mach number 2.1 jet were measured and are shown in Figure 66. The St = 0.22 and 0.23 components possess higher levels of fluctuation over the length of the jet than do the St = 0.26 and 0.28 components. However, the jet clearly

prefers the St = 0.22 component as was shown in the unexcited jet flow fluctuation spectra. Therefore, the St = 0.22 component was studied in the Mach number 2.1 jet and the results from the measurements of this component should be representative of the other frequencies in the jet (as was the case for the Mach number 2.5 jet). The St = 0.33 component was studied in the Mach number 1.4 jet, since that jet has only one unstable frequency.

Figure 67 shows the axial variation of the flow fluctuation amplitudes for the full spectrum (St = 0.05 to 0.72), the St = 0.22 (ΔSt = 0.02) component, and the St = 0.44 (ΔSt = 0.06) component for the Mach number 2.1 jet excited at St = 0.22. The full spectrum and the St = 0.22 component both grow exponentially from x/D = 2 to 9. The rate of growth of the full spectrum is the same as the St = 0.22 component. The harmonic (St = 0.44) also grows exponentially over this region of the jet but at a different rate. The growth rates, $-k_i d$, are summarized in Table IV.

The growth of the Mach number 1.4 flow fluctuations excited at St = 0.33 are shown in Figure 68. The full spectrum and St = 0.33 component grow at the same exponential rate from x/D = 2 to 7. The harmonic remains at a constant amplitude over the first 5 diameters of flow in the excited jet and then grows exponentially from x/D = 5 to 7. The axial distribution of the different spectral components of the Mach number 1.4 jet showed no change when the jet was excited except for the St = 0.66 component. It appears that the exciter causes a constant level of fluctuation near the exit of the nozzle that is not present in the natural jet for the St = 0.66 component. The St = 0.66 component's growth in the unexcited jet is shown in the figure to illustrate how

the harmonic grows exponentially from x/D = 4 to 7 when the jet is not excited.

For all three Mach number jets the harmonic grows exponentially while the fundamental is still growing exponentially. This indicates that the initial growth of the harmonic is probably not induced by a nonlinear interaction.

Relative Phase Measurements, Mach Number 1.4 and 2.1 Jets

Axial, radial and azimuthal relative phase measurements were made in the Mach 2.1 jet excited at St = 0.22. The axial phase measurements in Figure 69 were made on three different days. The wavelength of the St = 0.22 component is (2.50 $\pm$0.11) D. The speed at which the wave travels downstream is calculated to be 0.89 a_o, which is 0.58 of the exit velocity of the jet.

Azimuthal phase distributions shown in Figure 70 illustrate that the jet is initially in a flapping mode at x/D = 7 and then transforms into a helix (n = -1) by the time it reaches x/D = 13. As in the Mach number 2.5 jet case, the transformation to a helix is accompanied by a substantial decrease in the fraction of flow fluctuations which are coherent. The radial phase distribution at x/D = 7 is shown in Figure 71. These measurements show that the same type of instability is present in the Mach 2.1 jet as found in the Mach 2.5 jet. The only difference is the less rapidly varying phase distribution in the vertical profile (at x/D = 7) in the Mach 2.1 jet as compared to the Mach 2.5 jet when it was in the flapping mode at x/D = 8 or 12.

The axial variation of the relative phase for the St = 0.33 component of the Mach 1.4 jet is shown in Figure 72. The wavelength is 1.71 $\pm$0.07 D. The wave travels downstream at $0.72a_o$, which is 0.61 of the exit velocity. The wave is definitely traveling downstream subsonically. Azimuthal phase measurements made at x/D = 4 and 8 (shown in Figure 73) indicate that the wave is in the flapping mode. Radial surveys of the relative phase at x/D = 4 and 8 (Figures 74 and 75) show a slow variation in the phase across the shear layer.

The Mach 1.4 and 2.1 jets have axial wavelengths that are constant over the region of measurements as was the case for the Mach 2.5 jet. The two jets both contain a flapping instability at x/D = 7. The Mach 2.1 jet's instability transforms into a helix by x/D = 13. However, the instability in the Mach 1.4 jet lost its coherence before a tranformation into a helix was apparent.

Table VI contains a summary of the axial wavelengths measured in the three jets. Also shown are earlier axial wavelengths measured by us (52) (53) in three other Mach number jets. The wavelength of the instability increases as the Mach number of the jet increases. The wavelength of the instability decreases with increasing Strouhal number and the wave speed is approximately constant. The wave speed of the instability in all of the jets was found to be from about 60 to 70% of the exit velocity of the jet. As noted earlier, the jet nozzles used in the previous studies had simple conical contours. It seems apparent that the instability properties of the jets are not appreciably affected by the details of the nozzle.

Comparison of Measured Wave Properties to Predicted Values

Tam's work (9) contains a linear stability analysis for cold supersonic jets with a top hat profile. Once the frequency of the disturbance is known, the complex wave number k can be determined using this theory. Table VII contains both the measured and predicted values of k for the jets used in this study and two jets used in a previous study (52) (53). The predicted value of k for the Mach 1.4 jet was estimated, since Tam's theory is valid for Mach 1.5 to 3.0. Also shown is the growth rate and wave number for a jet with a top hat profile as predicted by Morris (69) for a Mach 1.4 isothermal jet. The disturbance used by Morris has a frequency of St = 0.30 and is an n = 1 mode. The predicted values of the real part of the wave number are all within 40% of the measured values. Both theories predict a larger value of growth rate, $-k_i d$, than was measured at all Mach numbers for these low Reynolds numbers. Morris predicts that as the shear layer grows wider the growth rate will decrease. Based on mean flow measurements, estimates of the shear layer thickness were made. Using this estimated value, Morris's theory still predicts the same growth rate. However, the value of $k_r d$ predicted by the theory raises to 3.53, essentially the same value as that measured. The values of $-k_i d$ measured for the full spectrum were found to increase with Reynolds number (see Table V). This indicates that the growth rate of individual spectral components will also increase, thus compensating for the majority of discrepancy observed between the values measured in the low Reynolds number jets and the values predicted for the high Reynolds number jets. Since the mean flow profile near the exit of the jet approximates a top hat profile better than at increased Reynolds numbers

this trend is reasonable. (Top hat profiles have typically larger growth rates (36).) These results indicate that it is possible to calculate the real part of the wave number with some degree of accuracy and to obtain reasonable estimates of the imaginary part ($-k_i d$) from existing theories.

Radial profiles of the hot-wire fluctuations as well as mean hot-wire voltage were recorded for the M = 1.4 and 2.1 jets with the same procedure used in the M = 2.5 jet. The data show the same features as were apparent in the M = 2.5 case and therefore are not repeated here.

CHAPTER VIII

ACOUSTIC MEASUREMENTS, MACH NUMBER 1.4 AND 2.5 JETS

Microphone SPL Contours and Spectra, Mach Number 1.4 and 2.1 Jets

Figures 76 and 77 show SPL contours for the Mach number 2.1 and 1.4 jets. Contours are shown for the natural jets and for the Mach number 2.1 jet excited at St = 0.22 and the Mach number 1.4 jet excited at St = 0.33. The SPL contours show that the acoustic field for both of these jets is highly directional as was seen in the Mach number 2.5 jet. The directivity of the radiated noise is the same for the excited and natural jets. As was observed in the Mach number 2.5 jet, there is a decrease in the maximum sound pressure level attained (for a given radial distance from the centerline of the jet) when the jet is excited. This difference in maximum sound pressure level becomes smaller with increasing Mach number (5 db at M = 1.4, 3 db at M = 2.1, and 2 db at M = 2.5). In the Mach number 1.4 and 2.1 jets, where the difference in maximum sound pressure level is larger, the cause is readily apparent upon close examination of microphone spectra which show a decrease in the level of the broad band random fluctuations when the jet is excited (Figures 78 and 79).

A spectrum of the sound radiated from the natural Mach number 2.1 jet is shown in Figure 78. The microphone is located at the point of maximum sound pressure level for a radial distance of 12 diameters. The

spectrum shows that the St = 0.22 component is definitely the dominant noise producer in the natural jet. Figure 78 also shows a microphone spectrum made at the same location when the jet was excited at St = 0.22. (The vertical scale is the same for both spectra.) The amplitude of the St = 0.22 component remains approximately the same when the jet is excited. However, the level of the random fluctuations has decreased.

Figure 79 shows microphone spectra for both the natural and excited (St = 0.33) Mach number 1.4 jet. The spectra were made at the point of maximum sound pressure level at a radial distance of 10 diameters. The natural spectrum shows that the St = 0.33 component is the dominant noise producer in the Mach number 1.4 jet. When the jet is excited at St = 0.33 the amplitude of the St = 0.33 component remains approximately the same but as in the M = 2.1 jet the level of the random flucutations has decreased. This, no doubt, is a direct result of the flow fluctuations "locking" onto the excitation frequency, suppressing the growth of other instability components, and remaining more coherent over a longer length of the jet.

The development of the spectra as the microphone approaches the axial location of maximum sound pressure levels from upstream while maintaining a constant radial distance was the same for the Mach number 1.4 and 2.1 jets as in the Mach number 2.5 jet (from x/D = 14 to 30). This was the case for both the excited and natural jet spectra. Close to the exit of the unexcited jet ($x/D \approx 5$) the spectrum is broad with no discrete peaks but maximizing in amplitude around St = 0.22 for the Mach number 2.1 jet and St = 0.33 for the Mach number 1.4 jet. When excited a small discrete peak appears at the frequency of excitation. As the microphone is moved downstream closer to the point of maximum sound

pressure level the spectrum shows successively larger discrete peaks (for both the excited and natural jets) at the Strouhal numbers of 0.22 and 0.33 for the Mach number 2.1 and 1.4 jets, respectively. This shows that the instability is producing larger portions of the noise in the areas of large sound pressure levels. The percent of coherent sound measured at a radius of 10 diameters increases from about 10% at x/D = 5 to about 60% at the point of maximum sound pressure level.

A directivity plot of the sound pressure levels generated by the full spectrum, the St = 0.22 component, and the coherent structure (phase averaged) are shown in Figure 80 for the Mach number 2.1 jet excited at St = 0.22. The sound pressure levels were measured along an arc 26 diameters in radius centered at the jet exit and then plotted as a function of β, the angle from the jet axis. This was also done in Figure 81 for the full spectrum, the St = 0.33 component, and the coherent structure of the sound radiated by the Mach number 1.4 jet excited at St = 0.33. The sound radiated by the single spectral component whose frequency is the same as the frequency of excitation comprises a large portion of the overall sound level at the angle of maximum noise level for both jets. As β is increased the sound pressure levels of this component decreases more rapidly than the overall sound pressure levels. This was also observed in the Mach number 2.5 jet and indicates that the sound radiated by the coherent structure controls the directivity pattern for all three Mach number jets.

A directivity plot for several Mach number jets is shown in Figure 82. The natural Mach number 2.5, 2.1, and 1.4 jets used in this study are shown along with data estimated from directivity plots for Mach number 2.0 and 1.5 high Reynolds number jets measured by Yu and Dosanjh

(50) (70). The low Reynolds number jets are generating comparable levels of noise, accounting for the Mach number effect, thus showing that the instability is a powerful noise generator. The directivity of the M = 2.0 high Reynolds number jet (50) is different from the others shown in the figure. This is due to two factors. First, the arc radius used in this study is smaller than required to be completely in the far field. The M = 2.0 data was originally based on an arc radius of 180 diameters. Second, we (53) showed that the maximum noise generators are located farther downstream in the low Reynolds number jet. This affects the directivity patterns when recorded at the relatively small arc radius.

Acoustic Wave Front Measurements, Mach Number 1.4 and 2.1 Jets

Acoustic wave front measurements for the Mach number 1.4 and 2.1 jets are shown in Figure 83, with each jet excited at its dominant frequency. For both jets the wave fronts are shaped like arcs and are definitely not Mach waves. For $x/D \approx 8$ (near the end of the potential core) there is a region of no correlation present perpendicular to the jet axis. The Mach number 2.5 jet also had a similar region near the end of the potential core. However, farther upstream the Mach number 2.5 jet again showed organized wave fronts. In the Mach number 1.4 and 2.1 jets the end of the potential core is closer to the exit of the jet. Thus the development of the instability occurs over a much shorter axial length and the resulting acoustic response is compacted into a shorter axial length for the lower Mach number jets in comparison with the Mach number 2.5 jet. Due to this compacting effect and low sound pressure

levels, it was not possible to reliably determine the wave fronts for x/D less than 8.

Performing a simple ray trace on the acoustic wave fronts in the areas of maximum sound pressure levels indicates that the dominant noise source is near the end of the potential core where the flow fluctuations maximize. The acoustic measurements presented show that the instability of the jet generates a major portion of the noise radiated by the jet whether its axial wavespeed is supersonic or subsonic. The acoustic measurements also indicate that the noise production mechanism of the instability is the same for all three jets and that it is a relatively localized source. The localized source is the fast growth, saturation and decay of the instability which occurs near the end of the potential core for all three jets.

Proposed Noise Generation Mechanism in Higher Reynolds Number Jets

Flow fluctuation and microphone spectra presented in Figures 5, 6 and 7 show how the spectrum becomes broader with increasing Reynolds number. Like most free shear flow instabilities, a broader frequency range becomes unstable with increasing Reynolds number. Based upon the measurements made in this study and our preliminary work (53), it appears that the noise production mechanism in high Reynolds number jets may consist of the same type of instability as is present in the low Reynolds number jet. It is envisioned that the noise production mechanism consists of a wave-type instability with several different frequencies growing, saturating and decaying at different axial locations. Each spectral component generates noise in its frequency range in the same

manner (approximately) as the instability component measured in the low Reynolds number jets. The several different frequencies naturally account for the broadening of the spectrum.

CHAPTER IX

CONCLUSIONS

Flow field and acoustic measurements have been made in low Reynolds number Mach 1.4, 2.1, and 2.5 jets. There is a band of unstable frequencies present in each jet. This band is very narrow for the Mach number 1.4 jet and becomes wider as the Mach number increases. It was observed that for all three Mach numbers the mode of the instability was initially the n = +1 and n = -1 modes occurring simultaneously (resulting in the jet flapping up and down). In the Mach number 2.1 and 2.5 jets it was observed that the mode transformed into a helix (n = -1) shortly past the end of the potential core. The transformation to a helix is accompanied by a substantial decrease in the coherence of the flow fluctuations. The instability in the Mach number 1.4 jet lost its coherence before such a transformation could be observed.

Axial relative phase measurements show that the instability in all three jets can be characterized as waves traveling downstream at speeds between 60% and 70% of the jet exit velocity. The disturbances were found to grow in amplitude exponentially over a region of the jet where the potential core was present. Thus, a linear stability theory can be applied to the jet using a wave representation of the flow fluctuations for at least this region of the jet.

When the measured wave properties were compared to those predicted by Tam (9) and Morris (69), it was found that the predicted value for the

real part of the wave number ($k_r d$) compared favorably. However, the growth rate ($k_i d$) did not compare as well for the low Reynolds number jets. However, measurements indicate that as the Reynolds number is increased the growth rate will increase to a value more comparable to those predicted. The frequency selection scheme of Tam's theory was found to be invalid in the present experiments.

Acoustic measurements show that the majority of the sound in the areas of high sound pressure levels is generated by the instability of the jets. The sound radiated by the instability governs the directivity pattern of the acoustic field. It is estimated that the major noise sources are located near the end of the potential core. This corresponds to the axial location where the flow fluctuations reach a maximum level. Acoustic wave front measurements show that the sound is not radiated as Mach waves, even in the Mach number 2.5 jet where the waves travel downstream supersonically with respect to the ambient air. Instead, the acoustic wave fronts are characteristic of noise generated by a relatively localized source.

For all three Mach number jets the major portion of the sound radiated by the jets is produced by the instability's rapid growth and decay that occur near the end of the potential core. This takes place over a relatively short distance (approximately one wavelength of the instability) in the jet. The coherence of the instability drastically decreases after this and the level of random fluctuations increases.

BIBLIOGRAPHY

(1) Lighthill, M. J. "On Sound Generated Aerodynamically, I General Theory." Proc. Roy. Soc., A211 (1952), pp. 546-587.

(2) Lighthill, M. J. "On Sound Generated Aerodynamically, II Turbulence as a Source of Sound." Proc. Roy. Soc., A222 (1954), pp. 1-32.

(3) Ffowcs Williams, J. E. "The Noise From Turbulence Convected at High Speed." Phil. Trans. Roy. Soc., A255 (1963), pp. 459.

(4) Ribner, H. S. "The Generation of Sound by Turbulent Jets." Advances in Applied Mechanics, Vol. 8 (1964), pp. 103-182.

(5) Phillips, O. M. "On the Generation of Sound by Supersonic Turbulent Shear Layer." J. Fluid Mech., Vol. 9 (1960), pp. 1-28.

(6) Pao, S. P. and M. V. Lowson. "Some Applications of Jet Noise Theory." AIAA Paper No. 70-233, 1970.

(7) Lilley, G. M., P. Morris, and B. J. Tester. "On the Theory of Jet Noise and its Applications." AIAA Paper 73-987, 1973.

(8) Doak, P. E. "Analysis of Internally Generated Sound in Continuous Materials: 2. A Critical Review of the Conceptual Adequacy and Physical Scope of Existing Theories of Aerodynamic Noise, with Special Reference to Jet Noise." Journal of Sound and Vibration., Vol. 25 (1972), pp. 263-335.

(9) Tam, C. K. W. "On the Noise of a Nearly Ideally Expanded Supersonic Jet." J. Fluid Mech., Vol. 51 (1972), pp. 69-95.

(10) Tam, C. K. W. "Directional Acoustic Radiation From a Supersonic Jet Generated by Shear Layer Instabilities." J. Fluid Mech., Vol. 46 (1971), pp. 757-768.

(11) Tam, C. K. W. "Supersonic Jet Noise Generated by Large Scale Disturbances." AIAA Paper 73-992, 1973.

(12) Tam, C. K. W. "Supersonic Jet Noise Generated by Large Scale Disturbances." J. Sound and Vibration., Vol. 38 (1974), pp. 51-79.

(13) Chan, Y. Y. "Discrete Acoustic Radiation From a High-Speed Jet as a Singular Pertubation Problem." Canadian Aeronautics and Space Journal., Vol. 38 (1974), pp. 51-79.

(14) Chan, Y. Y. "Noise Generated Wavelike Eddies in a Turbulent Jet." ICAS Paper No. 76-42, 1976.

(15) Liu, J. T. C. "Developing Large-Scale Wavelike Eddies and the Near Jet Noise Field." J. Fluid Mech., Vol. 62 (1974), pp. 437-464.

(16) Morris, P. J. "The Spatial Viscous Instability of Axisymmetric Jets." J. Fluid Mech., Vol. 77, Part 3 (1976), pp. 511-529.

(17) Morris, P. J. "Flow Characteristics of the Large-Scale Wave-Like Structure of a Supersonic Round Jet." (Submitted for publication to the J. Sound and Vibration.)

(18) Brown, G., and Roshko, A. "The Effect of Density Difference on the Turbulent Mixing Layer." AGARD Conference on Turbulent Shear Flows. Conf. Proc. No. 93 (1971), p. 23.

(19) Bradshaw, P., Ferris, D. H., and Johnson, R. F. "Turbulence in the Noise Producing Region of a Circular Jet." J. Fluid Mech., Vol. 19 (1964), pp. 591-624.

(20) Crow, S. C., and F. H. Champagne. "Orderly Structure in Jet Turbulence." J. Fluid Mech., Vol. 48 (1971), pp. 547-591.

(21) Winant, C. D., and F. K. Browand. "Vortex Pairing, the Mechanism of Turbulent Mixing Layer Growth at Moderate Reynolds Number." J. Fluid Mech., Vol. 63 (1974), pp. 237-256.

(22) Lau, J. C., M. J. Fisher, and H. V. Fuchs. "The Intrinsic Structure of Turbulent Jets." J. Sound and Vibration, Vol. 22, No. 4 (1972), pp. 379-406.

(23) Browand, F. K., and P. D. Weidman. "Large Scales in the Developing Mixing Layer." J. Fluid Mech., Vol. 76, Part 1 (1976), pp. 127-144.

(24) Roshko, A. "Structure of Turbulent Shear Flows: A New Look." AIAA J., Vol. 14 (1976), pp. 1349-1357.

(25) Mollo-Christensen, E. "Jet Noise and Shear Flow Instability Seen from an Experimenter's Viewpoint." J. Appl. Mech., Vol. 34 (1967), pp. 1-7.

(26) Bishop, K. A., J. E. Ffowcs Williams, and W. Smith. "On the Noise Sources of the Unsuppressed High-Speed Jet." J. Fluid Mech., Vol. 50 (1971), pp. 21-31.

(27) Laufer, J., R. E. Kaplan, and W. T. Chu. "On the Generation of Jet Noise." AGARD Conf. Proc. No. 131 on Noise Mechanisms, 1973.

(28) Browand, F. K. "An Experimental Investigation of the Instability of an Incompressible Separated Shear Layer." J. Fluid Mech., Vol. 26, Part 2 (1966), pp. 281-307.

(29) Tollmien, W. "The Production of Turbulence." NACA Technical Memorandum Number 609, 1931.

(30) Schubauer, G. B., and H. K. Skramstad. "Laminar-Boundary Layer Oscillations and Transition on a Flat Plate." NACA Report Number 909, 1948.

(31) Lees, L., and C. C. Lin. "Investigation of the Stability of the Laminar Boundary Layer in a Compressible Fluid." NACA TN 1115, 1946.

(32) Mack, L. M. "Inviscid Stability of the Laminar Compressible Boundary Layer for Three-Dimensional Disturbances." JPL Space Program Summary No. 37-36, Vol. IV (1966), pp. 143-147.

(33) Demetriades, A. "An Experimental Investigation of the Stability of the Hypersonic Laminar Boundary Layer." Guggenheim Aeronautical Laboratory, California Institute of Technology, Hypersonic Research Project Memorandum No. 43, May 15, 1958.

(34) Kendall, J. M. "Supersonic Boundary Layer Stability Experiments." Proceedings of the Boundary Layer Transition Study Group Meeting, Vol. II, Aerospace Report No. TR-0158 (S3816-63)-1, 1967.

(35) Laufer, J., and T. Vrebalovich. "Stability and Transition of Supersonic Laminary Boundary Layer on an Insulated Flat Plate." J. Fluid Mech., Vol. 9 (1960), pp. 257-299.

(36) Gold, H. "Stability of Axisymmetric Laminar Wakes." AIAA Entry Technical Conference, Williamsburg and Hampton, Virginia, October 12-24, 1964.

(37) Sato, H., and O. Okada. "The Stability and Transition of an Axisymmetric Wake." J. Fluid Mech., Vol. 26, Part 2 (1966), pp. 237-253.

(38) McLaughlin, D. K. "Experimental Investigation of the Mean Flow and Stability of the Laminar Supersonic Cone Wake." AFOSR No. 70-0072TR, January, 1970.

(39) Behrens, W., and D. R. S. Ko. "Experimental Stability Studies in Wakes of Two Dimensional Slender Bodies at Hypersonic Speeds." AIAA J., Vol. 9, No. 5 (1971), pp. 859-865.

(40) Miksad, R. W. "Experiments on the Non-Linear Stages of Free-Shear-Layer Transition." J. Fluid Mech., Vol. 56, Part 4 (1972), pp. 695-719.

(41) McLaughlin, D. K. "Experimental Investigation of the Stability of the Laminar Supersonic Cone Wake." AIAA J., Vol. 9, No. 4 (April, 1971), pp. 696-702.

(42) Reynolds, W. C., and A. K. M. F. Hussain. "The Mechanics of an Organized Wave in Turbulent Shear Flow. Part 3. Theoretical Models and Comparisons with Experiments." J. Fluid Mech., Vol. 54, Part 2 (1972), pp. 263-288.

(43) Moore, C. J. "The Role of Shear-Layer Instability Waves in Jet Exhaust Noise." J. Fluid Mech., Vol. 80, Part 2 (1977), pp. 321-357.

(44) Ollerhead, J. B. "Some Shadowgraph Experiments with a Cold Supersonic Jet." Wyle Laboratory Research Report, No. WR 66-44, 1966.

(45) Ollerhead, J. B. "On the Prediction of the Near Field Noise of Supersonic Jets." NASA, CR-857, 1967.

(46) Lowson, M. V., and J. B. Ollerhead. "Visualization of Noise from Cold Supersonic Jets." J. Acoust. Soc. Am., Vol. 44 (1968), p. 624.

(47) Salant, R. F. "Investigation of Jet Noise Using Optical Holography." Department of Transportation Report No. DOT-TSC-OST-73-11, 1973.

(48) Eggers, J. M. "Velocity Profiles and Eddy Viscosity Distributions Downstream of a Mach 2.2 Nozzle Exhausting to Quiescent Air." NASA Technical Note, D-3601, 1966.

(49) Jones, I. S. F. "Finite Amplitude Waves from a Supersonic Jet." AIAA Paper No. 71-151, 1971.

(50) Dosanjh, D. S., and J. C. Yu. "Noise from Underexpanded Axisymmetric Jet Flow Using Radial Jet Flow Impingement." Proceedings, AFQSR-UTIAS Symposium on Aerodynamic Noise, Toronto, 1968, pp. 169-188.

(51) McLaughlin, D. K., G. L. Morrison, and T. R. Troutt. "Experiments on the Instability Waves in a Supersonic Jet and Their Acoustic Radiation." J. Fluid Mech., Vol. 69 (1976), pp. 73-95.

(52) McLaughlin, D. K., G. L. Morrison, and T. R. Troutt. "Experiments on the Instability Waves in a Supersonic Jet and Their Acoustic Radiation." In Proceedings of the Second Interagency Symposium on University Research in Transportation Noise, Raleigh, North Carolina, June, 1974.

(53) McLaughlin, D. K., G. L. Morrison, and T. R. Troutt. "Reynolds Number Dependence in Supersonic Jet Noise." AIAA J., Vol. 15 (1977), pp. 526-532.

(54) Johnson, C. B., and L. R. Boney. "A Method for Calculating a Real-Gas Two-Dimensional Nozzle Contour Including the Effects of Gamma." NASA TM X-3243, Langley Research Center, Hampton, Virginia, 1975.

(55) Rott, N., and L. F. Crabtree. "Simplified Laminar Boundary-Layer Calculations for Bodies of Revolution and for Yawed Wings." J. Aero. Sci., Vol. 19 (1952), pp. 553-563.

(56) Matthews, M. L. "An Experimental Investigation of Viscous Effects on Static and Impact Pressure Probes in Hypersonic Flow." Pasadena, California: GALCIT, Hypersonic Research Project, Memo No. 44, 1958.

(57) Behrens, W. "Viscous Interaction Effect on a Static Pressure Probe at M = 6." AIAA J., Vol. 1 (1963), pp. 2364-2366.

(58) Johnson, D. A., and W. C. Rose. "Laser Velocimeter and Hot-Wire Anemometer Comparison in a Supersonic Boundary Layer." AIAA J., Vol. 13, No. 4 (1975), pp. 512-515.

(59) Rose, W. C. "The Behavior of a Compressible Turbulent Boundary Layer in a Shock-Wave-Induced Adverse Pressure Gradient." NASA TN D-7092, 1973.

(60) McLaughlin, D. K., J. E. Carter, M. Finston, and J. A. Forney. "Experimental Investigation of the Mean Flow of the Laminar Supersonic Cone Wake." AIAA J., Vol. 9, No. 3 (March, 1971), pp. 479-484.

(61) Hussain, A. K. M. F., and K. B. M. Q. Zaman. "Effect of Acoustic Excitation on the Turbulent Structure of a Circular Jet." In Proceedings of the Third Interagency Symposium on University Research in Transportation Noise. University of Utah, Salt Lake City, Utah, November, 1975.

(62) Mack, L. M. "Viscous and Inviscid Amplification Rates of Two- and Three-Dimensional Disturbances in a Compressible Boundary Layer." JPL Space Program Summary 37-42, Vol. IV (1966), pp. 158-162.

(63) Kistler, A. L. "Fluctuation Measurements in a Supersonic Turbulent Boundary Layer." The Physics of Fluids, Vol. 2, No. 3 (May-June, 1959), pp. 290-296.

(64) Laderman, A. J., and A. Demetriades. "Mean and Fluctuating Flow Measurements in the Hypersonic Boundary Layer Over a Cooled Wall." J. Fluid Mech., Vol. 63, No. 1 (March, 1974), pp. 121-144.

(65) Morkovin, M. V. Fluctuations and Hot-Wire Anemometry in Compressible Fluids. AGARDograph No. 24. Paris: NATO, November, 1956.

(66) Owen, F. K., C. C. Horstman, and M. I. Kussoy. "Mean and Fluctuating Flow Measurements of a Fully-Developed, Non-Adiabatic, Hypersonic Boundary Layer." J. Fluid Mech., Vol. 70, Part 2 (August, 1975), pp. 393-413.

(67) Rose, W. C. "Turbulence Measurements in a Compressible Boundary Layer." AIAA J., Vol. 12, No. 8 (August, 1974), pp. 1060-1064.

(68) Ko, C. L., D. K. McLaughlin, and T. R. Troutt. "Improved Techniques for Hot-Wire Fluctuation Measurements in Supersonic Flows." AIAA Paper No. 76-398, 1976.

(69) Plumbee, H. E., Jr. (Editor). "The Generation and Radiation of Supersonic Jet Noise. Vol. II." Air Force Aero Propulsion Laboratory Report No. AFAPL-TR-76-65, June, 1976.

(70) Yu, J. C., and D. S. Dosanjh. "Noise Field of Supersonic Mach 1.5 Cold Model Jet." J. Acoust. Soc. Am., Vol. 51 (1973), pp. 1400-1410.

(71) Schubert, L. K. "Refraction of Sound by a Jet: A Numerical Study." UTIAS Report No. 144, December, 1969.

(72) Laufer, J., R. S. Schlinker, and R. E. Kaplan. "Experiments on Supersonic Jet Noise." AIAA Paper No. 75-478, 1975.

(73) Goldstein, Marvin E. Aeroacoustics. New York: McGraw-Hill International Book Co., 1976.

(74) Ffowcs Williams, J. E., J. Simson, and V. J. Virchis. "Crackle: An Annoying Component of Jet Noise." J. Fluid Mech., Vol. 71 (1976), pp. 251-271.

(75) Morris, P. J. "Turbulence Measurements in Subsonic and Supersonic Axisymmetric Jets in a Moving Stream." AIAA Paper No. 76-25, 1976.

(76) Knott, P. et al. "Laser Velocimeter Developments for Noise Source Location. Vol. II." Air Force Aero Propulsion Laboratory Report No. TR-(to be assigned), Chapter 3, August, 1975.

(77) Nagamatsu, H. T., and R. E. Sheer, Jr. "Subsonic and Supersonic Jets and Supersonic Suppressor Characteristics." AIAA Paper No. 73-999, 1973.

(78) Lau, J. C., P. J. Morris, and M. J. Fisher. "Turbulence Measurements in Subsonic Jets Using a Laser Velocimeter." AIAA Paper No. 76-348, 1976.

(79) Kovasznay, L. S. G. "The Hot-Wire Anemometer in Supersonic Flow." J. Aero. Sci., Vol. 17, No. 9 (September, 1950), pp. 565-572.

(80) Kovasznay, L. S. G. "Turbulence in Supersonic Flow." J. Aero. Sci., Vol. 20, No. 10 (October, 1953), pp. 657-674.

APPENDIX A

EFFECTS OF ARTIFICIAL EXCITATION

The effects of artificial excitation were studied in the Mach number 2.1 and 2.5 jets. Hot-wire spectra were presented earlier in Figures 13, 14, 56, and 57 for the Mach number 2.1 and 2.5 jets both in the excited and natural states. These spectra show that the main effect of excitation on the flow fluctuations was the stabilization of the jet onto the excited frequency (and its harmonics) and the suppression of the other unstable components present in the natural jet. This stabilization also causes a reduction in the amount of broad band random fluctuations.

The fluctuation levels and growth rate of the Mach number 2.1 jet were altered very little by excitation while in the Mach number 2.5 jet the level of fluctuation near the exit of the jet was increased slightly. This resulted in the amplitude of the flow fluctuations saturating closer to the exit of the jet in the excited jet than in the natural one for the Mach number 2.5 jet. However, the rate of growth and the maximum level of fluctuation remained the same. Figure 84 shows radial profiles of the full spectrum (St = 0.03 to 0.64) flow fluctuations in the excited and natural Mach number 2.5 jets. There is no detectable difference in the profiles that can be attributed to the excitation.

In order to better understand the disturbance induced in the jet by the glow discharge, extensive hot-wire measurements were performed at x/D = 3 at the top (downstream of the exciter) and the bottom shear layer in the Mach number 2.1 jet. From Kovasznay mode diagrams* made from the hot-wire data, estimates of mass velocity and stagnation temperature fluctuations were obtained. The level of stagnation temperature

---

*The Kovasznay mode diagrams and the technique used to obtain them are discussed in Appendix B.

fluctuation is the y-axis intercept on the Kovaznay mode diagram and the level of mass velocity fluctuation is the slope that the curve asymptotically approaches for large values of A_m/A_T. The mode diagrams shown in Figure 85 at x/D = 3 for the top and bottom shear layers do indicate a larger level of fluctuations in the top shear layer. This is probably due to the probe being located exactly downstream of the exciter in the top shear layer and to the probe interference caused by the probe support spanning the flow from the top to the bottom of the jet.

The mode diagrams shown in Figure 85 illustrate that the ratio of total temperature fluctuations compared to the mass velocity fluctuations is the same whether the probe is directly downstream of the exciter or on the opposite side of the jet. Consequently, the local intense temperature fluctuations induced by the glow discharge, decay rapidly downstream of the glow leaving little history of the intense temperatures characteristic of the glow.

The above measurements were made when the excitation device was drawing a current of 0.2 ma DC at 415 volts DC (modulated by a 135 volt peak to peak alternating voltage). If the level of excitation was too large, it was found that the acoustic field was altered. Sound pressure level contours for the full spectrum made in the Mach number 2.5 jet presented earlier (Figure 39) show the natural jet and the jet excited using 0.2 ma of current. The effects of the excitation are a slight upstream shifting of the SPL contours and a 2 db decrease in the maximum sound pressure level attained at a constant radial distance from the centerline. The upstream shifting of the SPL contours is attributed to the flow fluctuations maximizing closer to the exit of the jet in the excited case. The decrease in maximum sound pressure level is due to

the reduction of random fluctuations in the areas of maximum noise levels when the jet is excited. The directivity of the contours remains the same. If a much larger level of excitation is used (≈ 2 ma DC) the SPL contours shown in Figure 86 result. Here the shape of the contours have been altered by the addition of a spurious lobe. Since the SPL contours are no longer the same as in the natural jet at this high level of excitation, it was decided to operate the exciter with no more than 0.2 ma current where there is not an appreciable effect on the flow fluctuation of the acoustic field. Moore (43) has also determined for subsonic jets that it is possible to excite the jet excessively resulting in a jet which is substantially different from the naturally occurring one.

The effects of excitation on the mean flow were also observed. Figure 87 shows mean hot-wire voltage profiles for both the natural and excited Mach number 2.5 jet. The excitation causes no detectable difference in the mean flow profiles.

Another check on the residual heating of the top shear layer due to the excitation was made by measuring the mean stagnation temperature radial distribution at x/D = 1 along the y-axis. The glow exciter is mounted on the + y-axis. Both the excited and natural stagnation temperature profiles are shown in Figure 88. The profiles are not affected by the excitation of the jet. All of the above measurements show that the excitation of the jet, when maintained at a low level, causes minimal changes in the flow and acoustic field.

APPENDIX B

HOT-WIRE DATA REDUCTION TECHNIQUE

A hot-wire data reduction technique similar to that outlined by Rose (58) (59) was used in this study. This method directly calibrates the sensitivity of the hot-wire to axial mass velocity and radial velocity for each hot-wire probe used. In this manner the substantial conduction end losses are accounted for. The sensitivity of the hot-wire to stagnation temperature fluctuations (A_T) is calculated using hot-wire voltage and resistance data recorded at constant flow conditions. This technique is a modification of the original methods proposed by Kovasznay (79) and Morkovin (65).

The bridge voltage, E_b, of the hot-wire is comprised of two parts, a fluctuating component, e', and a time averaged mean value, E. An oblique hot-wire responds to axial mass velocity (m), stagnation temperature (T_o), and radial velocity (v) fluctuations according to:

$$\frac{e'}{E} = A_m \frac{m'}{\bar{m}} - A_T \frac{T_o}{\bar{T}_o} \pm A_v \frac{v'}{\bar{u}} \tag{1}$$

The validity of this decomposition requires the local Mach number normal to the hot-wire to be greater than 1.2 (59) (65) (80). The sensitivity coefficients A_m, A_T, and A_v can be evaluated as follows (59).

$$A_m = \left.\frac{\partial \ell n\ E}{\partial \ell n(\rho u)}\right|_{T_o,\ R_w,\ \alpha \text{ constant}} \tag{2}$$

$$A_v = \left.\frac{\partial \ell n\ E}{\partial \alpha}\right|_{\bar{\rho}\bar{u},\ T_o,\ R_w \text{ constant}} \tag{3}$$

$$A_T = -\left.\frac{\partial \ell n\ E}{\partial \ell n\ \bar{T}_o}\right|_{\bar{\rho}\bar{u},\ R_w,\ \alpha \text{ constant}} \tag{4}$$

Both A_m and A_v were evaluated by direct calibration of each wire in the flow using the relations above. Following the method of Rose (59) the stagnation temperature fluctuation sensitivity was evaluated as follows:

$$A_T = \frac{\partial \ell n\ T_w}{\partial \ell n\ R_w}\left[\frac{\partial \ell n\ E}{\partial \ell n\ R_w} + \frac{1}{2} - \frac{R_w}{R_w + R_s}\right] + 0.765\ A_m - 0.9425 \qquad (5)$$

Normal Wire Measurements

When using a normal wire the RMS value of e' is measured. In order to determine values for the mass velocity fluctuations and the total temperature fluctuations, values of e'_{rms} and E were recorded using five overheats (wire temperatures). These data points were then used to solve (by 2nd order polynomial regression) the following equation as was done by Ko et al. (68).

$$\theta^{*2} = \tilde{m}^2\ (A_m/A_T)^2 - 2R_{mT_o}\ \tilde{m}\ \tilde{T}_o\ (A_m/A_T) + \tilde{T}_o^2 \qquad (6)$$

where

$$\theta^* = \frac{e'_{rms}/E}{A_T}$$

$$\tilde{m} = (\rho u)'_{rms}/\bar{\rho}\bar{u}$$

$$\tilde{T}_o = (T'_o)_{rms}/\bar{T}_o$$

$$R_{mT_o} = \frac{(\rho u)'\ T'_o}{(\rho u)'_{rms}\ (T'_o)_{rms}}$$

By using the second order curve fit, values for $\tilde{m}$, $\tilde{T}_o$, and R_{mT_o} were determined. Figures 89 and 90 show both the second order curve fit through the data points and the corresponding Kovaznay (80) mode diagram for the Mach number 2.1 jet at x/D = 14 excited and natural. The data fit the second order curve very well and are typical of the results obtained in this study. The Kovaznay mode diagram's y-axis intercept is the level of stagnation temperature fluctuation and the slope of the curve for large values of A_m/A_T asymptotically approaches the value of

the mass velocity fluctuation. The correlation coefficient between the mass velocity and stagnation temperature fluctuations (R_{mT_o}) was found to decrease from 0.95 at x/D = 2 to 0.62 at x/D = 14. This seems reasonable since the flow is very organized close to the exit of the jet and becomes less organized as the flow moves downstream. It was found that $\tilde{T}_o$ was usually about 10% of $\tilde{m}$. It is therefore possible to neglect $\tilde{T}_o$ and directly approximate $\tilde{m}$ by

$$\tilde{m} \doteq \frac{1}{A_m} \frac{e'_{rms}}{E} \tag{7}$$

for relatively large values of overheat. Figure 91 shows data in which this approximation was used to determine the axial growth of the fluctuations in the Mach number 2.1 jet. Also shown in the figure are the values of $\tilde{m}$ as determined from using the second order curve fit. The amount of error due to the approximation of Equation (7) is small. Therefore, this approximation was used in most of the hot-wire data reduction.

Crossed Hot-Wire Probe Measurements

A data reduction technique similar to the one used by Rose (58) was used for the crossed hot-wire probes. The crossed hot-wires were matched so that A_m and A_v were approximately the same for each wire. The output of the two wires were then instantaneously added and subtracted so that the two resulting voltages would be proportional to $\frac{m'}{\bar{m}}$ and $\frac{v'}{\bar{u}}$. Hence, neglecting stagnation temperature fluctuations:

$$(e'_1 - e'_2)_{rms} = (E_1 A_{v_1} + E_2 A_{v_2}) \left(\frac{v'}{\bar{u}}\right)_{rms} \tag{8}$$

$$(e'_1 + e'_2)_{rms} = (E_1 A_{m_1} + E_2 A_{m_2}) \tilde{m} \tag{9}$$

When this technique was used and the results for $\tilde{m}$ versus x/D were compared to the measurements made using a normal wire, the crossed hot-wire data was low in amplitude by 10 db. The reason for this discrepancy is that when the crossed hot-wire probes were operated by two Disa 55D05 constant temperature anemometers, the frequency response was only 4 kHz. If the 55M01 anemometer was used the hot-wires had a frequency response in excess of 40 kHz. However, since only one 55M01 anemometer was available and two anemometers were needed to operate the probes, it was decided to apply a correction factor to the measurements made using the 55D05 anemometers. For a 5μ wire the typical roll off due to frequency response is about 6 db/octave. The majority of the flow fluctuations occur at or below 12.5 kHz in the 9mm Mach 2.5 jet when excited at St = 0.18. The response of the hot-wire is down 13 db at 12.5 kHz due to the limited frequency response. It therefore seems reasonable that the 10 db drop in the measured values of the mass velocity fluctuations is due to the limited frequency response of the anemometers. In order to obtain an approximation of the amplitude of the radial flow fluctuations 10 db was added to the measured values of $\tilde{m}$ and $\tilde{v}$ so that $\tilde{m}$ measured by the crossed wire probe would be the same as $\tilde{m}$ measured by the normal hot-wire. The corrected results are presented in the main body of the report.

For shear flows with a large amount of velocity fluctuations it is common practice (63) through (67) to assume that the pressure fluctuations are negligible in comparison with the fluctuations in velocity, density and temperature. With this assumption the following relationships can be derived for the computations of the velocity, temperature and density fluctuations:

$$\tilde{u}^2 = \frac{1}{(s + b)^2} [\tilde{T}_o^2 + 2sR_{mT_o} \tilde{m} \tilde{T}_o + s^2 \tilde{m}^2] \tag{10}$$

$$\tilde{T}^2 = \tilde{\rho}^2 = \frac{1}{(s + b)^2} [\tilde{T}_o^2 - 2bR_{mT_o} \tilde{m} \tilde{T}_o + b^2 \tilde{m}^2] \tag{11}$$

where

$$s = \frac{1}{1 + \frac{(\gamma-1)}{2} M^2} \tag{12}$$

$$b = (\gamma-1) M^2 s. \tag{13}$$

APPENDIX C

FIGURES

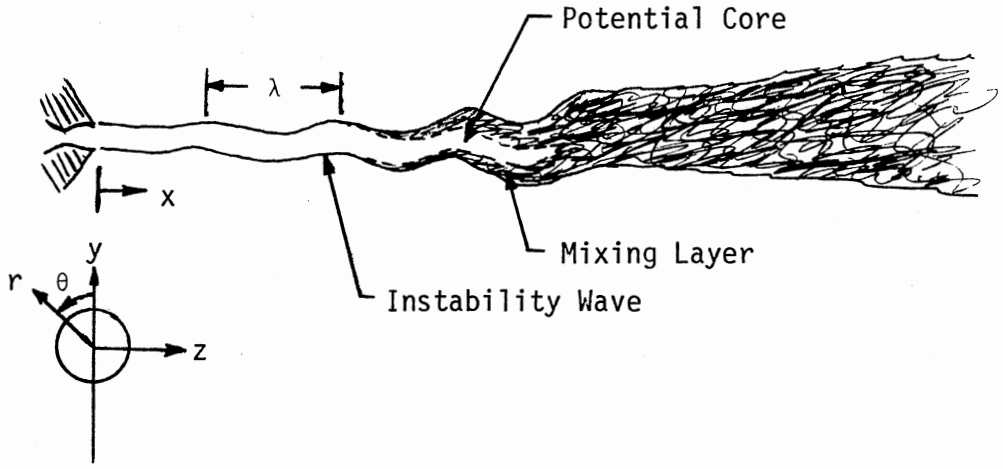

Figure 1. General Features of the Supersonic Jet

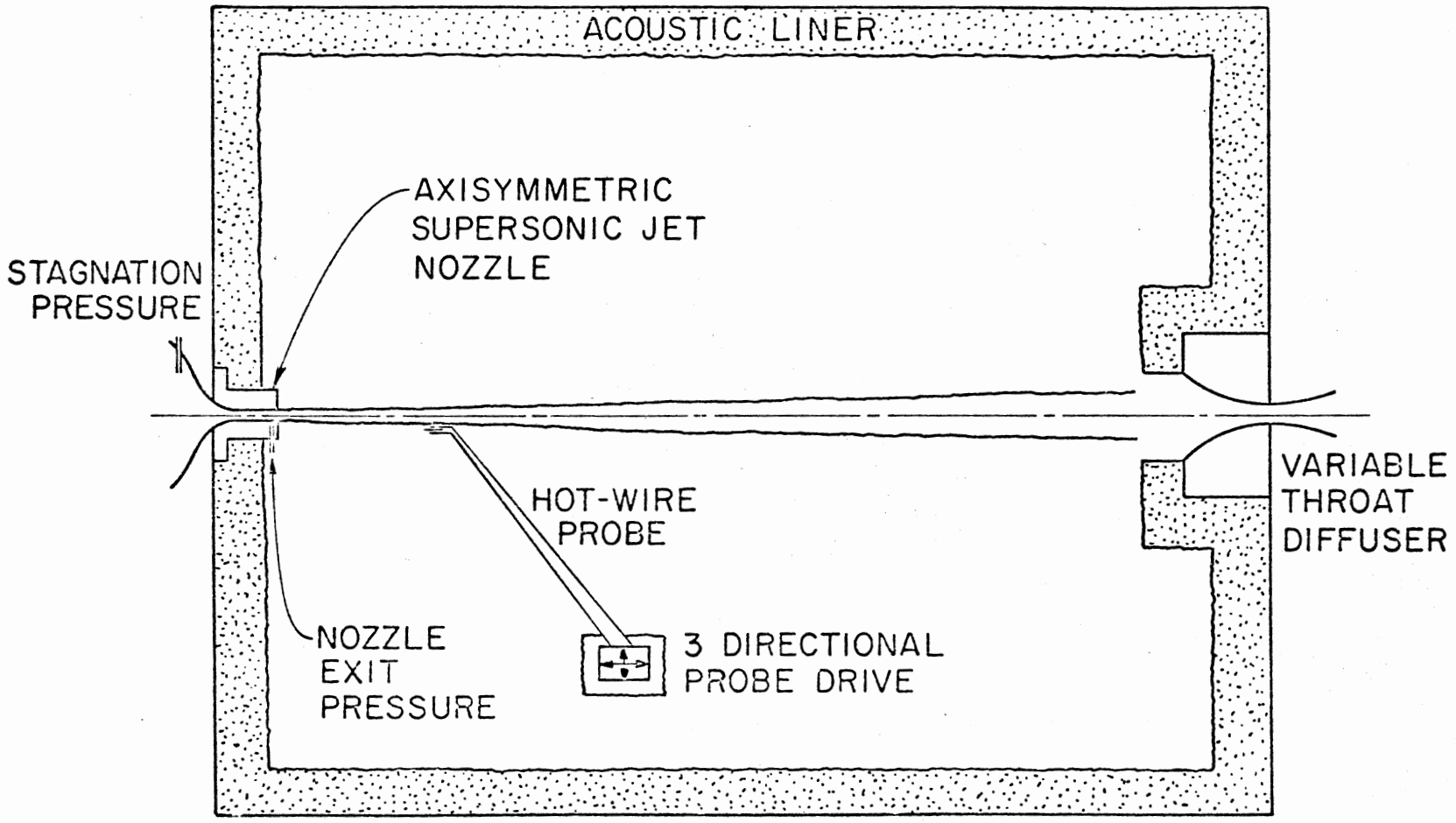

Figure 2. Schematic Diagram of Jet Test Facility

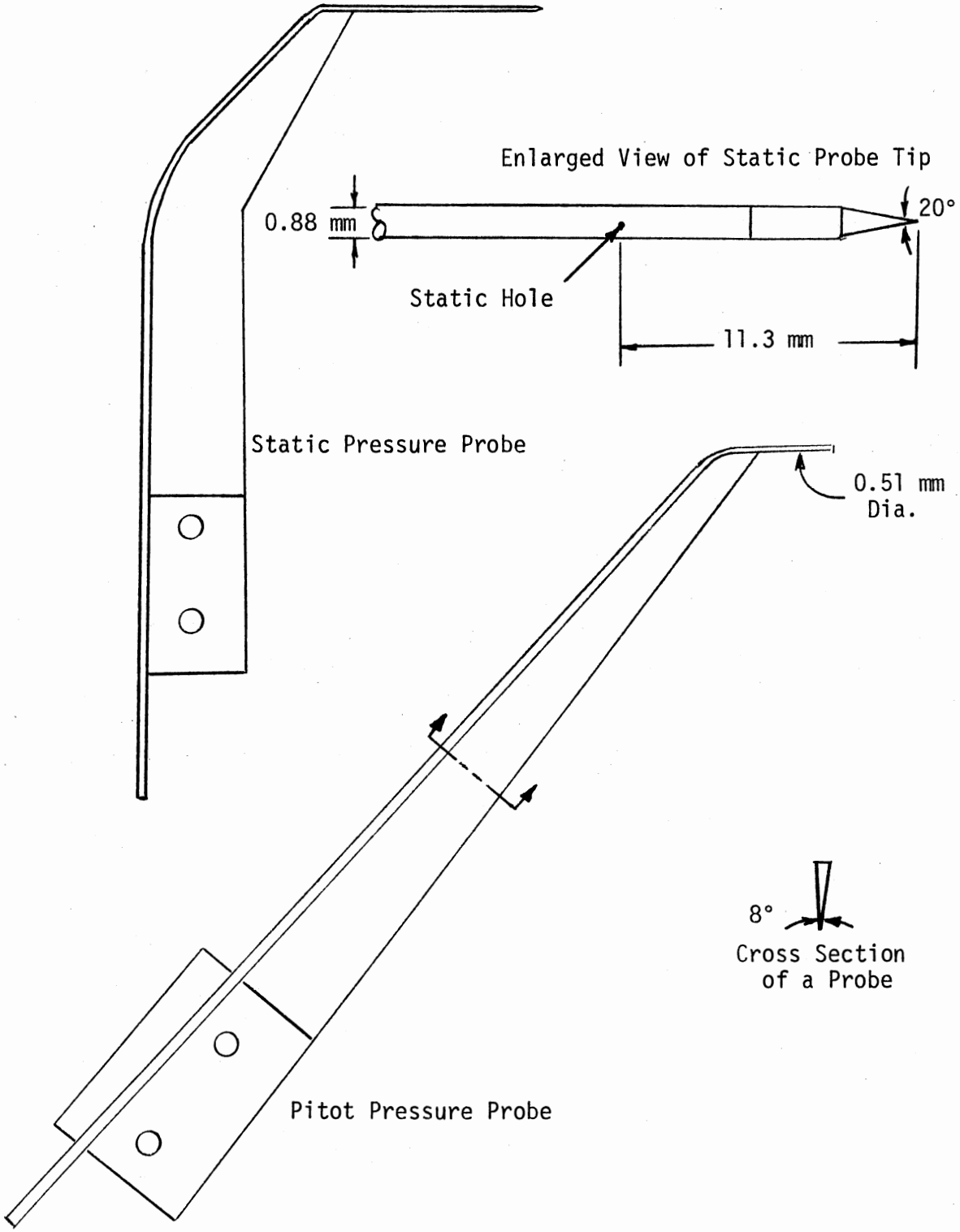

Figure 3. Static Pressure and Pitot Pressure Probes Drawn Full Scale

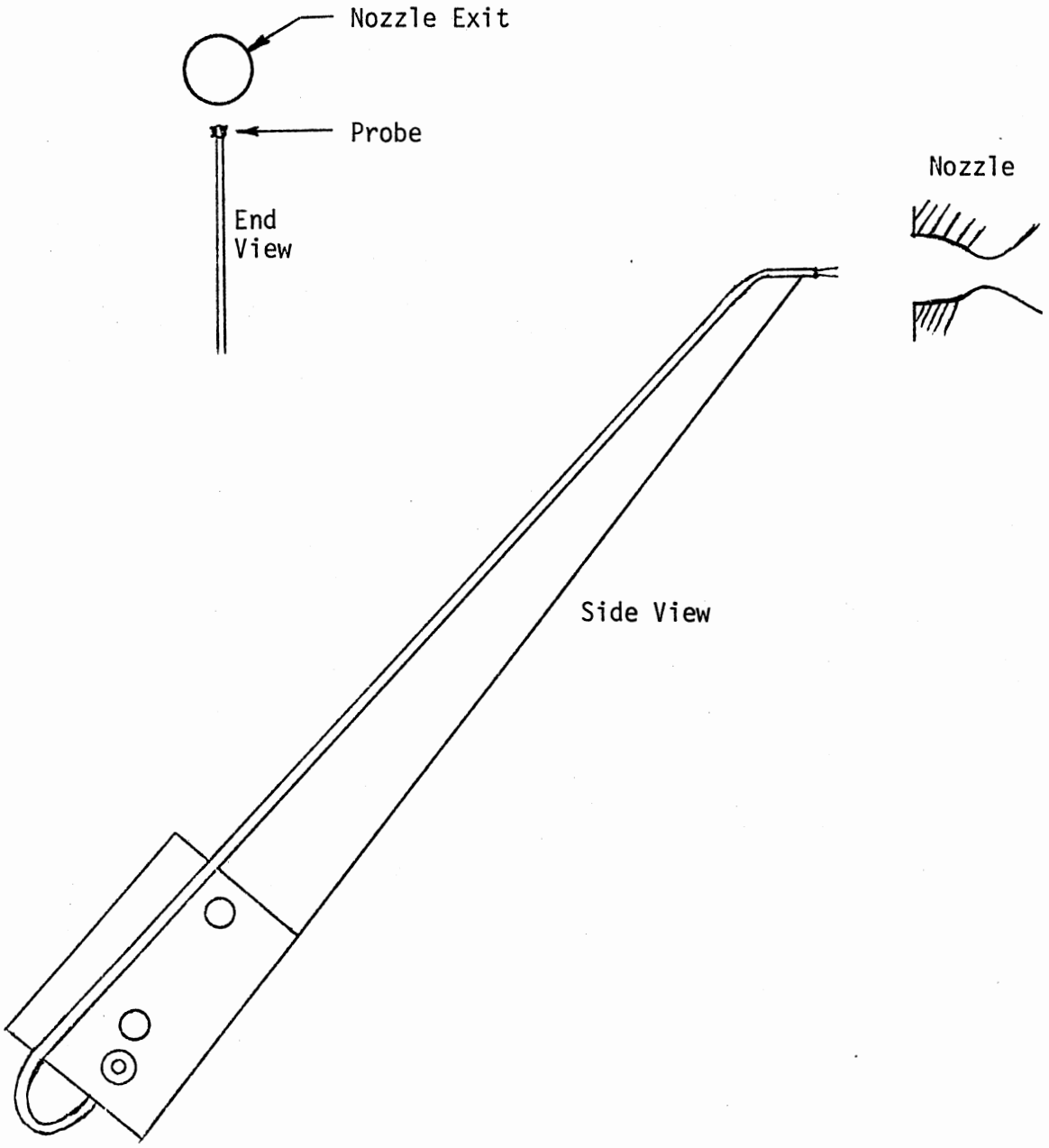

Figure 4. Crossed Hot-Wire Probe, Full Scale

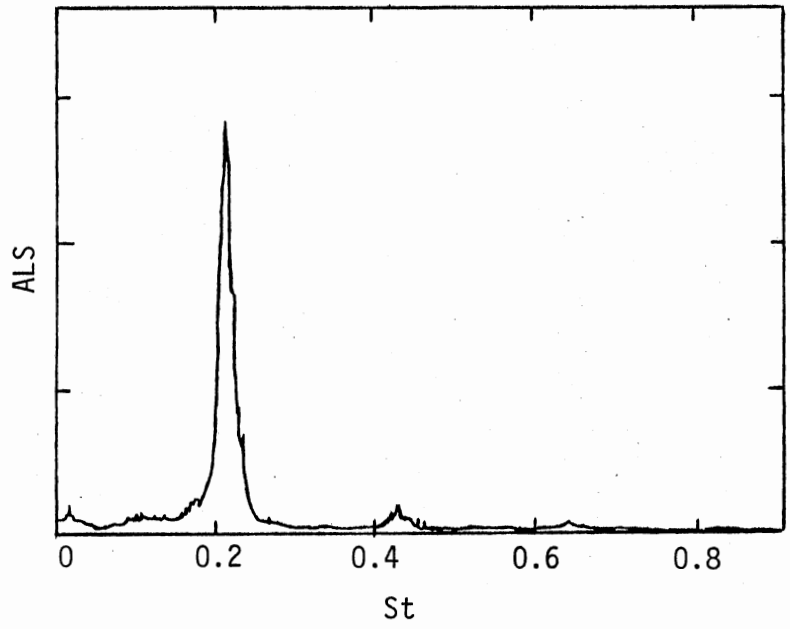

(a) Hot-Wire Spectrum, x/D = 10

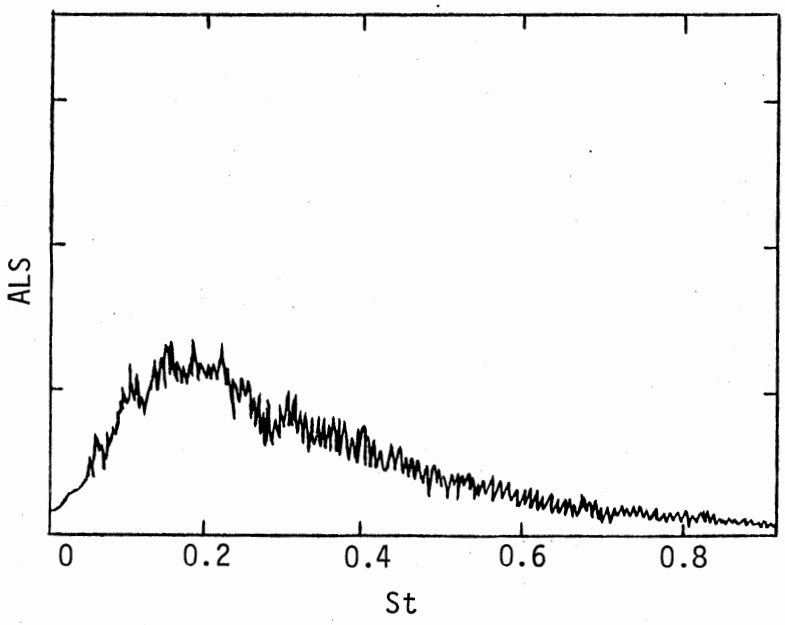

(b) Microphone Spectrum, x/D = 38, y/D - 12

Figure 5. M = 2.1 Spectra, Re_D = 4,900, U/d = 55,800 sec^{-1}, Analyzer Passband = 1 kHz, Sweep Rate = 1 kHz/sec, D = 10 mm

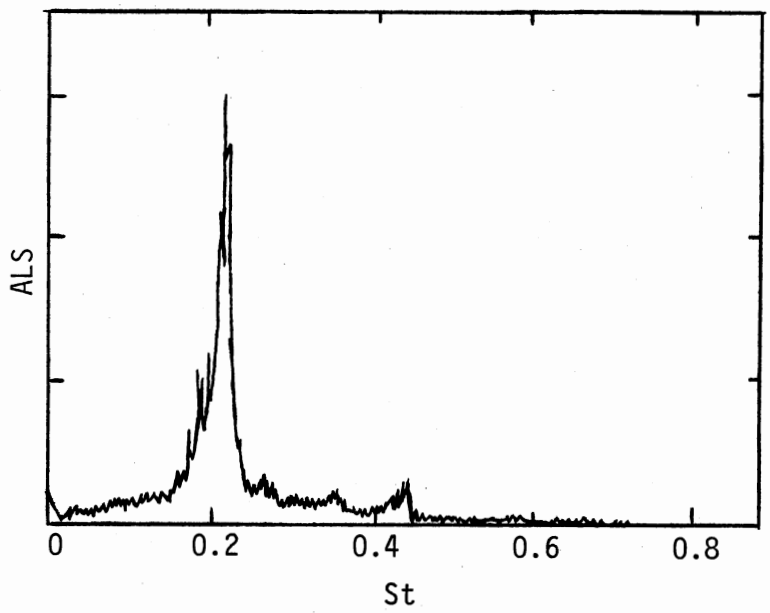

(a) Hot-Wire Spectrum, x/D = 10

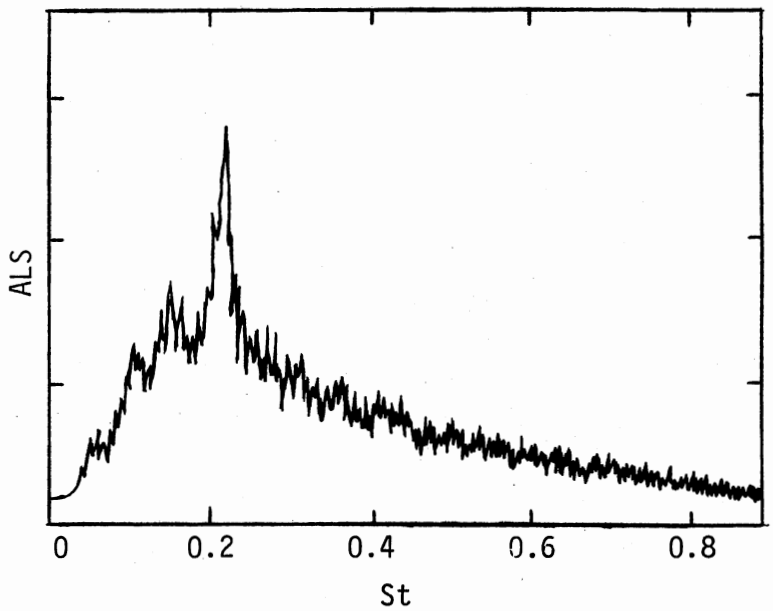

(b) Microphone Spectrum, x/D = 38, y/D = 12

Figure 6. M = 2.1 Spectra, Re = 7,900

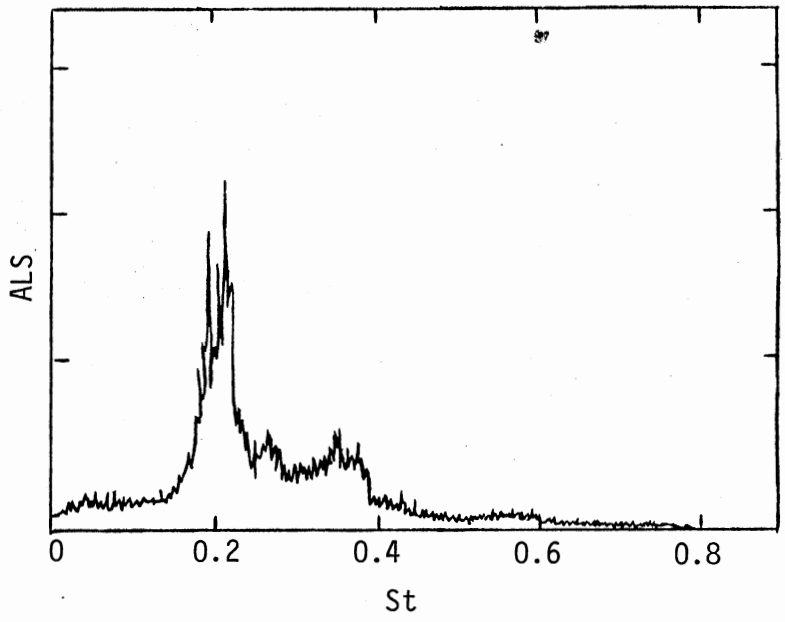

(a) Hot-Wire Spectrum, x/D = 8

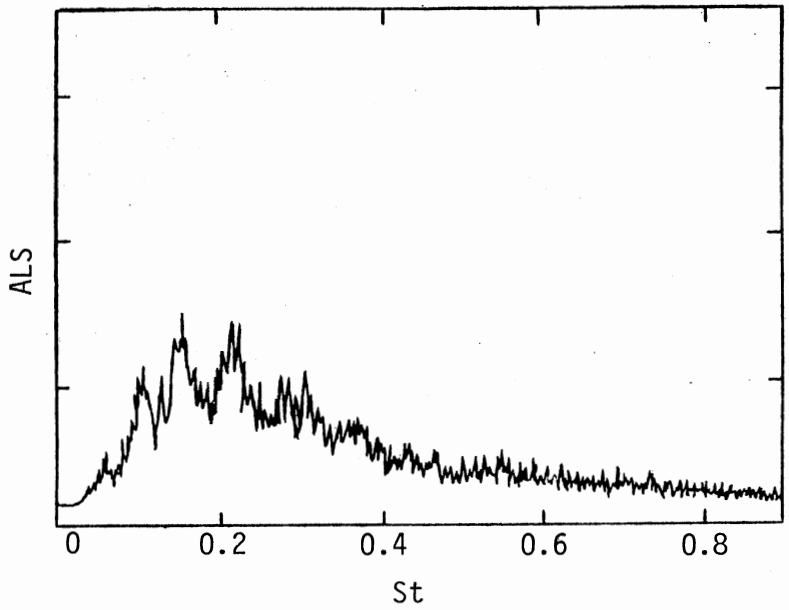

(b) Microphone Spectrum, x/D = 38, y/D = 12

Figure 7. M = 2.1 Spectra, Re = 11,750

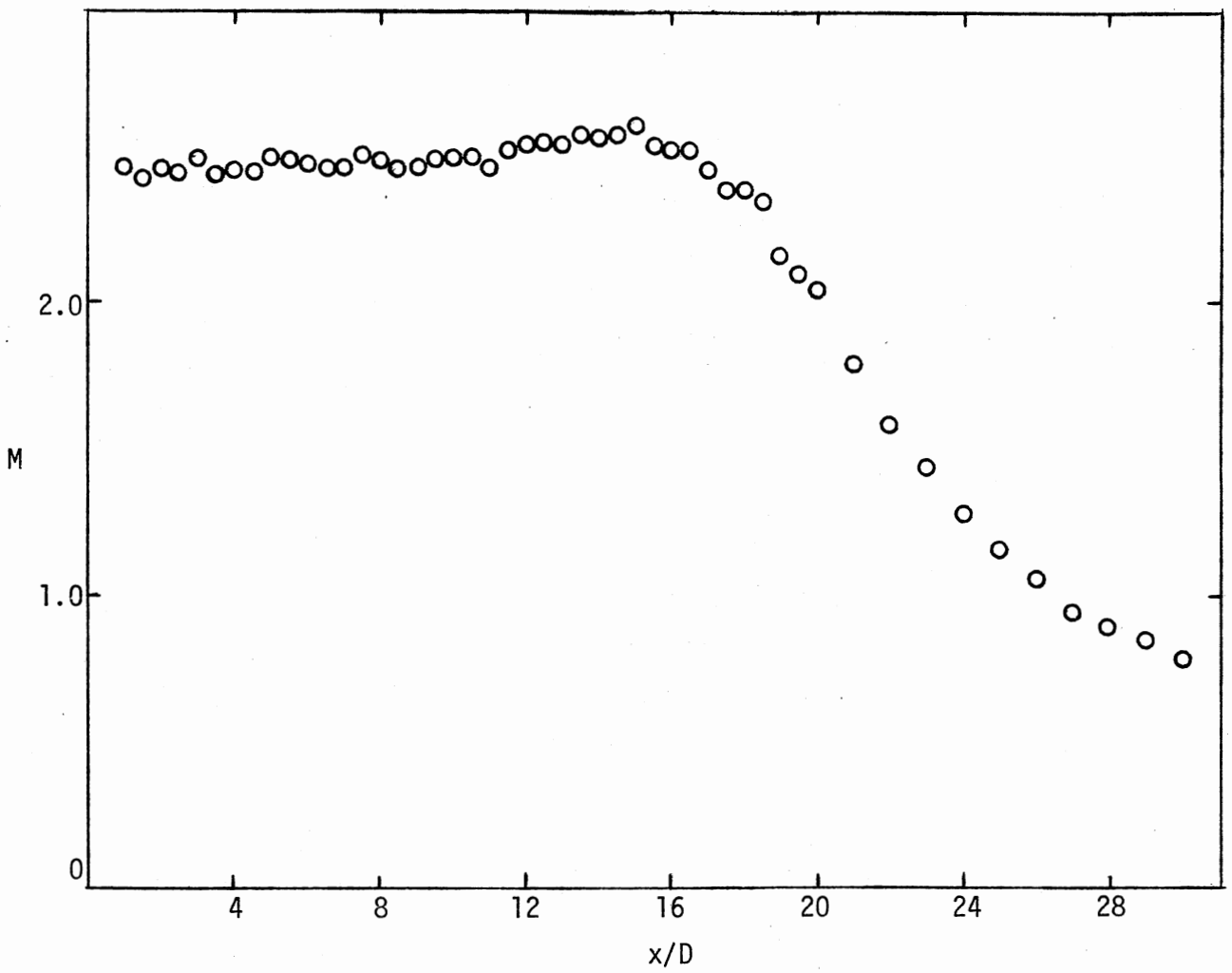

Figure 8. Axial Distribution of the Centerline Mach Number, M = 2.5

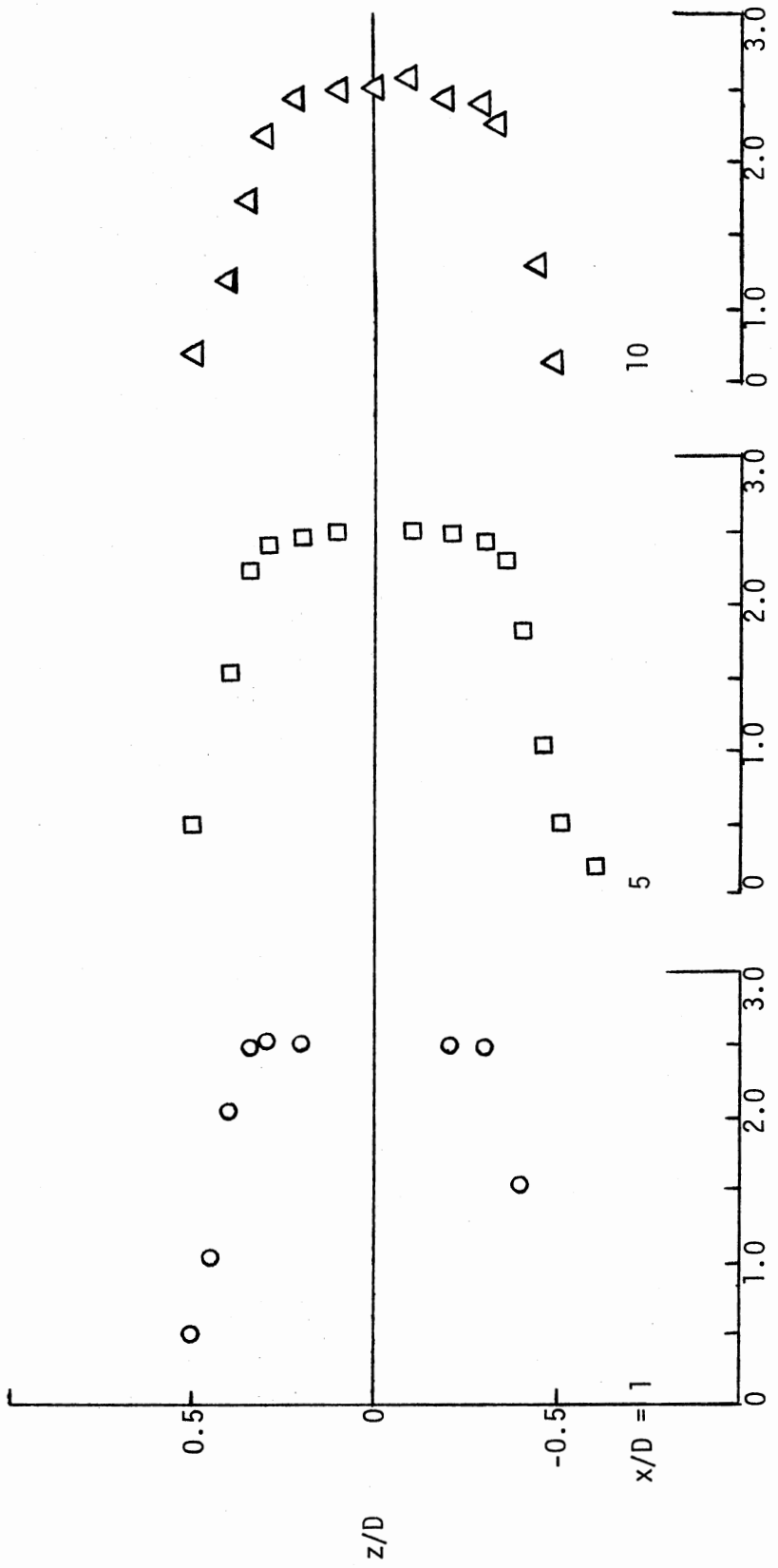

Figure 9. Radial Mach Number Distribution, M = 2.5

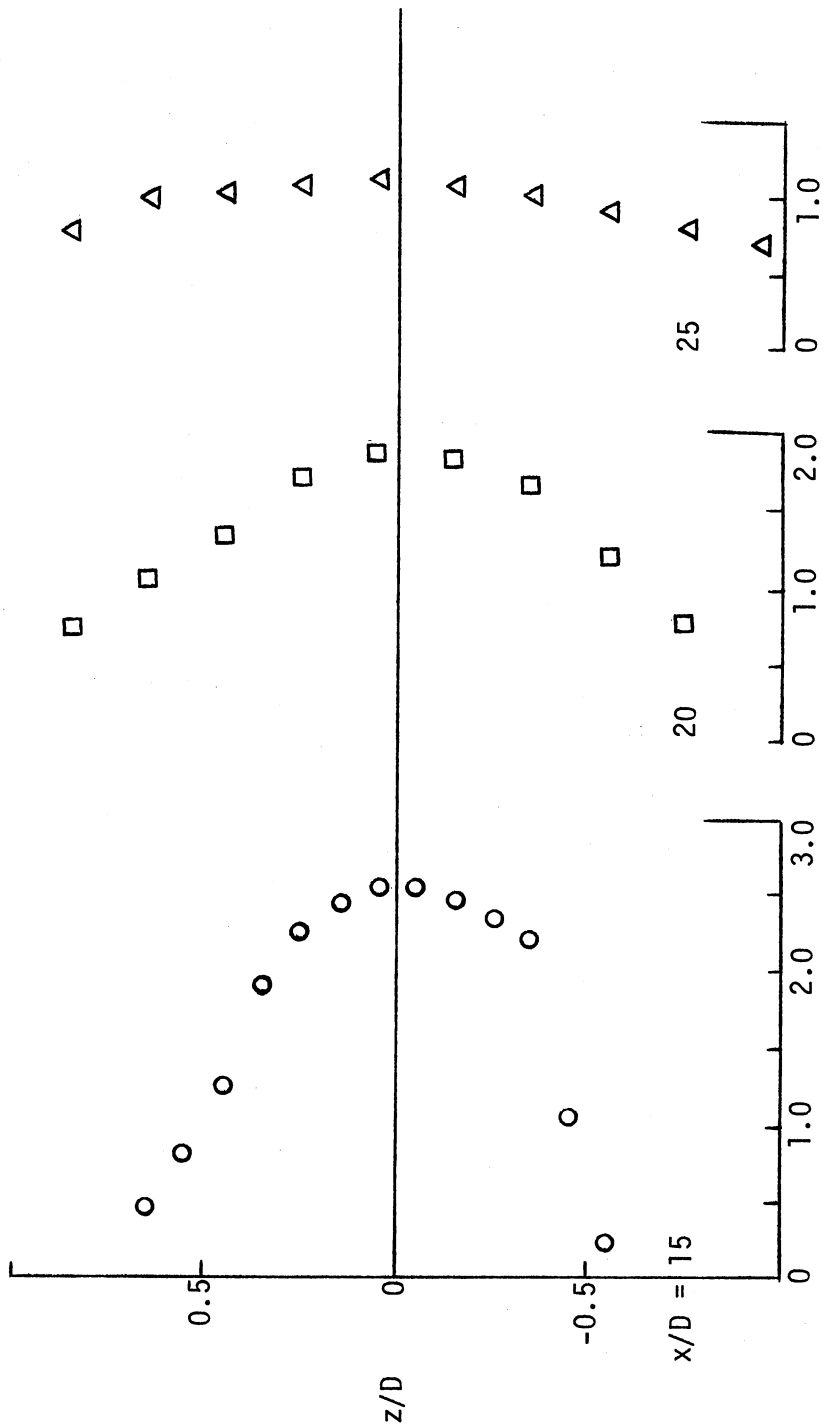

Figure 9. (Continued)

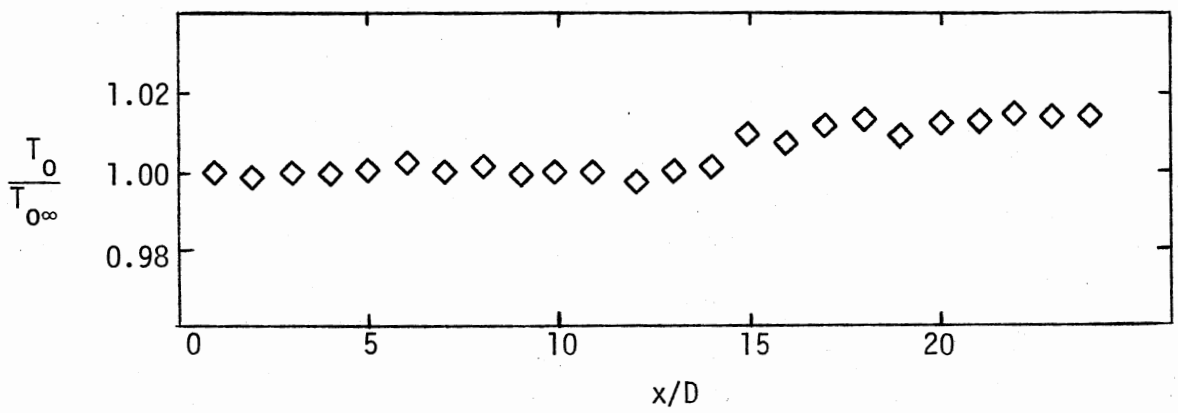

Figure 10. Axial Stagnation Temperature Distribution, M = 2.5

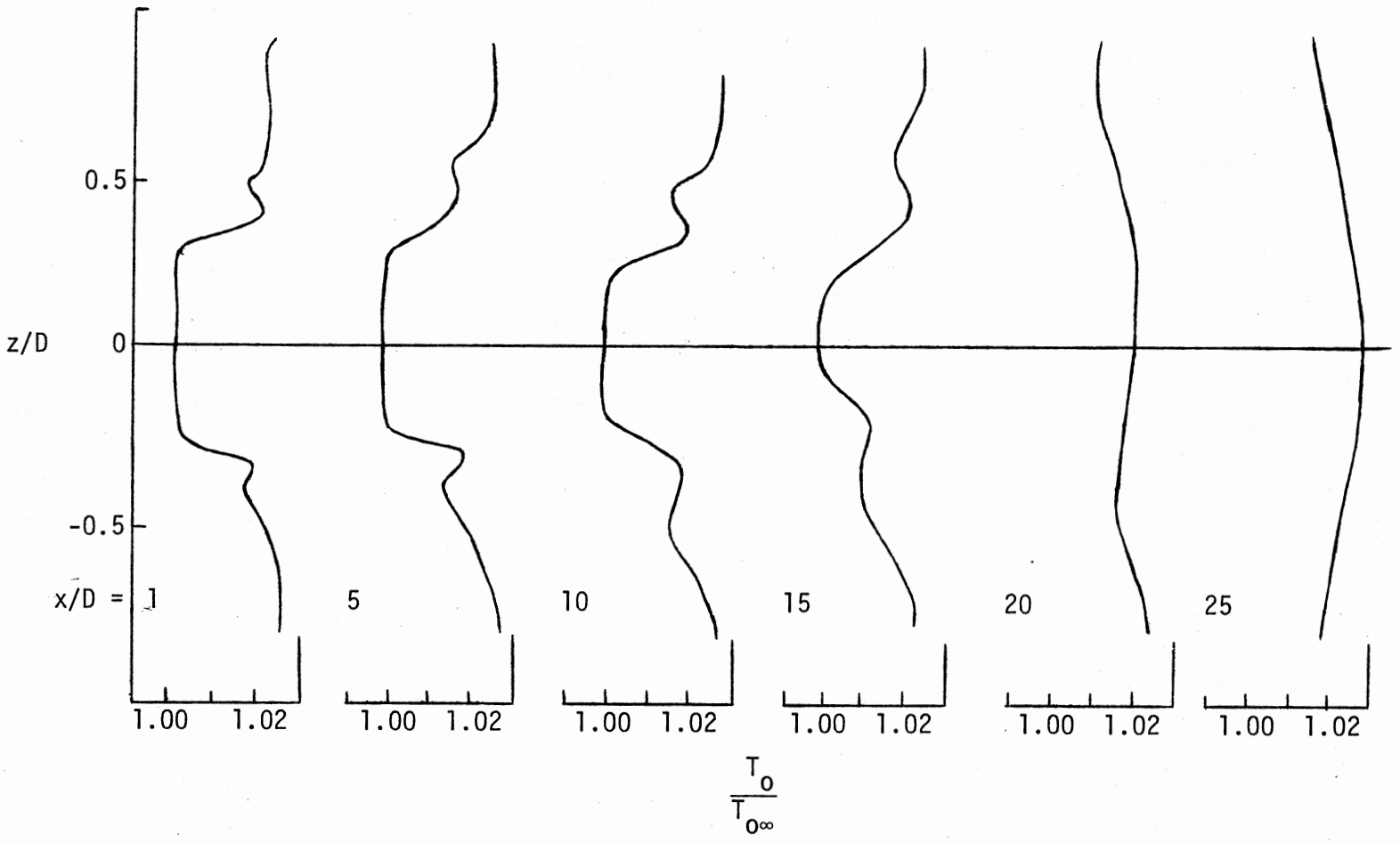

Figure 11. Radial Stagnation Temperature Profiles, M = 2.5

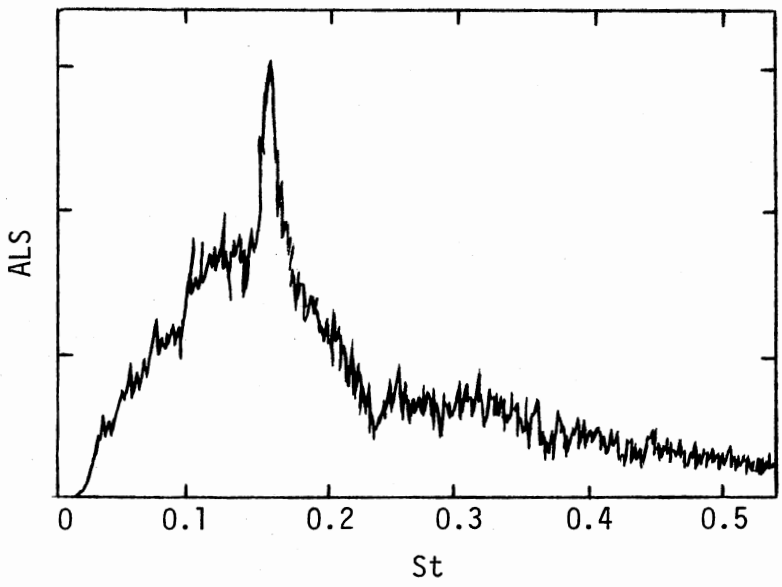

Figure 12. Microphone Spectrum, M = 2.5, x/D = 60, y/D = 32

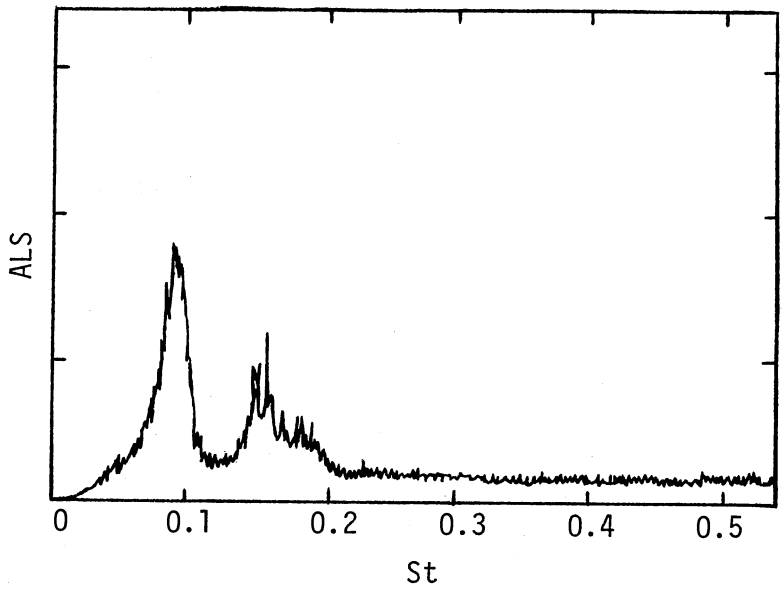

(a) x/D = 1

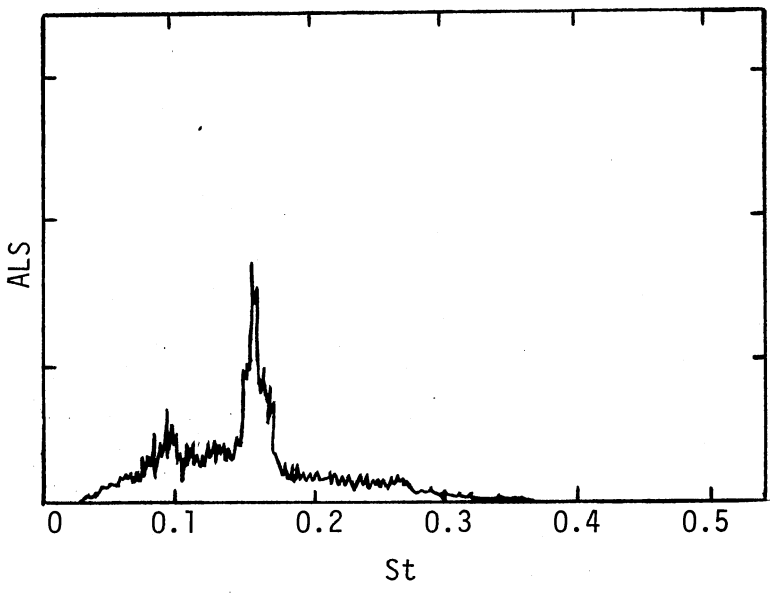

(b) x/D = 5

Figure 13. Hot-Wire Spectra, M = 2.5

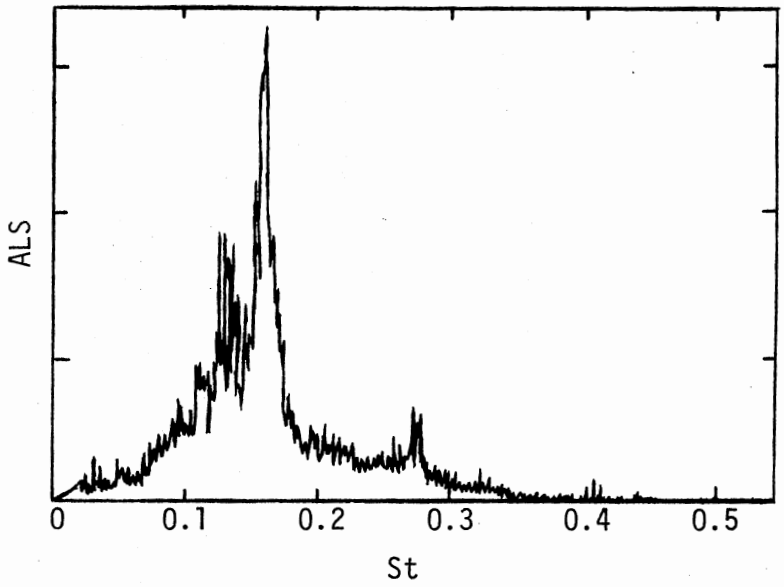

(c) x/D = 10

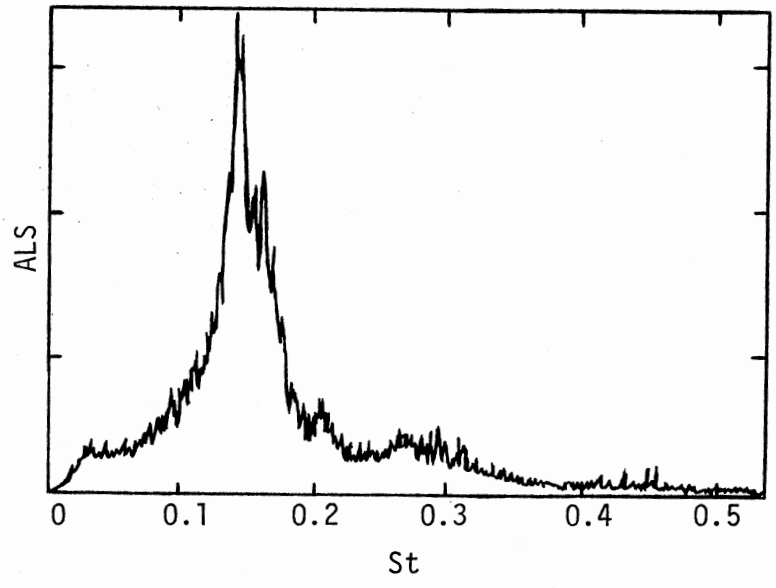

(d) x/D = 15

Figure 13. (Continued)

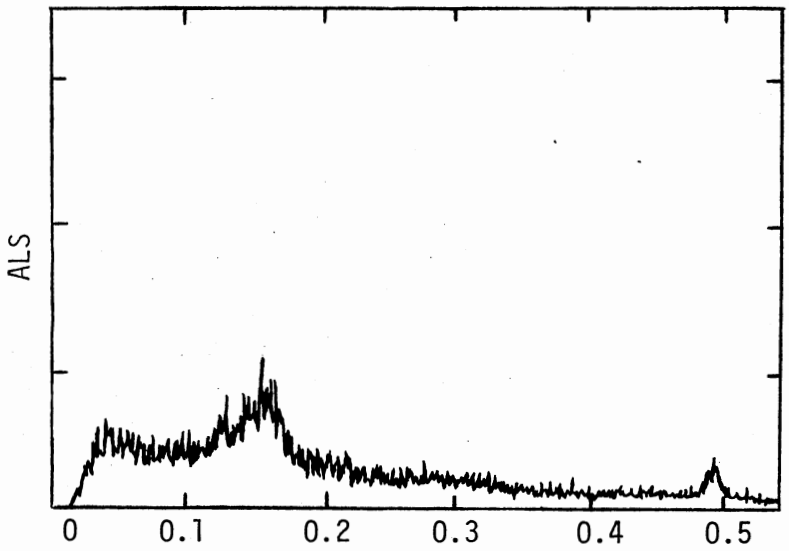

(e) x/D = 19

Figure 13. (Continued)

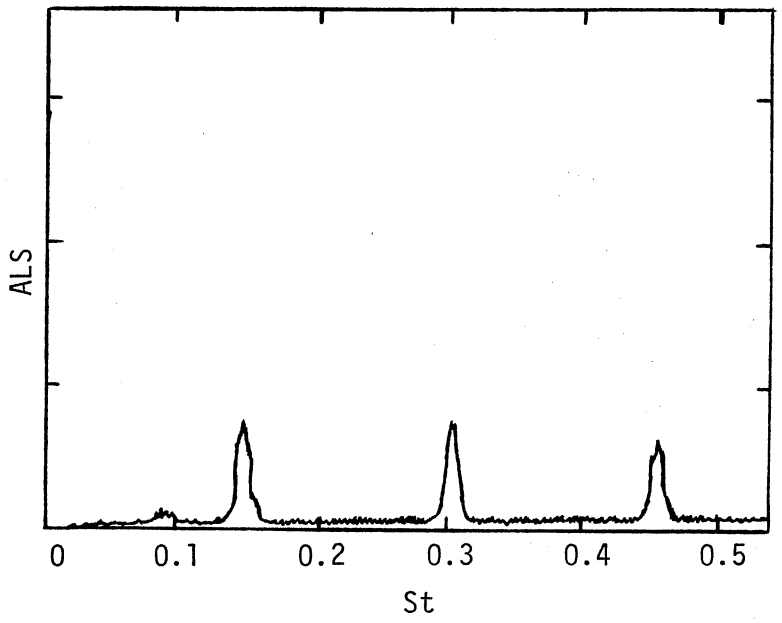

(a) x/D = 1

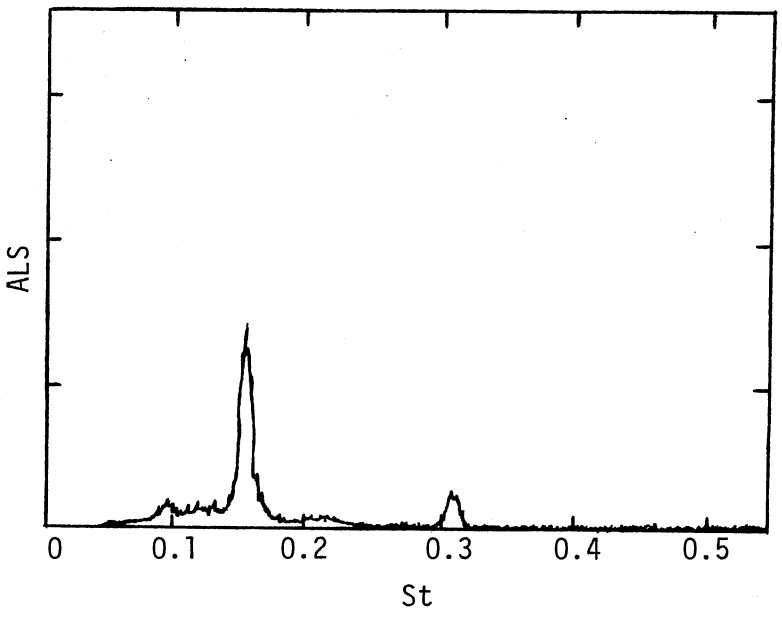

(b) x/D = 5

Figure 14. Hot-Wire Spectra, M = 2.5, Excited at St = 0.16

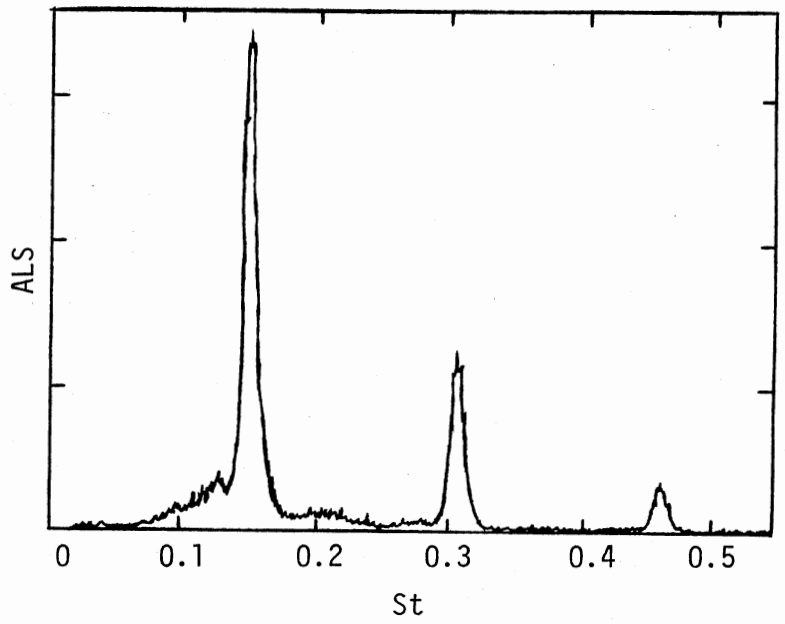

(c) x/D = 10

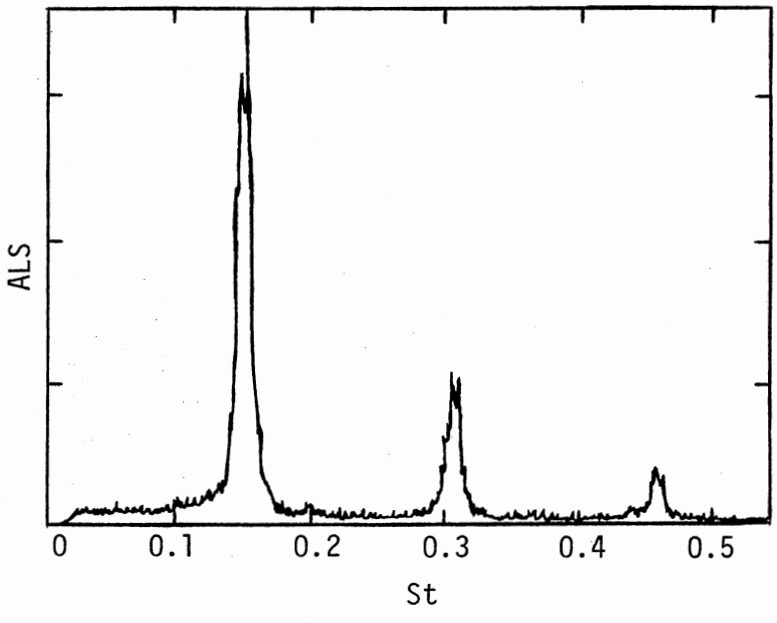

(d) x/D = 15

Figure 14. (Continued)

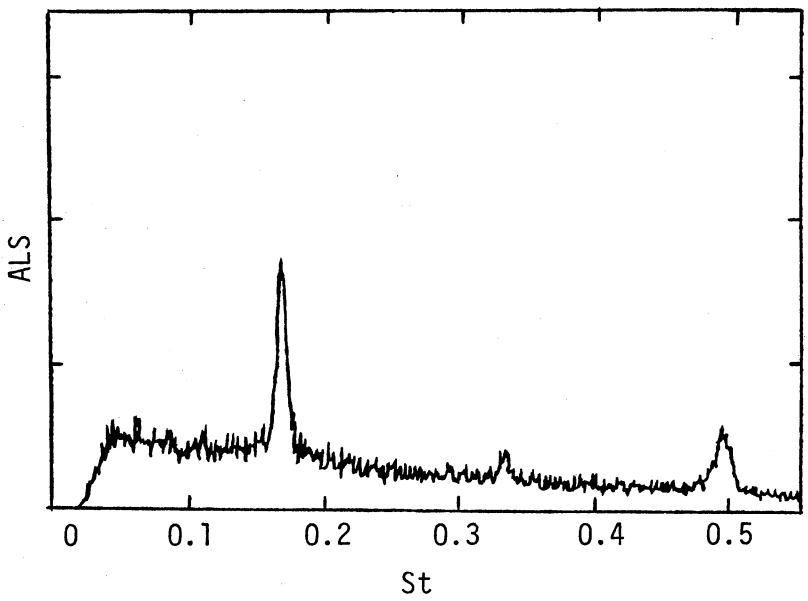

(e) x/D = 19

Figure 14. (Continued)

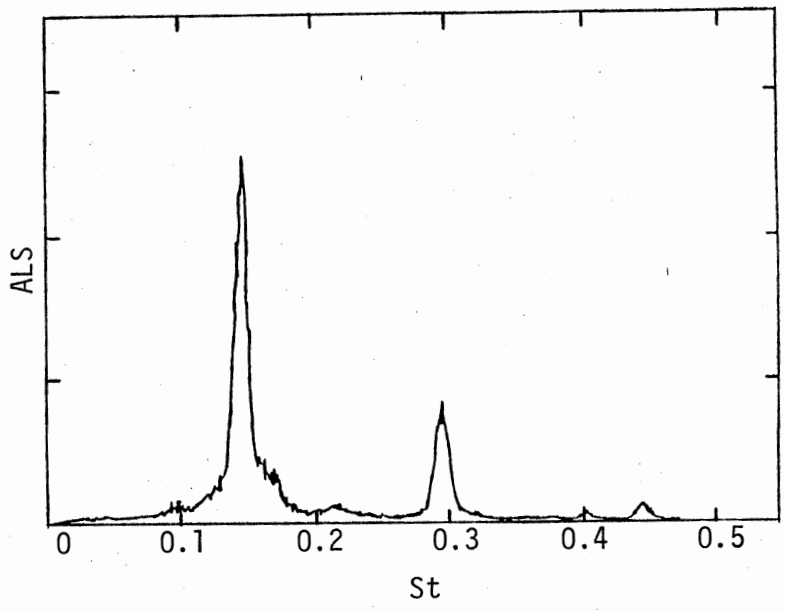

(a) x/D = 10

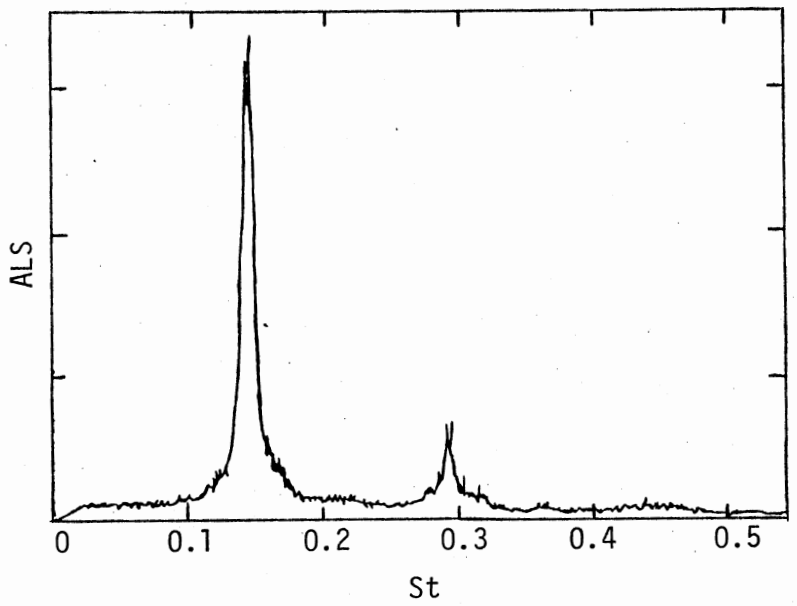

(b) x/D = 15

Figure 15. Hot-Wire Spectra M = 2.5, Excited at St = 0.14

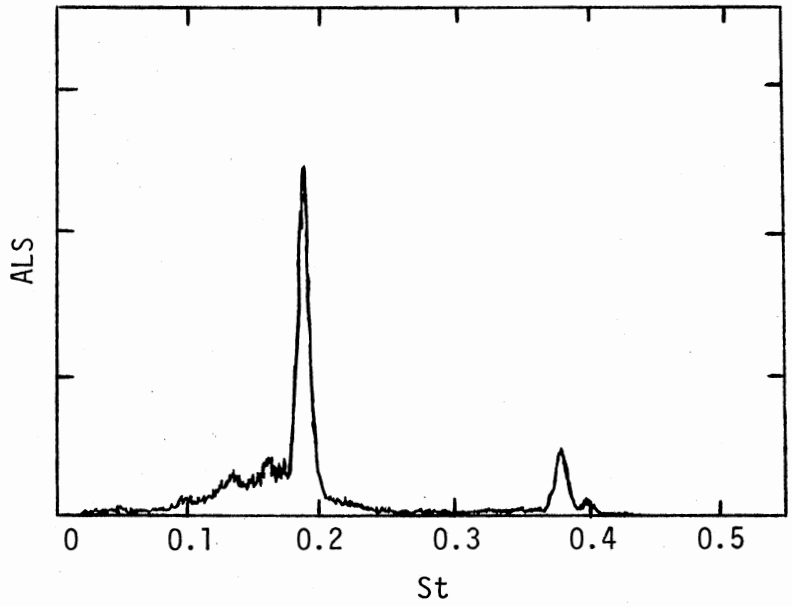

(a) x/D = 10

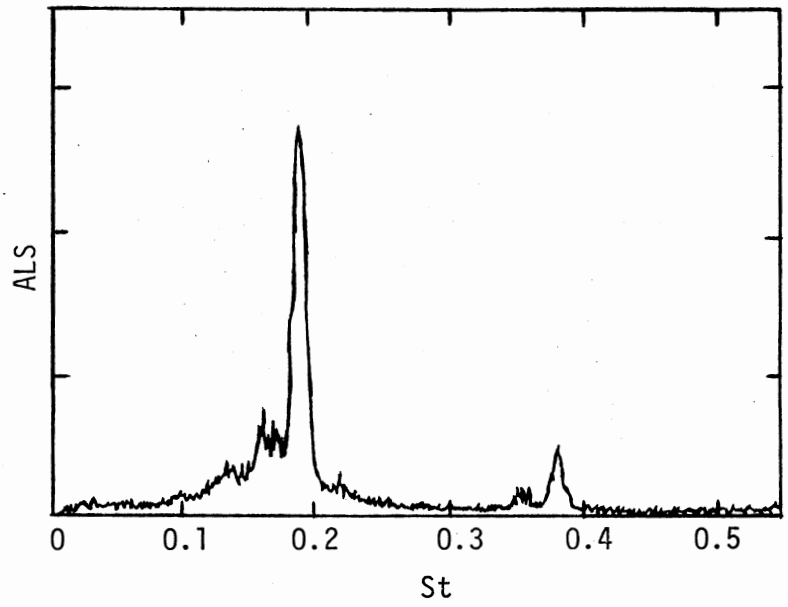

(b) x/D = 15

Figure 16. Hot-Wire Spectra M = 2.5, Excited at St = 0.18

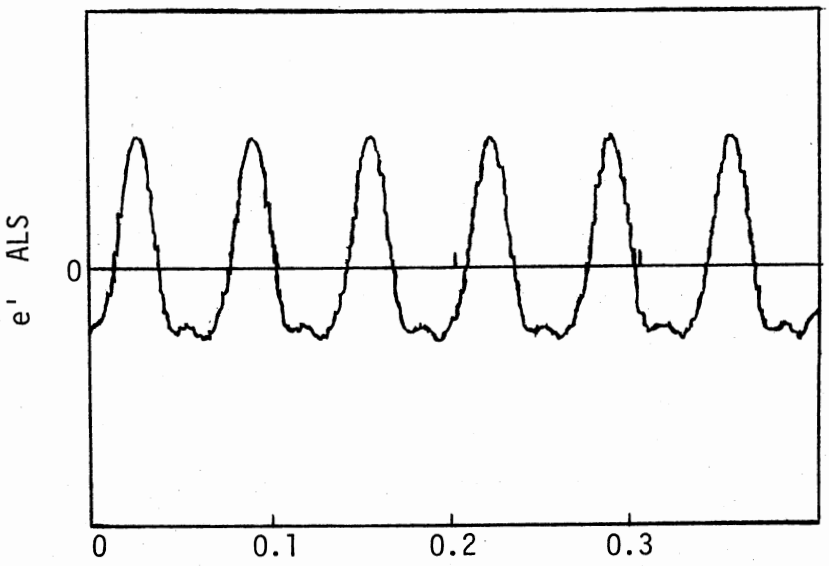

(a) Wave Form

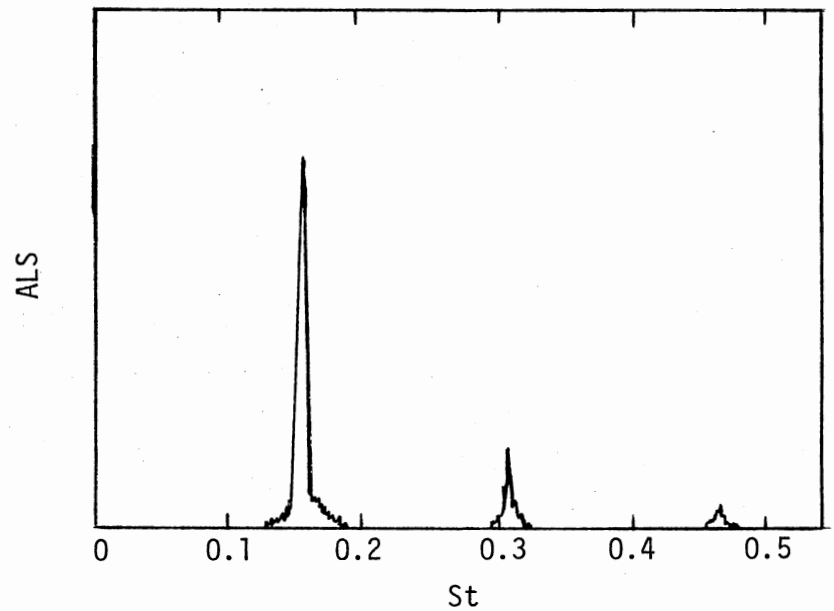

(b) Spectrum

Figure 17. Phase Averaged Hot-Wire Signal Wave Form and Spectrum, M = 2.5 Excited at St = 0.16

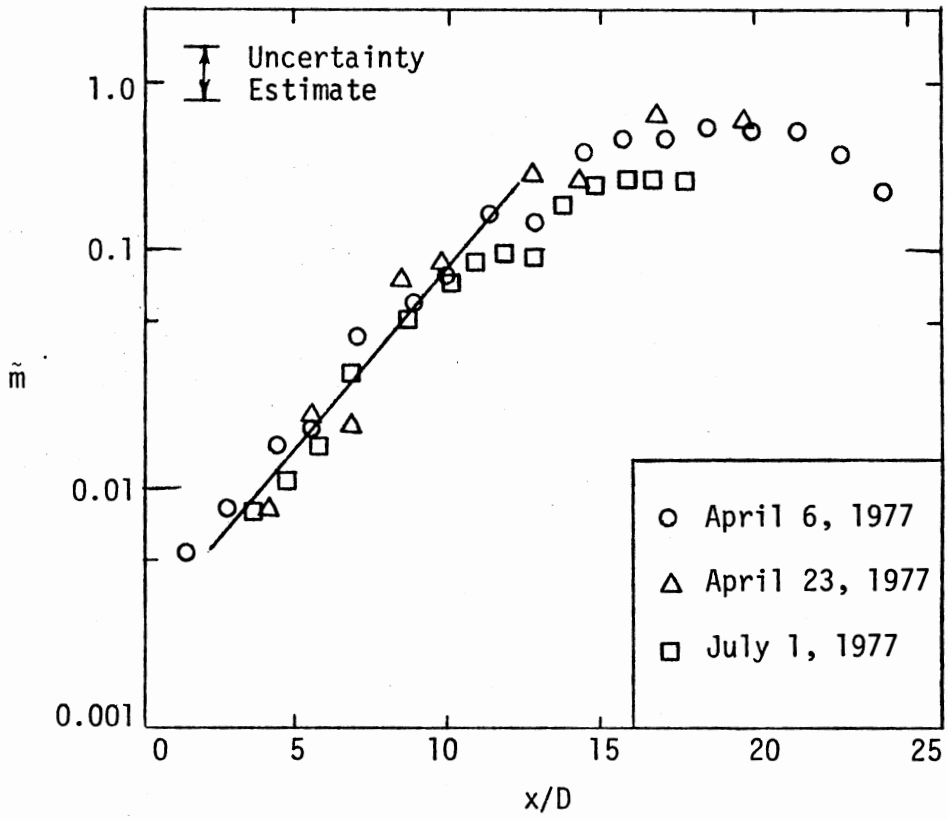

Figure 18. Axial Distribution of Peak $\tilde{m}$, M = 2.5

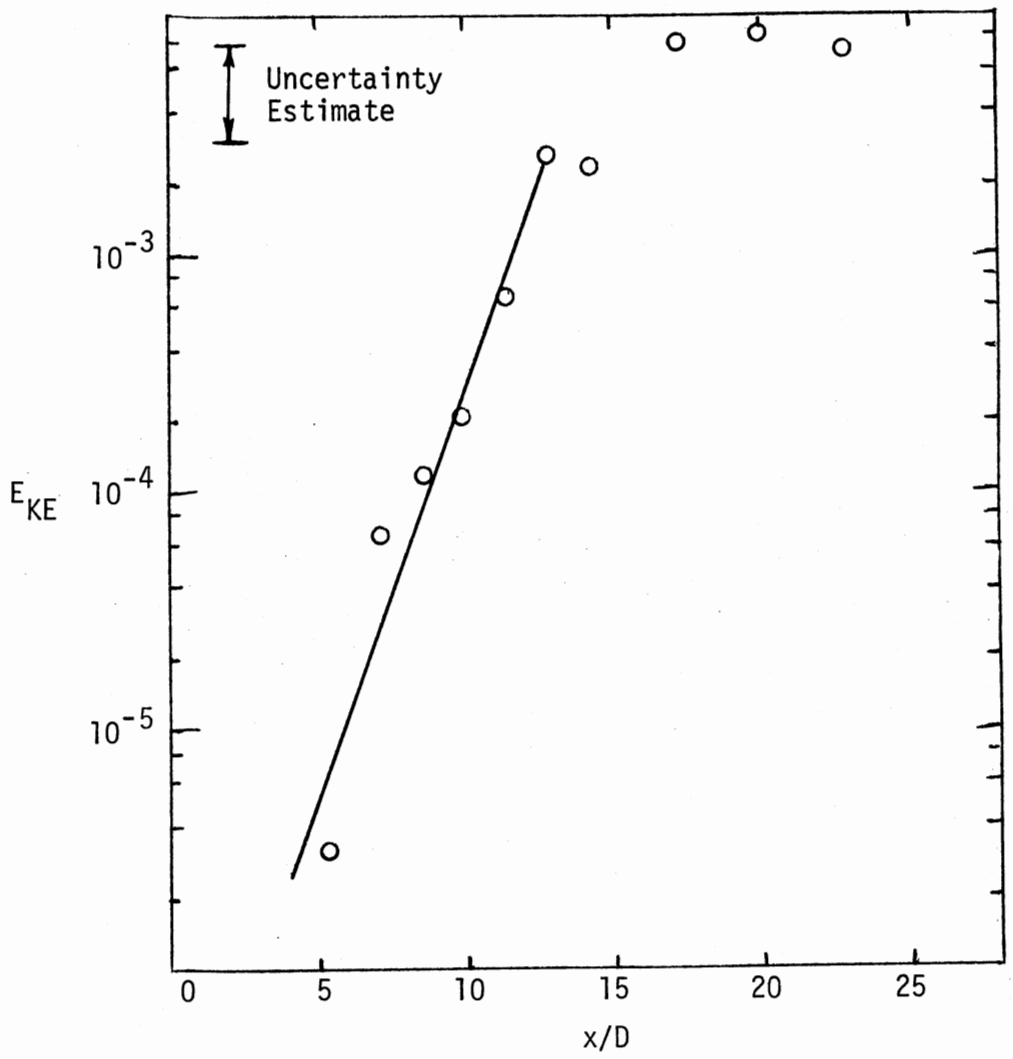

Figure 19. Axial Distribution of E_{KE}, M = 2.5

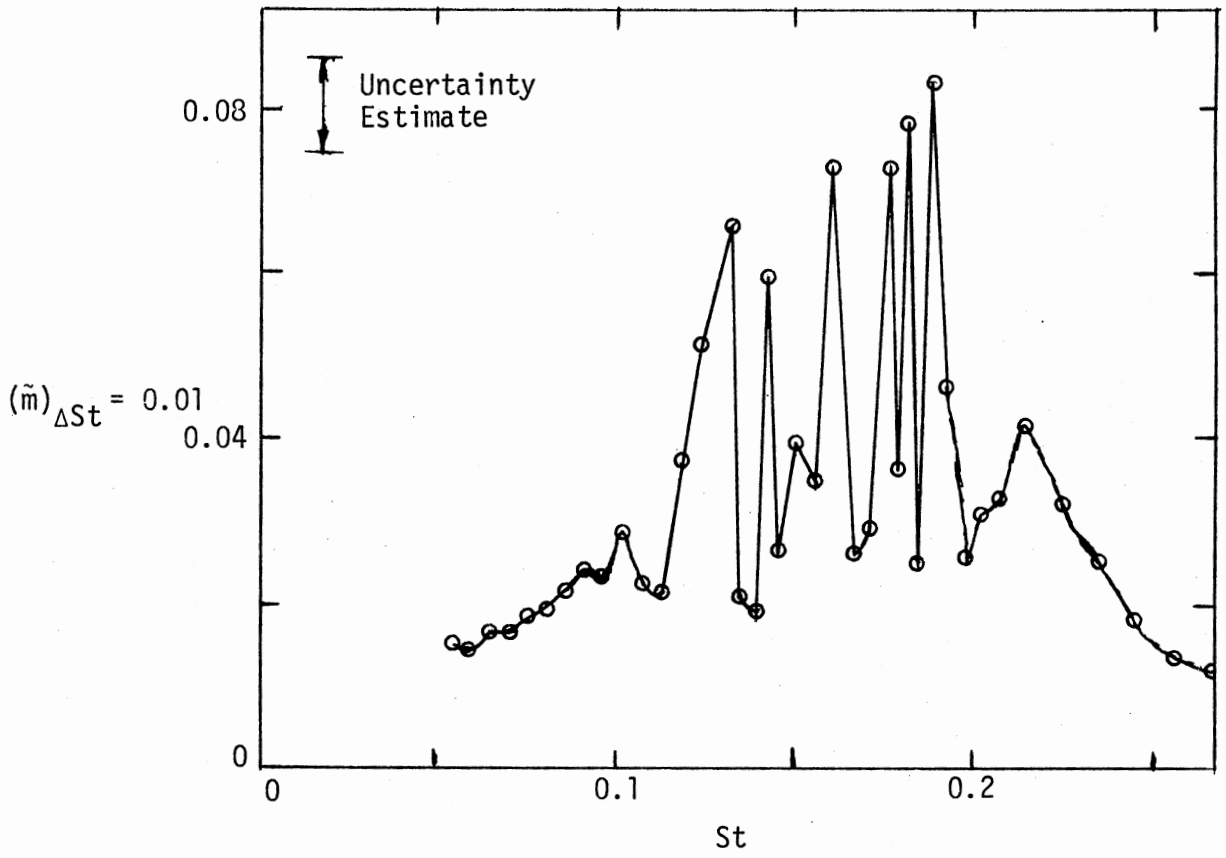

Figure 20. Response of the M = 2.5 Jet to Different Excitation Frequencies, x/D = 10

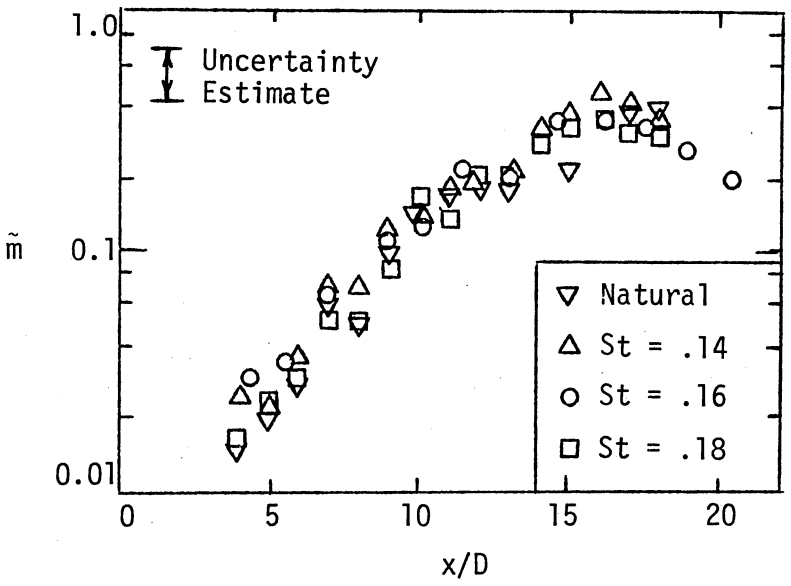

Figure 21. Full Spectrum Flow Fluctuation Amplitude Axial Distribution for Different Excitation Frequencies, M = 2.5

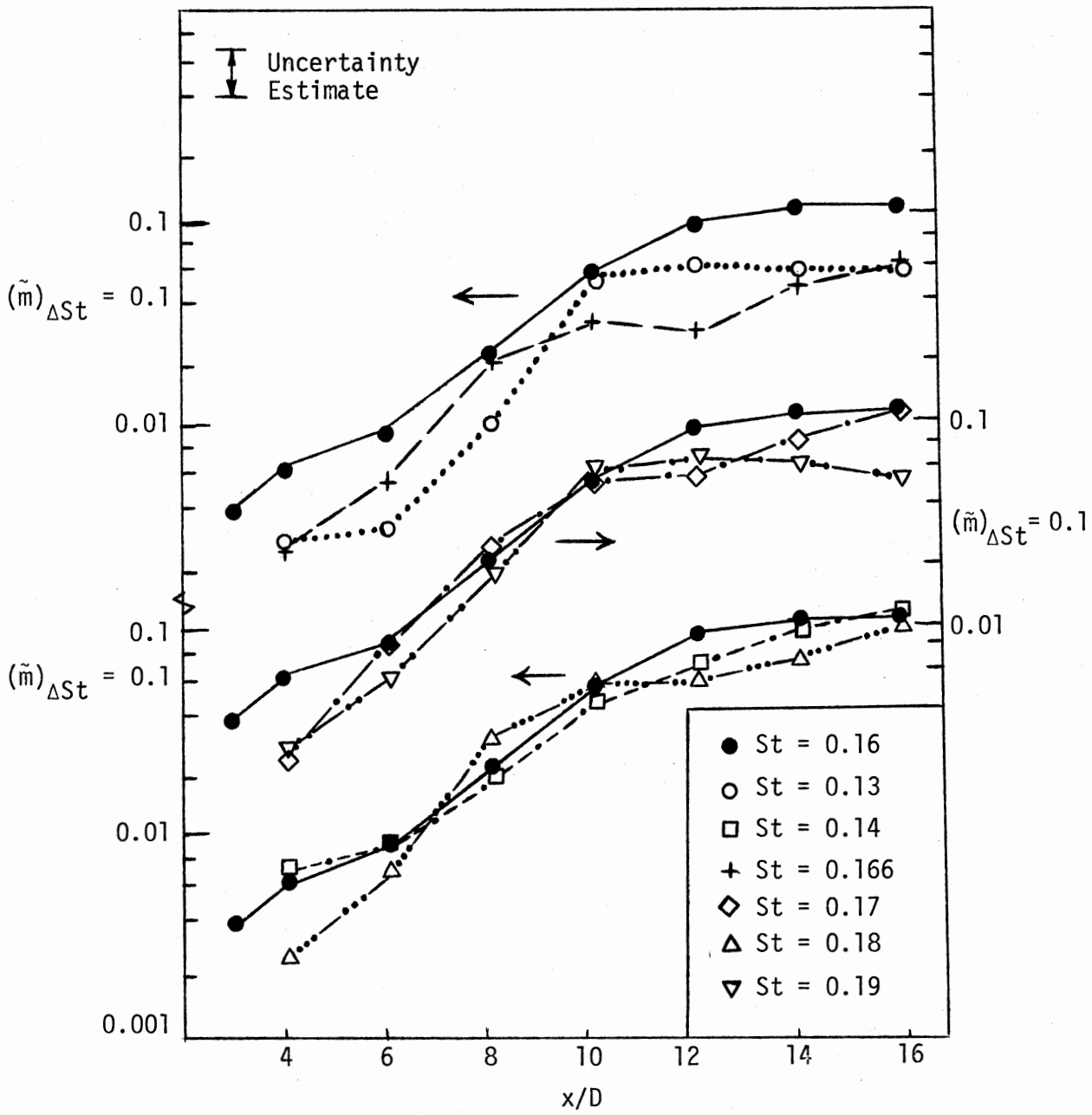

Figure 22. Flow Fluctuation Amplitude Distribution for 1 kHz Band (Δst = 0.01) Centered at the Frequency of Excitation, M = 2.5

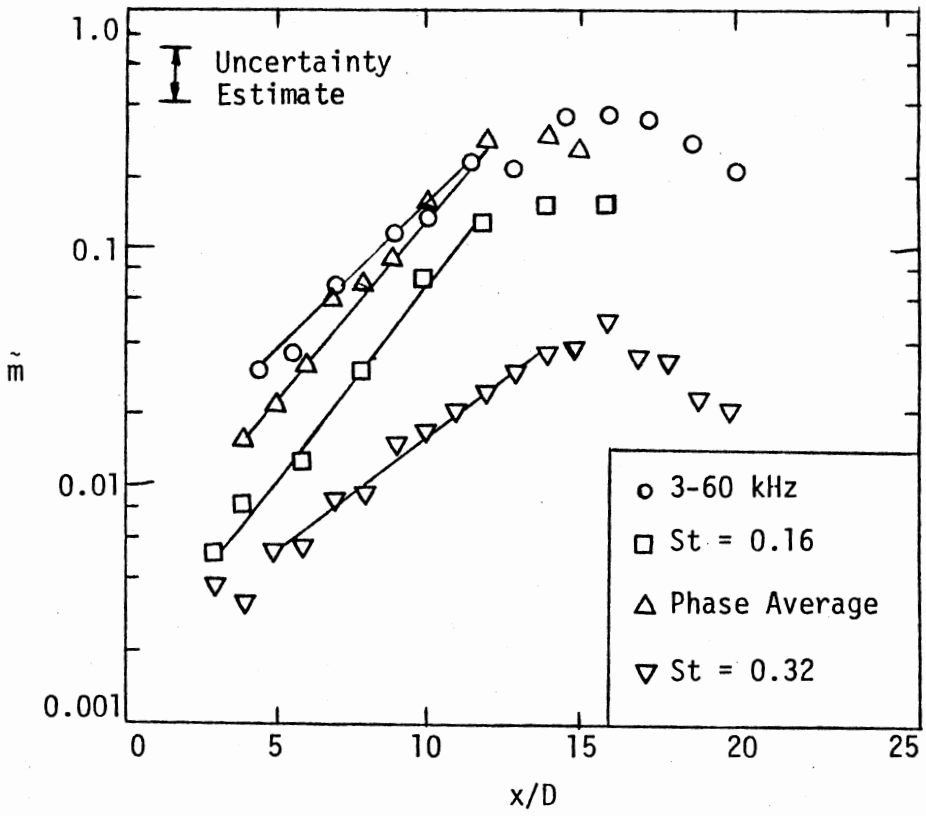

Figure 23. Axial Distribution of $\tilde{m}$ for Different Components, M = 2.5 Excited at St = 0.16

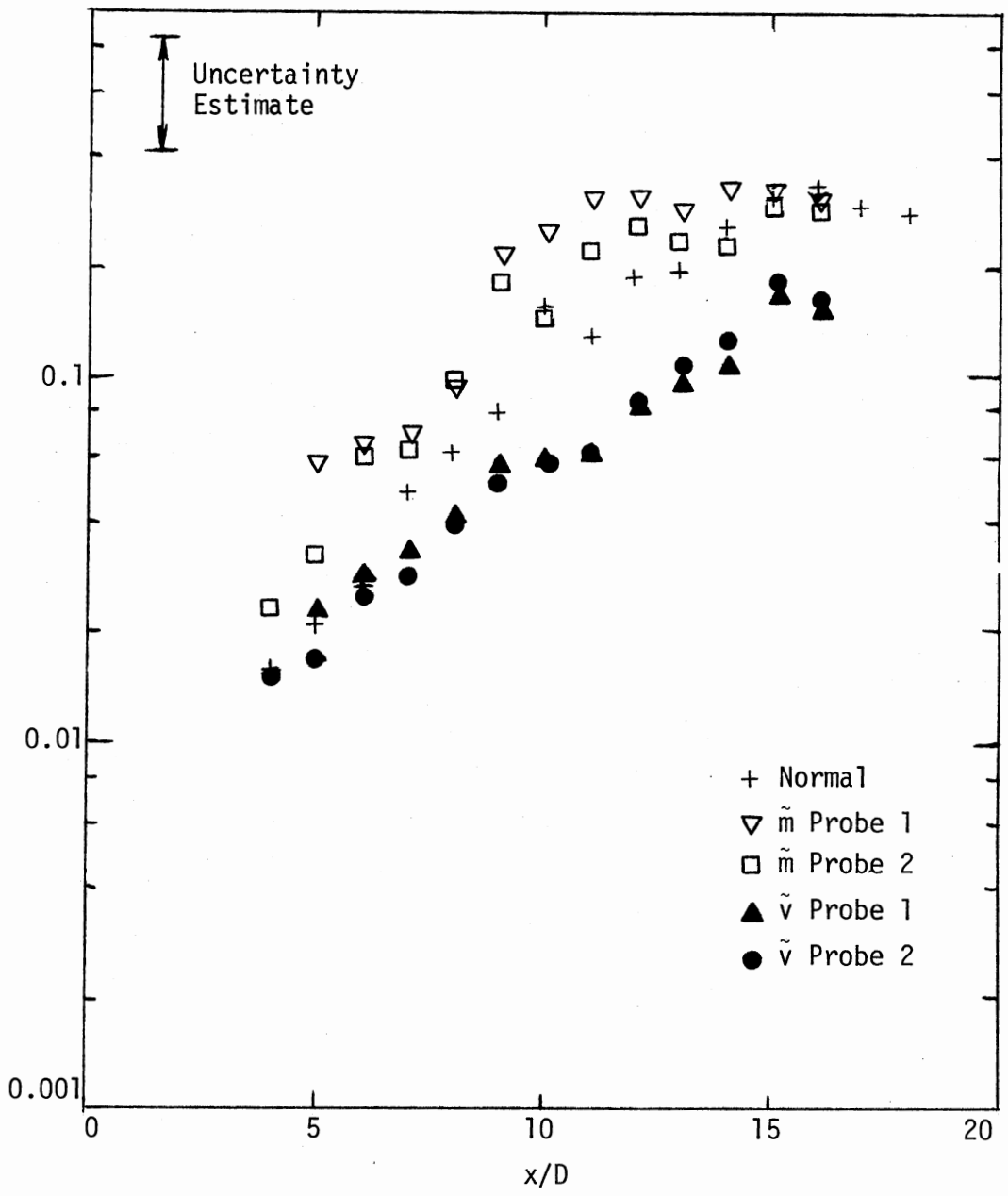

Figure 24. Radial and Axial Flow Fluctuations, M = 2.5 Excited at St = 0.18

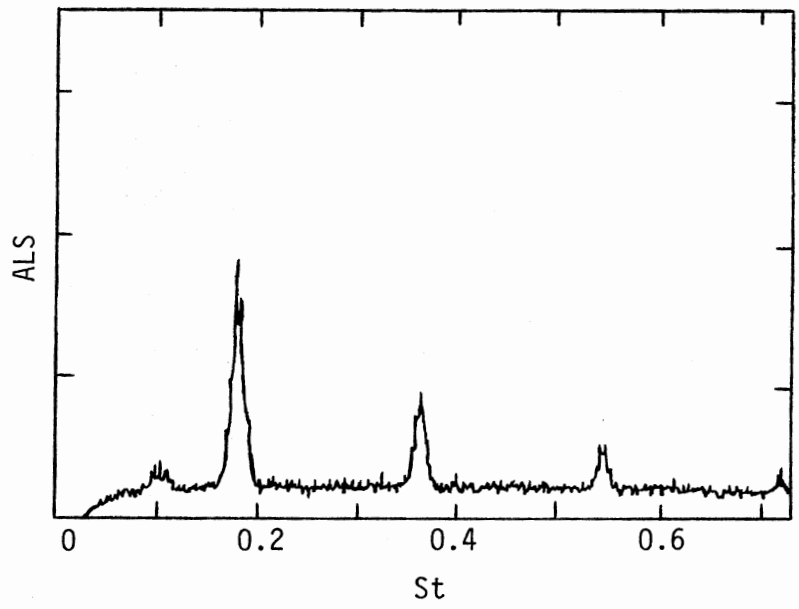

(a) x/D = 5

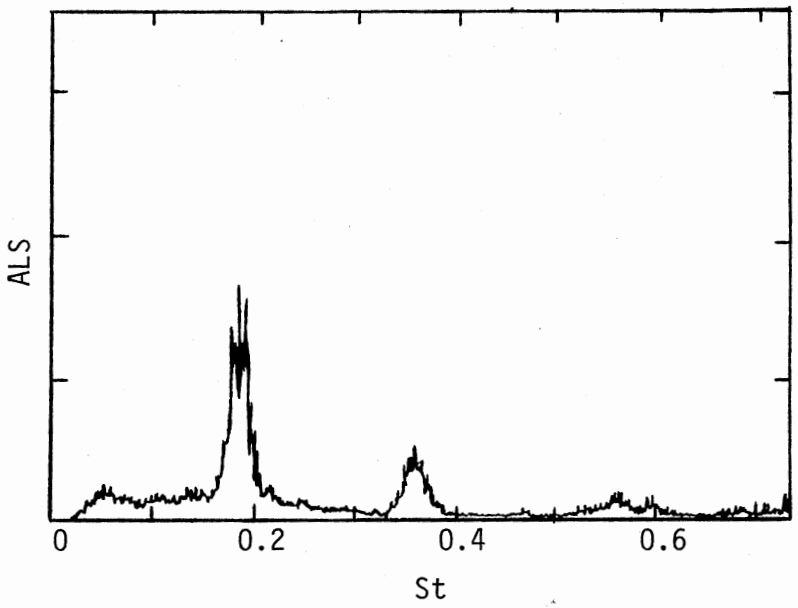

(b) x/D = 10

Figure 25. Radial Velocity Fluctuation Spectra, M = 2.5 Excited at St = 0.18

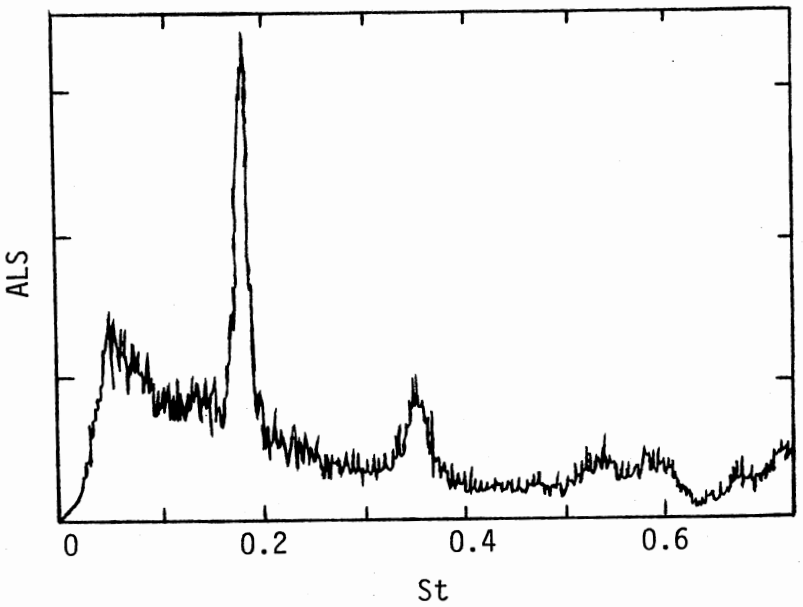

(c) x/D = 15

Figure 25. (Continued)

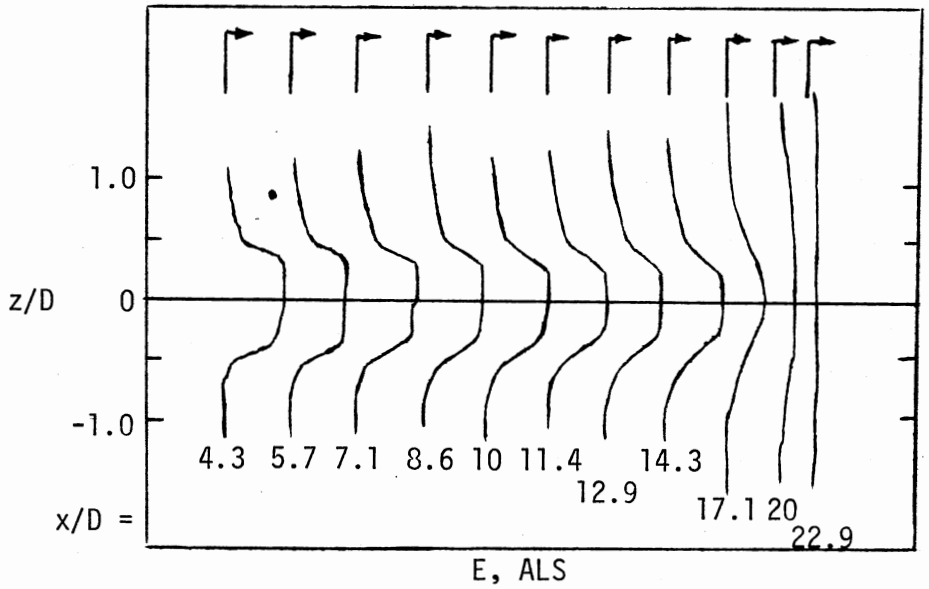

Figure 26. Mean Hot-Wire Voltage Radial Profile, M = 2.5 Excited at St = 0.16

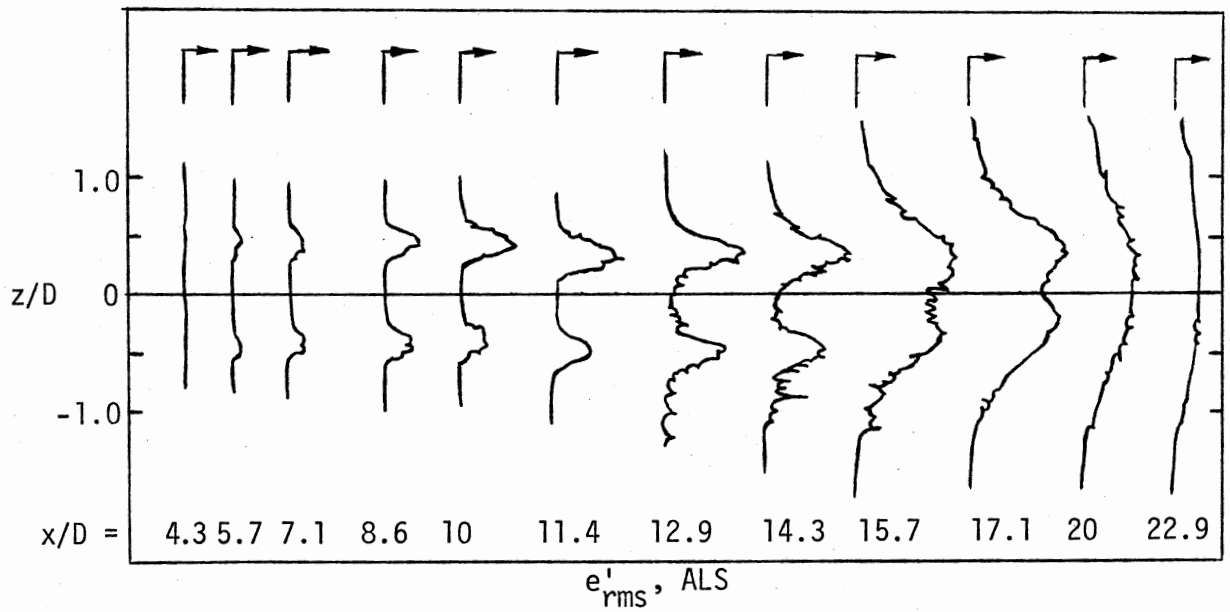

Figure 27. Full Wave Hot-Wire Voltage Fluctuation Level Radial Profile, M = 2.5 Excited at St = 0.16

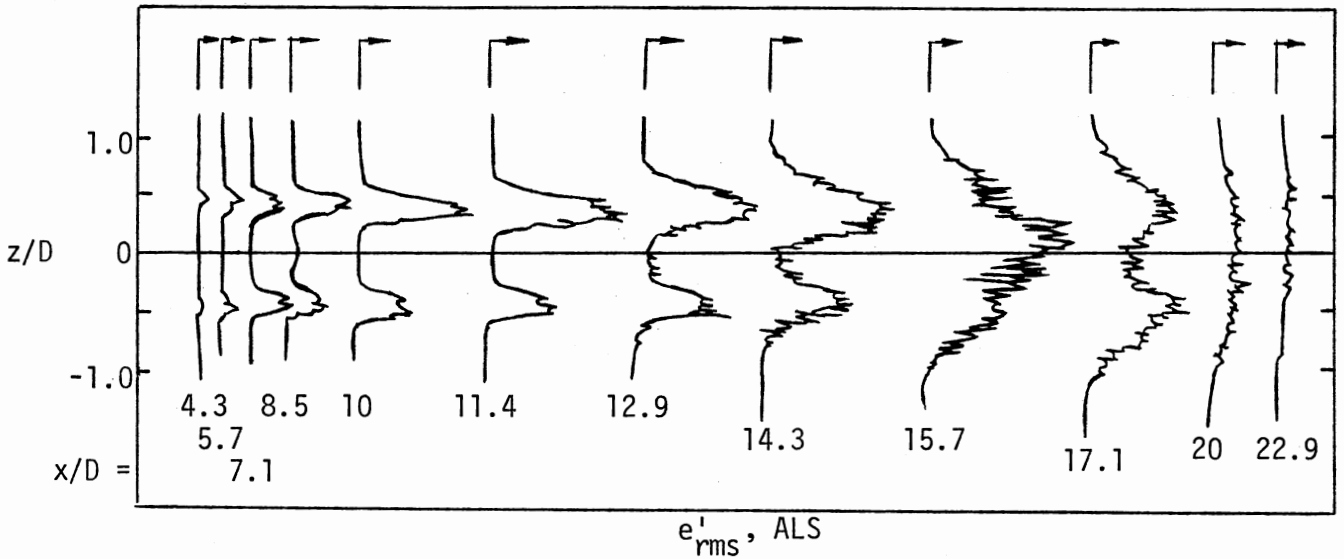

Figure 28. St = 0.16 Mode Hot-Wire Voltage Fluctuation Level Radial Profile, M = 2.5 Excited at St = 0.16

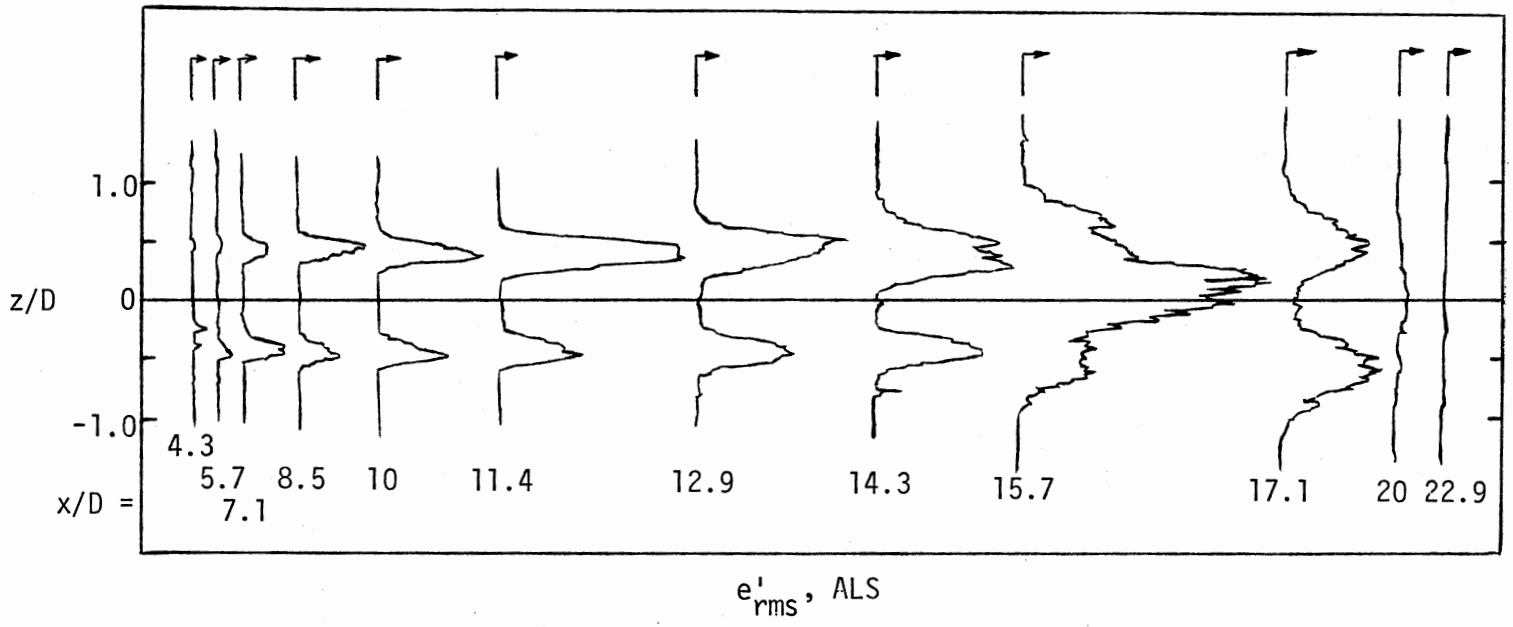

Figure 29. Phase Averaged Hot-Wire Signal Fluctuation Level Radial Profile, M = 2.5 Excited at St = 0.16

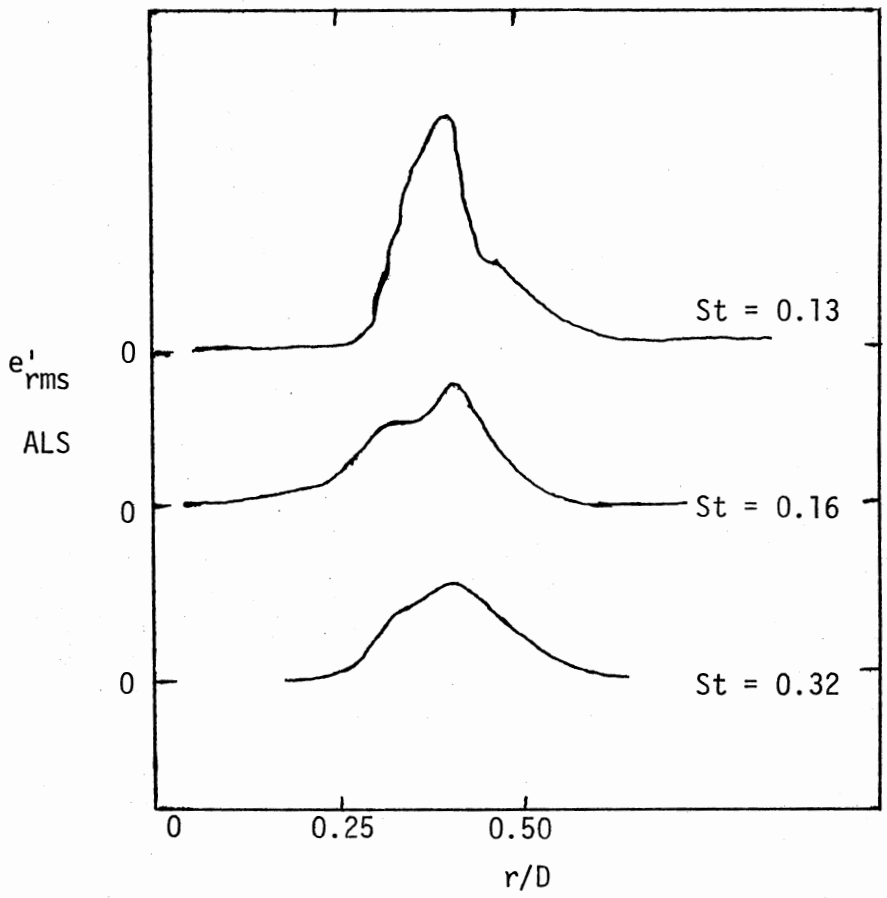

(a) x/D = 10

Figure 30. Hot-Wire Voltage Fluctuation Level Radial Profiles, M = 2.5

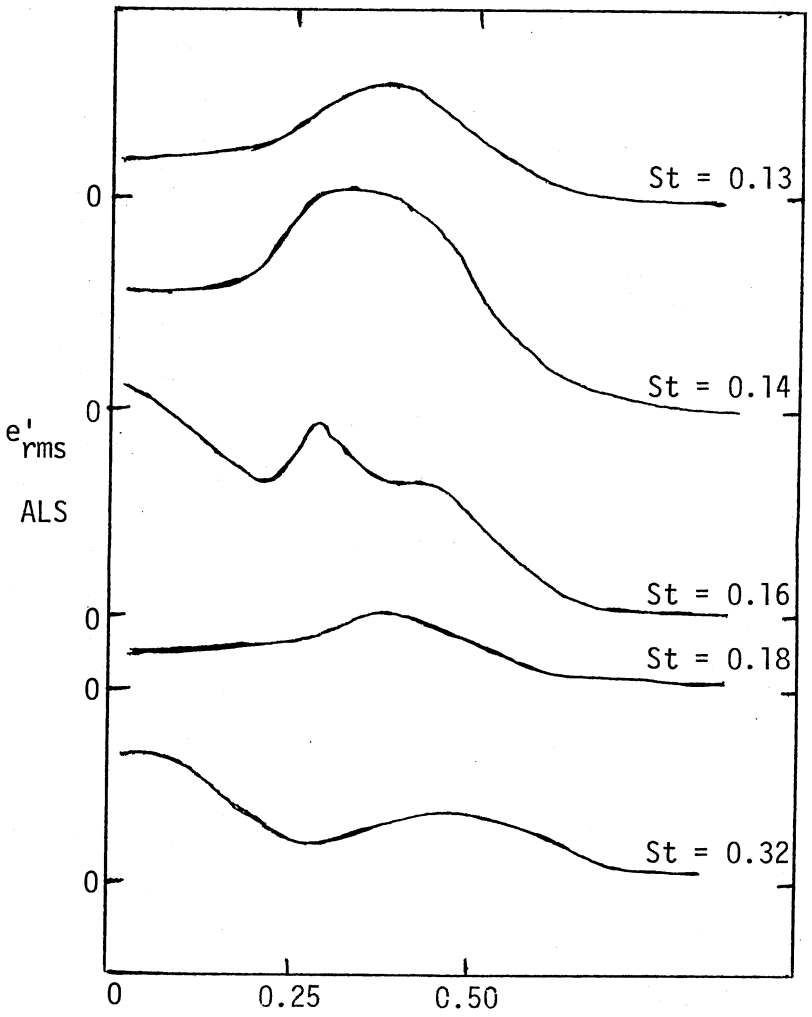

(b) x/D = 15

Figure 30. (Continued)

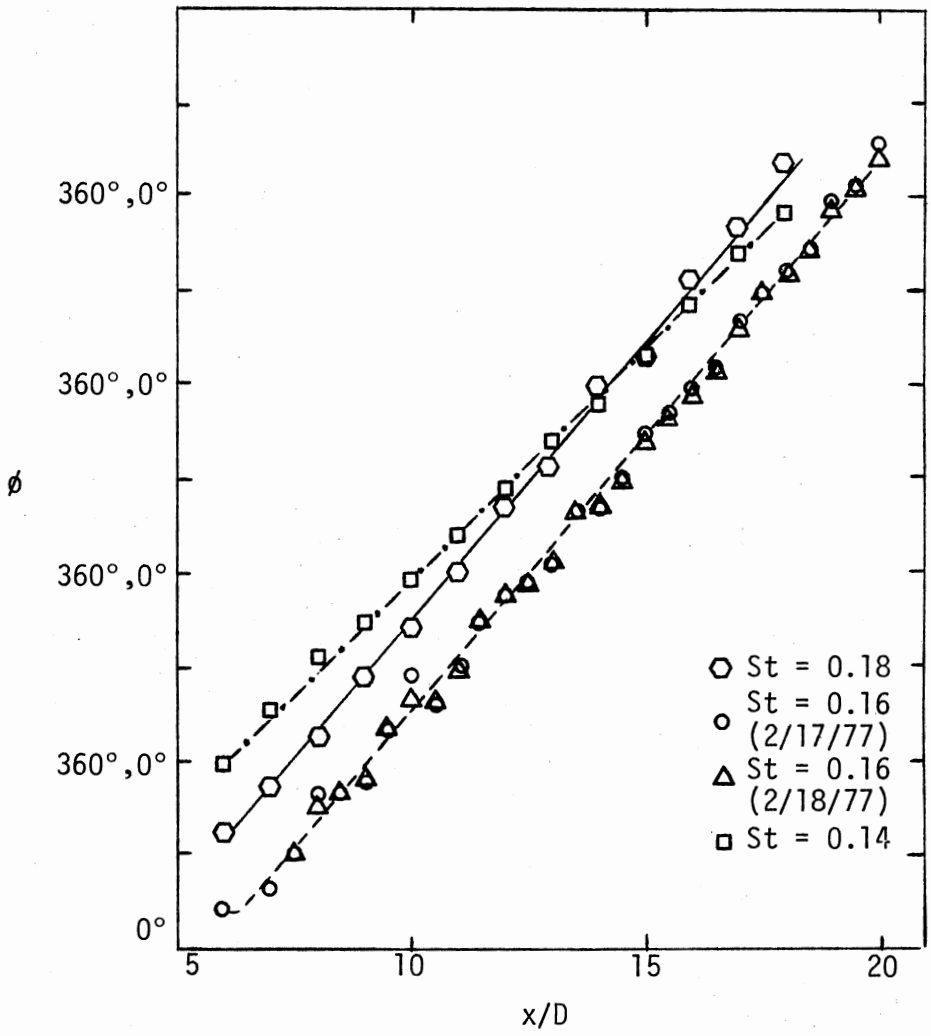

Figure 31. Axial Phase Distribution, M = 2.5

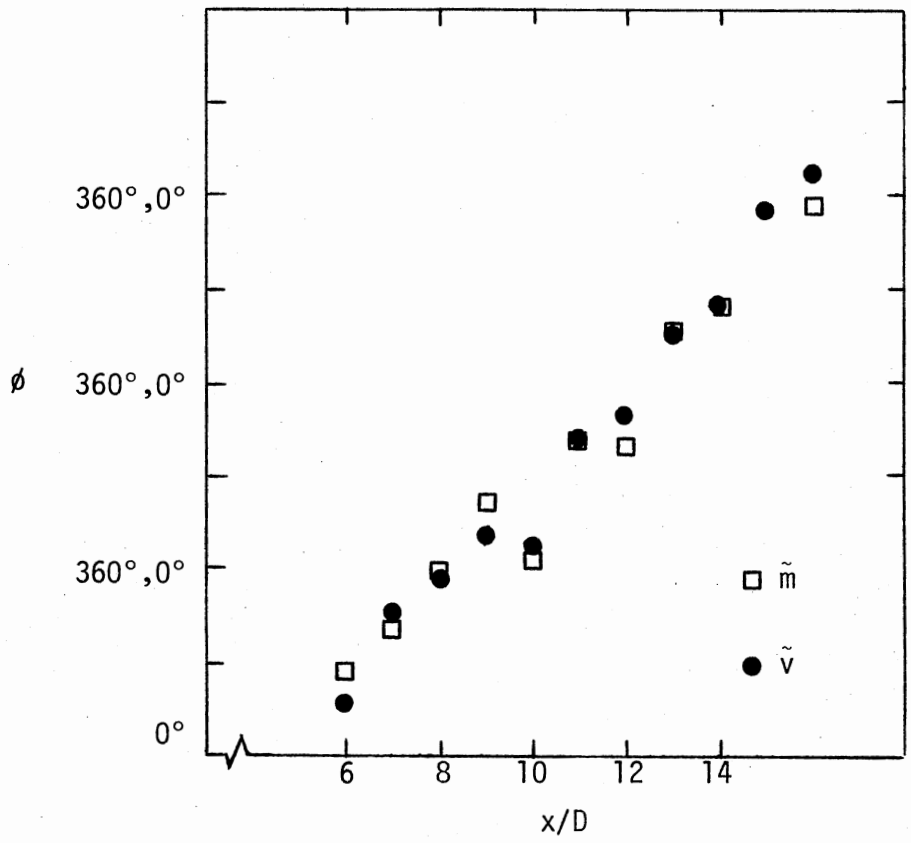

Figure 32. Axial Phase Distribution, Crossed Wire Probe, M = 2.5, St = 0.16

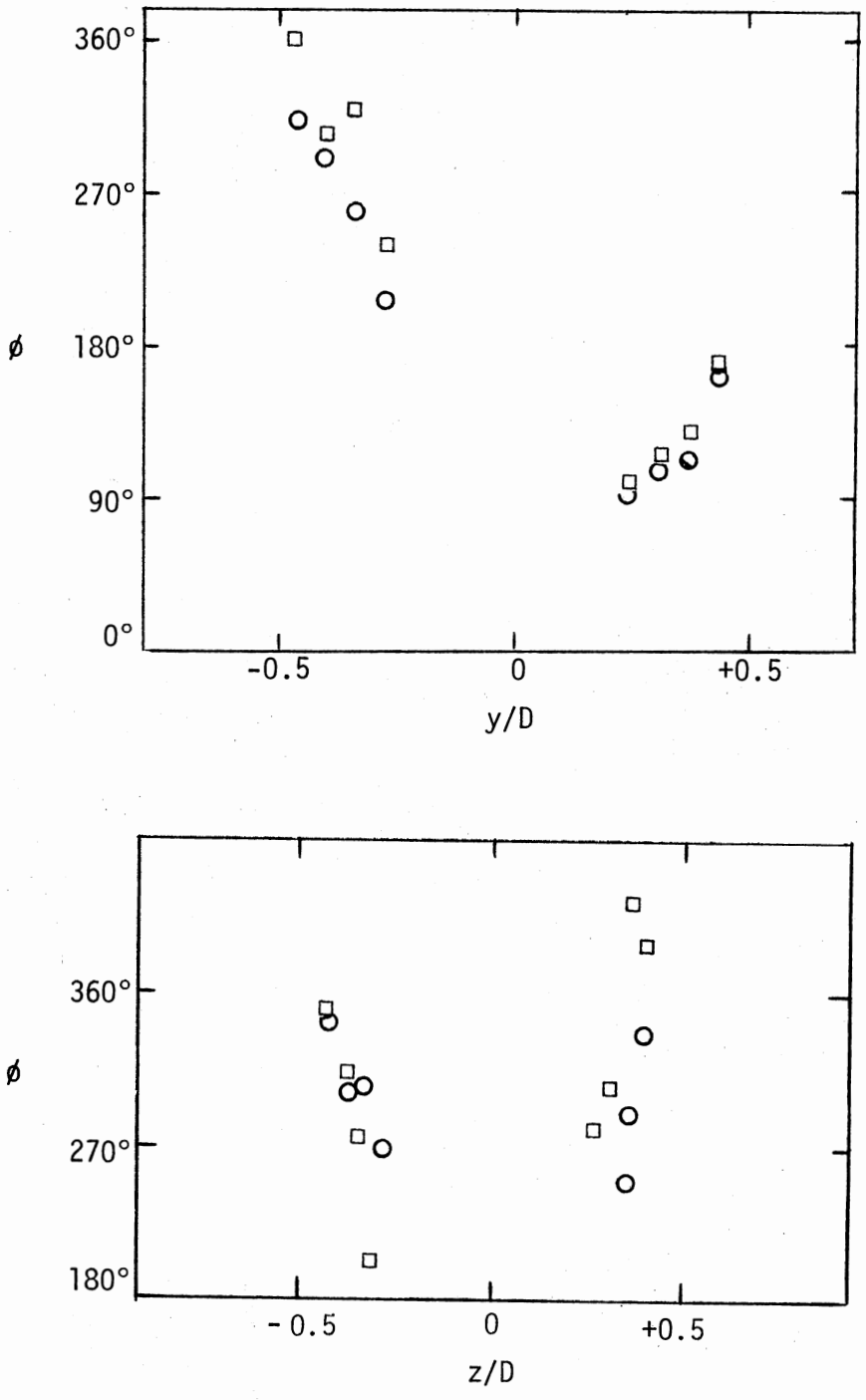

Figure 33. Radial Phase Distribution M = 2.5, St = 0.16, x/D = 8 (□ Feb. 25, 1977, ○ Feb. 28, 1977)

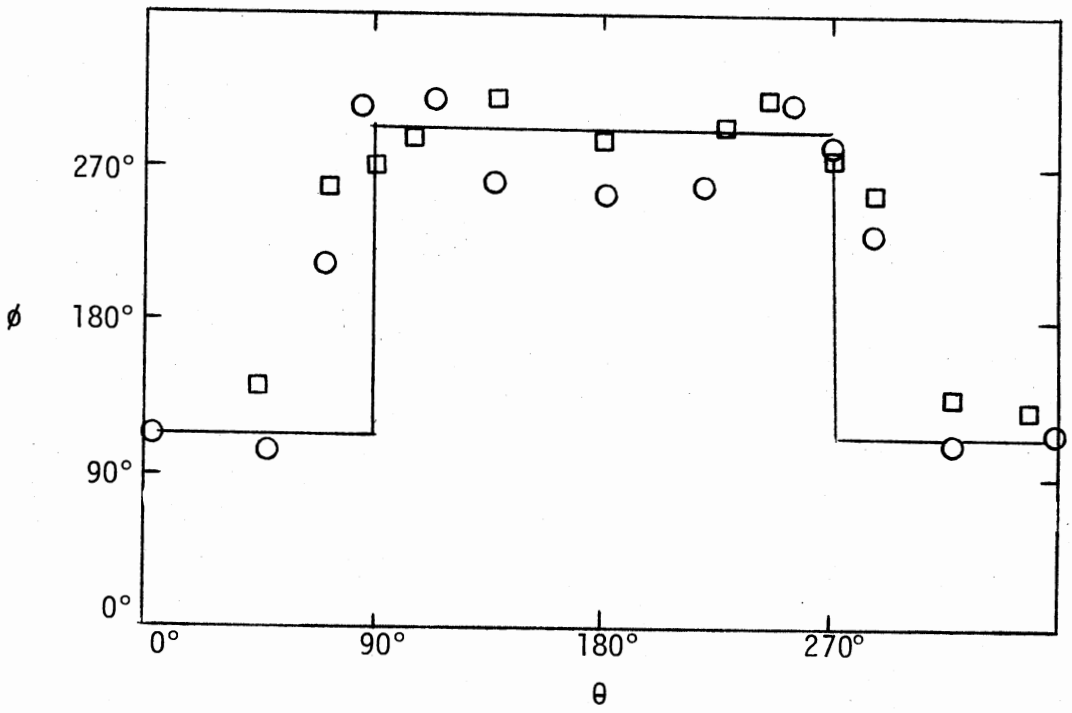

Figure 34. Azimuthal Phase Distribution, M = 2.5, St = 0.16, x/D = 8 (□ Feb. 25, 1977, ○ Feb. 28, 1977)

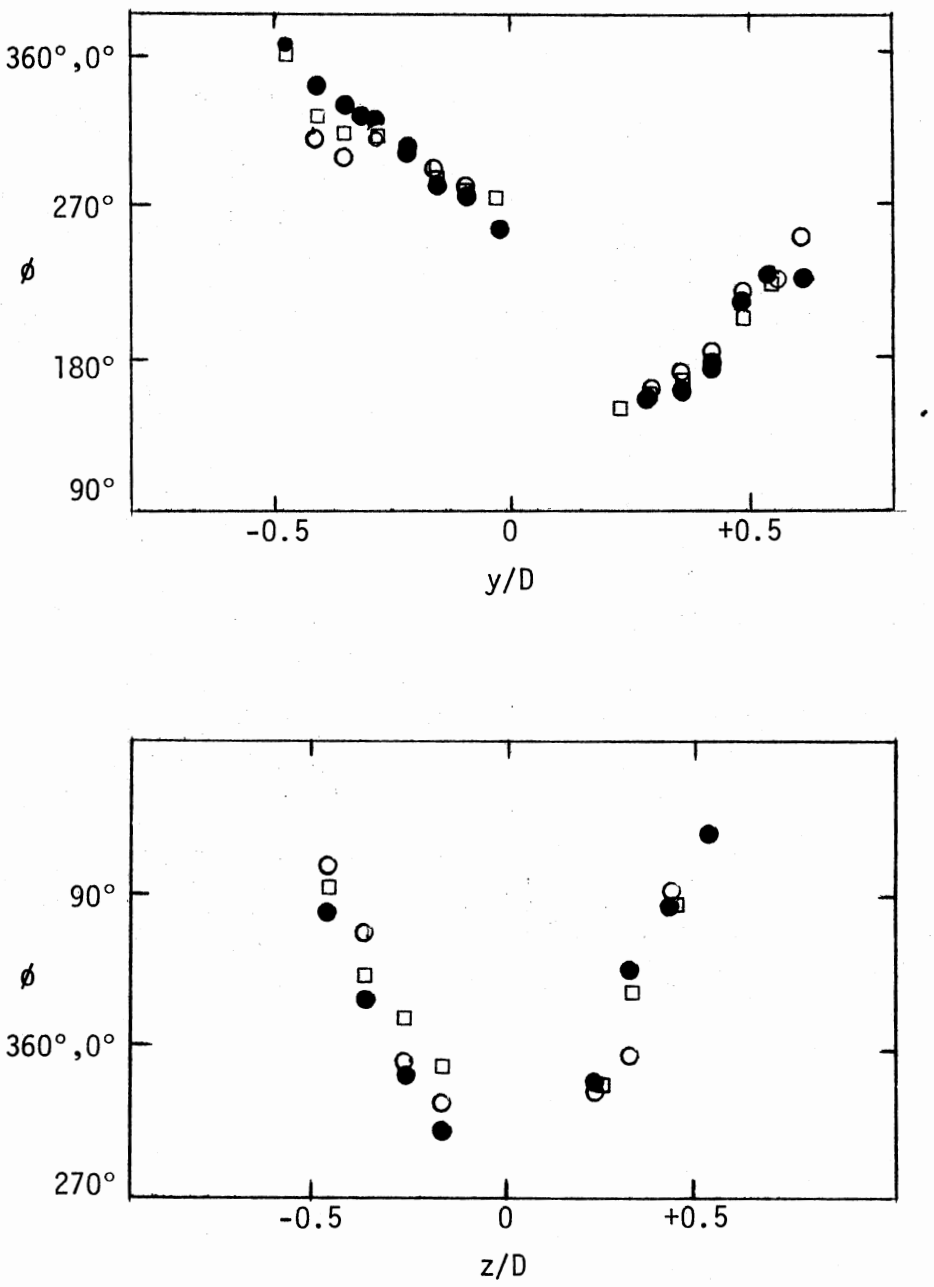

Figure 35. Radial Phase Distribution, M = 2.5, St = 0.16, x/D = 12 (● Feb. 14, 1977, □ Feb. 16, 1977, ○ Feb. 17, 1977)

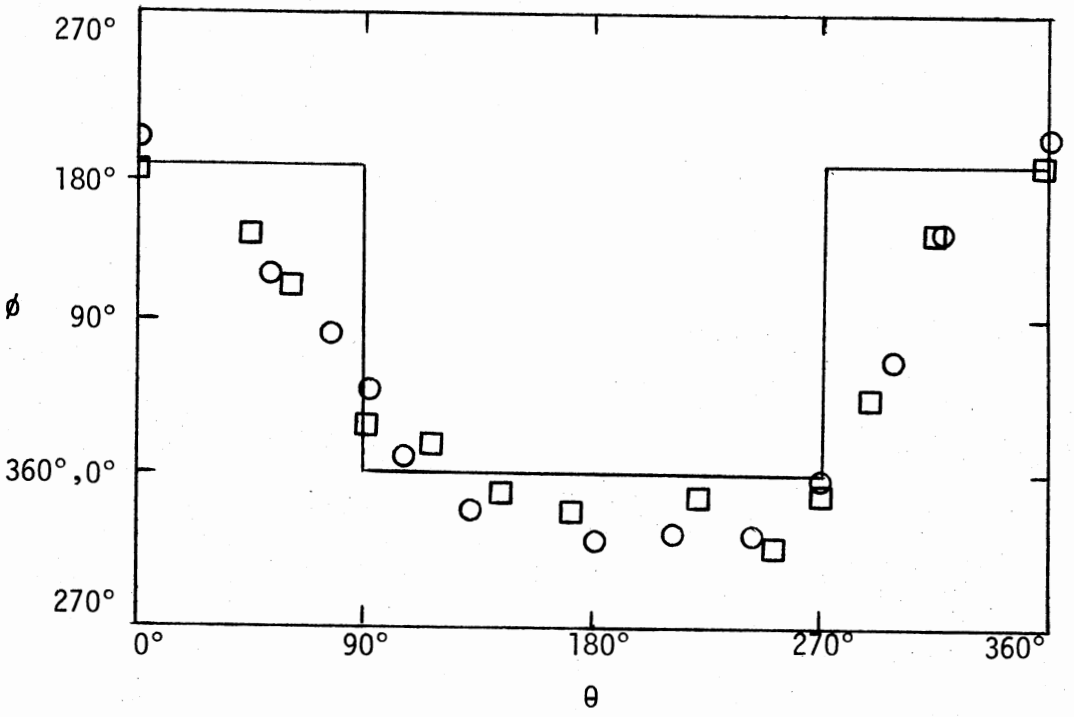

Figure 36. Azimuthal Phase Distribution, M = 2.5, St = 0.16, x/D = 12 (□ Feb. 25, 1977, ○ Feb. 28, 1977)

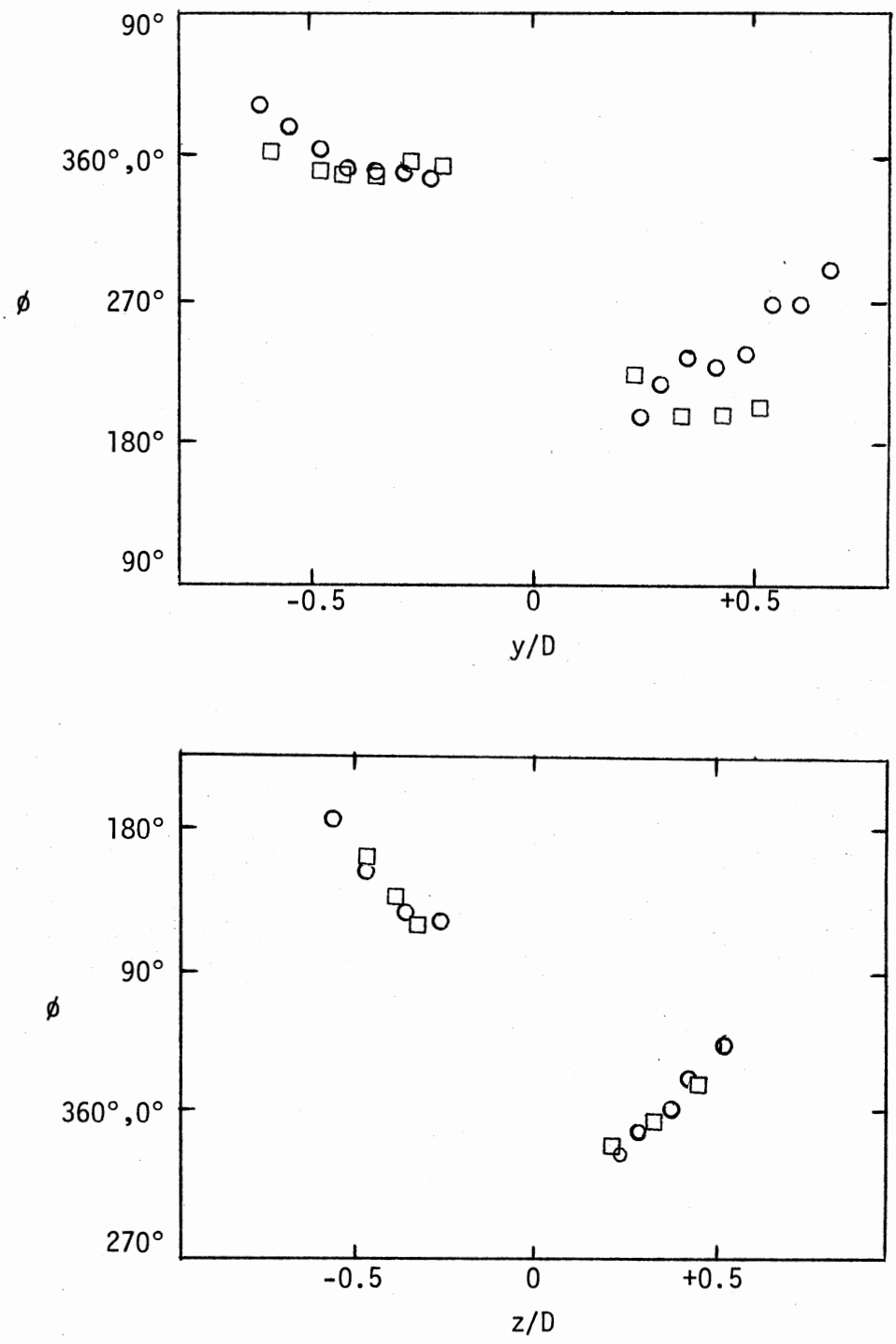

Figure 37. Radial Phase Distribution, M = 2.5, St = 0.16, x/D = 16 (○ Feb. 18, 1977, □ March 23, 1977)

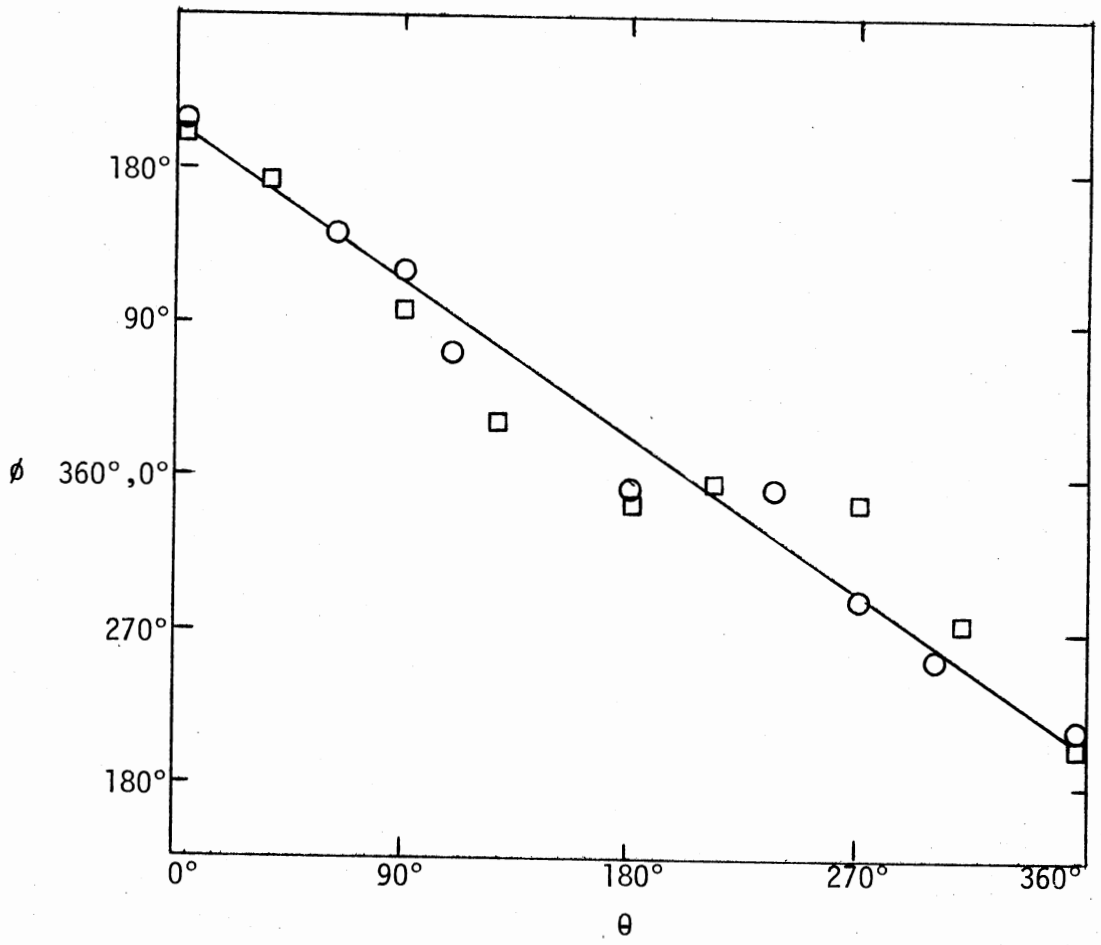

Figure 38. Azimuthal Phase Distribution, M = 2.5, St = 0.16, x/D = 16 (○ Feb. 28, 1977, □ March 23, 1977)

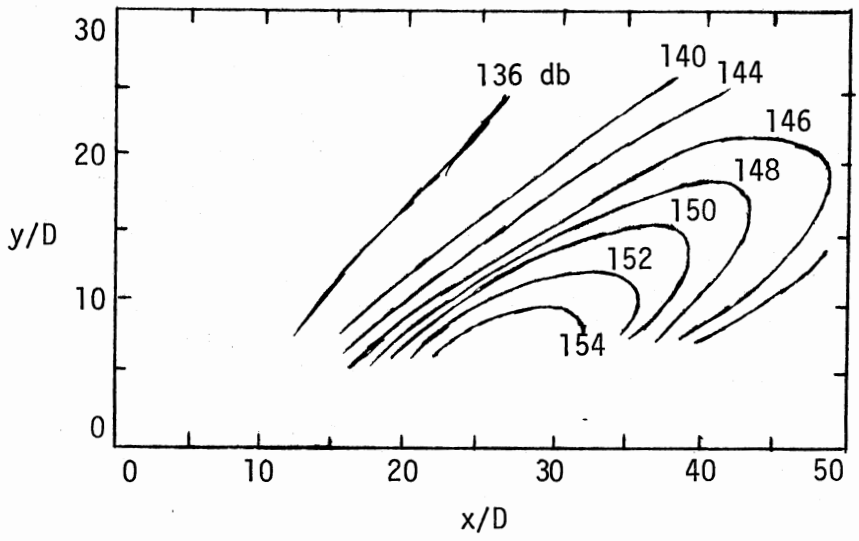

(a) Natural

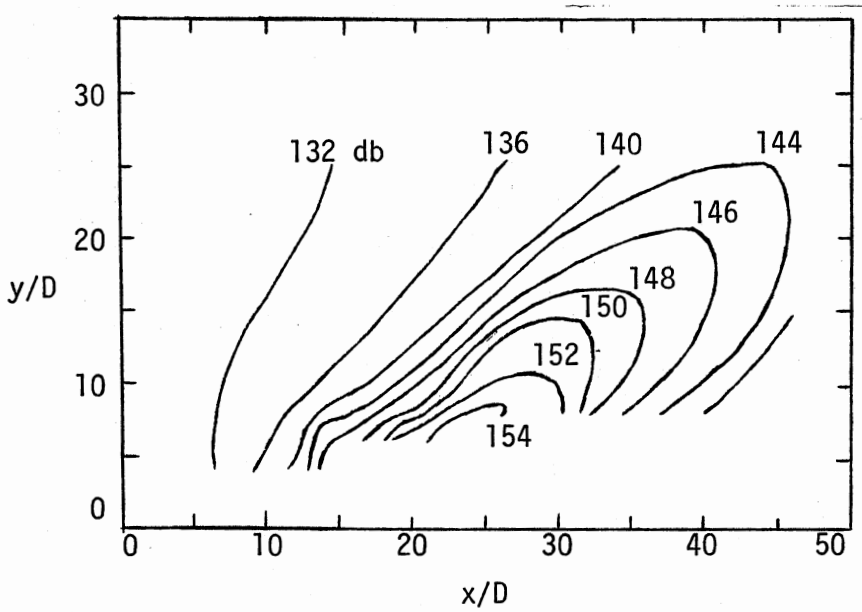

(b) Excited at St = 0.16

Figure 39. Full Spectrum SPL Contours, M = 2.5

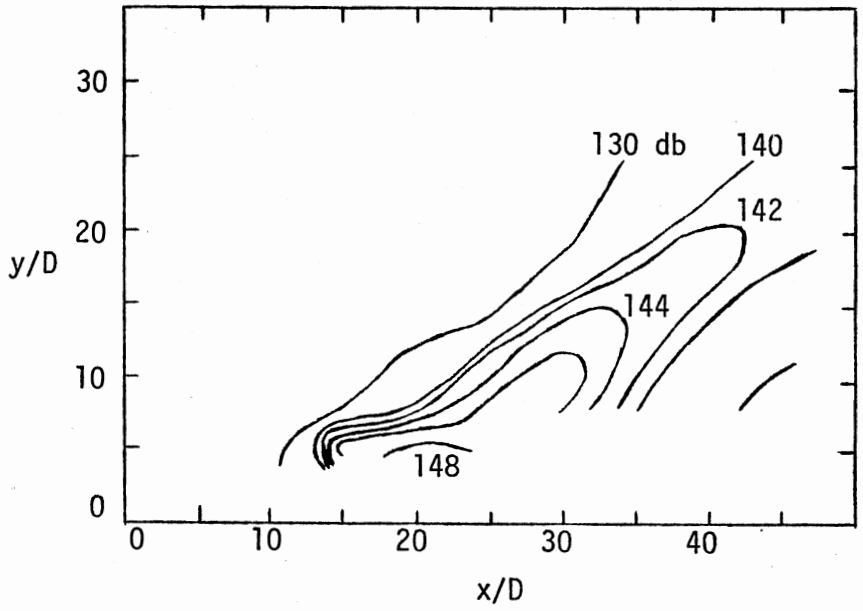

(a) St = 0.16 Component

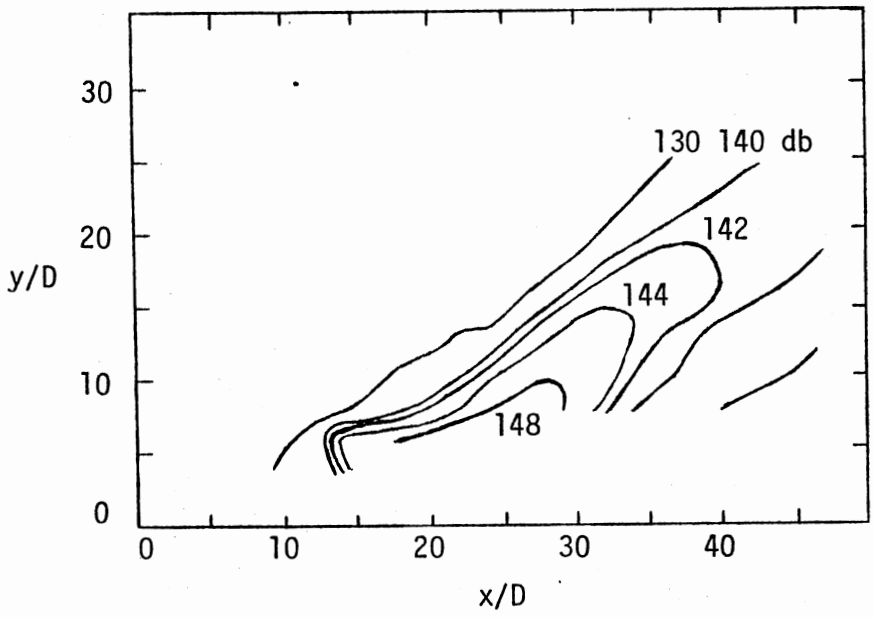

(b) Phase Averaged SPL

Figure 40. SPL Contours, M = 2.5, Excited at St = 0.16

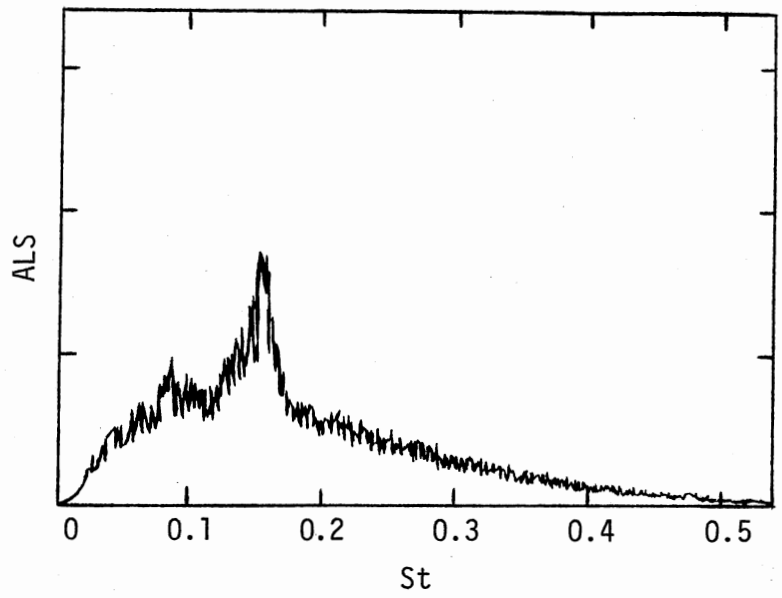

(a) x/D = 6

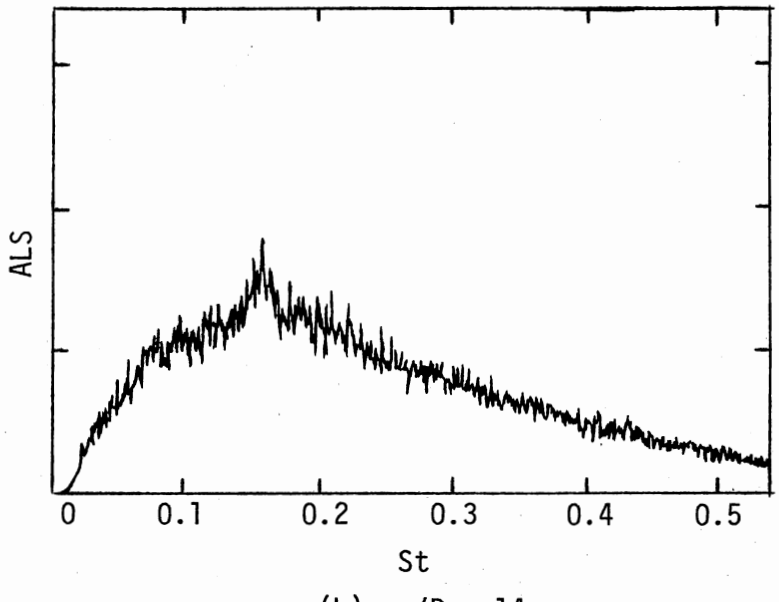

(b) x/D = 14

Figure 41. Microphone Spectra, M = 2.5, y/D = 12

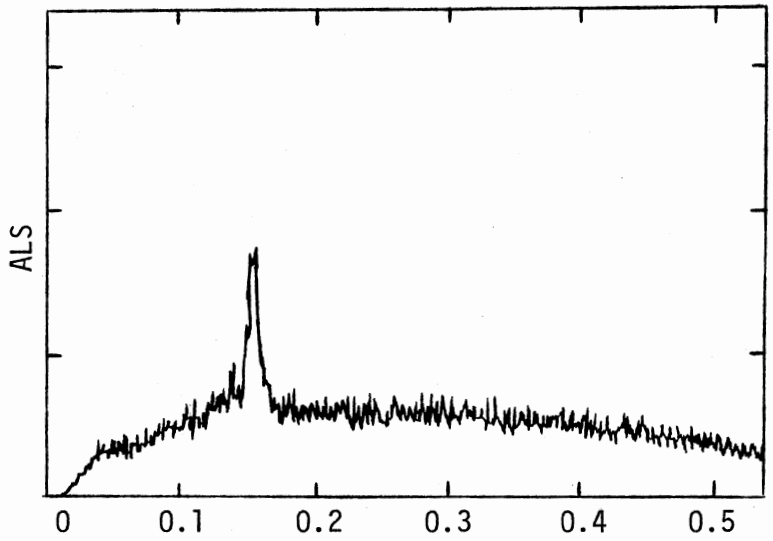

(c) x/D = 24

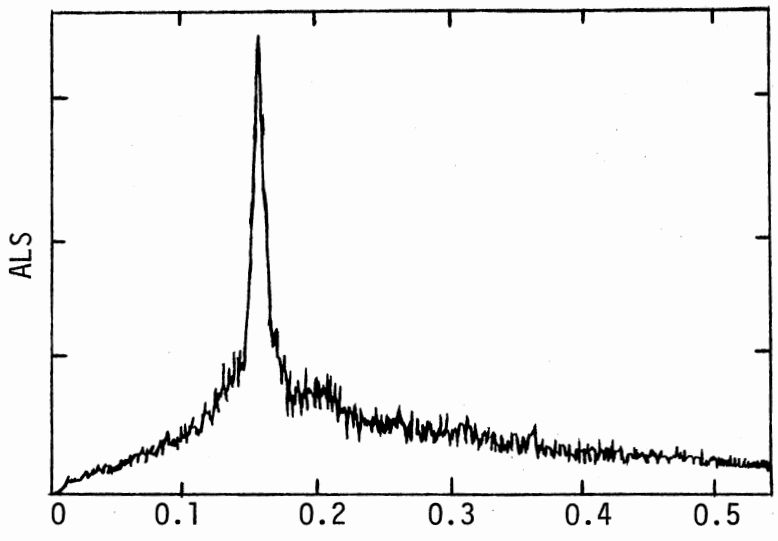

(d) x/D = 30

Figure 41. (Continued)

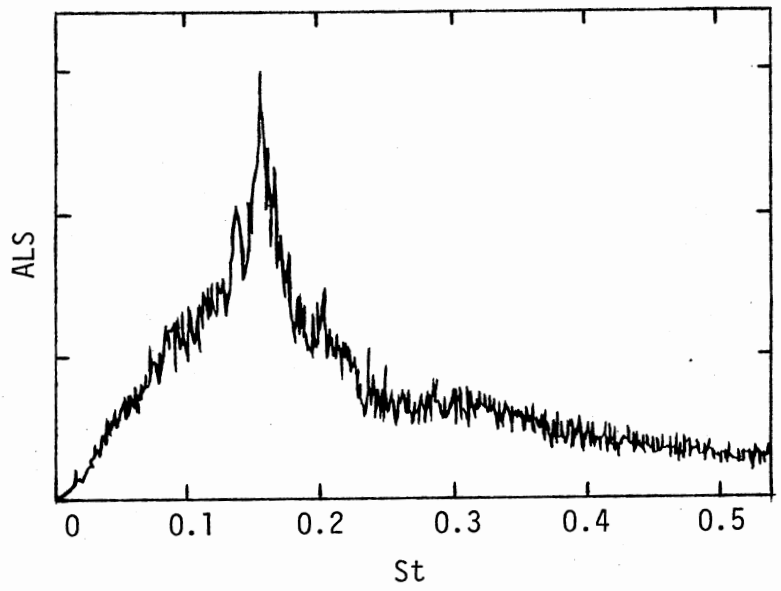

(e) x/D = 40

Figure 41. (Continued)

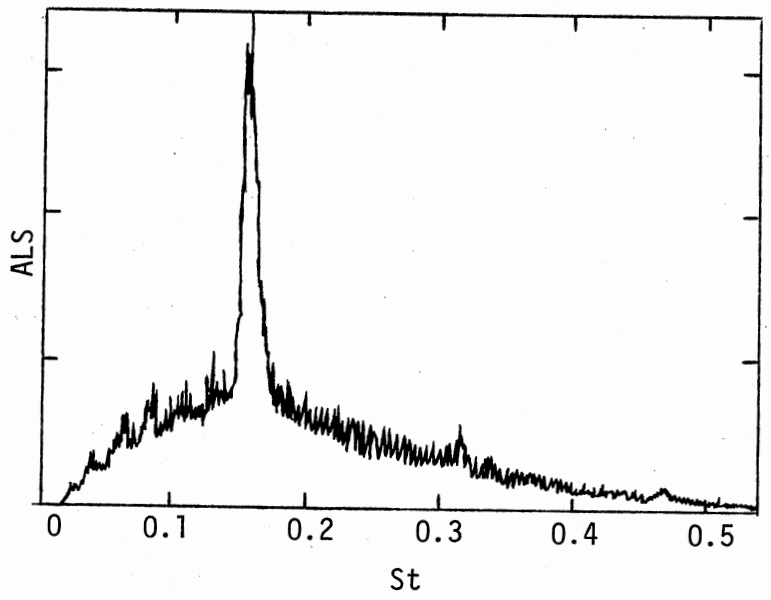

(a) x/D = 6

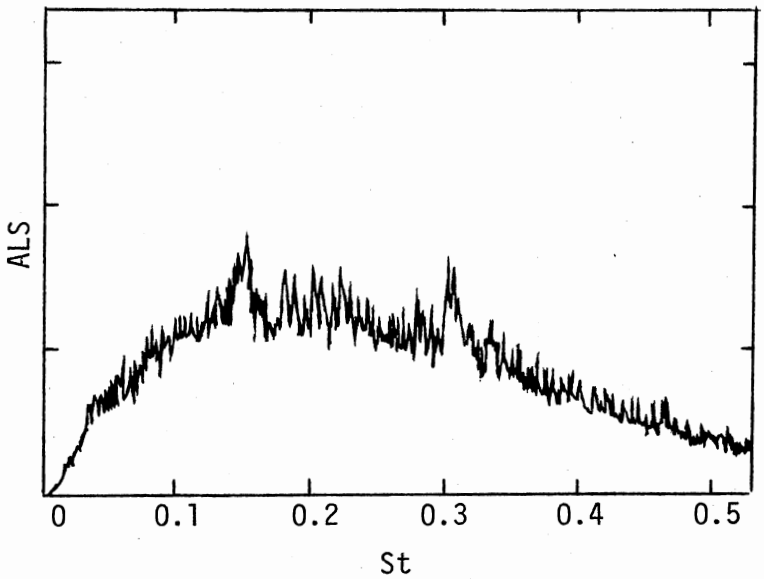

(b) x/D = 14

Figure 42. Microphone Spectra, M = 2.5, Excited at St = 0.16, y/D = 12

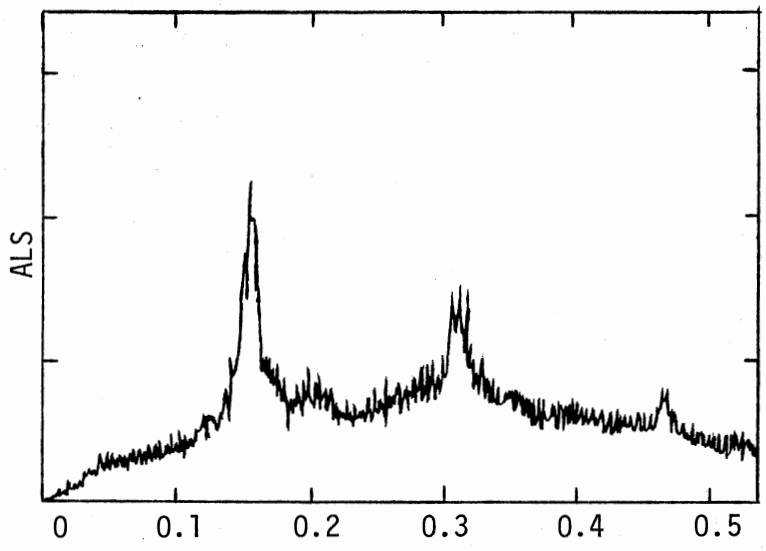

(c) x/D = 24

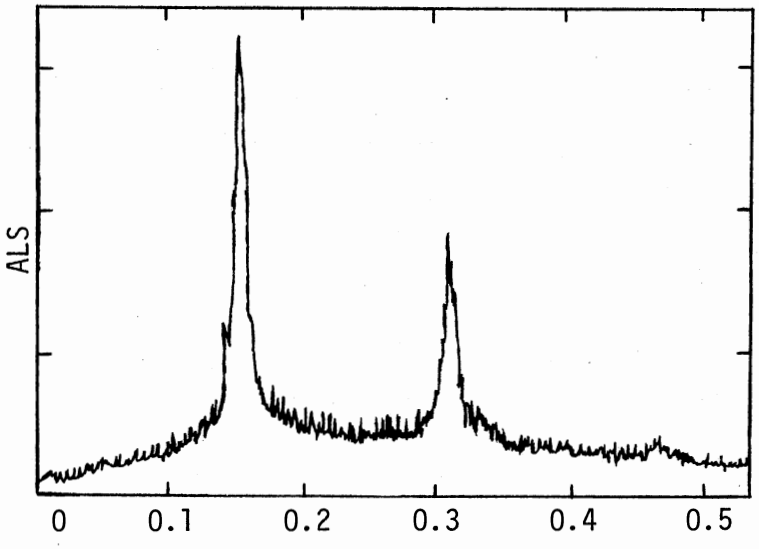

(d) x/D = 30

Figure 42. (Continued)

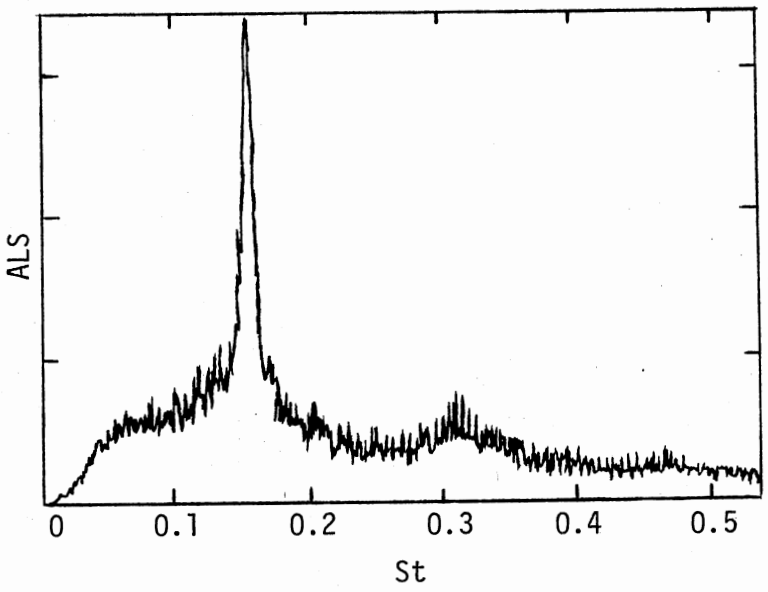

(e) x/D = 40

Figure 42. (Continued)

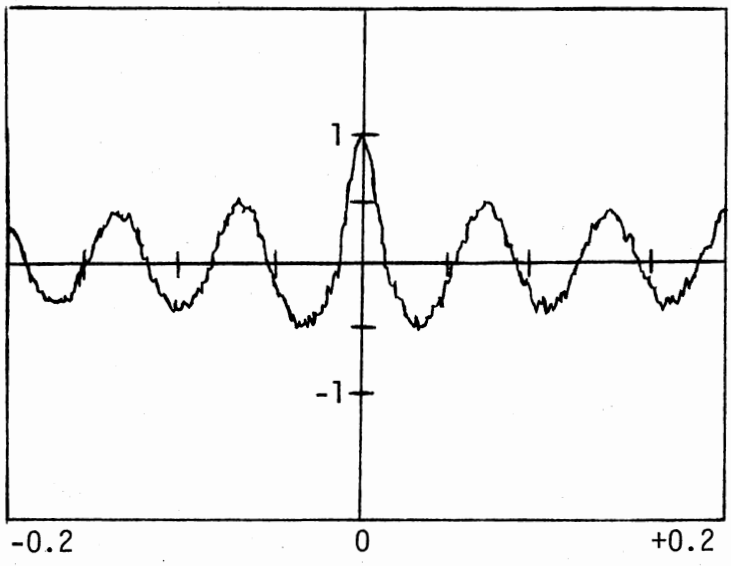

(a) Natural

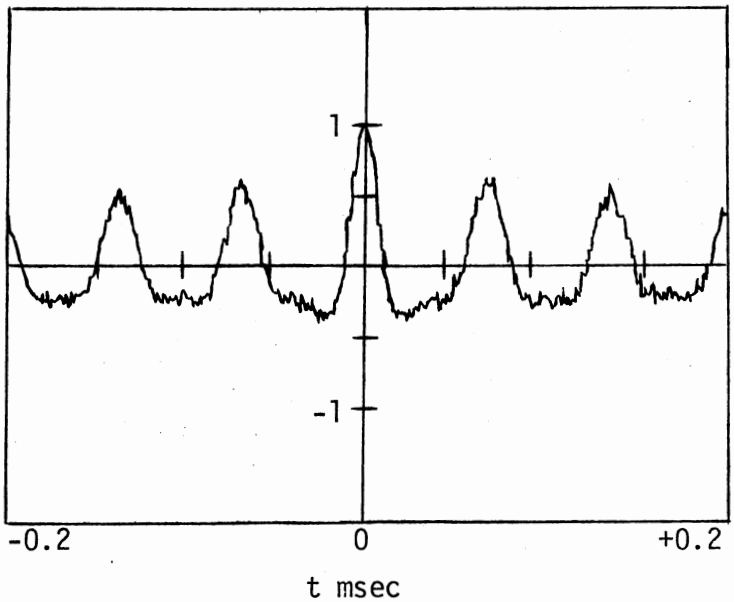

(b) Excited at St = 0.16

Figure 43. Microphone Autocorrelation, M = 2.5, x/D = 30, y/D = 12

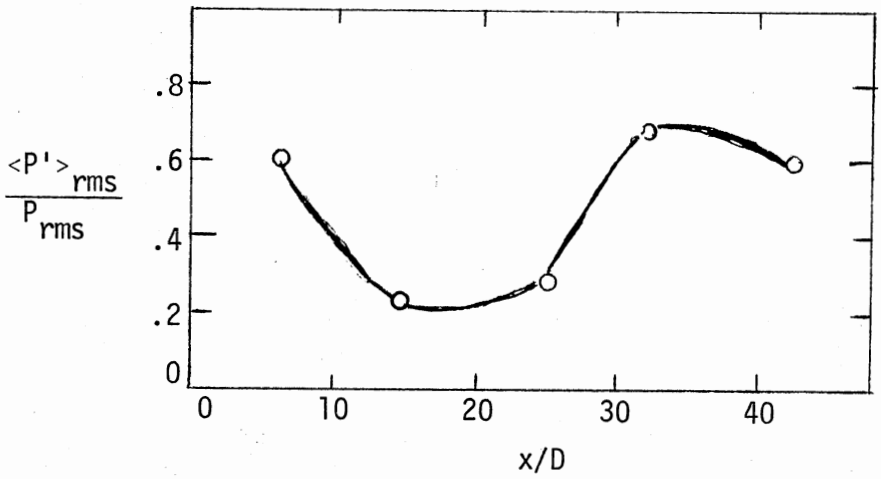

Figure 44. Axial Distribution of the Fraction of Coherent Pressure Fluctuations, M = 2.5, Excited at St = 0.16, y/D = 12

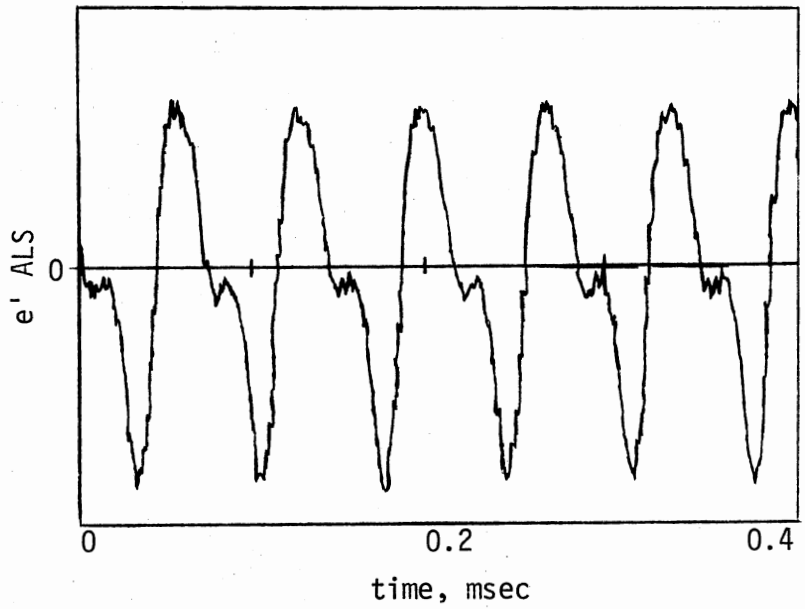

(a) Phase Averaged Signal Wave Form

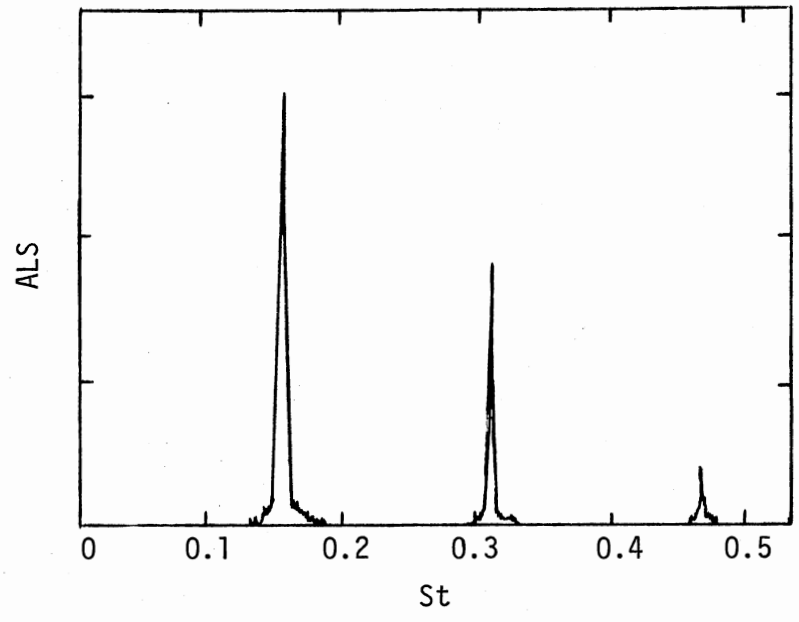

(b) Phase Averaged Signal Spectrum

Figure 45. Phase Averaged Microphone Signal, M = 2.5, Excited at St = 0.16, x/D = 30, y/D = 12

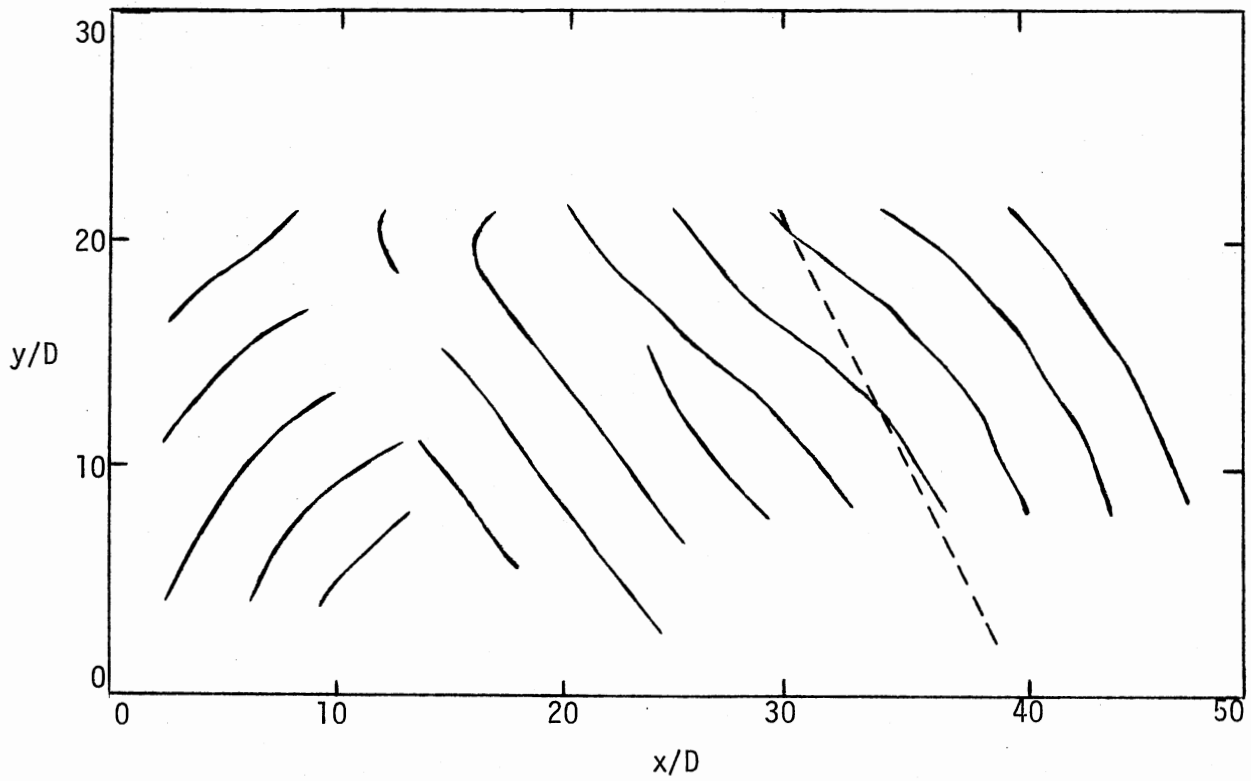

Figure 46. Acoustic Wave Fronts, M = 2.5, Excited at St = 0.16,
--- Calculated Mach Wave

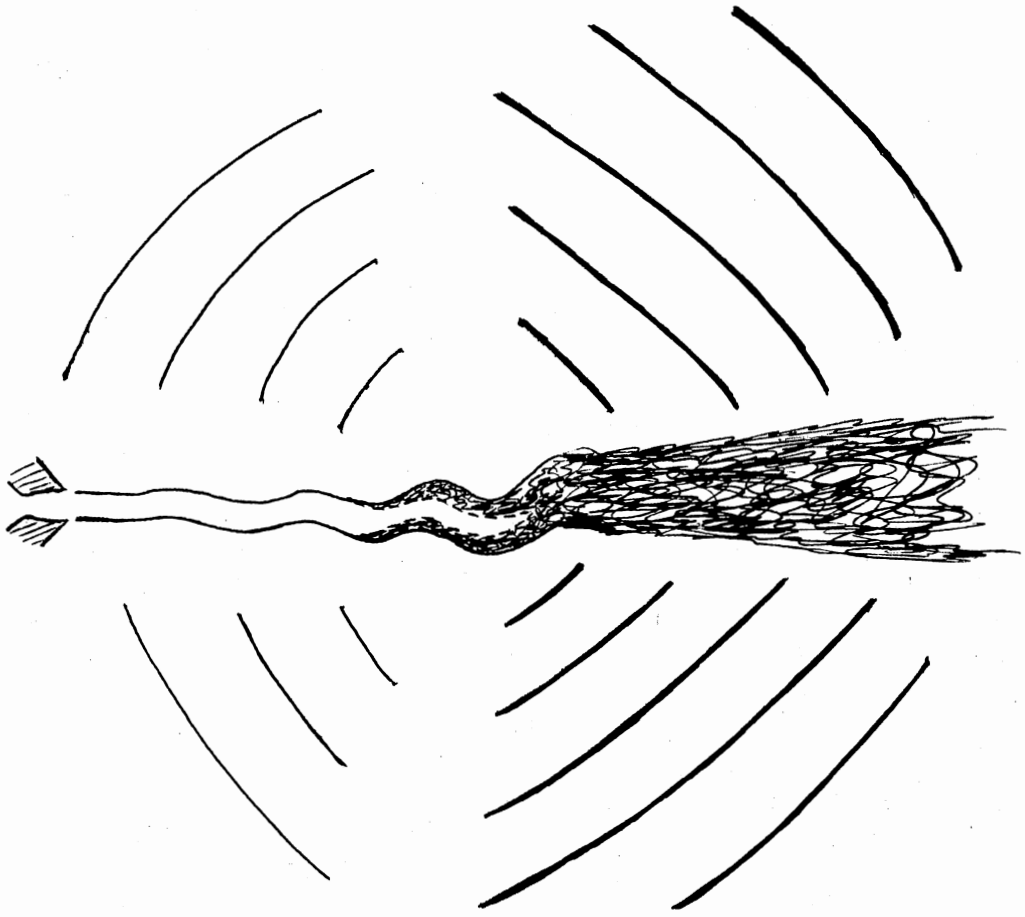

Figure 47. Diagram of Flow Instability and Acoustic Wave Fronts, M = 2.5

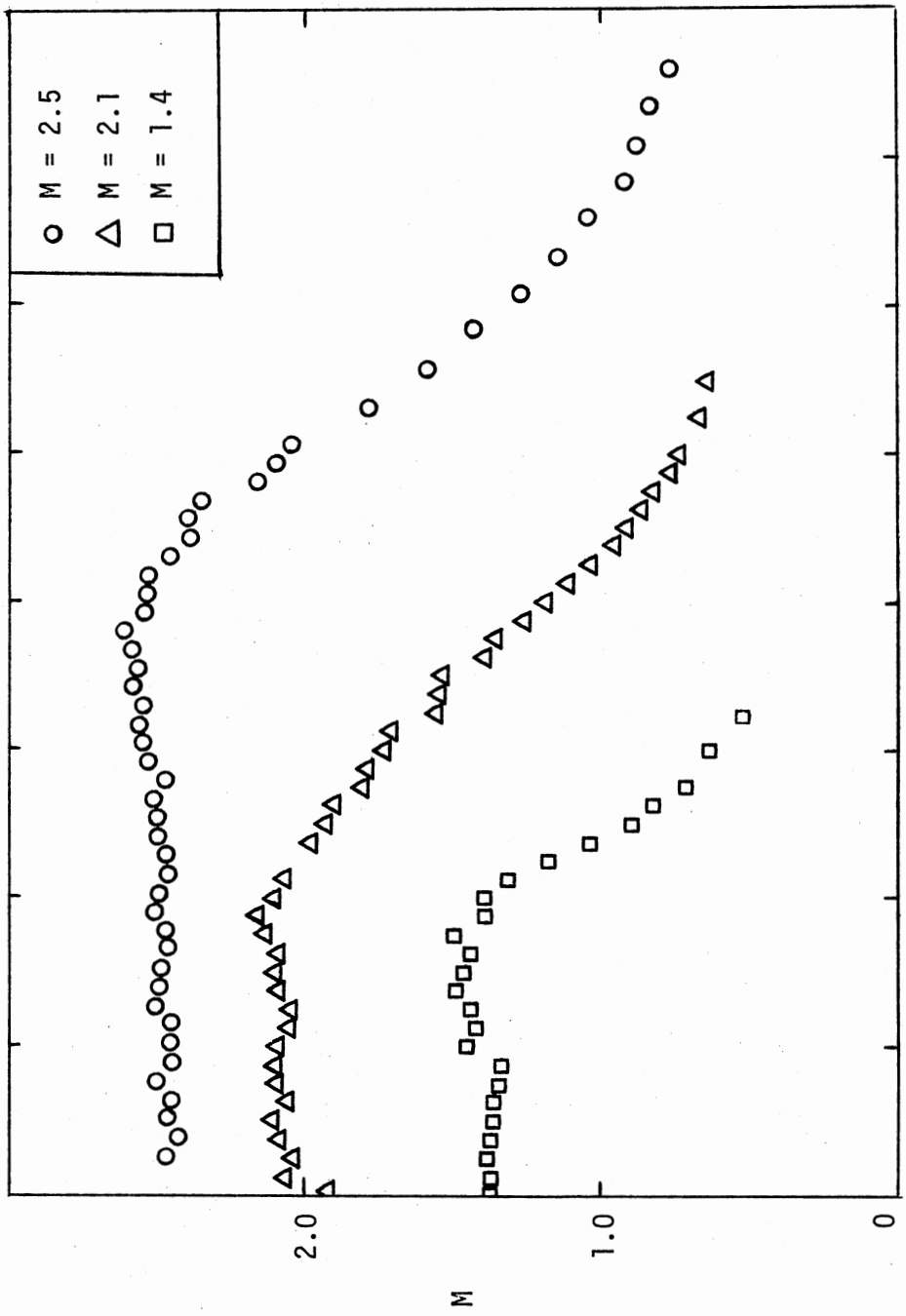

Figure 48. Centerline Mach Number Distributions

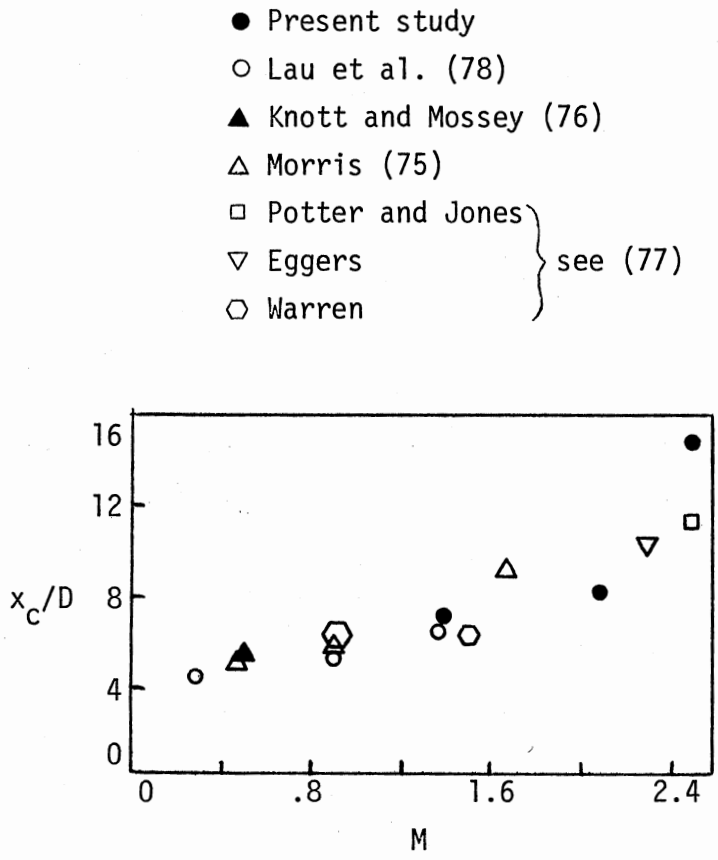

Figure 49. Length of Potential Core as a Function of Mach Number

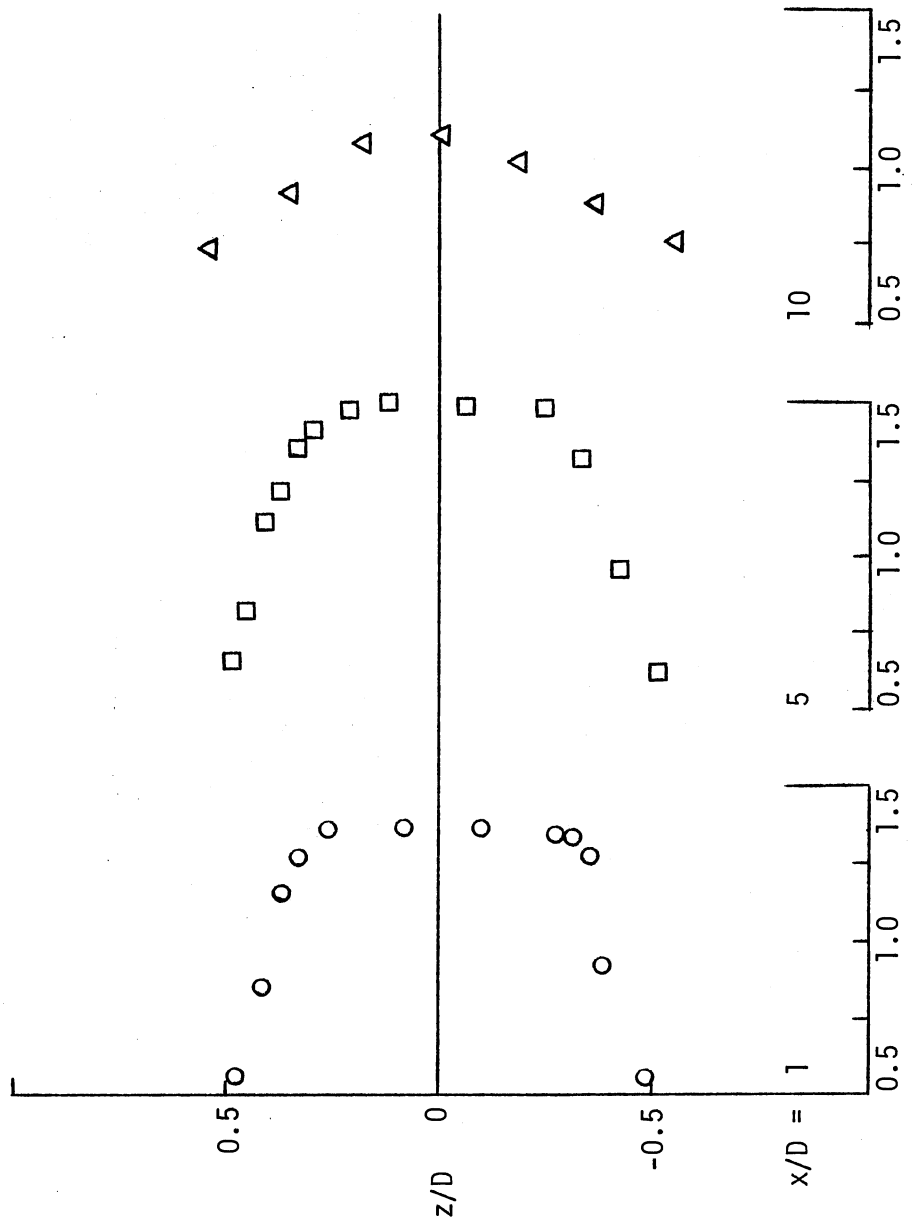

Figure 50. Radial Mach Number Distributions, M = 1.4

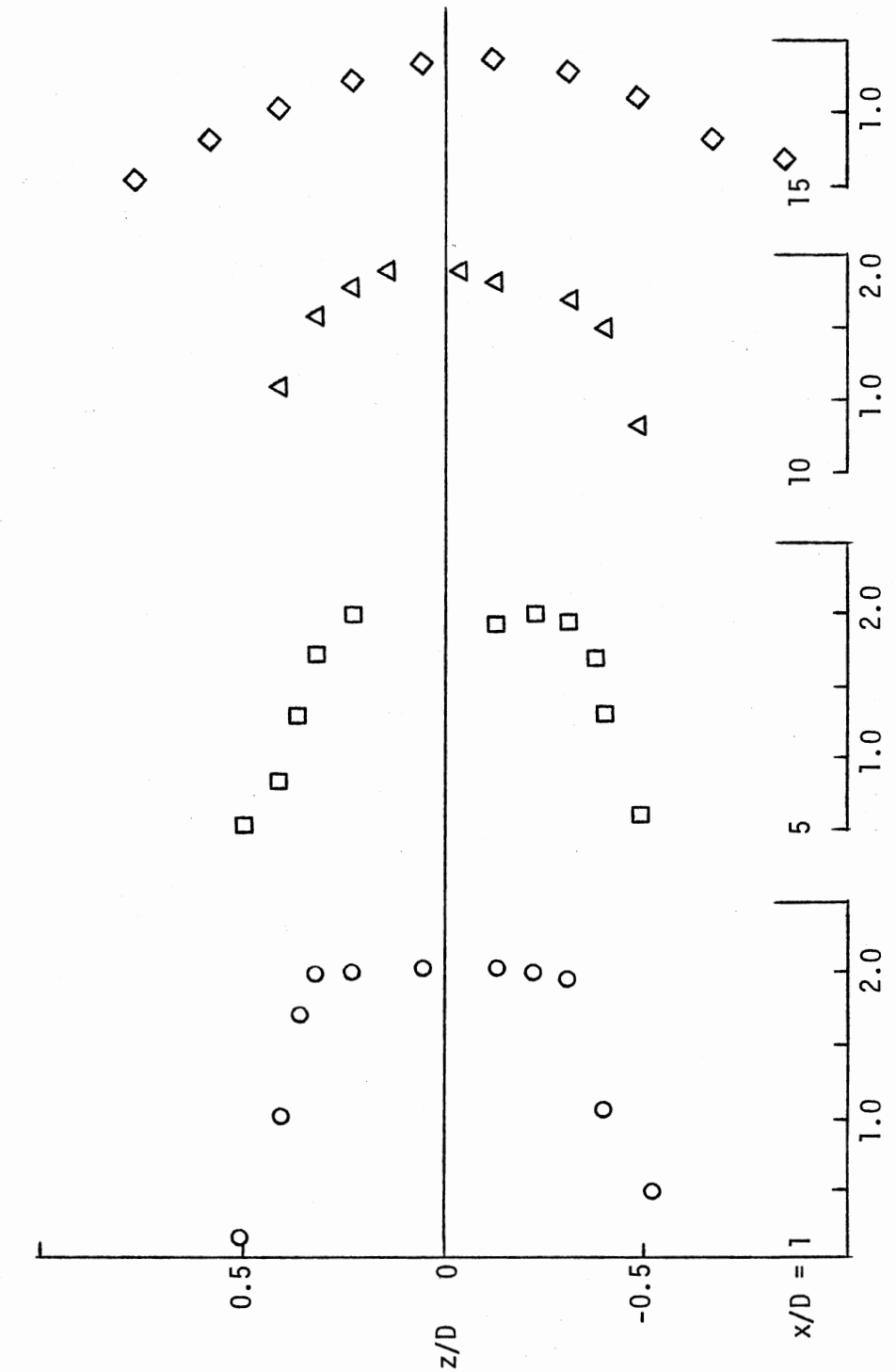

Figure 51. Radial Mach Number Distributions, M = 2.1

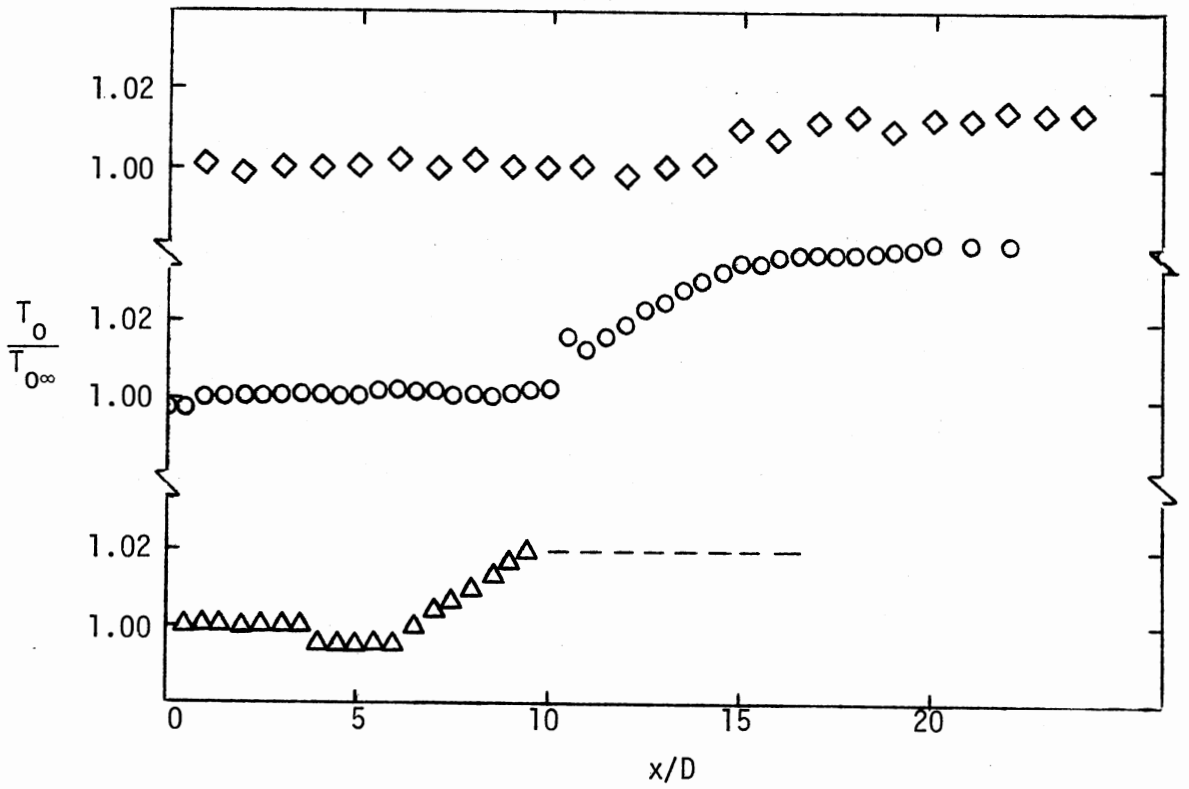

Figure 52. Axial Stagnation Temperature Distributions
(△ M = 1.4, ○ M = 2.1, ◇ M = 2.5)

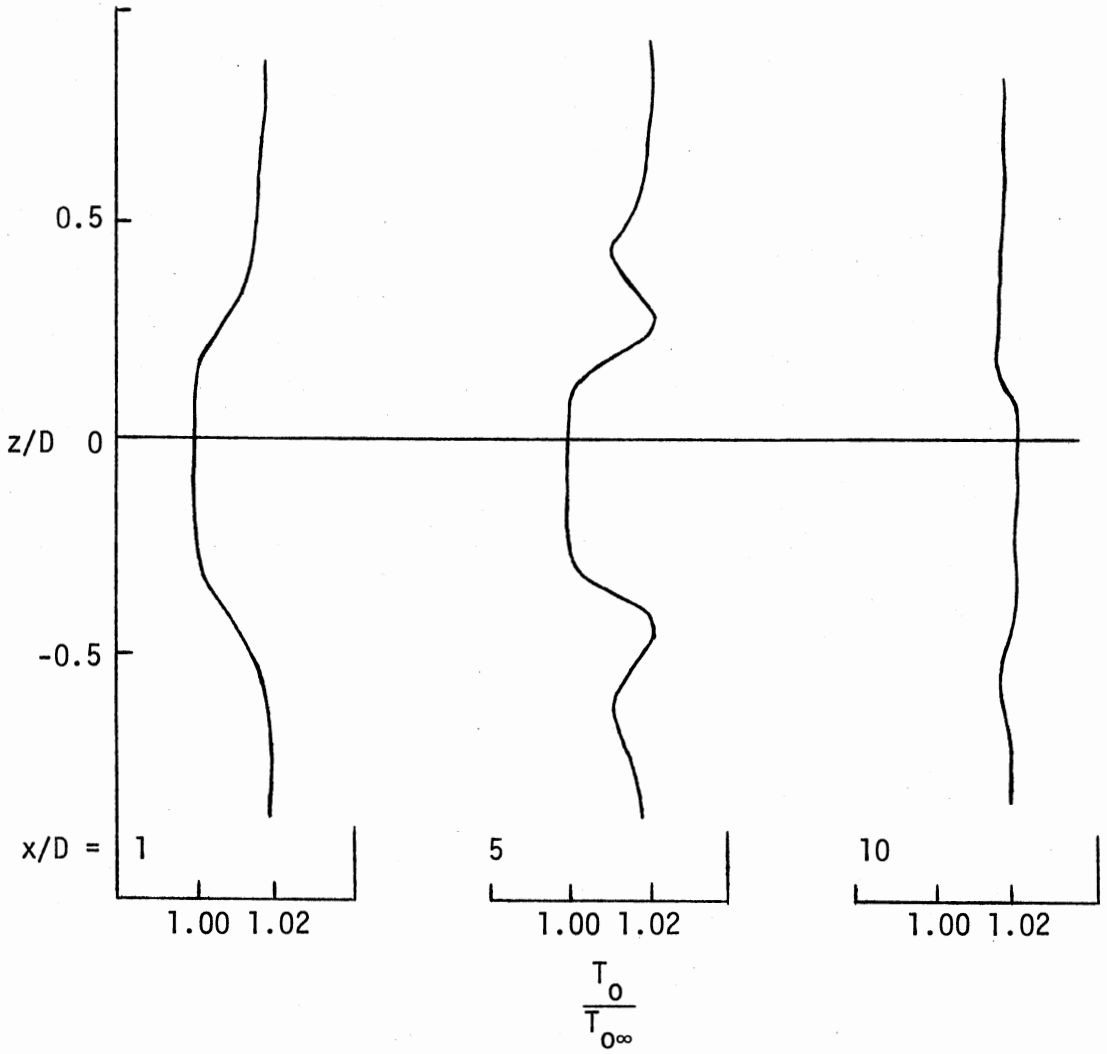

Figure 53. Radial Stagnation Temperature Distributions, M = 1.4

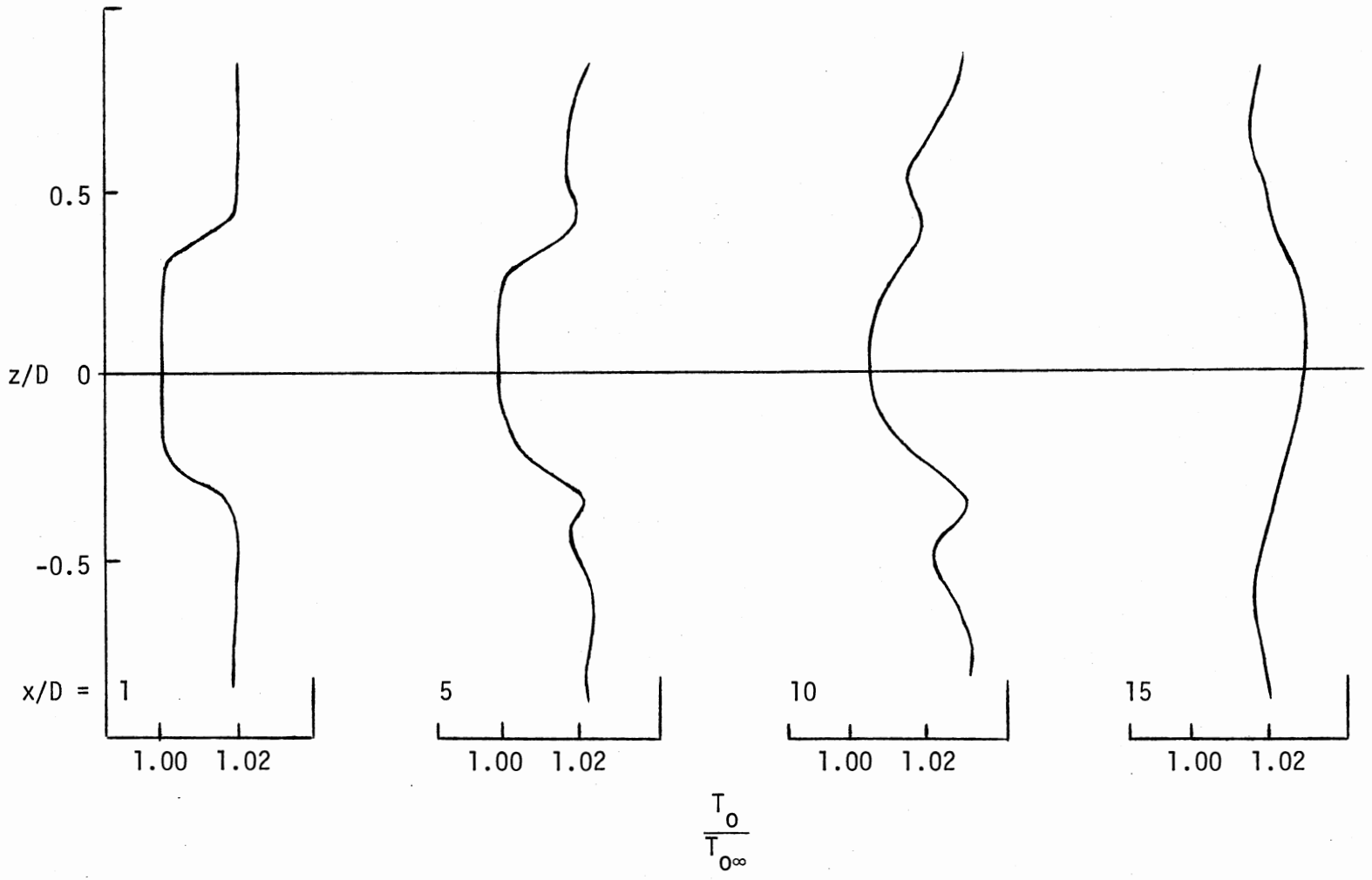

Figure 54. Radial Stagnation Temperature Distributions, M = 2.1

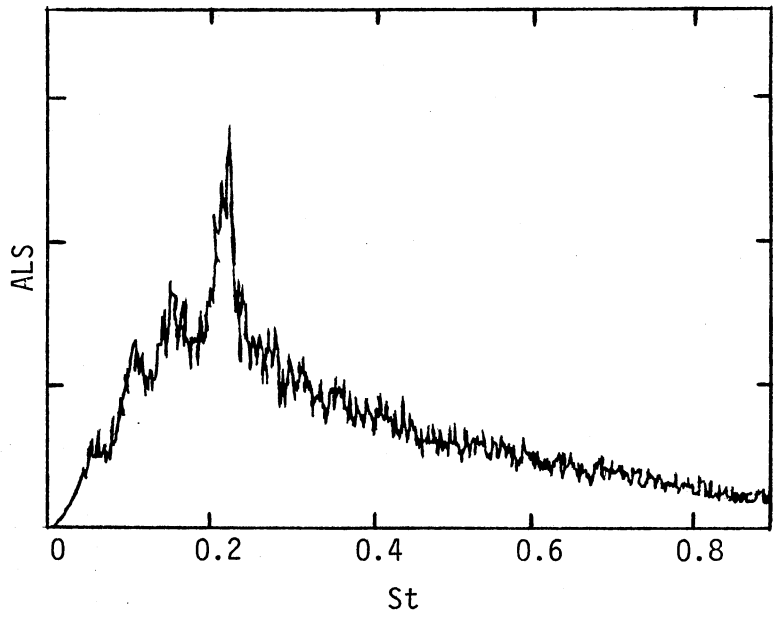

Figure 55. Microphone Spectrum, M = 2.1, x/D = 38, y/D = 21

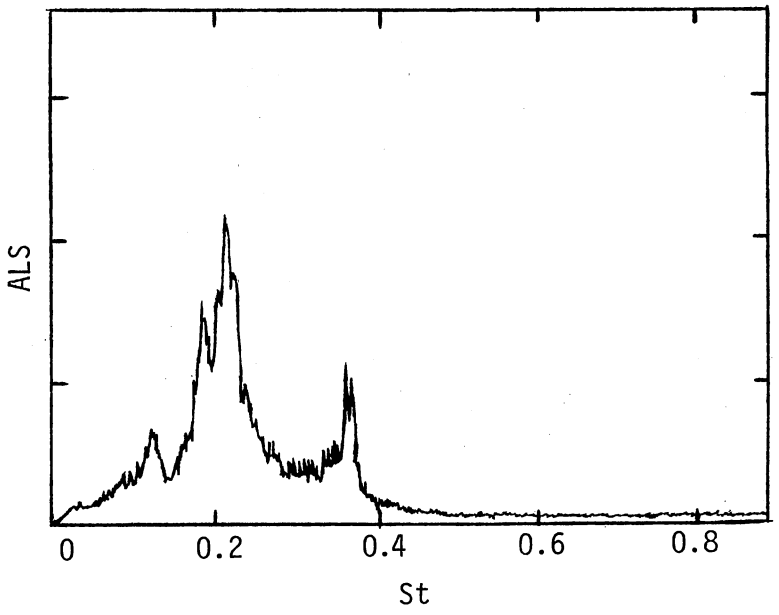

(a) x/D = 5

Figure 56. Hot-Wire Spectrum, M = 2.1

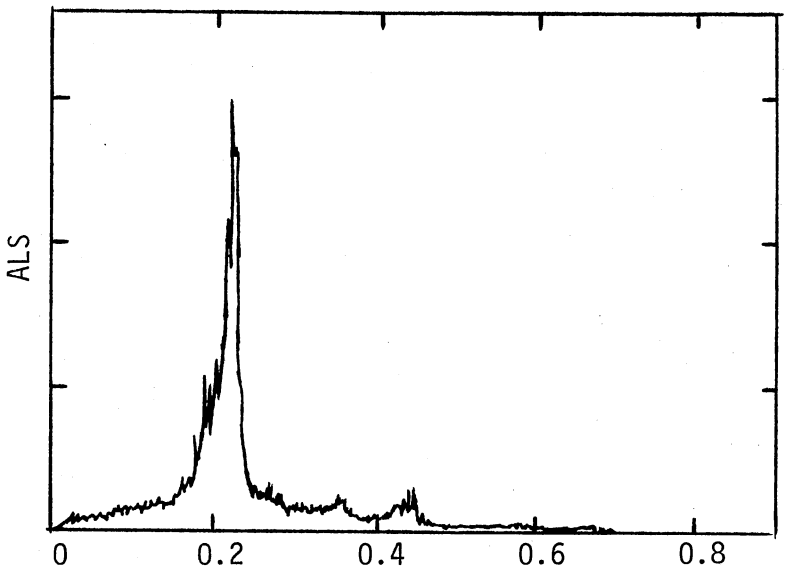

(b) x/D = 10

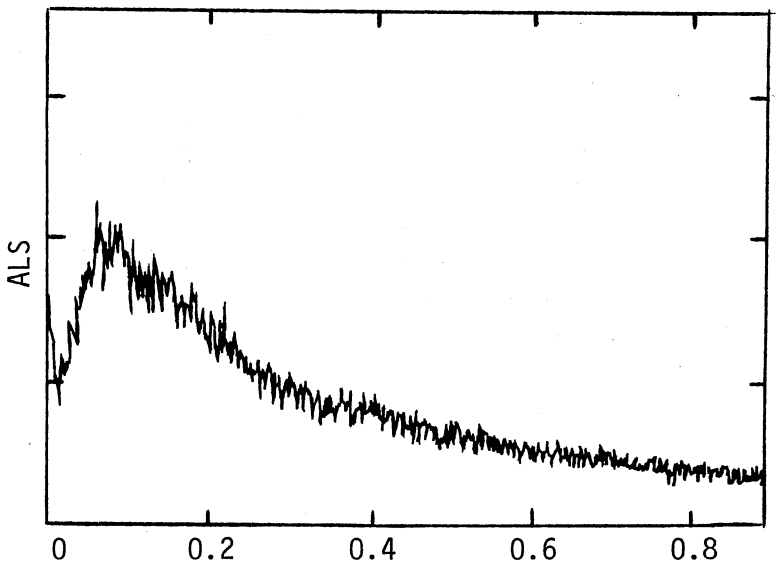

(c) x/D = 15

Figure 56. (Continued)

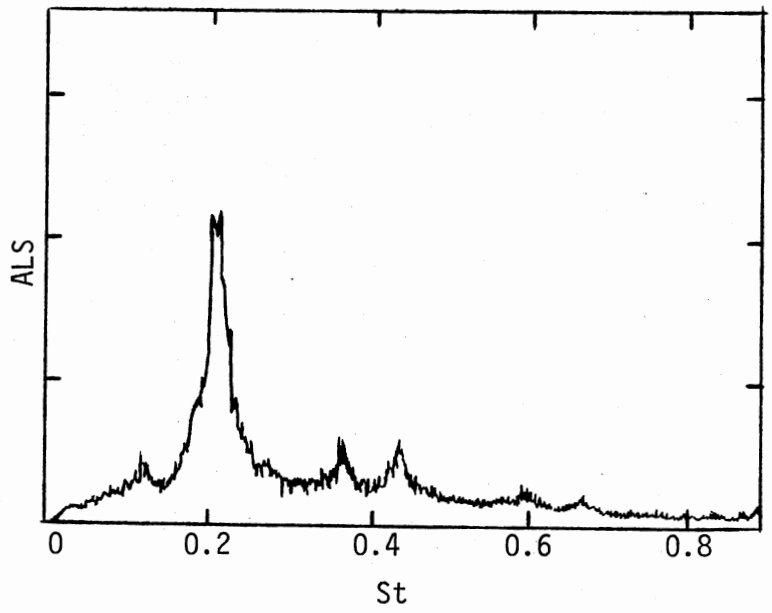

(a) x/D = 5

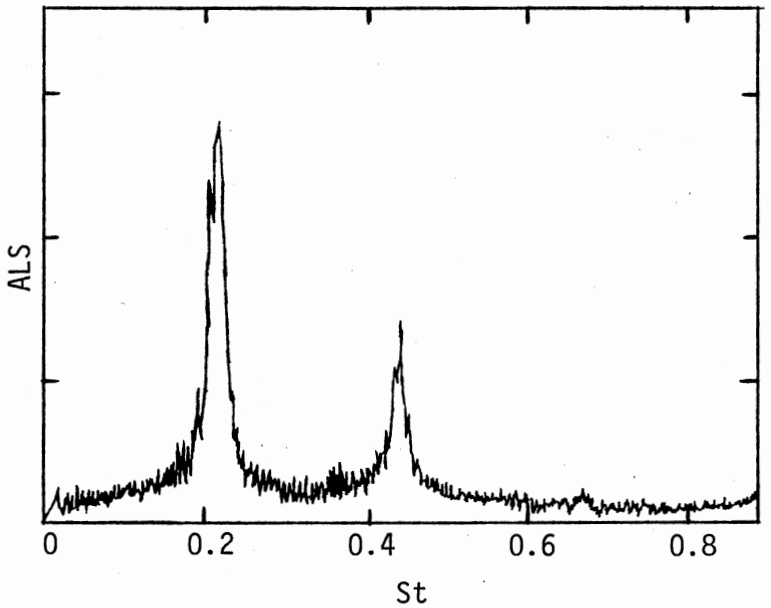

(b) x/D = 10

Figure 57. Hot-Wire Spectra, M = 2.1, Excited at St = 0.22

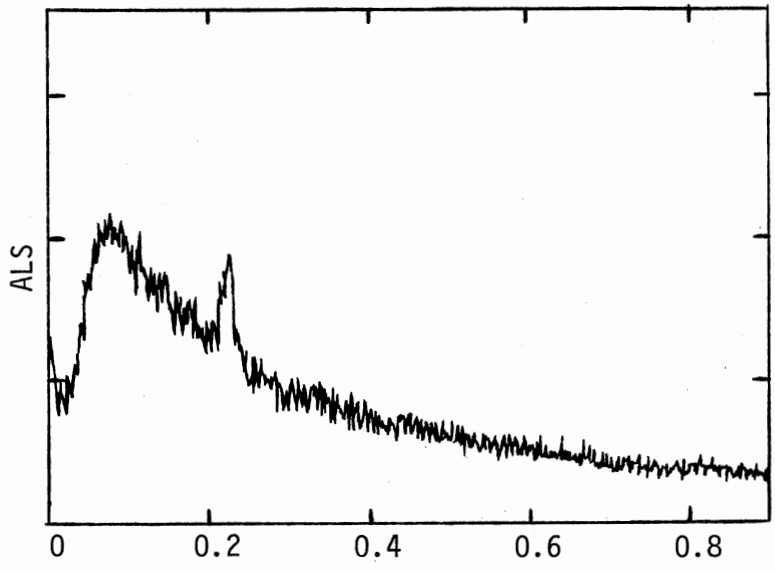

(c) x/D = 15

Figure 57. (Continued)

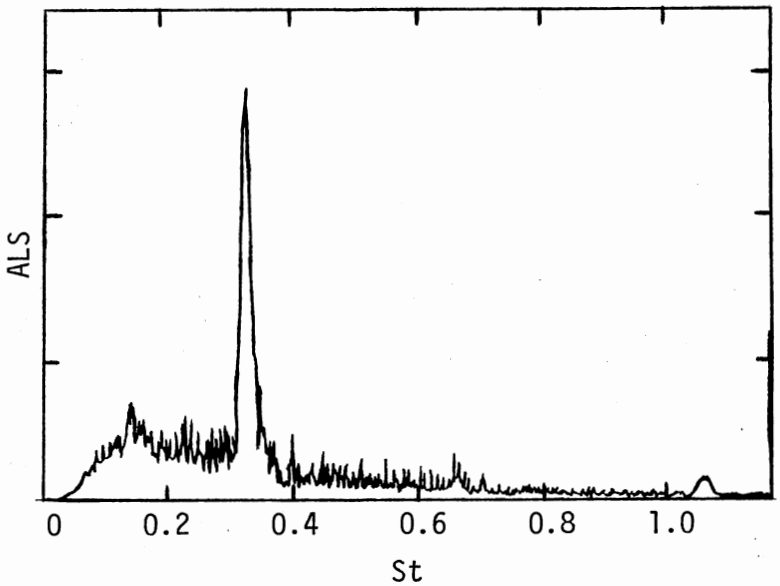

Figure 58. Microphone Spectrum, M = 1.4, x/D = 41, y/D = 21

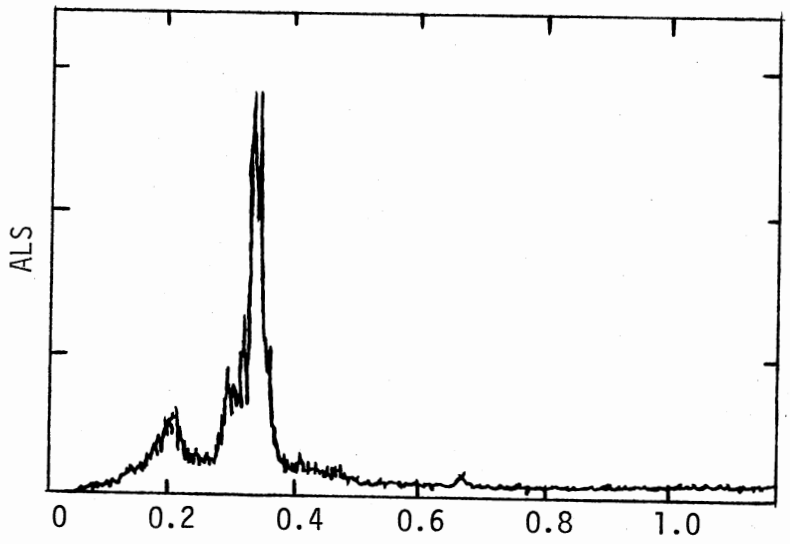

(a) x/D = 4

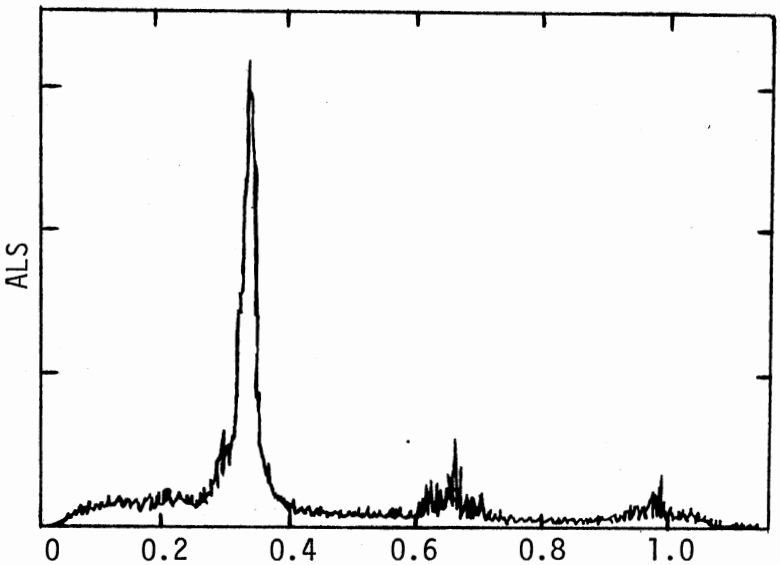

(b) x/D = 8

Figure 59. Hot-Wire Spectra, M = 1.4

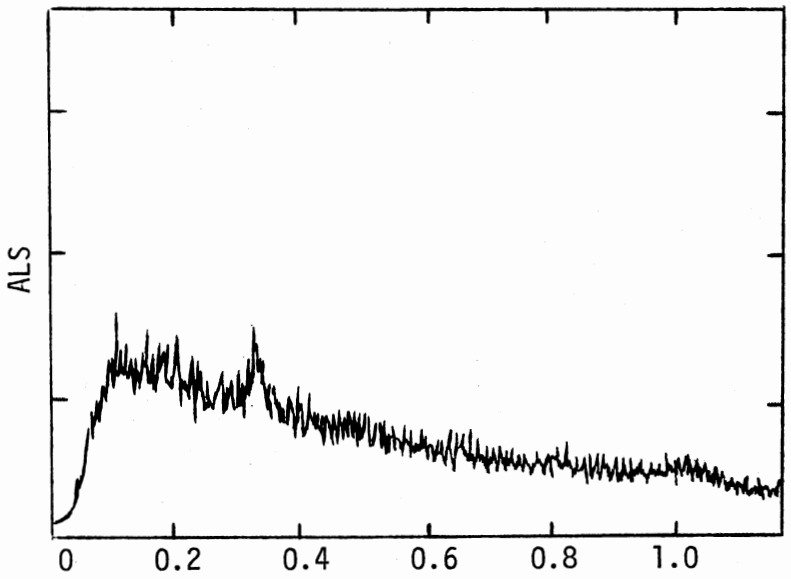

(c) x/D = 12

Figure 59. (Continued)

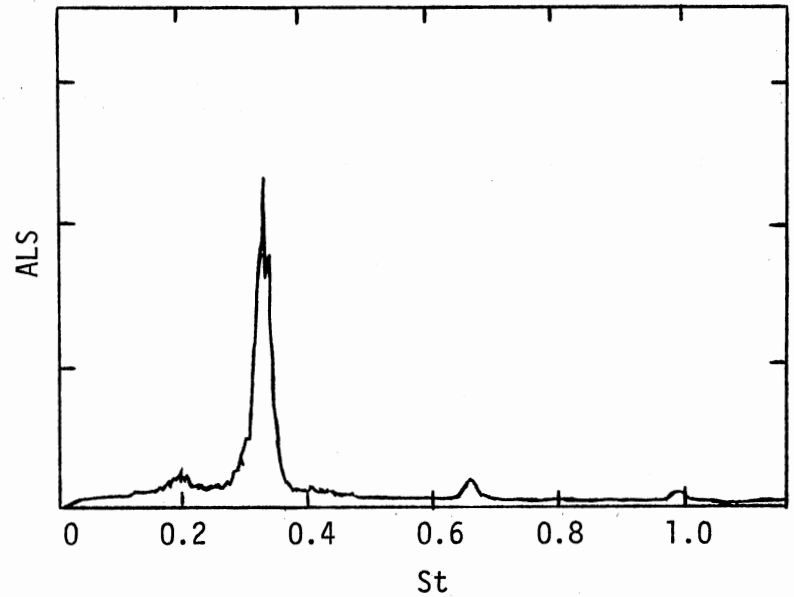

(a) x/D = 4

Figure 60. Hot-Wire Spectrum, M = 1.4, Excited at St = 0.33

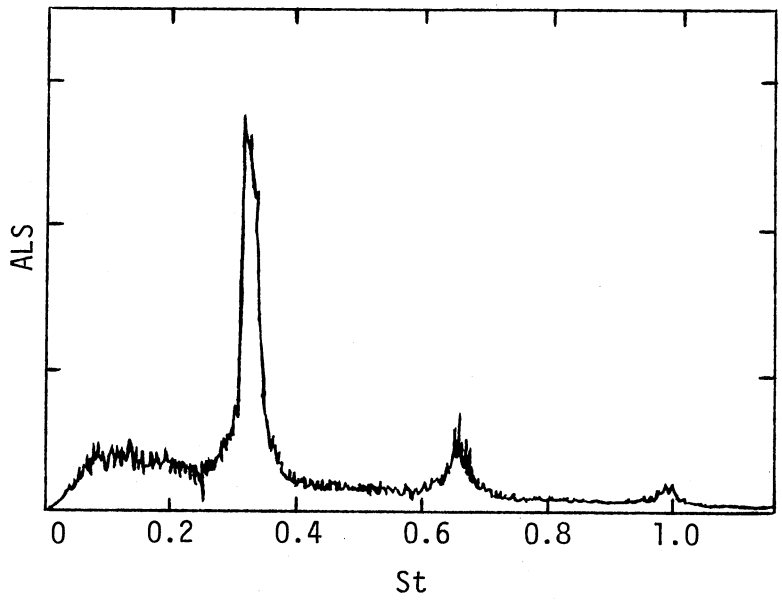

(a) x/D = 8

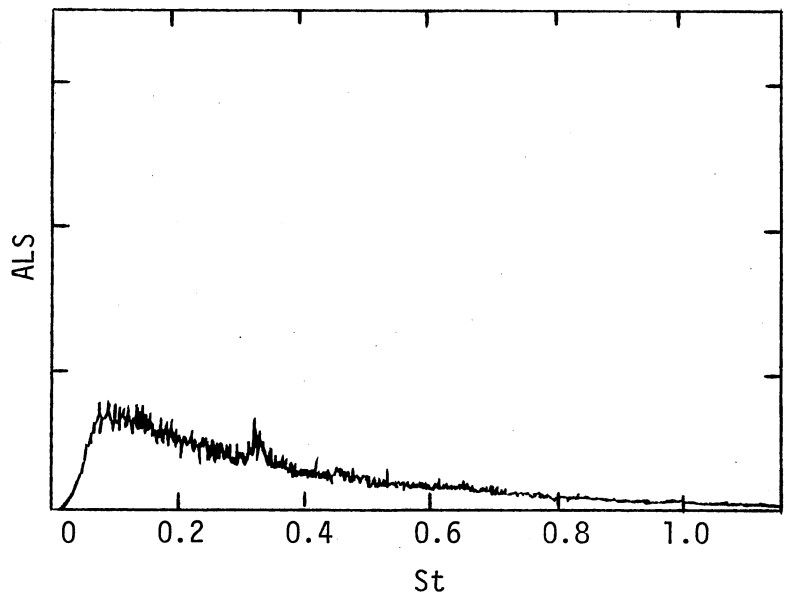

(b) x/D = 12

Figure 60. (Continued)

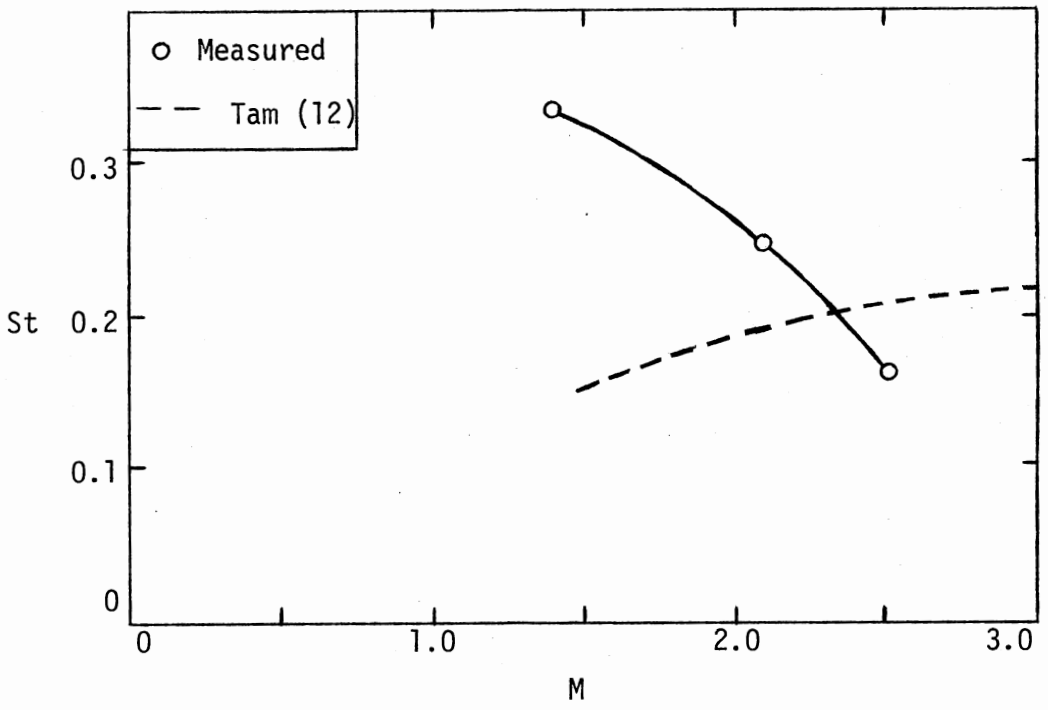

Figure 61. Strouhal Number Variation with Mach Number

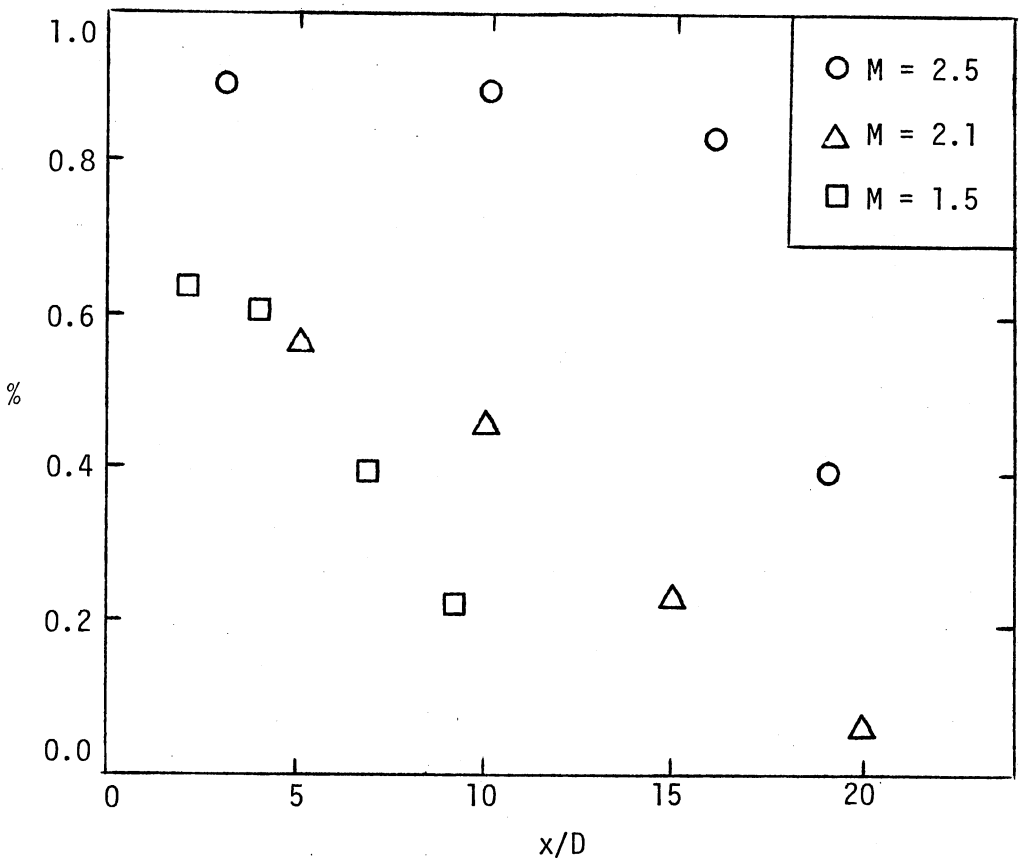

Figure 62. Axial Distribution of Percent Coherent Structure in the Flow

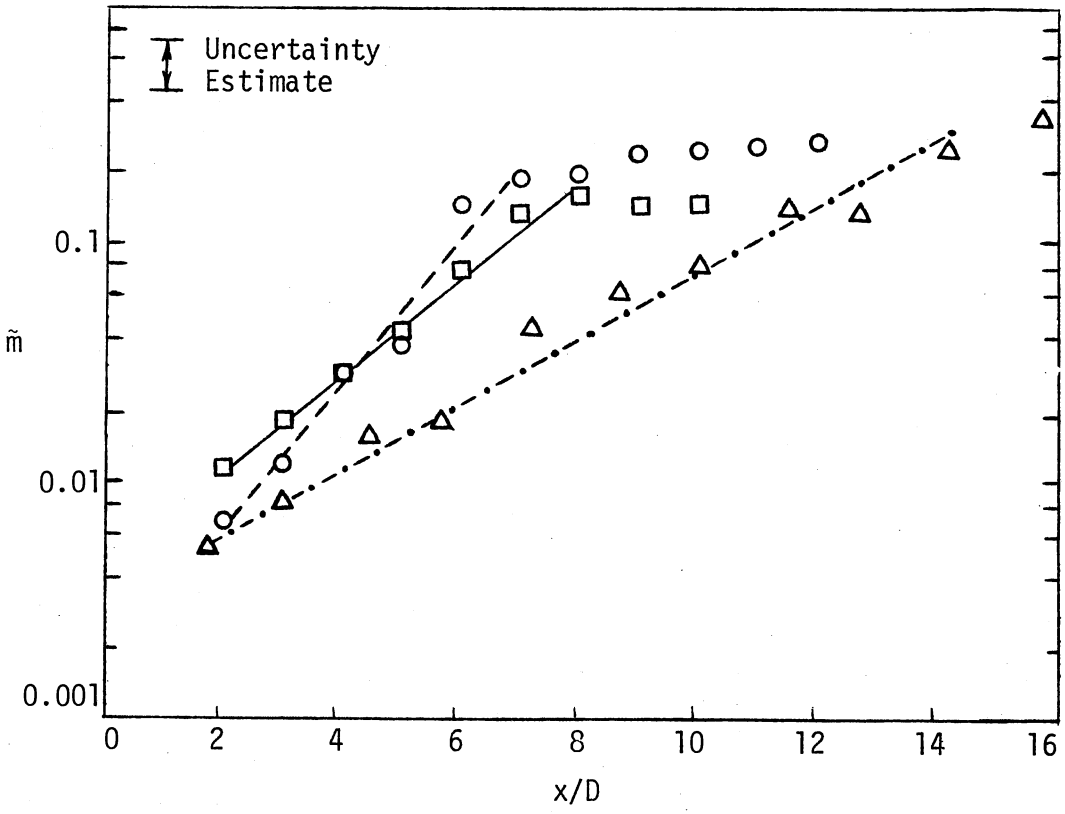

Figure 63. Axial Full Wave $\tilde{m}$ Distributions (□ M = 1.4, ○ M = 2.1, △ M = 2.5)

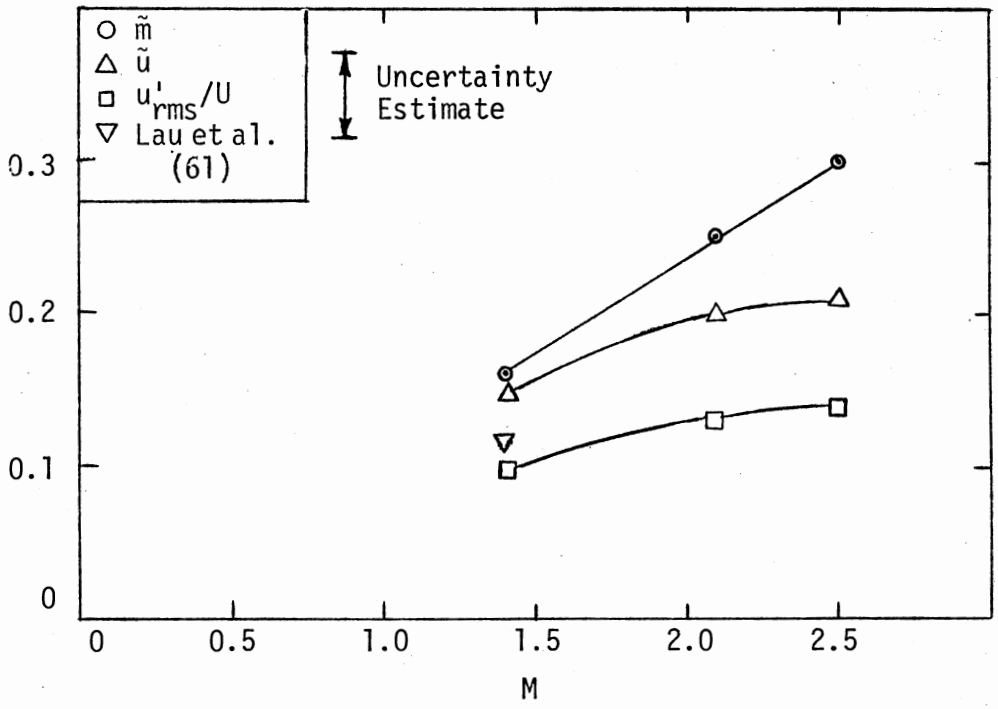

Figure 64. Maximum Flow Fluctuation Levels as a Function of Mach Number, 3,700 $\leq$ Re $\leq$ 8,700

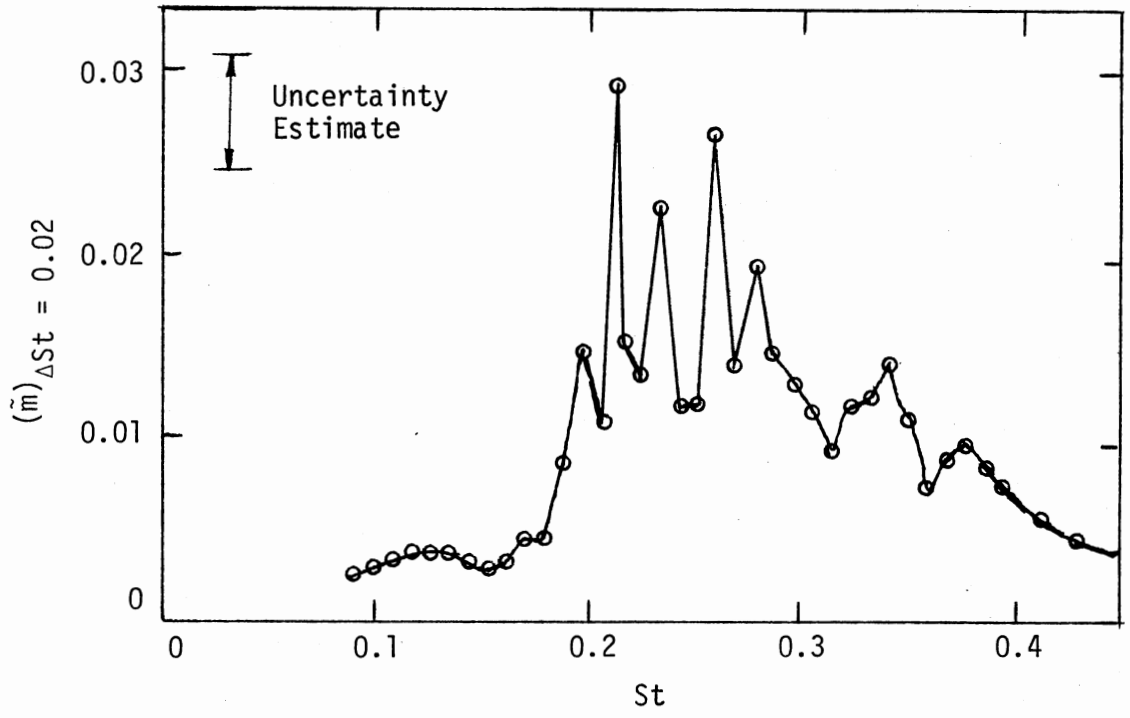

(a) M = 2.1, x/D = 5

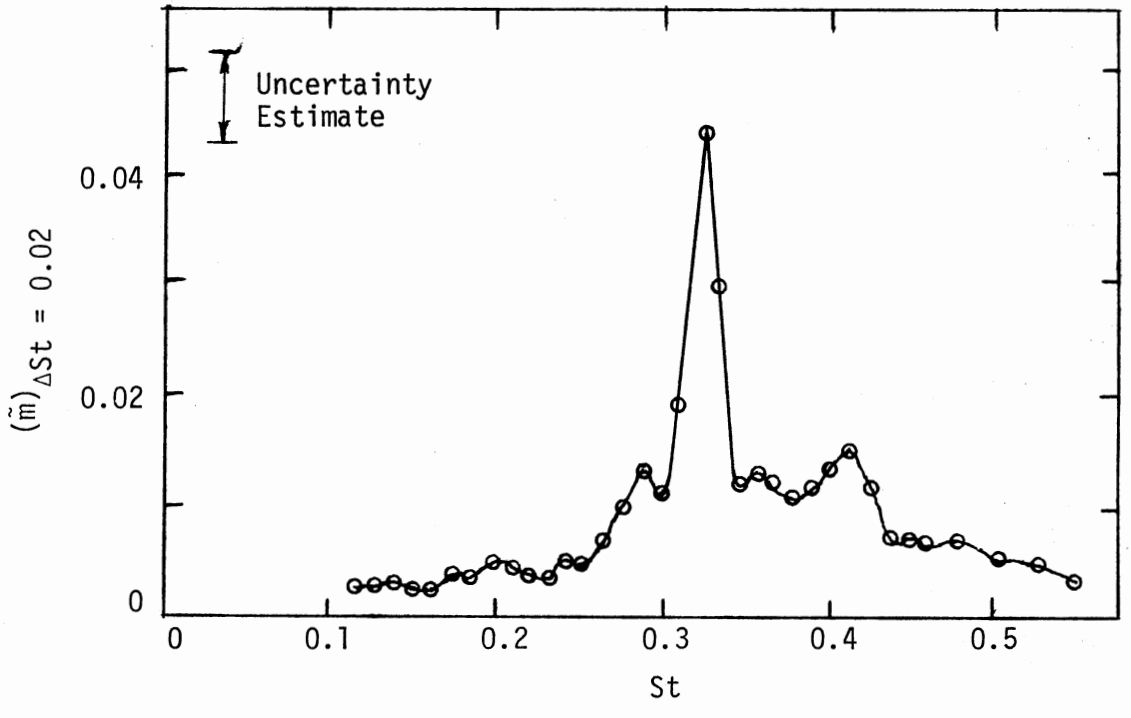

(b) M = 1.4, x/D = 4

Figure 65. Response of the M = 1.4 and 2.1 Jets to Different Excitation Frequencies

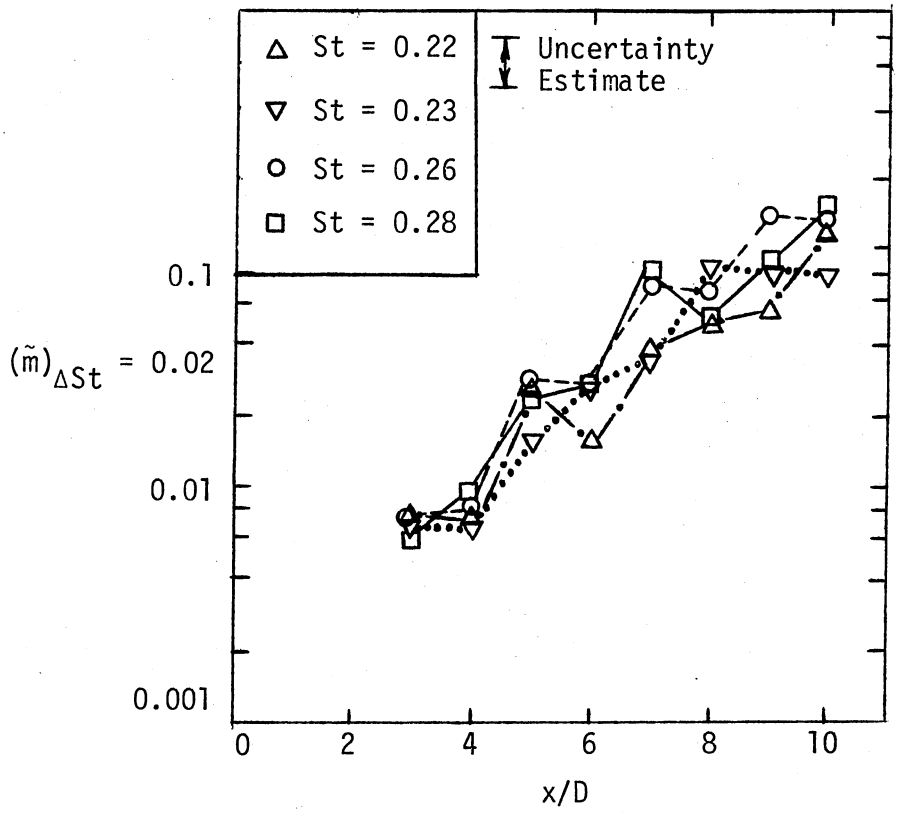

Figure 66. Flow Fluctuation Amplitude Distribution for 1 kHz Band Centered at the Frequency of Excitation, M = 2.1, ΔSt = 0.02

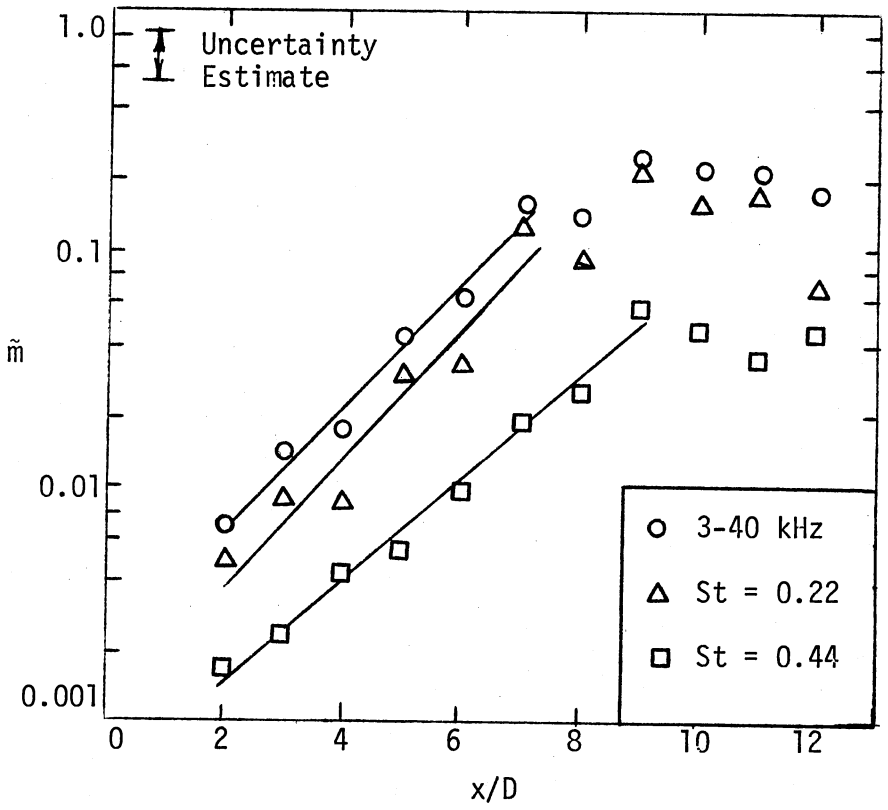

Figure 67. Axial Distribution of $\tilde{m}$ for Different Components, M = 2.1, Excited at St = 0.22

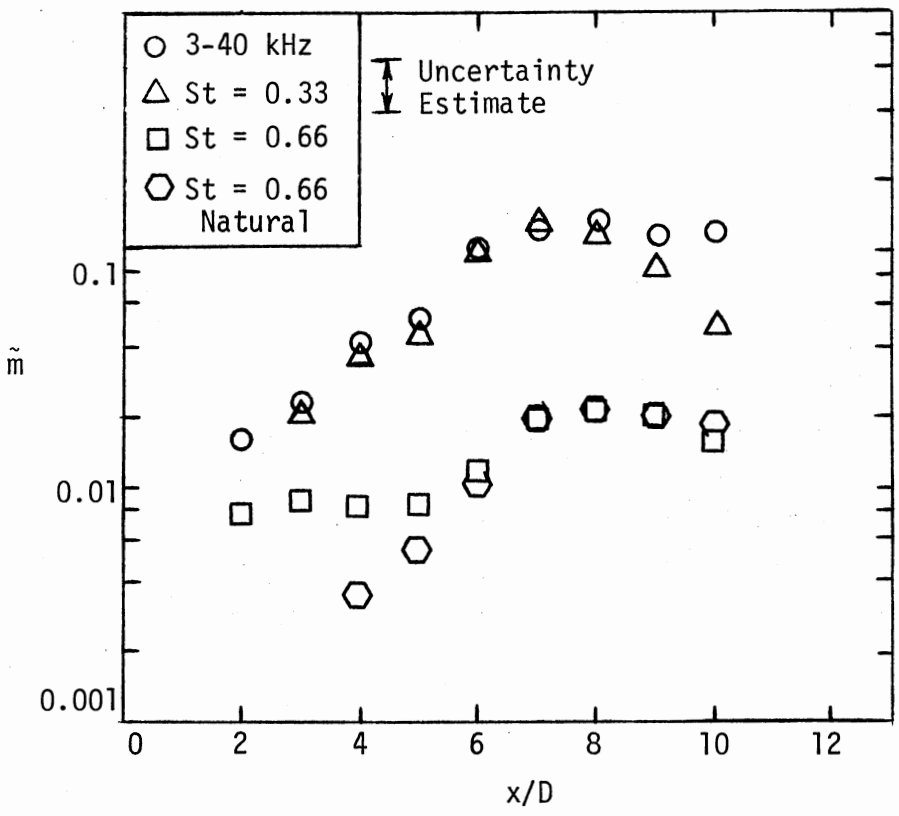

Figure 68. Axial Flow Fluctuation Distribution for Different Spectral Components, M = 1.4, Excited at St = 0.33

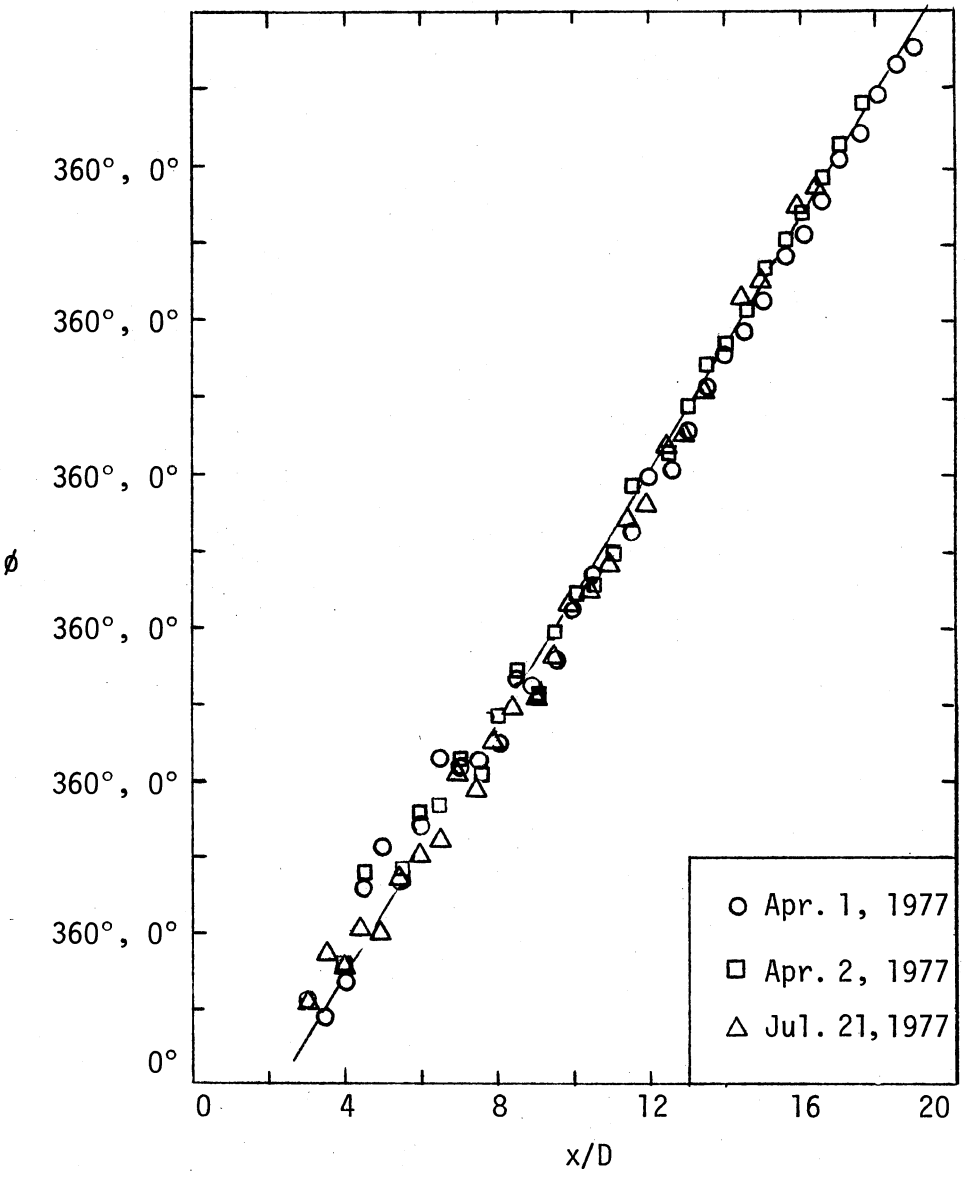

Figure 69. Axial Phase Distribution, M = 2.1, St = 0.22

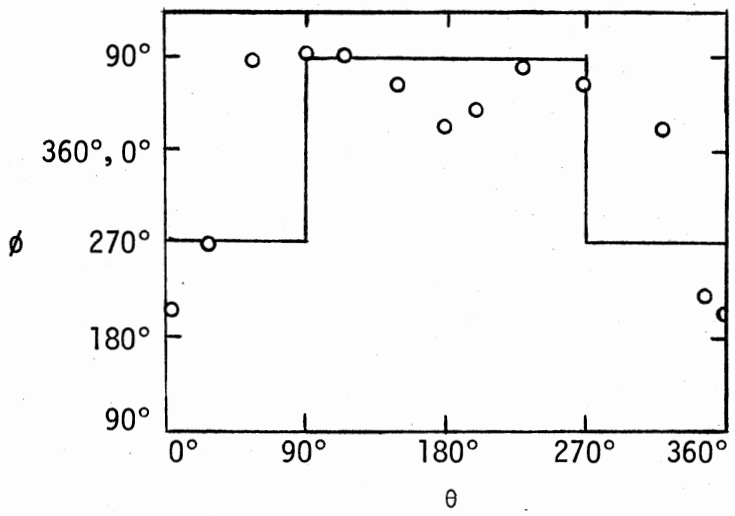

(a) x/D = 7

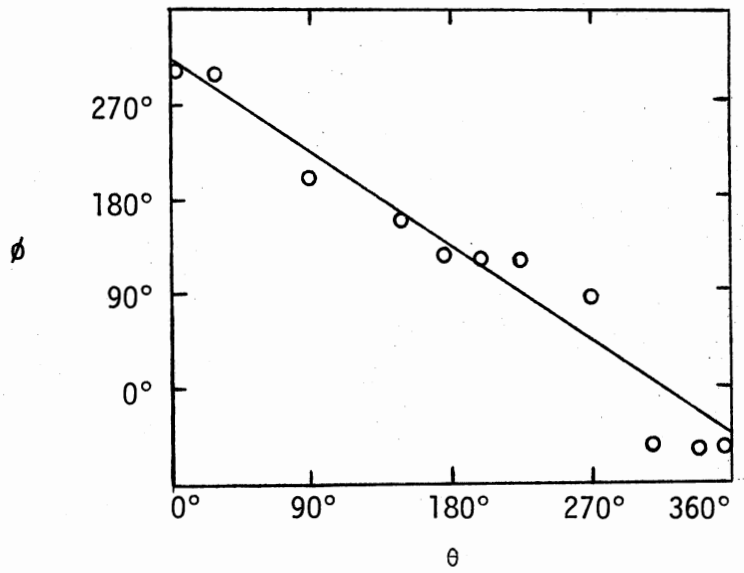

(b) x/D = 13

Figure 70. Azimuthal Phase Distribution, M = 2.1, St = 0.22

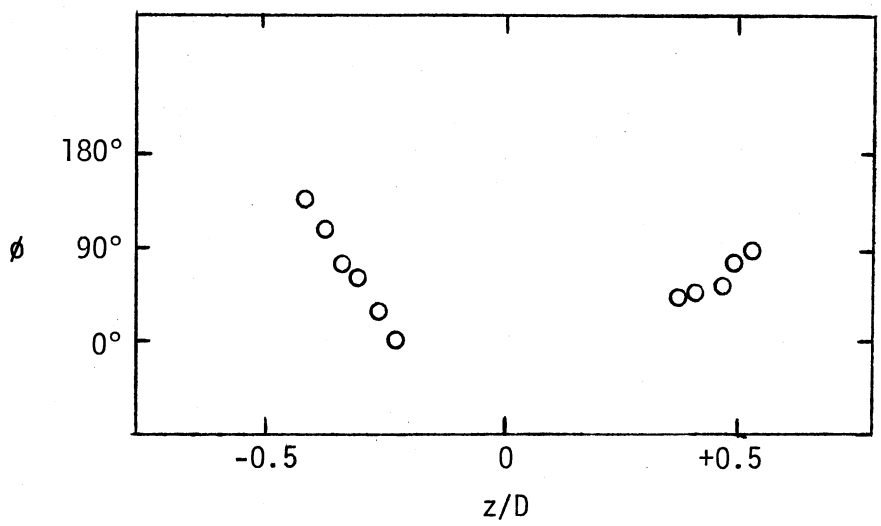

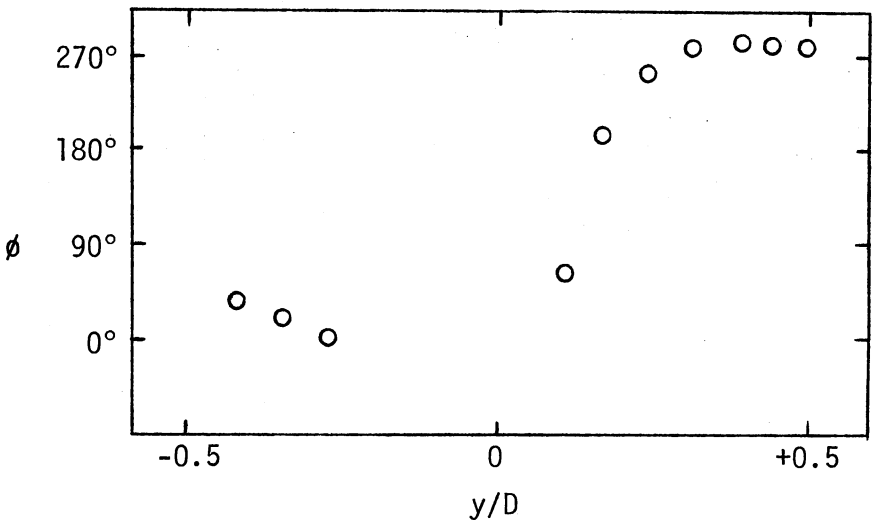

Figure 71. Radial Phase Distribution, M = 2.1, St = 0.44, x/D = 7

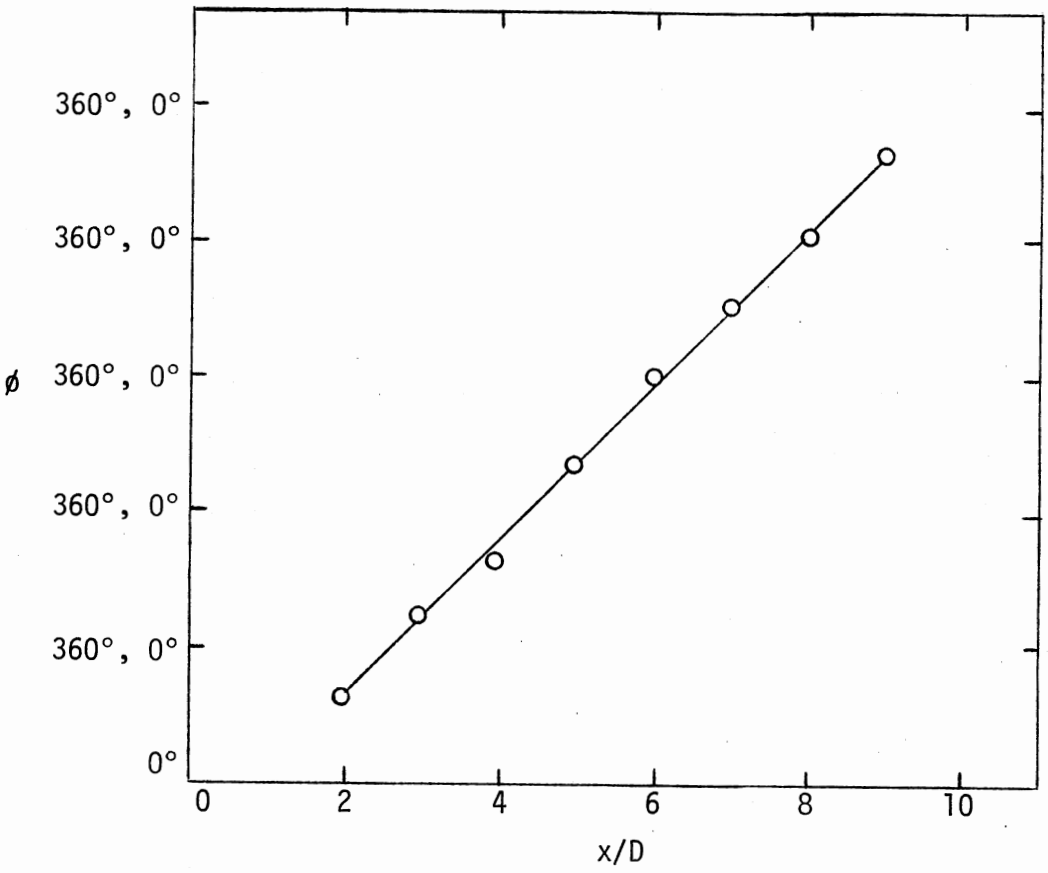

Figure 72. Axial Phase Distribution, M = 1.4, St = 0.33

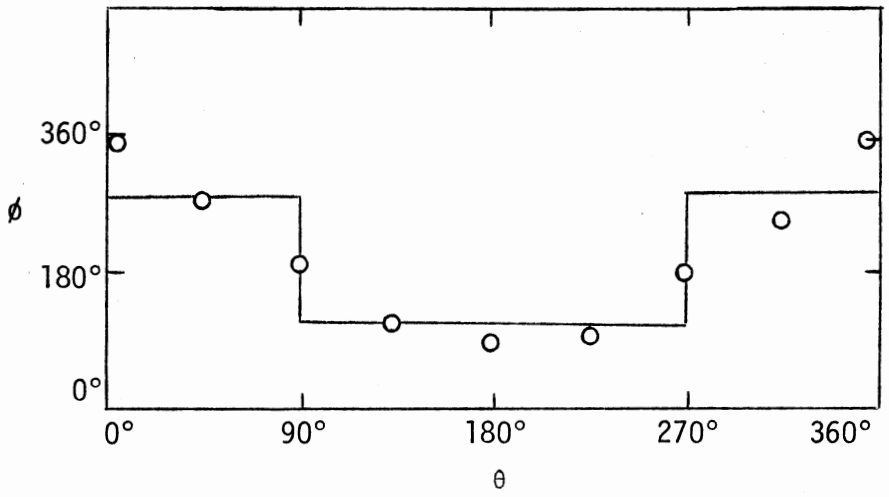

(a) x/D = 4

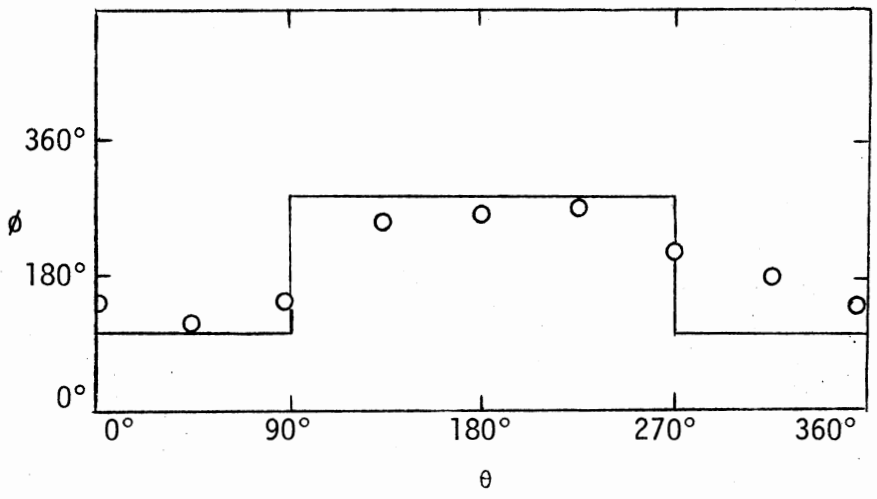

(b) x/D = 8

Figure 73. Azimuthal Phase Distribution, M = 1.4, St = 0.33

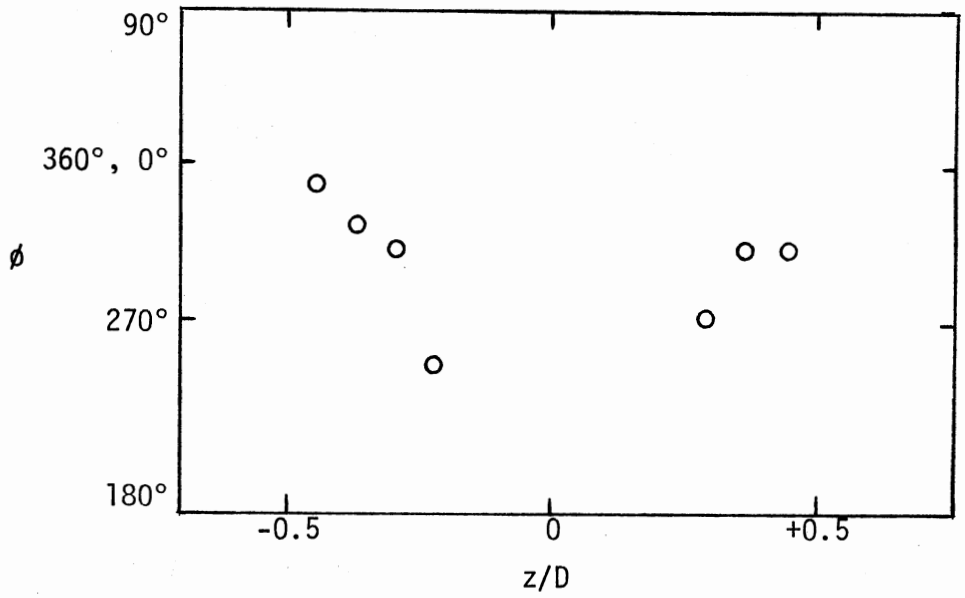

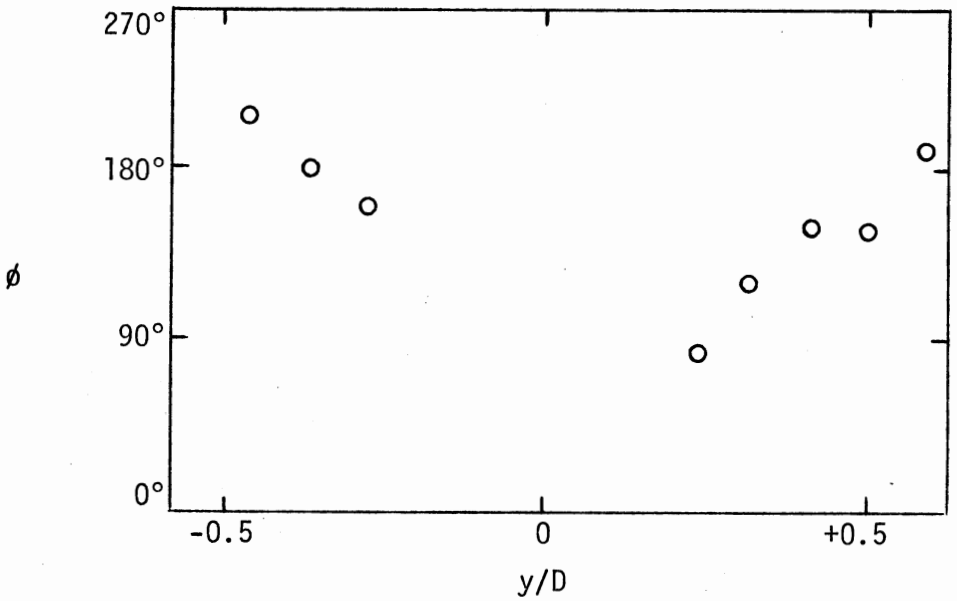

Figure 74. Radial Phase Distribution,
M = 1.4, St = 0.33,
x/D = 4

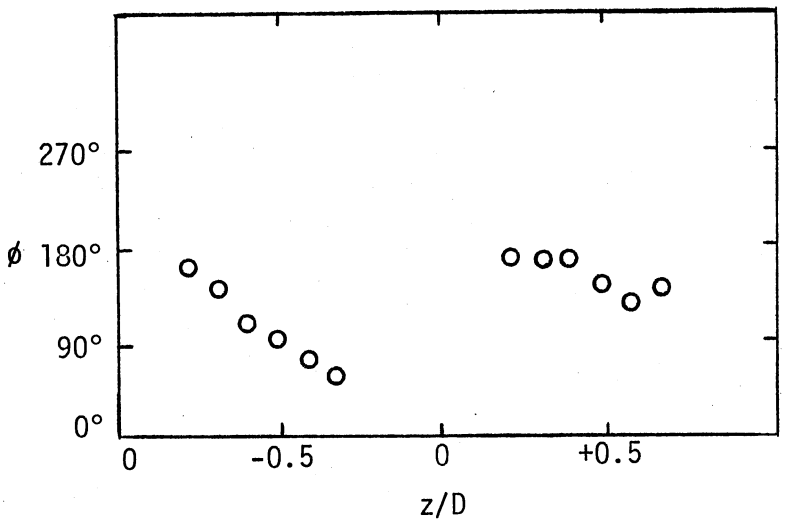

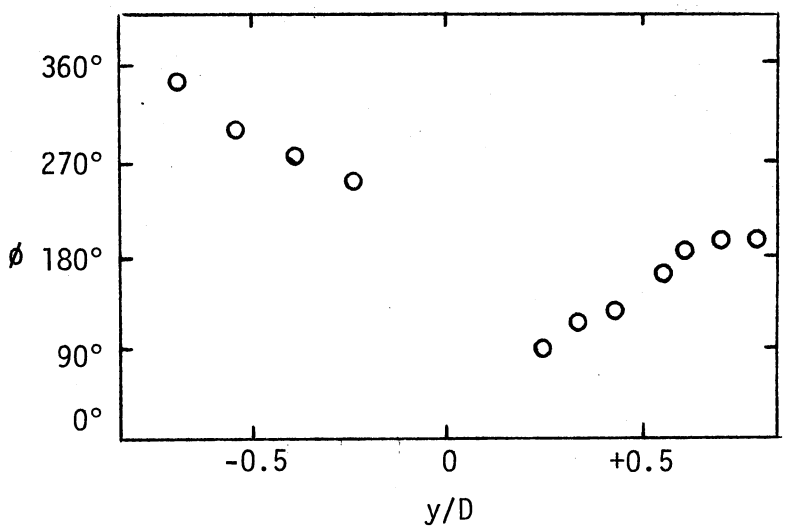

Figure 75. Radial Phase Distribution, M = 1.4, St = 0.33, x/D = 8

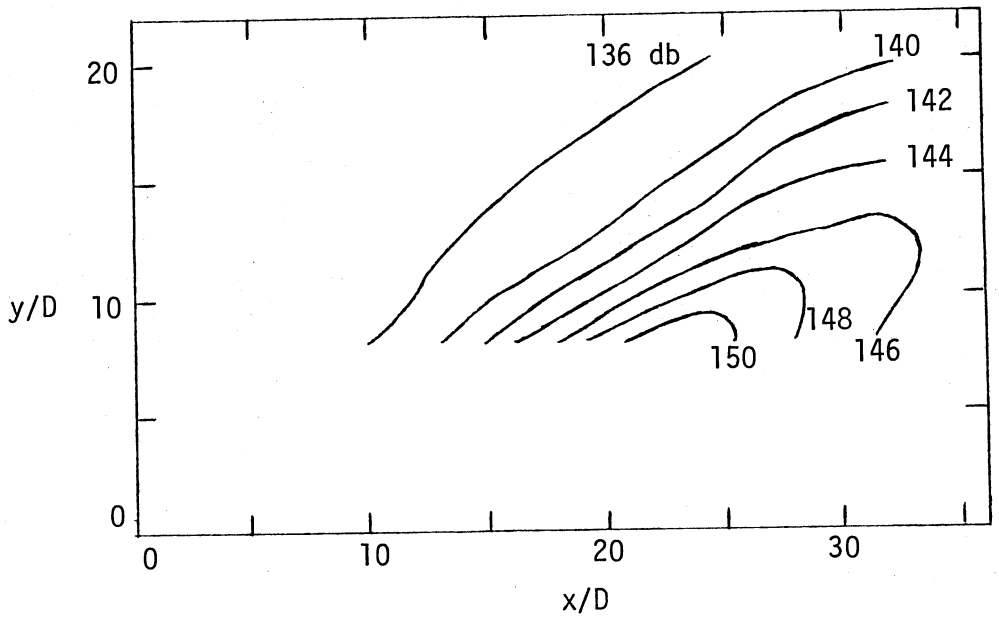

(a) Natural

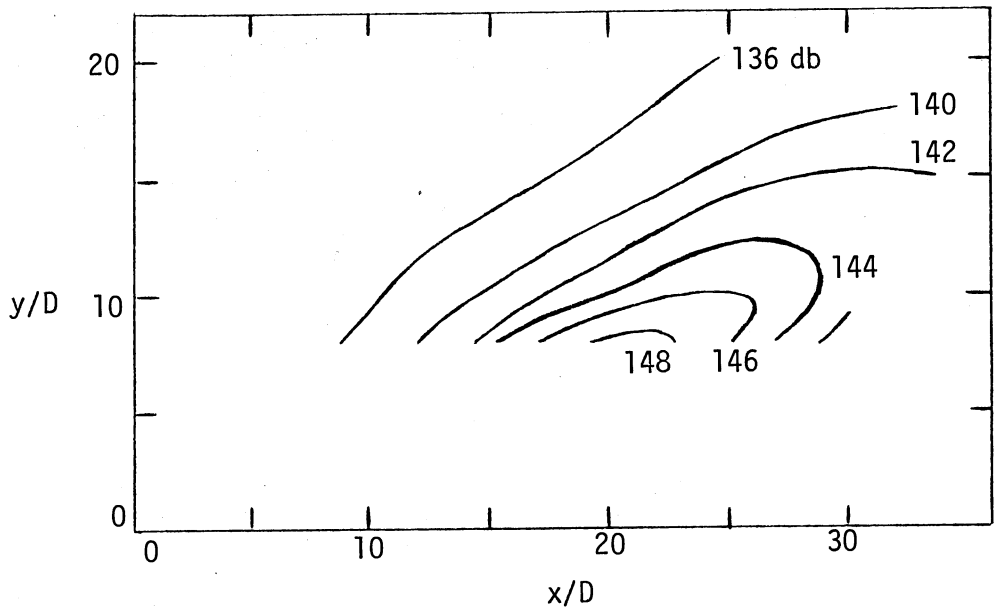

(b) Excited at St = 0.22

Figure 76. Full Spectrum SPL Contours, M = 2.1

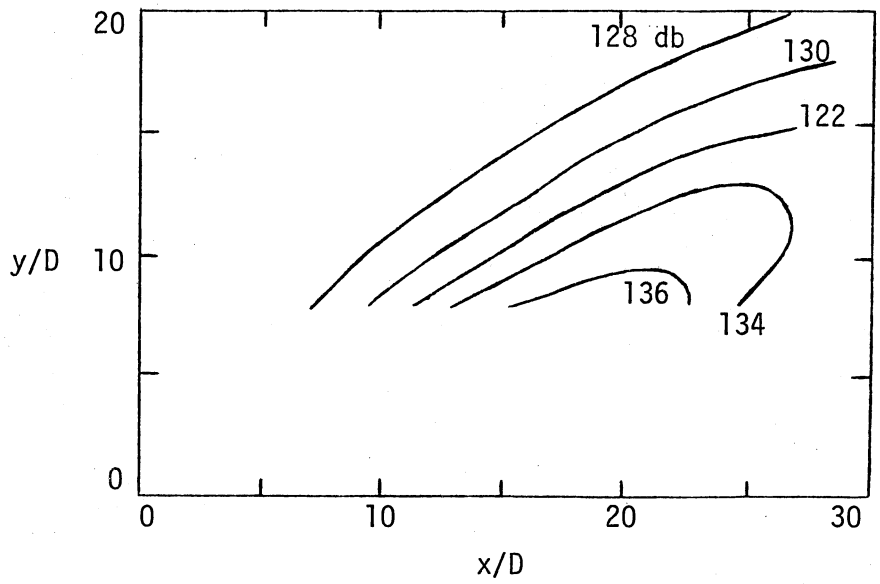

(a) Natural

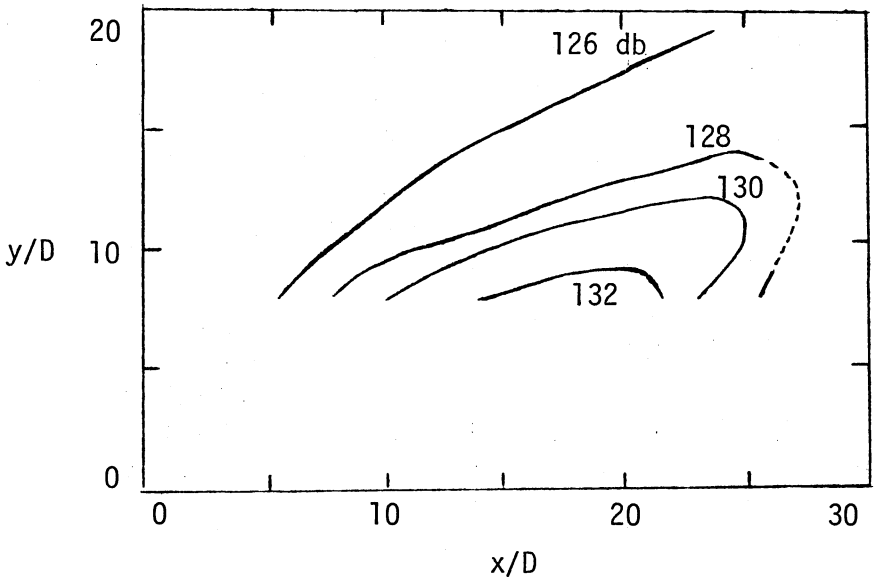

(b) Excited at St = 0.33

Figure 77. Full Spectrum SPL Contours, M = 1.4

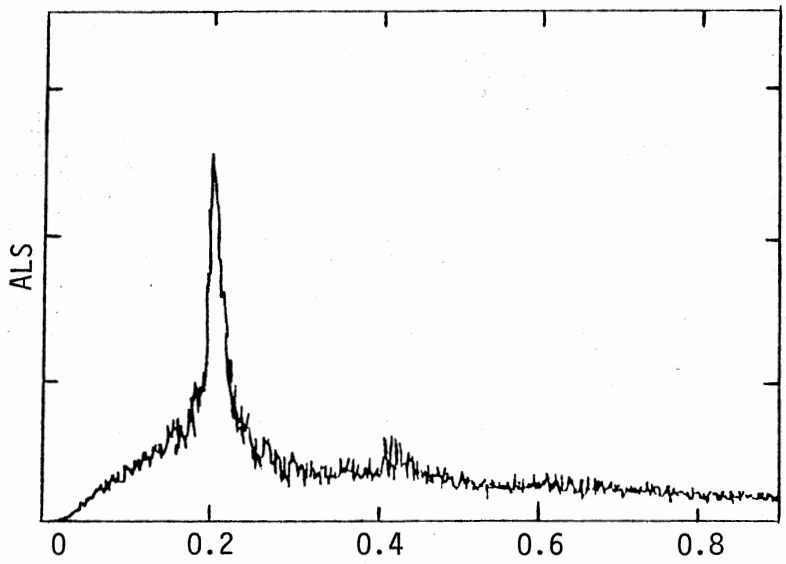

(a) Natural

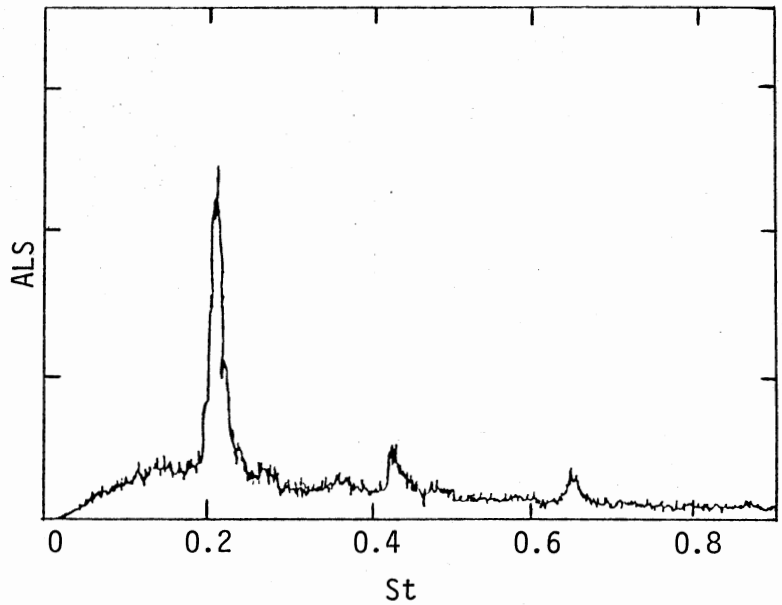

(b) Excited at St = 0.22

Figure 78. Microphone Spectra, M = 2.1, x/D = 28, y/D = 12

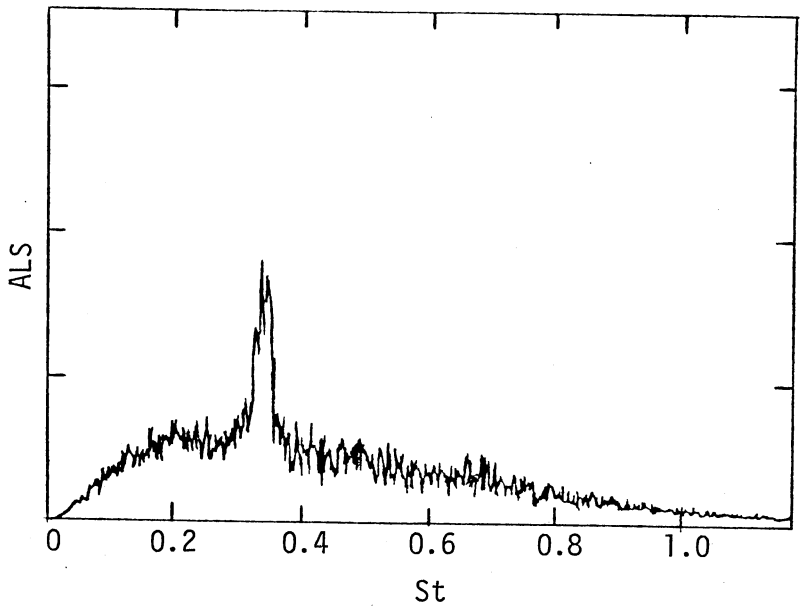

(a) Natural

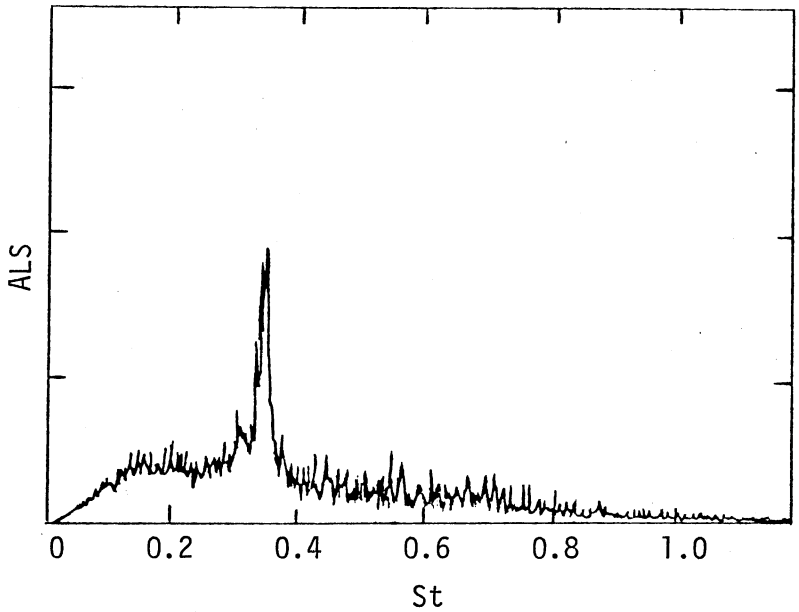

(b) Excited at St = 0.33

Figure 79. Microphone Spectra, M = 1.4, x/D = 22, y/D = 10

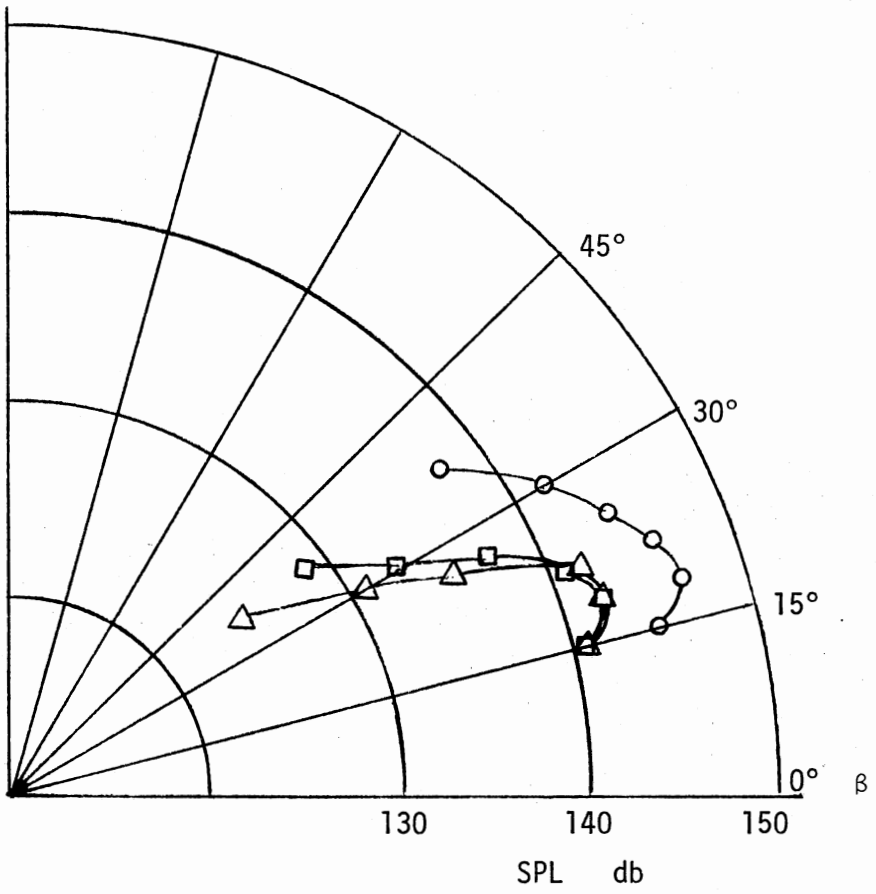

Figure 80. SPL Directivity Distributions (○ Full Spectrum, □ St = 0.22, △ Phase Average, M = 2.1)

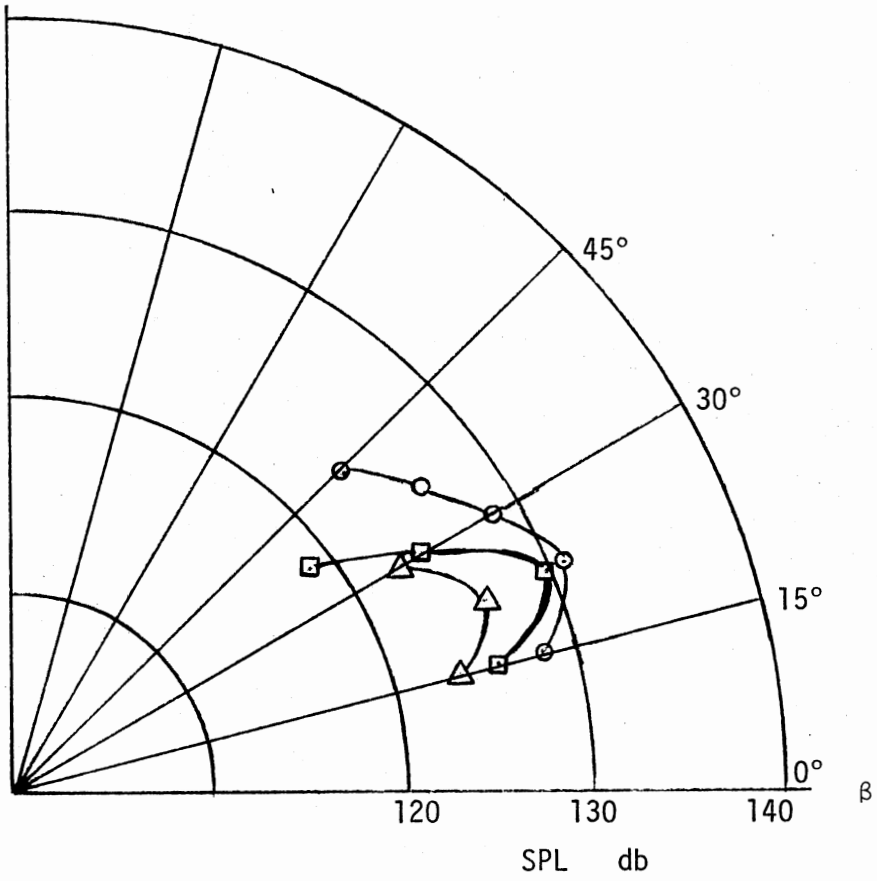

Figure 81. SPL Directivity Distributions (○ Full Spectrum, □ St = 0.33, △ Phase Average, M = 1.5)

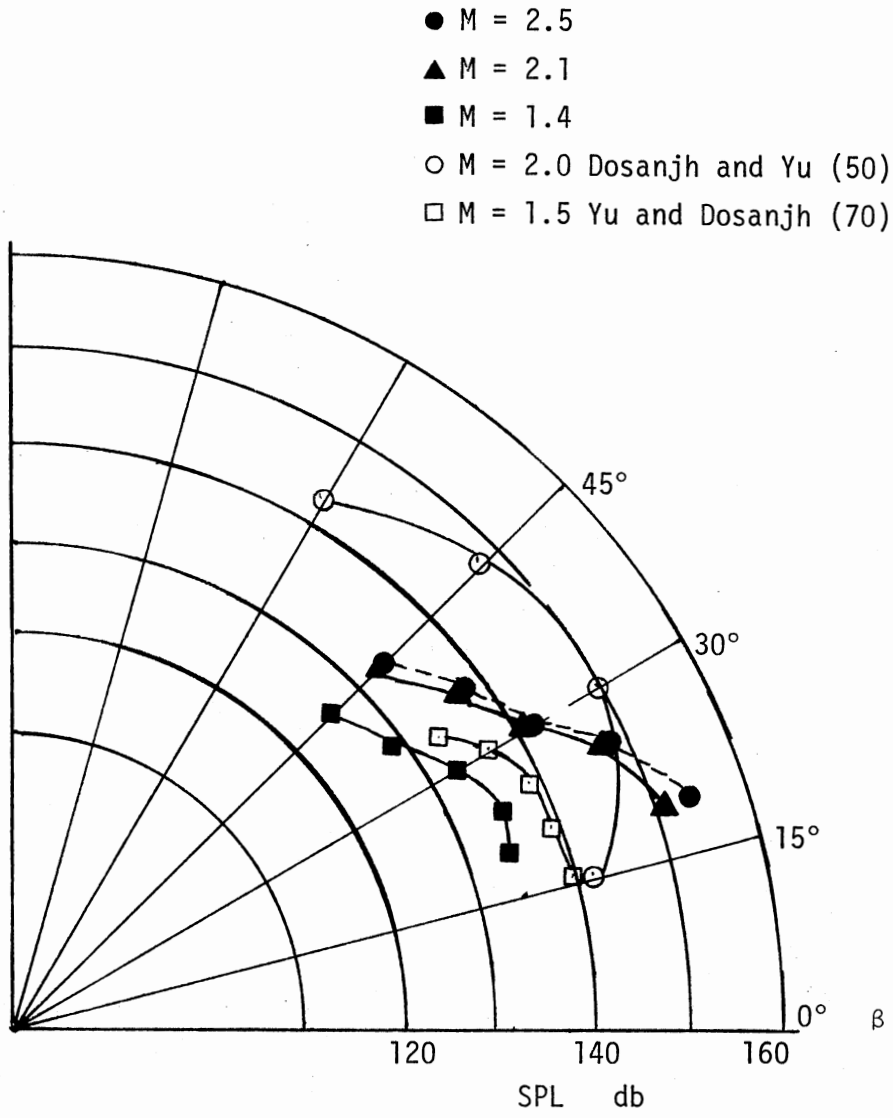

Figure 82. SPL Directivity Distributions

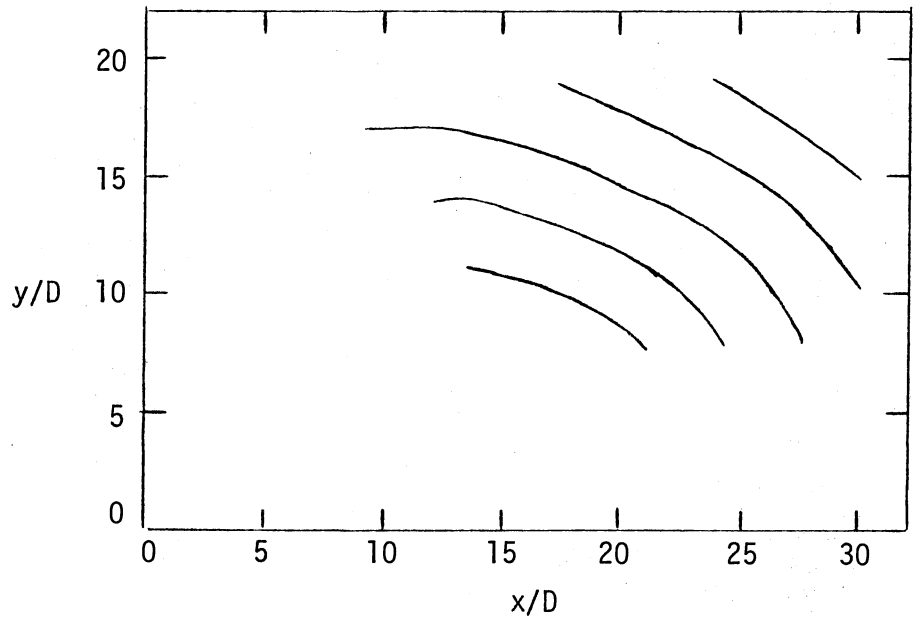

(a) M = 2.1, St = 0.22

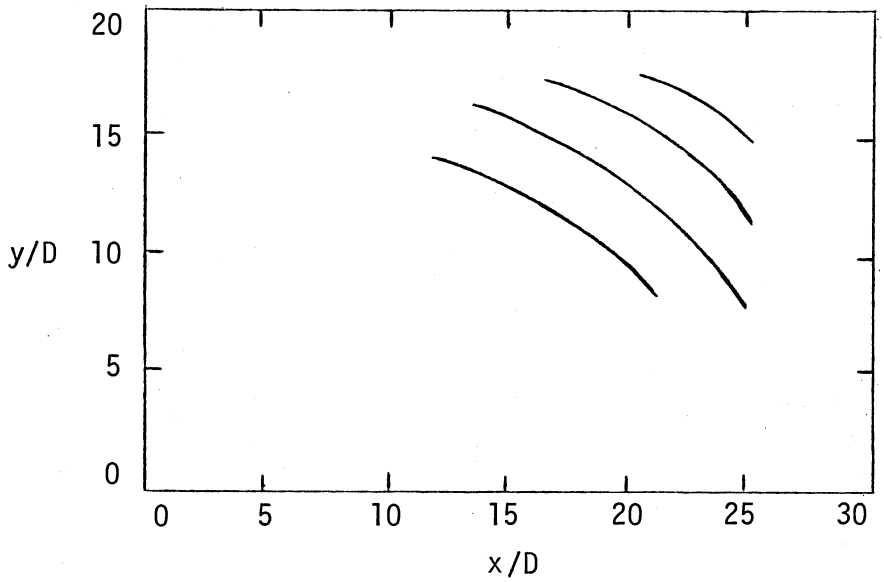

(b) M = 1.4, St = 0.33

Figure 83. Acoustic Wave Fronts

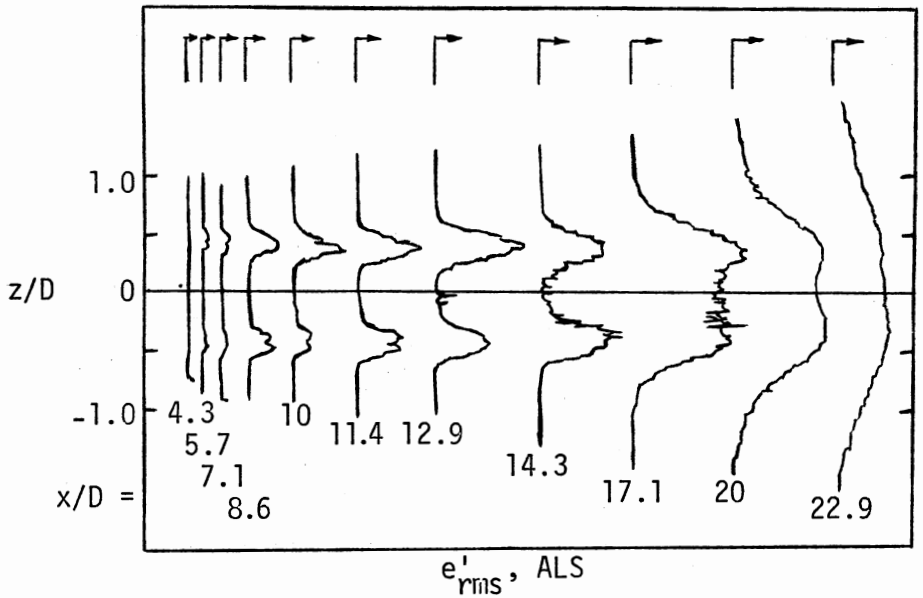

(a) Natural

Figure 84. Hot-Wire Voltage Fluctuation Level Radial Profile, M = 2.5, Full Spectrum

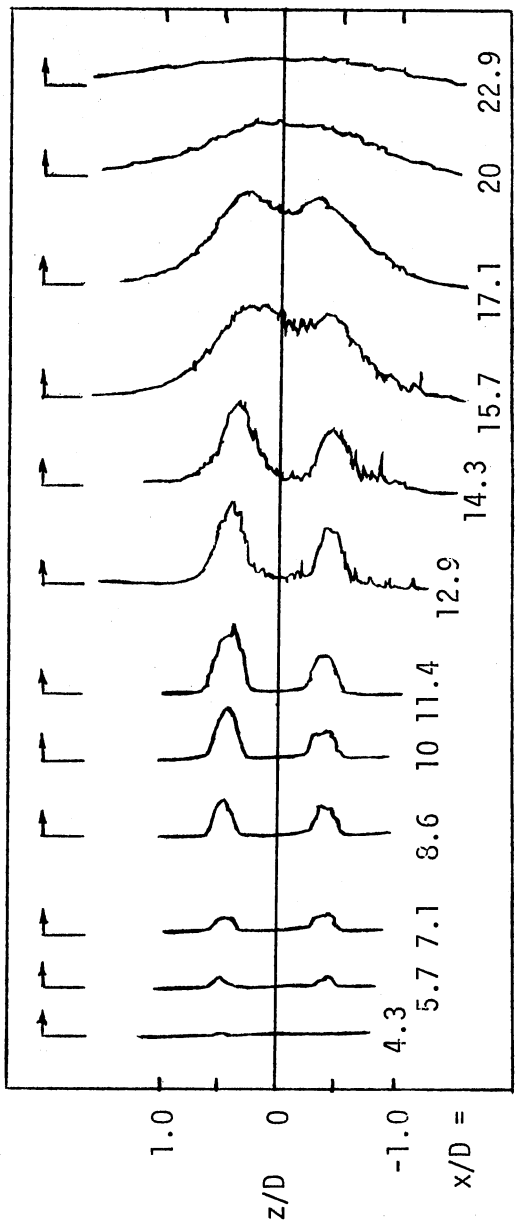

(b) Excited at St = 0.16

Figure 84. (Continued)

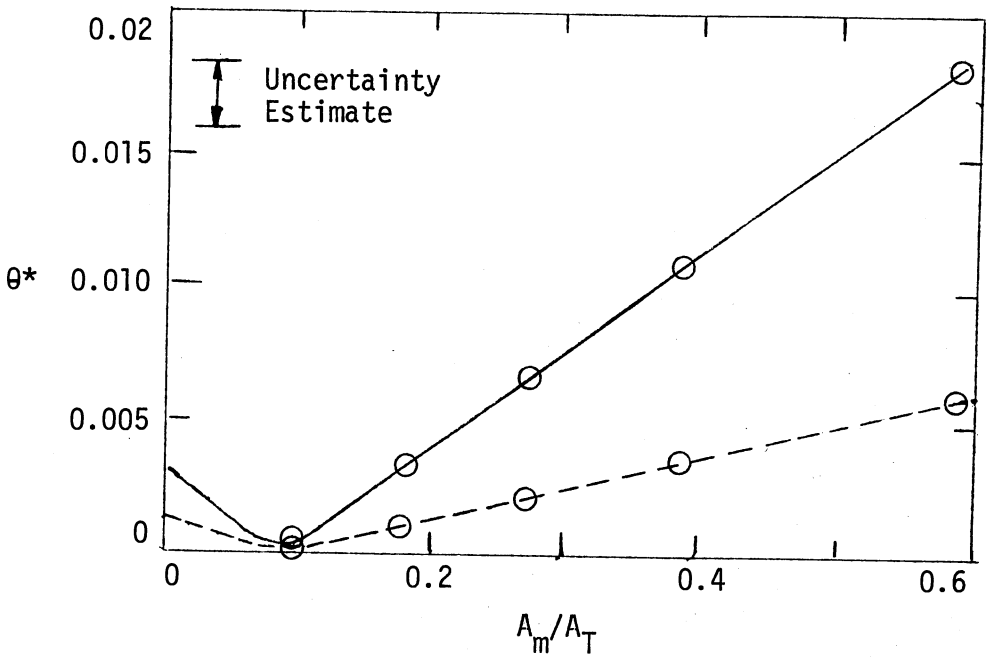

Figure 85. Hot-Wire Mode Diagram, M = 2.1, Excited at St = 0.22 (x/D = 3, —— Top of Jet, $\tilde{m}$ = 0.036, $\tilde{T}_o$ = 0.003, R_mT_o = 1.00; --- Bottom of Jet, $\tilde{m}$ = 0.012, $\tilde{T}_o$ = 0.001, R_mT_o = 0.89)

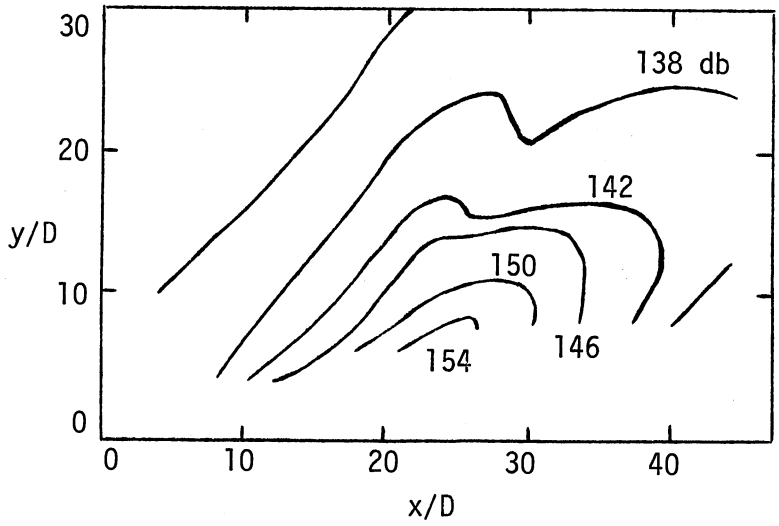

Figure 86. SPL Contour, M = 2.5 Excited at St = 0.16, High Level of Excitation

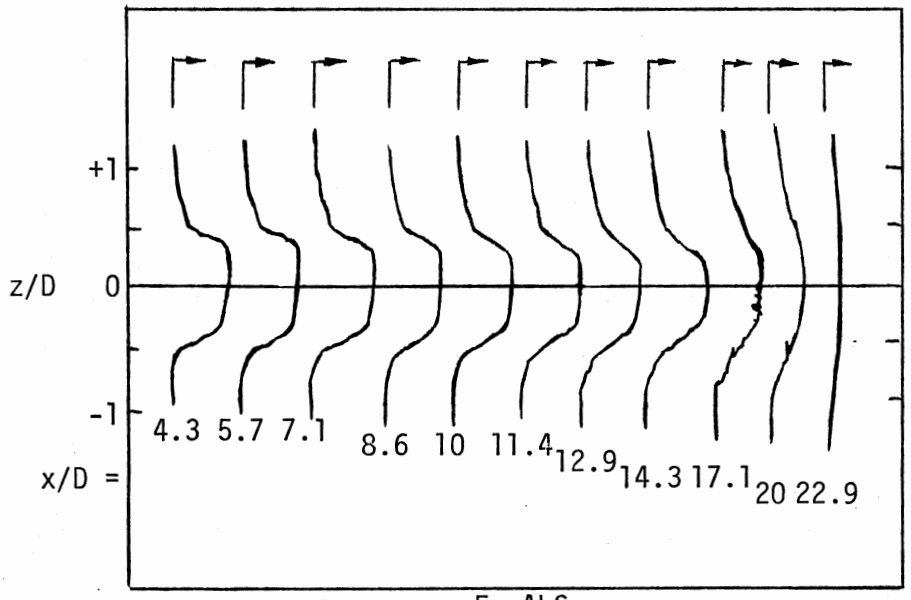

E, ALS

(a) Natural

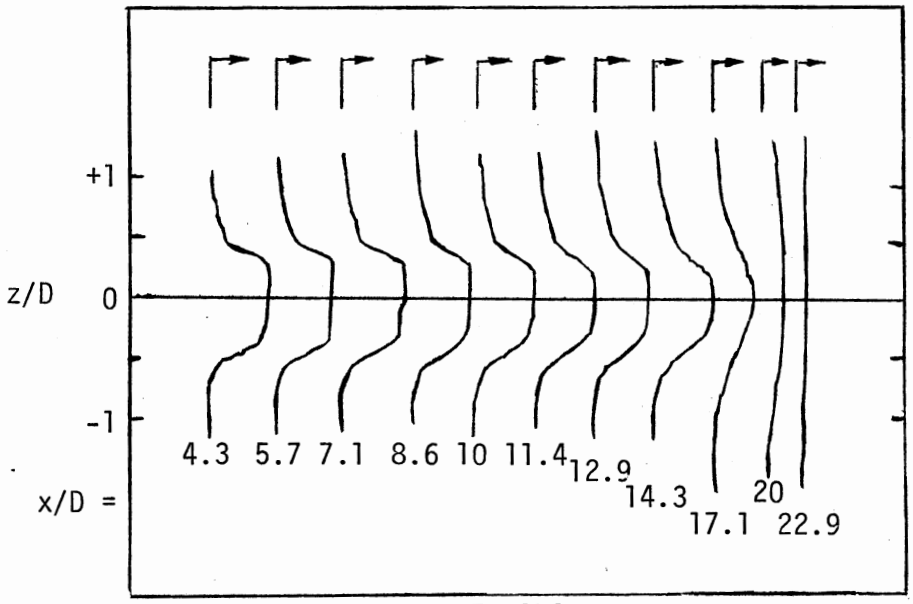

E, ALS

(b) Excited at St = 0.16

Figure 87. Mean Hot-Wire Voltage Profiles, M = 2.5

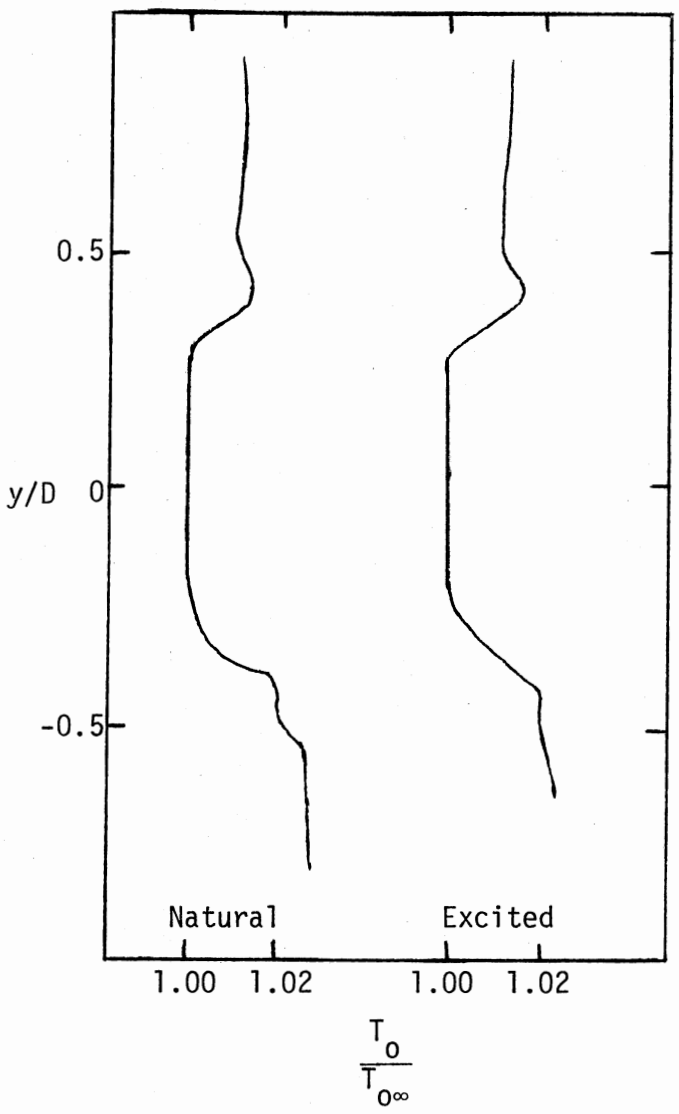

Figure 88. Radial Stagnation Temperature Distributions, M = 2.5, x/D = 1

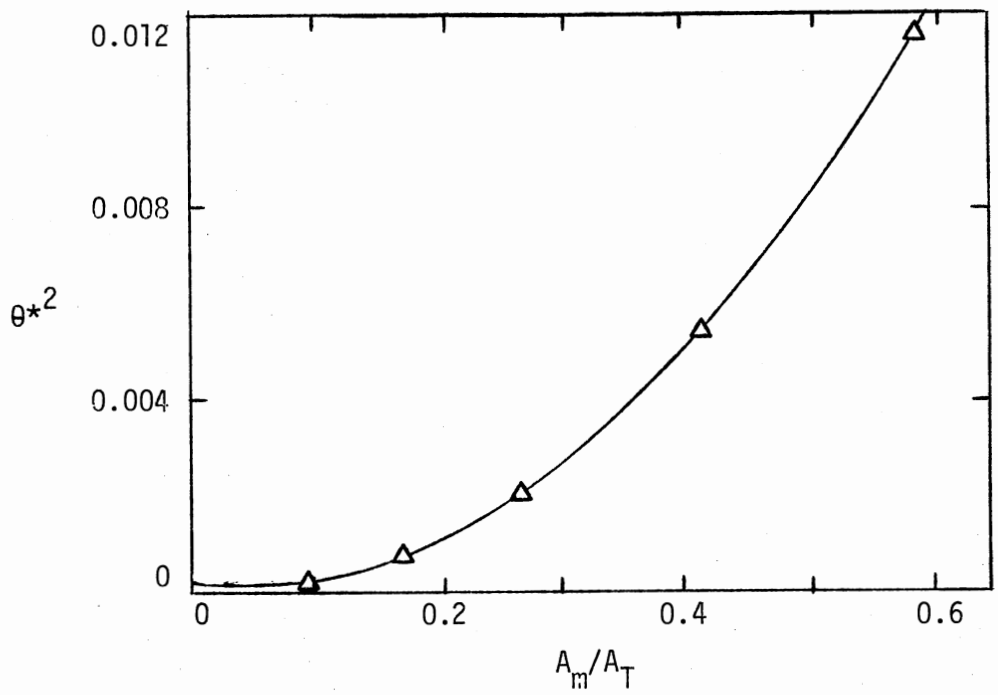

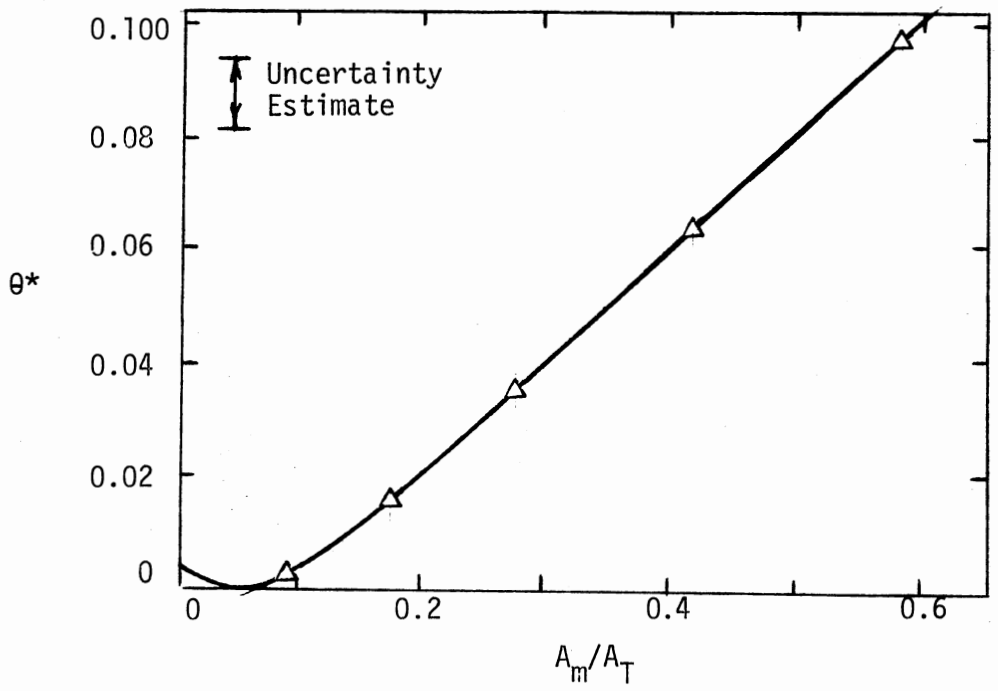

Figure 89. Mode Diagrams for Normal Hot-Wire ($M = 2.1$, $x/D = 14$, $\tilde{m} = 0.20$, $\tilde{T}_o = 0.015$, $R_{mT_o} = 0.65$)

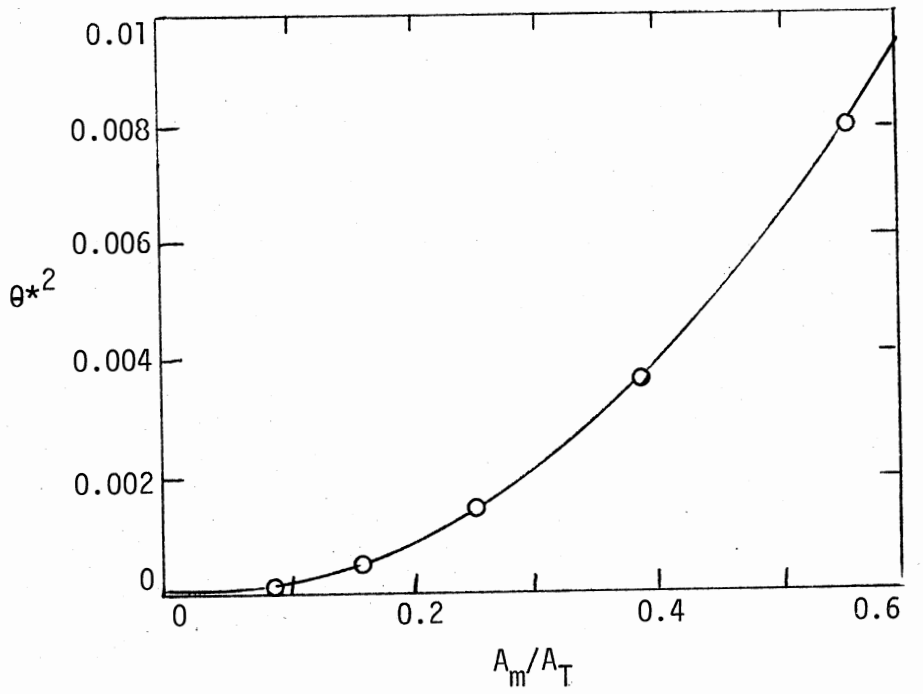

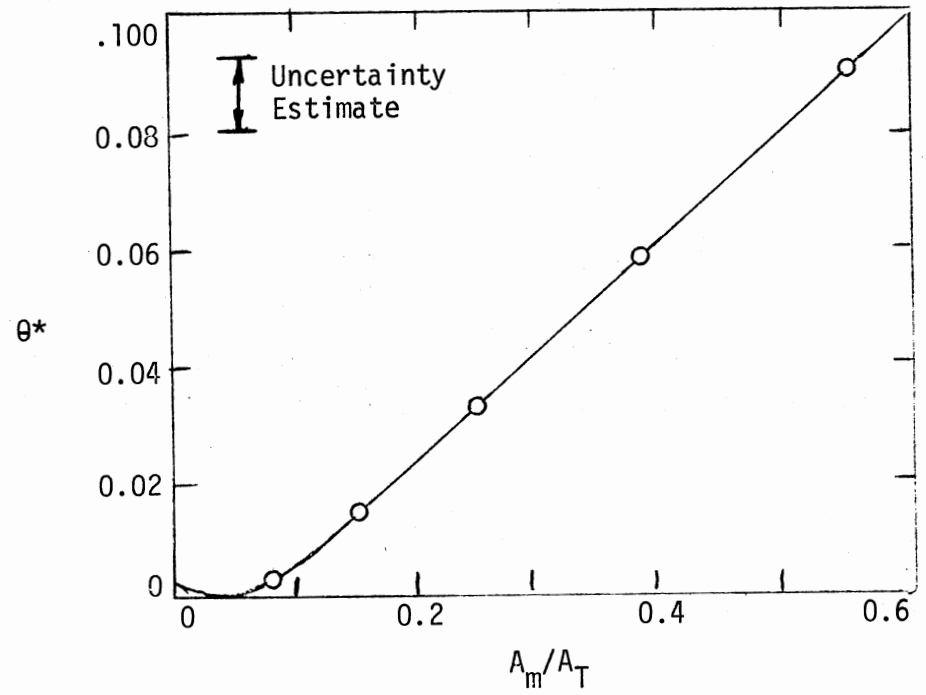

Figure 90. Mode Diagrams for Normal Hot-Wire, M = 2.1, Excited at St = 0.22 (x/D = 14, $\tilde{m}$ = 0.17, $\tilde{T}_o$ = 0.011, R_{mT_o} = 0.62)

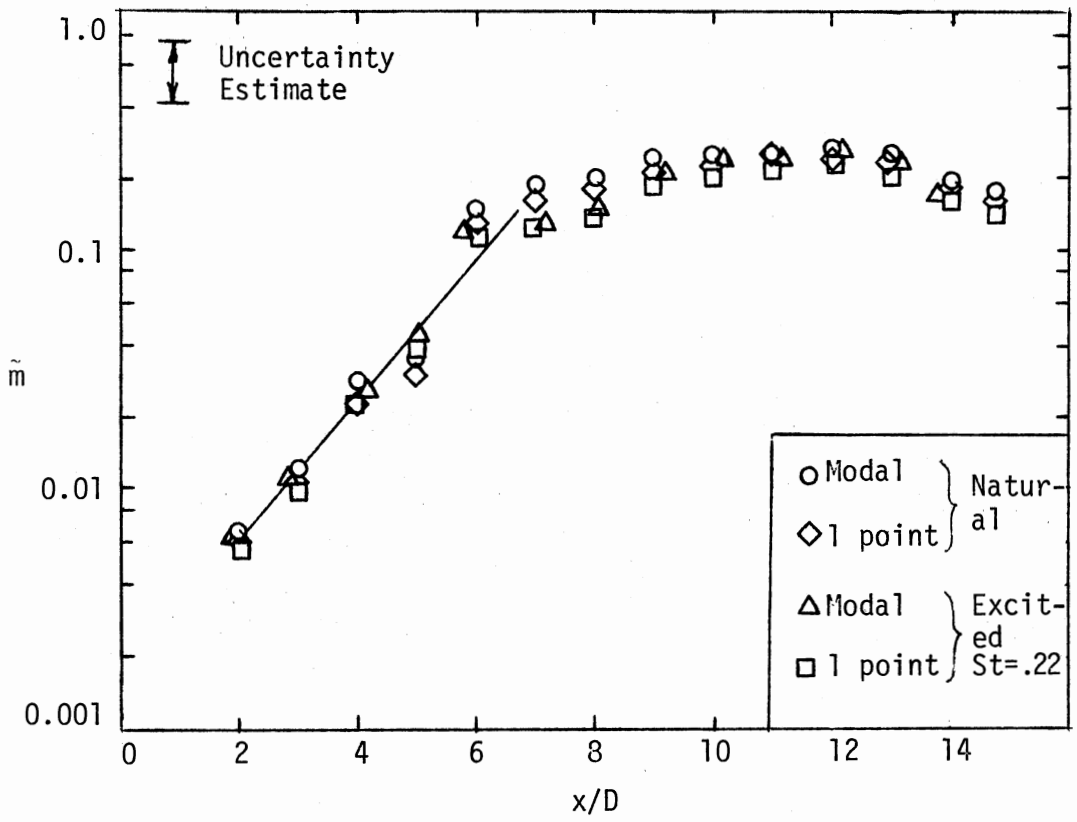

Figure 91. Axial Growth of Flow Fluctuations, M = 2.1

APPENDIX D

TABLES

TABLE I

TEST CONDITIONS

M	D	Re	D/d	U/d
Basic Measurements				
2.5	6.86 mm	8,700	1.12	93,300 sec^{-1}
2.5	9 mm	8,700	1.12	71,100 sec^{-1}
2.1	10 mm	7,900	1.06	55,800 sec^{-1}
1.4	10 mm	3,700	1.07	43,700 sec^{-1}
Additional Measurements				
1.4	10 mm	6,400	1.07	43,700 sec^{-1}
2.1	10 mm	4,900	1.06	55,800 sec^{-1}
2.1	10 mm	11,750	1.06	55,800 sec^{-1}

TABLE II

GROWTH RATES ($-k_i d$), M = 2.5, Re = 8,700

St	Natural or Excitation Frequency	$-k_i d$
0.03 - 0.64	Natural	0.29 ± 0.05
0.03 - 0.64	St = 0.14	0.28 ± 0.09
0.03 - 0.64	St = 0.16	0.28 ± 0.07
0.03 - 0.64	St = 0.18	0.30 ± 0.07
0.16	St = 0.16	0.32 ± 0.05
0.32	St = 0.16	0.20 ± 0.03
Phase Averaged	St = 0.16	0.30 ± 0.07

TABLE III

AXIAL WAVELENGTHS, M = 2.5

St	λ/D	$k_r d$	c/a_0	c/U
0.14	4.19 ± 0.07	1.34 ± 0.03	1.15	0.69
0.16	3.74 ± 0.06	1.50 ± 0.03	1.11	0.67
0.18	3.40 ± 0.18	1.65 ± 0.08	1.12	0.68

TABLE IV

SUMMARY OF ALL GROWTH RATES ($-k_i d$)

M	St	Natural or Excitation Frequency	$-k_i d$	Re
Present Study				
1.4	0.07 - 0.92	Natural	0.54 ± 0.13	3,700
1.4	0.07 - 0.92	Natural	0.81 ± 0.08	6,400
1.4	0.07 - 0.92	St = 0.33	0.48 ± 0.08	3,700
1.4	0.33	St = 0.33	0.50 ± 0.10	3,700
1.4	0.66	Natural	0.63 ± 0.10	3,700
2.1	0.05 - 0.72	Natural	0.60 ± 0.12	7,900
2.1	0.05 - 0.72	St = 0.22	0.56 ± 0.08	7,900
2.1	0.22	St = 0.22	0.59 ± 0.22	7,900
2.1	0.44	St = 0.22	0.46 ± 0.06	7,900
2.5	0.03 - 0.64	Natural	0.29 ± 0.04	8,700
2.5	0.03 - 0.64	St = 0.14	0.28 ± 0.07	8,700
2.5	0.03 - 0.64	St = 0.16	0.28 ± 0.05	8,700
2.5	0.03 - 0.64	St = 0.18	0.30 ± 0.05	8,700
2.5	0.16	St = 0.16	0.32 ± 0.04	8,700
2.5	0.32	St = 0.16	0.20 ± 0.02	8,700
2.5	Phase Ave	St = 0.16	0.30 ± 0.05	8,700
2.5	$\tilde{m}$ X - probe	St = 0.18	0.29 ± 0.07	8,700
2.5	$\tilde{v}$ X = probe	St = 0.18	0.17 ± 0.01	8,700
Previous Studies (52) (53)				
1.3	0.07 - 0.92	Natural	1.01 + 0.62	5,600
2.2*	0.15	St = 0.15	0.58 + 0.10	28,900
2.2*	0.18	St = 0.18	0.44 + 0.10	28,900

TABLE IV. (Continued)

M	St	Natural or Excitation Frequency	$-k_i d$	Re
2.2*	0.19	St = 0.19	0.44 ± 0.10	28,900
2.3*	0.03 - 0.64	Natural	0.41 ± 0.02	9,900
2.4*	0.03 - 0.64	Natural	0.80 ± 0.14	58,000

*Conical nozzle contours.

TABLE V

GROWTH RATE ($-k_i d$) OF THE FULL SPECTRUM, NATURAL JET

M	Re	$-k_i d$
1.3	5,600	1.01 $\pm$ 0.62
1.4	6,400	0.81 $\pm$ 0.08
2.1	7,900	0.60 $\pm$ 0.12
2.3	9,900	0.41 $\pm$ 0.02
2.5	8,700	0.29 $\pm$ 0.04
1.4	3,700	0.54 $\pm$ 0.13
2.4	58,000	0.80 $\pm$ 0.14

TABLE VI

WAVE PROPERTIES

M	St	λ/d	$k_r d$	c/a_o	c/U_{exit}
Present Study					
1.4	0.33	1.83 ± 0.17	3.43 ± 0.29	0.72	0.61
2.1	0.22	2.65 ± 0.12	2.37 ± 0.10	0.89	0.58
2.5	0.14	4.69 ± 0.08	1.34 ± 0.03	1.15	0.69
2.5	0.16	4.19 ± 0.07	1.50 ± 0.03	1.11	0.67
2.5	0.18	3.81 ± 0.20	1.65 ± 0.08	1.12	0.68
Previous Studies (52) (53)					
1.3	0.39	1.80 ± 0.20	3.50 ± 0.30	0.27	0.64
2.2*	0.15	4.70 ± 0.50	1.30 ± 0.10	1.10	0.70
2.3*	0.18	3.90 ± 0.40	1.60 ± 0.20	1.13	0.72
2.2*	0.21	3.10 ± 0.30	2.00 ± 0.20	1.04	0.66
2.3*	0.17	3.80 ± 0.40	1.70 + 0.20	1.04	0.65

*Conical nozzle contours.

TABLE VII

COMPARISON OF MEASURED VALUES OF k TO VALUES PREDICTED BY TAM AND MORRIS

Measured				Tam		Morris	
M	St	$k_r d$	$-k_i d$	$k_r d$	$-k_i d$	$k_r d$	$-k_i d$
Present Study							
1.4	0.33	3.43 ± 0.29	0.50 ± 0.10	2.44*	1.70*	2.17	0.72
2.1	0.22	2.37 ± 0.10	0.59 ± 0.22	1.68	0.96	---	---
2.5	0.14	1.34 ± 0.03	0.28 ± 0.07	1.08	0.60	---	---
2.5	0.16	1.50 ± 0.03	0.32 ± 0.04	1.16	0.65	---	---
2.5	0.18	1.65 ± 0.08	0.30 ± 0.05	1.40	0.75	---	---
Previous Studies (52) (53)							
2.2	0.15	1.34 ± 0.13	0.58 ± 0.10	1.10	0.64	---	---
2.2	0.18	1.61 ± 0.16	0.44 ± 0.10	1.42	0.76	---	---
2.2	0.21	2.03 ± 0.20	---	1.66	---	---	---
2.3	0.17	1.65 ± 0.17	---	1.28	---	---	---

*Estimated values.

VITA

Gerald Lee Morrison

Candidate for the Degree of

Doctor of Philosophy

Thesis: FLOW INSTABILITY AND ACOUSTIC RADIATION MEASUREMENTS OF LOW REYNOLDS NUMBER SUPERSONIC JETS

Major Field: Mechanical Engineering

Biographical:

Personal Data: Born in Bartlesville, Oklahoma, October, 1951, the son of Mr. and Mrs. E. R. Morrison.

Education: Graduated from Sooner High School in Bartlesville, Oklahoma in May, 1969; received the Bachelor of Science degree, Mechanical Engineering at Oklahoma State University in May, 1973; received the Master of Science degree at Oklahoma State University in May, 1974; completed requirements for the Doctor of Philosophy degree at Oklahoma State University in December, 1977.

Honors: Phi Kappa Phi, Pi Tau Sigma, Sigma Tau, Tau Beta Pi, and Gulf Oil Fellowship.

Professional Societies: American Institute of Aeronautics and Astronautics.